



**HAL**  
open science

# Oligomerization and fibrillization properties of amyloid peptides and interactions with inhibitors

Anais Hoffmann

► **To cite this version:**

Anais Hoffmann. Oligomerization and fibrillization properties of amyloid peptides and interactions with inhibitors. Biophysics. Université Pierre et Marie Curie - Paris VI, 2015. English. NNT : 2015PA066442 . tel-01372204

**HAL Id: tel-01372204**

**<https://theses.hal.science/tel-01372204>**

Submitted on 27 Sep 2016

**HAL** is a multi-disciplinary open access archive for the deposit and dissemination of scientific research documents, whether they are published or not. The documents may come from teaching and research institutions in France or abroad, or from public or private research centers.

L'archive ouverte pluridisciplinaire **HAL**, est destinée au dépôt et à la diffusion de documents scientifiques de niveau recherche, publiés ou non, émanant des établissements d'enseignement et de recherche français ou étrangers, des laboratoires publics ou privés.

# Université Pierre et Marie Curie

Ecole doctorale Chimie Physique et Chimie Analytique de Paris (ED 388)

*Laboratoire des BioMolécules / Equipe Structure et Dynamique des biomolécules*

## **Oligomerization and fibrillization properties of amyloid peptides and interactions with inhibitors**

Par Anais Hoffmann

Thèse de doctorat de Biophysique

Dirigée par Lucie Khemtemourian en co-direction avec Olivier Lequin

Soutenu le 25 septembre 2015

Devant un jury composé de :

Mme Sophie LECOMTE

Directrice de recherches, CNRS

M. Arnaud BONDON

Directeur de recherches, CNRS Rennes

Mme Antoinette KILLIAN

Professeur, Utrecht University, The Netherlands

M. Thierry FOULON

Professeur, Université Pierre et Marie Curie

Mme Lucie KHEMTEMOURIAN

Chargée de recherche, CNRS Paris

M. Olivier LEQUIN

Professeur, Université Pierre et Marie Curie



# Abstract

Amyloid diseases, including Alzheimer's (AD), Parkinson's, Prion diseases and type 2 diabetes mellitus (T2DM), are characterized by the accumulation of insoluble fibrillar aggregates in tissues. These diseases are the result of the aberrant folding of proteins that constitute the main component of the fibrils. My thesis project focused on two amyloid peptides:  $\beta$ -amyloid peptide, a 40/42 residue peptide involved in AD, and Islet Amyloid PolyPeptide (IAPP), a 37 residue peptide linked with T2DM.

Although the mechanism of oligomerization is still unclear, it is known to be a stepwise process that includes a nucleation phase, where the peptides are mainly monomeric and slowly form aggregates, followed by an elongation phase, characterized by the formation of large prefibrillar oligomers leading to mature fibrils. A first part of my project focused on the early stages of fibrillation of IAPP, using a set of complementary biophysical techniques. This study showed that the oligomerization pathway of IAPP involved no or short time lived oligomers favoring the formation of large aggregates.

In a second step, I investigated the effect of residue 18 and global charge of IAPP by a mutational analysis of residue His18 and biophysical analysis at pH 5.5 and 7.4. The results showed that (1) the substitution of His18 slowed down the kinetics of fibrillation of IAPP by affecting the interactions between monomers, (2) acidic pH was unfavorable for the process.

Finally, we examined the interaction of amyloid peptides with potential inhibitors of synthetic (sugar or fluor-based peptides) or natural origin (epigallocatechingallate). Different mechanisms of action could be characterized.





# Acknowledgments

Une thèse, c'est fait de hauts et de bas, de joies et de larmes. Ce sont trois années éprouvantes, riches en émotions mais inoubliables desquelles nous ressortons grandis.

Le manuscrit qui suit relate le travail que j'ai effectué au long de ces trois années passées au laboratoire des BioMolécules. Travail, qui n'aurait pas été le même sans le soutien de personnes que je souhaiterais remercier.

En premier lieu, je souhaiterais remercier le Pr. Solange Lavielle et le Dr. Sandrine Sagan pour m'avoir accueillies chaleureusement dans le laboratoire où j'ai passé ces trois années.

Je remercie également les Dr. Sophie Lecomte, Dr. Arnaud Bondon ainsi que les Pr. Antoinette Killian et Pr. Thierry Foulon d'avoir accepté d'évaluer ma thèse. J'ai été ravie que vous ayez pris part à mon jury et de discuter avec vous sur le sujet passionnant qu'est celui des amyloïdes.

Merci à Lucie Khemtemourian et Olivier Lequin, mes deux directeurs de thèse. Lucie, pour avoir cru en mes capacités, m'avoir encouragé à faire une thèse et de ce fait, permis de travailler sur un sujet aussi complexe qu'ambitieux. Olivier, merci pour toutes les connaissances que tu as pu m'apporter, tes conseils et surtout... ta patience malgré mon mauvais caractère !

Je tiens également à remercier à tous les membres du LBM en premier lieu les « RMN-istes ». Ludovic, Emeric et Jean-Jacques, merci pour votre aide et conseils que vous m'avez fourni en différentes occasions lors de ces trois ans. Mention spéciale pour Ludovic : l'expression bactérienne et la purification de peptides amyloïdes vont définitivement me marquer à vie ! Isabelle, je te remercie pour ta patience et toutes les explications que tu as pris le temps de me donner lorsque nous avons travaillé sur le projet « inhibiteurs ». Lumi, merci pour ton aide en RMN et avec Mathematica. Une pensée pour les stagiaires de l'équipe 3, dont j'ai autrefois fait partie : Manon, Alexandra et Sridévi. Merci pour votre bonne humeur et votre implication dans le travail, vous avez été des stagiaires au top.

Merci également aux autres membres du laboratoire, en particulier Françoise pour avoir chouchouté « mes » cellules et pour avoir appris à la non-biologiste que je suis à faire des tests de cytotoxicité. Nicolas, merci pour ta bonne humeur et tes conseils, c'est toujours un plaisir de discuter avec toi. L'équipe de spectro de masse : Gilles, Emmanuelle et Gérard pour leur sympathie et pour m'avoir aidé à me dépatouiller avec la technique du MALDI-TOF. Les « anciens » thésards : Séverine, Tom et Shahid. Merci pour vos conseils et votre soutien.

Je remercie tout particulièrement Lucie « C. ». Il n'y a pas assez de mots pour exprimer ma reconnaissance. Merci de ton soutien, de tes conseils, de ta bonne humeur avant, pendant et après ma thèse. Je suis très fière d'être ta « petite sœur de thèse ».

Ma thèse n'aurait également pas été la même au LBM sans « les filles du bureau » à savoir mon homonyme (Anaïs T), Enicule (Lucile), Aude à la joie (pas de traduction ici) et Mathildou (qui n'est pas dans le bureau mais c'est pareil). Merci pour toutes les petites discussions, les gros fous rires et votre soutien... Et oui, entre filles on se serre les coudes !!! Merci aux « thésards du quatrième » (anciennement nommés les « gars du quatrième » mais ça ne marche plus...): Fred pour sa bonne humeur contagieuse (quand il n'est pas au muséum), Seb pour son humour sans failles, Mehdi pour toutes les discussions et fous rires que l'on a pu avoir (vive la salle de HPLC au bâtiment F !) et Claudia dont le sourire est contagieux ! Pierre, je ne te remercie pas car 1/ tu trouverais ça bizarre, 2/ ça t'apprendra à quitter le bureau des thésards. Trêves de plaisanterie, merci pour tous tes conseils, ton soutien et tous les bons moments que l'on a pu passer au labo.

Je remercie également les « gars de l'ENS » : Cyril pour tes conseils et ton soutien, notamment lors de la dernière ligne droite de ma thèse... Je ne savais plus où donner de la tête et tu as réussi à me faire garder mon calme malgré tout ! Samuel, merci pour ton soutien et pour ta bonne humeur, c'est un bonheur de pouvoir travailler avec toi. Et de manière générale... Merci à vous deux pour l'aide que vous m'avez apportée pour l'utilisation de Mathematica !!! Sans vous, je crois que mon ordinateur n'aurait pas fait long feu...

Merci aux personnes avec lesquelles j'ai également pu travailler lors de ma thèse. Géraldine Toutirais pour m'avoir fait découvrir la microscopie électronique à transmission et Christophe Desmarets qui m'a permis de monopoliser l'appareil de dichroïsme circulaire à plusieurs reprises. Merci également à Manikam Sadasivam Saravanan mon « correspondant des Pays-Bas » qui m'a accueillie dans le groupe de Membrane Biophysics and Biochemistry à Utrecht et formée pour les expériences sur les monocouches et que j'ai pu accueillir à mon

tour à Paris pour des expériences RMN. It was always a great pleasure to work with you Saran, thank you for being my « cheerboy ».

J'exprime également ma reconnaissance au Pr. Claude Pepe, merci de m'avoir permis d'effectuer mon tout premier stage en chimie analytique et pour vos conseils. Ce fut un vrai tremplin pour la suite de ma formation académique et de ma carrière.

Un énorme merci à Sophie Rochut, ton soutien et tes conseils précieux m'ont porté toutes ces années. Merci de m'avoir donné l'occasion de travailler avec toi et d'avoir toujours cru en moi, même quand moi je n'y croyais plus. Une partie de moi ne serait pas là où j'en suis aujourd'hui sans toi. Pour une fois, je peux dire que mon habitude d'arriver en retard en toutes circonstances m'aura porté chance !

Un grand merci également à Nicolas Haraczaj, pour m'avoir embarquée dans la folie et la complexité de l'application de la chimie analytique aux sciences forensiques. Merci pour m'avoir accueilli pendant toutes mes visites de courtoisies à l'IRC, « ma deuxième maison ou presque » et de m'avoir rappelé à maintes reprises qu'il fallait que je garde la pêche.

Enfin, je tiens tout spécialement à remercier mes proches pour m'avoir épaulée lors de ma thèse.

Mes amies « d'enfance », Alexandra et Diana, qui m'ont montré que la distance ne changeait rien à l'amitié. Les « filles du sport » : Emilie (mon double) et Séverine pour avoir toujours su me redonner le sourire dans les moments difficiles (et m'avoir encore plus fait rire, dans les bons moments !). Marine et son balcon (We are Wargirls !), qui m'ont aidé lors de la rédaction de ma thèse. Laetitia, Prisca et Anne-Caroline, merci d'avoir été là pour moi, votre soutien a été sans faille et m'a permis de tenir jusqu'au bout. Thomas, ma meilleure rencontre de la fac et mon frère de coeur, tu sais que je t'adore, merci de me supporter depuis ces 9 dernières années... Le blanchiment des coraux aura toujours une signification particulière pour moi.

Merci enfin à ma famille : mes parents parce qu'ils ont toujours cru en moi et surtout ma petite sœur (petite en âge mais plus grande par la taille !) pour notre complicité sans laquelle rien ne serait pareil (ah.)! My cousin, Aileen, thank you so much again for traveling from the US to France to support me on the day of my PhD defense. I still can't believe that you did that, I'm glad you came.

Merci enfin à toutes les personnes que j'ai sans doute oublié de citer ici.



# Table of contents

<b>Abstract</b> .....	<b>3</b>
<b>Acknowledgments</b> .....	<b>5</b>
<b>Table of contents</b> .....	<b>9</b>
<b>Glossary</b> .....	<b>13</b>
<b>Introduction</b> .....	<b>15</b>
<b>1. Amyloid diseases</b> .....	<b>17</b>
<b>2. Cytotoxicity hypotheses and mechanistic models of fibrillization</b> .....	<b>19</b>
<b>3. Type 2 diabetes mellitus and secretion of Islet Amyloid PolyPeptide</b> .....	<b>24</b>
a) Secretion of Islet Amyloid PolyPeptide.....	24
b) Development of type 2 diabetes mellitus .....	26
i. Extracellular origin.....	26
ii. Intracellular origin .....	27
c) Elongation and structure of the fibrils.....	28
d) Key residues of hIAPP in the amyloidogenesis .....	30
<b>4. Alzheimer's disease (AD) and formation of <math>\beta</math>-Amyloid (<math>A\beta</math>) peptide</b> .....	<b>31</b>
a) Formation of $\beta$ -Amyloid ( $A\beta$ ) peptide.....	31
b) Factors to the development of AD.....	32
i. Mutation of APP gene .....	33
ii. Presenilins.....	33
iii. ApolipoproteinE (APOE) .....	34
c) Structure of $A\beta_{42}$ in solution .....	34
i. $A\beta_{42}$ fibrils.....	34
ii. $A\beta$ intermediates.....	35
<b>5. Interactions between amyloid peptides and the cell membrane</b> .....	<b>37</b>
a) Influence of the cell membrane on the oligomerization .....	38
b) Structure of membrane bound amyloid peptides .....	39
c) Membrane models.....	40
<b>6. Interaction with inhibitors</b> .....	<b>41</b>
<b>7. Objectives of the thesis</b> .....	<b>42</b>
<b>Investigating the fibrillization mechanisms, the structure of amyloid peptides and the interactions between species</b> .....	<b>49</b>
<b>1. Monitoring the kinetics of fibrillation and oligomer formation by fluorescence</b> .....	<b>51</b>
a) Fluorescent probes .....	51

i.	Thioflavin T.....	52
ii.	Tryptophanol.....	54
b)	Experimental protocol.....	55
c)	Advantages, drawbacks and troubleshooting.....	56
<b>2.</b>	<b>Study of the membrane permeabilization by calcein leakage experiments.....</b>	<b>57</b>
a)	Calcein.....	57
b)	Experimental protocol.....	58
c)	Advantages, drawbacks and troubleshooting.....	59
<b>3.</b>	<b>Analysis of the secondary structure of the peptides with circular dichroism (CD) .</b>	<b>59</b>
a)	Principle.....	59
b)	Experimental protocol.....	61
c)	Advantages, drawbacks and troubleshooting.....	62
<b>4.</b>	<b>Nuclear Magnetic Resonance (NMR) spectroscopy.....</b>	<b>63</b>
a)	Principle.....	63
b)	1D spectrum acquisition.....	64
c)	Diffusion Ordered NMR-Spectroscopy (DOSY) / Pulse Field Gradient (PFG) experiment	67
d)	Saturation Transfer Difference (STD) experiments.....	69
e)	Sequential assignment of hIAPP.....	71
f)	Experimental protocol.....	72
g)	Advantages and drawbacks.....	73
<b>5.</b>	<b>Monolayer experiment.....</b>	<b>73</b>
a)	Principle.....	73
b)	Experimental protocol.....	74
c)	Advantages, drawbacks and troubleshooting.....	75
<b>6.</b>	<b>Transmission Electron Microscopy.....</b>	<b>75</b>
a)	Principle.....	75
b)	Experimental protocol.....	76
c)	Drawbacks and troubleshooting.....	77
<b>7.</b>	<b>Polyacrylamide gel electrophoresis.....</b>	<b>77</b>
a)	Principle.....	77
b)	Gel composition and electrophoresis conditions.....	78
c)	Advantages and drawbacks.....	81
<b>8.</b>	<b>Sample preparation.....</b>	<b>81</b>
a)	Materials.....	81
b)	Preparation of the peptides.....	82

c)	Preparation of the vesicles .....	82
i.	Choice of the lipids.....	82
ii.	Preparation of Small/Large Unilamellar Vesicles (S/LUV) .....	83
iii.	Preparation of calcein vesicles (LUV 200 nm).....	83
iv.	Quantification of the phospholipid concentration .....	84
<b>9.</b>	<b>Expression of A<math>\beta</math>42.....</b>	<b>85</b>
i.	Experimental protocol .....	85
ii.	Troubleshooting and protocol optimization.....	86
<b>Insights into the kinetics and mechanism of fibrillization of hIAPP in solution ....</b>		<b>97</b>
<b>1.</b>	<b>Results .....</b>	<b>101</b>
a)	Study of the early stages of fibrillization.....	101
i.	ThT and TROL fluorescence assays.....	101
ii.	CD spectroscopy .....	104
iii.	NMR spectroscopy .....	107
iv.	Gel electrophoresis .....	113
b)	Interaction with fluorescent probes .....	118
i.	Influence on A $\beta$ 42 kinetics of fibrillization.....	118
ii.	Influence on hIAPP kinetics of fibrillization.....	122
<b>2.</b>	<b>Discussion.....</b>	<b>130</b>
<b>3.</b>	<b>Conclusion .....</b>	<b>135</b>
<b>4.</b>	<b>Materials and Methods.....</b>	<b>136</b>
<b>Effect of charge and mutation of residue 18 on the aggregation properties of the Islet Amyloid PolyPeptide (IAPP) in membrane environment .....</b>		<b>143</b>
<b>1.</b>	<b>Introduction.....</b>	<b>145</b>
<b>2.</b>	<b>Results and discussion .....</b>	<b>148</b>
a)	Fibrillization occurs for all mutants under both pH conditions.....	148
b)	Quantification of hIAPP wild type and mutant monomers over time by NMR.....	151
d)	Circular dichroism show shows the formation of large $\beta$ -sheet aggregates .....	157
e)	Mutation and change of pH does not influence the peptide insertion into the membrane 164	
f)	Calcein leakage experiment .....	165
<b>3.</b>	<b>Conclusion .....</b>	<b>168</b>
<b>4.</b>	<b>Material and Methods.....</b>	<b>169</b>
<b>Interactions of amyloid peptides with inhibitors .....</b>		<b>175</b>
<b>1.</b>	<b>Introduction.....</b>	<b>177</b>



2. Effect of a (R)- $\alpha$ -trifluoromethylalanine containing short peptide in the inhibition of amyloid- $\beta$ fibrillation.....	179
3. Study of the effect of small glycopeptidomimetics on the oligomerization and fibrillization of A $\beta$ 42.....	182
4. Effect of (-)-epigallocatechin-3-gallate on the oligomerization of hIAPP .....	186
5. Conclusion` .....	194
<b>Conclusion</b> .....	<b>199</b>
<b>Publications</b> .....	<b>205</b>
<b>Summary (French)</b> .....	<b>249</b>
<b>Abstract (French)</b> .....	Erreur ! Signet non défini.

# Glossary

(h)IAPP	: (human)Islet Amyloid PolyPeptide
A $\beta$	: Amyloid- $\beta$ peptide
AD	: Alzheimer's Disease
APP	: Amyloid Protein Precursor
ER	: Endoplasmic Reticulum
UPR	: Unfolded Protein Response
DOPC	: 1,2-dioleoyl-sn-glycero-3-phosphatidylcholine
DOPS	: 1,2-dioleoyl-sn-glycero-3-phosphatidylserine
EGCG	: (-)-epigallocatechin-3-gallate
SUV	: Small Unilamellar Vesicle
LUV	: Large Unilamellar Vesicle
ThT	: Thioflavin T
TROL	: Tryptophanol
CD	: Circular Dichroism
NMR	: Nuclear Magnetic Resonance
STD	: Saturation Transfer Difference
PFG	: Pulse Field Gradient
DOSY	: Diffusion Ordered NMR-Spectroscopy
TEM	: Transmission Electron Microscopy
TOCSY	: TOtal Correlation Spectroscopy
NOESY	: Nuclear Overhauser Effect Spectroscopy
TEM	: Transmission Electron Microscopy



# **Chapter 1:**

## **Introduction**



## 1. Amyloid diseases

The term “amyloid” was introduced by the physician and biologist Rudolph Virchow in the late-19th century, after he identified macroscopic abnormal-looking cerebral tissues that were able to exhibit a positive iodine staining reaction in presence of sulfuric acid.<sup>1</sup> The fibrils were starch-like, similar to cellulose, hence the term “amyloid” (*amylum* in Latin, ἄμυλον *amylon* in Greek). This initial discovery was followed by a descriptive stage where amyloid fibrils were observed by light microscopy using a variety of histologic dyes. Around the 1920s, it was agreed that one of the properties of amyloid fibrils was their capacity to bind to Congo red dye, exhibiting enhanced colored anisotropy after observation under polarized light. The introduction of electron microscopy allowed further descriptions of amyloid fibrils morphology. The observation of amyloid deposits of human and animal origins showed that the aggregates were constituted of straight, rigid fibrils that were 6 to 13 nm wide and 100 to 1600 nm long<sup>2,3</sup>. Amyloid fibrils, that are, as it was later discovered, built as a repetition of a specific peptide or protein, were located in various tissues types and associated with neurodegenerative and metabolic impairments and other diseases (table 1).

<b>Disease</b>	<b>Aggregation protein or peptide</b>
<i>Neurodegenerative diseases</i>	
Alzheimer's disease	Amyloid- $\beta$ peptide
Spongiform encephalopathies	Prion protein
Parkinson's disease	$\alpha$ -synuclein
Amyotrophic lateral sclerosis	Superoxide dismutase 1
Huntington disease	Huntingtin
<i>Non-neuropathic systemic amyloidosis</i>	
Amyloid light chain amyloidosis	Immunoglobulin light chain or its fragments
Amyloid A amyloidosis	Serum amyloid A1 protein fragments
Senile systemic amyloidosis	Wild-type transthyretin
Haemodialysis-related amyloidosis	$\beta$ 2-microglobulin
<i>Non-neuropathic localized amyloidosis</i>	
Type 2 diabetes mellitus	Islet Amyloid PolyPeptide
Apolipoprotein A1 amyloidosis	APO-A1 fragments
Injection-localized amyloidosis	Insulin

**Table 1: Some human diseases associated with amyloid aggregation. Adapted from Knowles *and al.* 2014<sup>4</sup>**

Further investigation about amyloid fibrils show that they are the result of the aberrant folding of the peptides or proteins that accumulate in the organism and constitute the main components of the fibrils. Although the mechanism of fibrillization is still unclear, it is known to be a two-step process that includes a nucleation phase, where the peptides are mainly monomeric and form small soluble aggregates, followed by an elongation phase, characterized by the formation of large prefibrillar oligomers leading to mature fibrils (figure 1). The fibrillization, as it is associated with an aberrant folding of peptides/proteins, is therefore characterized by a conformational change in the peptide from its native or disordered structure into a cross  $\beta$ -sheet conformation as depicted in figure 1. This leads to highly structured fibrils, with the  $\beta$ -strands of the peptides being oriented perpendicularly to the fibril axis (figure 2).

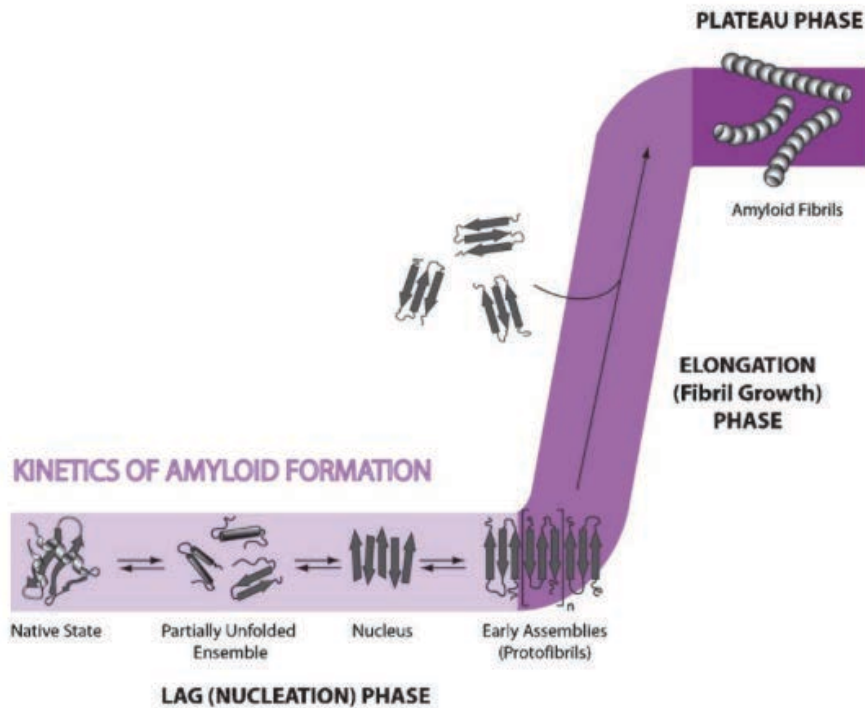


Figure 1: Schematic representation of amyloid fibril formation. The fibrillization is a two-step process composed of the nucleation phase/lag phase in which prefibrillar assemblies are formed triggered by the aberrant folding of the constitutive peptide, followed by an exponential elongation phase during which the fibrils are formed. The plateau represents the state where maximum fibril growth has occurred. Adapted from Wilson and al. 2007<sup>5</sup>

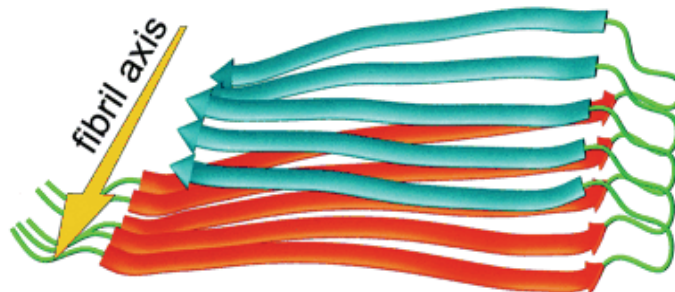


Figure 2: Schematic representation A $\beta$ 40 fibrils incorporating the cross- $\beta$  motif common to all amyloid fibrils. Adapted from Petkova and al, 2002.<sup>6</sup>

## 2. Cytotoxicity hypotheses and mechanistic models of fibrillization

The first hypothesis suggested that the fibrils were the main pathogenic entities related to amyloid disorders. Since amyloid diseases were correlated to the presence of large insoluble fibrils at the surface of membranes, it was initially believed that they were the most pathogenic species inducing cell death and progression of the disease they were related to. However, more recent studies have challenged this initial hypothesis by cytotoxicity studies showing that fibrillar aggregates have less impact on cell death than small soluble oligomers.



Nowadays, a second hypothesis has risen and indicates that rather than the mature fibrils, some specific intermediate states and/or the whole oligomerization process are responsible for amyloid disorders and are potentially more harmful for the cells. The involvement of those intermediate species in the development of the diseases has been shown, especially for Alzheimer, Parkinson and Huntington diseases, from *in vitro* studies on primary cell cultures<sup>7</sup>.

Further investigations of the link between amyloid intermediates and cell death have shown that oligomers interact greatly with the cell membrane, disturbing the structural integrity of the lipid bilayer.<sup>8</sup> Although the mechanisms for membrane permeabilization or membrane disruption are yet unknown, different coexisting models have been proposed to explain the deleterious effect of amyloid oligomers on membranes. These models include the “ion channel” hypothesis, insertion of the peptide into the membrane leading to its disruption, and the “lipid uptake hypothesis” (figure 3).

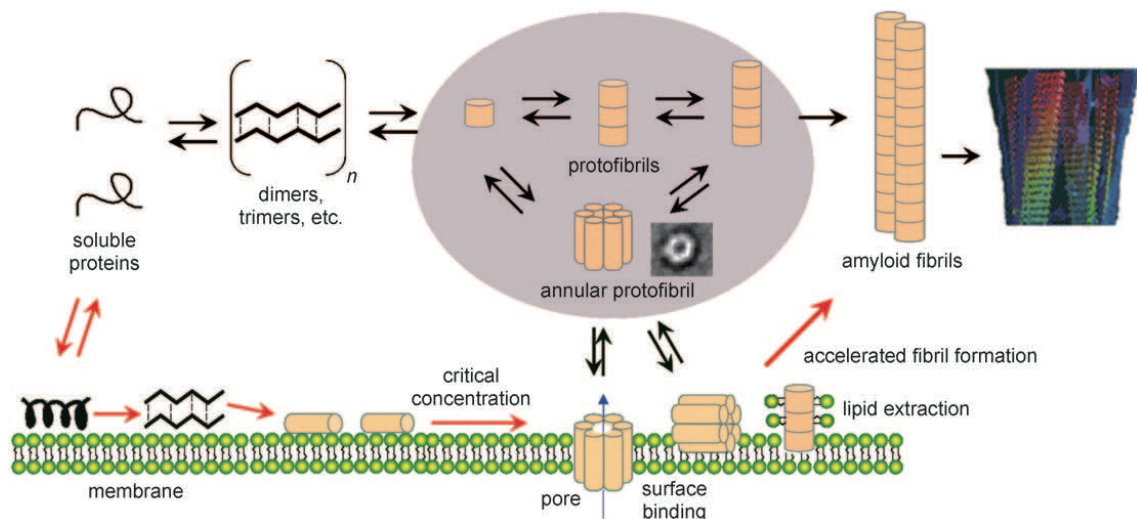


**Figure 3: Interconnectivity between amyloid formation and membrane disruption. Top: The process of amyloid-fibril formation.**

**Amyloid formation involves the misfolding of soluble proteins into  $\beta$ -sheet oligomers, which further aggregate into protofibrils, including ring-like annular protofibrils, and then into amyloid fibrils. Bottom: The role of membranes in amyloid formation and toxicity. Soluble proteins bind to membrane surfaces with a conformational transition to an  $\alpha$ -helix structure. The accumulation of proteins on the surface of the membrane induces their oligomerization into  $\beta$ -sheet aggregates. When a critical threshold concentration is reached, a transmembrane pore (annular protofibril) develops in the membrane and enables the leakage of membrane contents. As other possible or coexistent mechanisms, annular protofibrils formed in solution may insert into the membrane, undefined prefibrillar aggregates may bind to the membrane surface and induce membrane thinning, and lipids may be extracted from the membrane and incorporated into the developing fibril in a detergent-like process.**

From Butterfield and Lashuel.<sup>17</sup>

The “ion channel” hypothesis, demonstrated the ability of amyloid peptides, to form ion channels through the membrane. Experiments of vesicle permeabilization by amyloid- $\beta$  ( $A\beta$ ) peptide, human Islet Amyloid Polypeptide (hIAPP) and  $\alpha$ -synuclein have shown that those

channels were the results of annular shaped oligomers that interacted with the membrane. The formation of those “ion channels” induces a loss of the selectivity of the membrane by allowing ions to either leak into the intercellular compartment or enter into the cytoplasm. The disruption of the ion concentration inside or outside the cell, which is detrimental to its function, contributes to trigger apoptosis.<sup>9, 10, 11, 12</sup>

The mechanisms for pore formation of amyloid peptides were suggested to be similar to the mode of action of antimicrobial peptides on the membrane. Indeed, both amyloid and antimicrobial peptides share many characteristics, such as the capacity to adopt amphipathic structures in presence of lipid bilayers and the capacity to permeabilize the membrane. These physiochemical similarities could therefore suggest that the two classes of peptides have similar mechanisms of membrane disruption.<sup>13</sup> Different models were proposed to describe the mode of action of antimicrobial peptides, on the membrane (figure 4). In the barrel-stave model the hydrophobic region of the peptide comes in contact with the hydrophobic membrane interior, while the hydrophilic region is oriented towards the aqueous medium. The result is the formation of a peptide lined, hydrophilic pore that increases in size as the monomer aggregates and allows molecules to leak out of or into the cell. The toroidal-pore model suggests metastable structure where the hydrophilic part of the peptide remains in contact with the hydrophilic lipid groups, inducing a curvature of the membrane and allowing the passage of molecules through the membrane. The sinking-raft and carpet models locate the associating peptides on the surface of the membrane in a “carpet like” manner. Upon a critical concentration, the membrane dissociates and breaks down creating a pore. Following the disruption, either the lipid bilayer is resealed (sinking raft model) or disintegrates in a detergent-like manner (carpet model).<sup>14,15,16</sup>

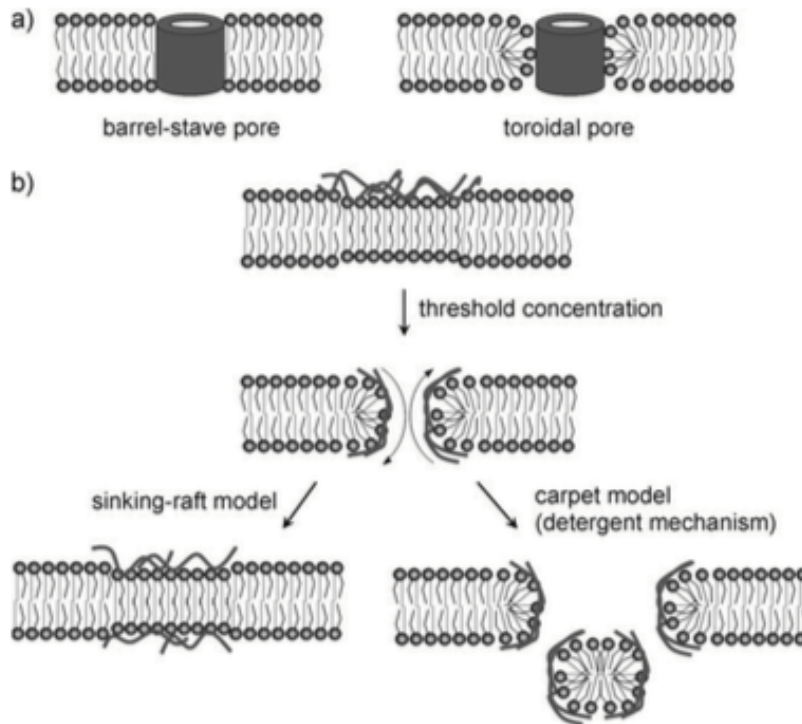


Figure 4: a) Models of barrel-stave and toroidal pores. b) Two dimensional representations of the sinking-raft and carpet models for membrane permeabilization. From Butterfield and Lashuel.<sup>17</sup>

Finally, the « lipid uptake » hypothesis suggests a concerted mechanism of membrane disruption and fibril formation on the surface of the lipid bilayer. The study, which monitored the kinetics of fibril formation of hIAPP as well as the permeabilization of large unilamellar vesicles, mimicking the membrane, showed a close link between the fibrillization process and membrane disruption. Observation by cryomicroscopy showed that the formation of a rigid fibril on the surface of the vesicle induced to a change in the membrane curvature, which leads to membrane leakage (figure 5).

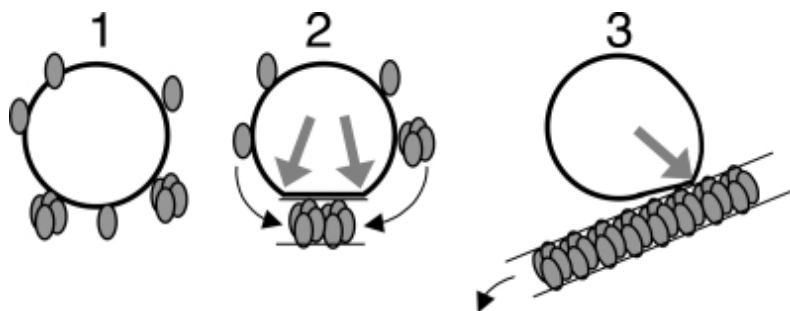
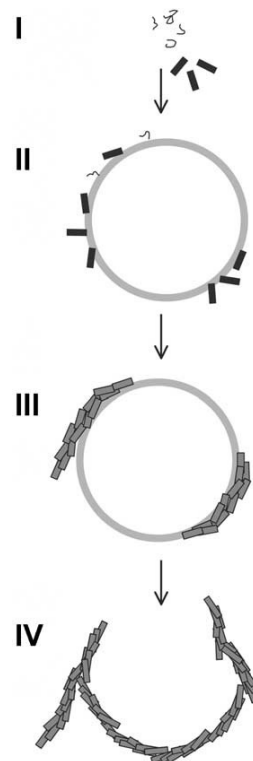


Figure 5: Simplified schematic representation of the different stages of the proposed membrane-associated hIAPP fibril growth that results in membrane damage.

Starting from an intact membrane (black circle) and monomeric hIAPP (gray ellipsoids), hIAPP monomers or oligomers adsorb on or insert into the membrane (*Left*). Next, membrane-located hIAPP participates in initiation and propagation of fibril growth at the membrane leading to a forced change in membrane curvature and concomitant temporal membrane leakage, at the locations where fibrils and membrane separate (gray arrows) (*Center*). Finally, mature hIAPP fibrils that line the surface of a distorted membrane start detaching, initiating recovery of vesicle shape (*Right*). Oligomers have been depicted arbitrarily as a cluster of four hIAPP monomers. Black arrows indicate the movement of hIAPP species. From Engel *and al.*<sup>18</sup>

The lipid uptake process was also observed by confocal microscopy. Results have shown that addition of hIAPP on membrane models induced a permeabilization and disintegration of the membrane simultaneously with the aggregation of the peptide. The presence of fluorescent lipids, as well as the amyloid specific Congo red dye, showed that the aggregates contained a substantial amount of lipids, as a result of an uptake from the membrane by the growing fibrils. The extraction of lipids by hIAPP and their incorporation to the growing fibril consequently leads to the disruption then disintegration of the membrane over time (figure 6).<sup>18,19</sup>



**Figure 6: Schematic representation of the proposed mechanism for the formation of amyloid protein–lipid aggregates in the presence of lipid membranes.**

**I: The aggregation process starts when monomeric proteins are added to the aqueous solution. II: Attractive interaction between the lipid bilayer and the protein oligomers and/or monomers leads to accumulation of proteins at the lipid bilayer. III: Aggregation continues at the lipid membrane, whereby lipids are taken up by the forming aggregates. The extraction of lipids from the membrane also causes local disruption of the membrane barrier. IV: Aggregation continues. Large protein–lipid aggregates are formed for which the membrane may serve as a template. The aggregates include amyloid proteins as well as lipids from the membrane. From Sparr and al.<sup>19</sup>**

The mechanisms of oligomerization and fibril formation are therefore very intricate and, although common pathways of oligomerization were suggested, some specific stages of aggregation can vary with the studied amyloid peptide. During my thesis, I focused on the oligomerization and fibrillization of two amyloid peptides: human Islet Amyloid Polypeptide (hIAPP) involved in type 2 diabetes mellitus, and  $\beta$ -amyloid peptide linked to Alzheimer's disease.

### 3. Type 2 diabetes mellitus and secretion of Islet Amyloid PolyPeptide

Diabetes is a disease that affects over 380 million people in the world. Among those patients, 90% suffer from type 2 diabetes mellitus, otherwise known as the non-insulin dependent diabetes mellitus (WHO, 2014). Linked to a resistance to insulin, it is a chronic disease that is associated to a combination of lifestyle such as a poor diet, overweight and sedentarity and genetic factors. The development of the disease shortens the lifespan of 10 years and leads to multiple complications such as cardiovascular disease, which affect about 50 to 80% of the diabetes patients and blindness or kidney failures.

#### a) Secretion of Islet Amyloid PolyPeptide

Pancreatic sections of type 2 diabetes patients have shown the presence of extracellular amyloid plaques on the surface of  $\beta$ -cells in the Islets of Langerhans (figure 7). Those amyloid fibrils were mainly composed of a 37 residue peptide called Islet Amyloid PolyPeptide (IAPP) also known as amylin<sup>20</sup>. The accumulation of fibrillar IAPP on the pancreatic  $\beta$ -cells was shown to have a significant role in the destruction of the cells therefore in the pathogenesis of type 2 diabetes mellitus.<sup>21</sup>

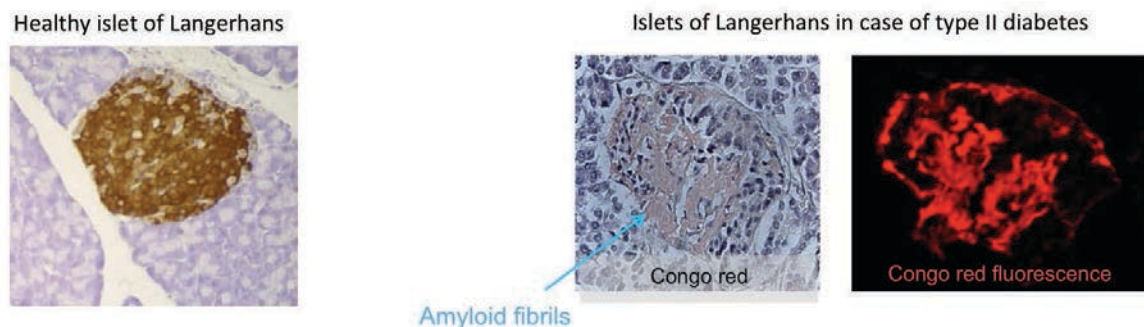


**Figure 7: Microscopic sections of mouse pancreatic tissue, including an islet of Langerhans.** Left : Using an immunohistochemical staining with an antiserum raised against insulin, the insulin-producing  $\beta$ -cells in this healthy islet of a non-transgenic mouse are clearly visible (brown staining) amongst the exocrine tissue (purple counterstaining). Right: Using the amyloid-specific dye Congo red, the presence of amyloid can easily be detected in this islet of a hIAPP transgenic mouse. Using brightfield light microscopy, the Congo red stained amyloid is visible as pink deposits. In this severely affected islet, the  $\beta$ -cell mass is largely reduced. Due to auto-fluorescence of amyloid-bound Congo red, the amyloid can be visualized even better with fluorescence microscopy (bright red colour). From Höppener and al. 2006<sup>22</sup>

IAPP is initially cosecreted with insulin in the pancreatic  $\beta$ -cells islet of Langerhans as a 89 residue peptide precursor (pre-proIAPP). After its expression, PreProIAPP undergoes several post-translational modifications that lead to mature IAPP. First, the cleavage of a signal sequence consisting of 22 residue located on the N-terminus of the polypeptide

generates the 67 residue pro-IAPP. Second, a subsequent cleavage by two prohormone convertases PC2 and PC1/3 of two peptide bonds located on both C-terminus and N-terminus of proIAPP leads to a 40 residue peptide consisting of IAPP and three residues glycine-lysine-arginine located in its C-terminus. The peptide then undergoes the last post-translational processing step, with the removal of the two dibasic residues Lys39 and Arg40 by carboxypeptidase E (CPE) and amidation of the C-terminus, with Gly38 serving as a nitrogen donor. The mature 37 residue IAPP is also composed of an intramolecular disulfide bridge between residues Cys2 and Cys7. Once IAPP is formed at a slightly acidic pH of 5.5 within the intracellular vesicles, it is released in the extracellular medium at a pH of 7.4 where, under favorable conditions, it is prone to aggregate into insoluble fibrils (Figures 8 and 9).<sup>23,24,25,26</sup>

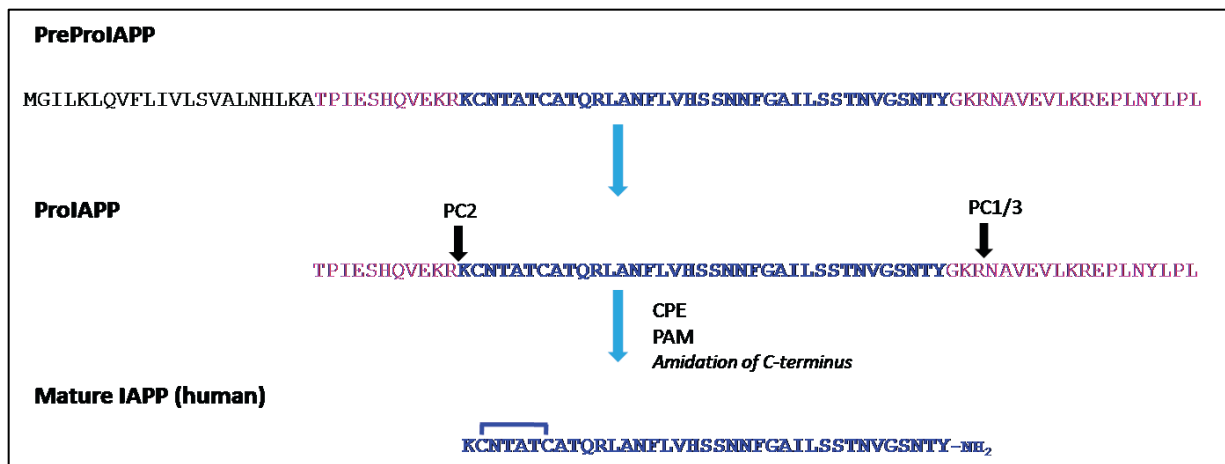


Figure 8: Processing of PreProIAPP to mature IAPP (human form). IAPP is synthesized as an 89 residue PreProHormone.

The cleavage of the signal sequence leads to the 67 residue ProIAPP. ProIAPP is cleaved in its N-terminus and C-terminus parts respectively by PC2 and PC1/3. The further processing of the cleaved peptide by CPE/PAM leads to the amidation of the C-terminus. Mature IAPP also undergoes the formation of the disulfide bridge between Cys2 and Cys7.

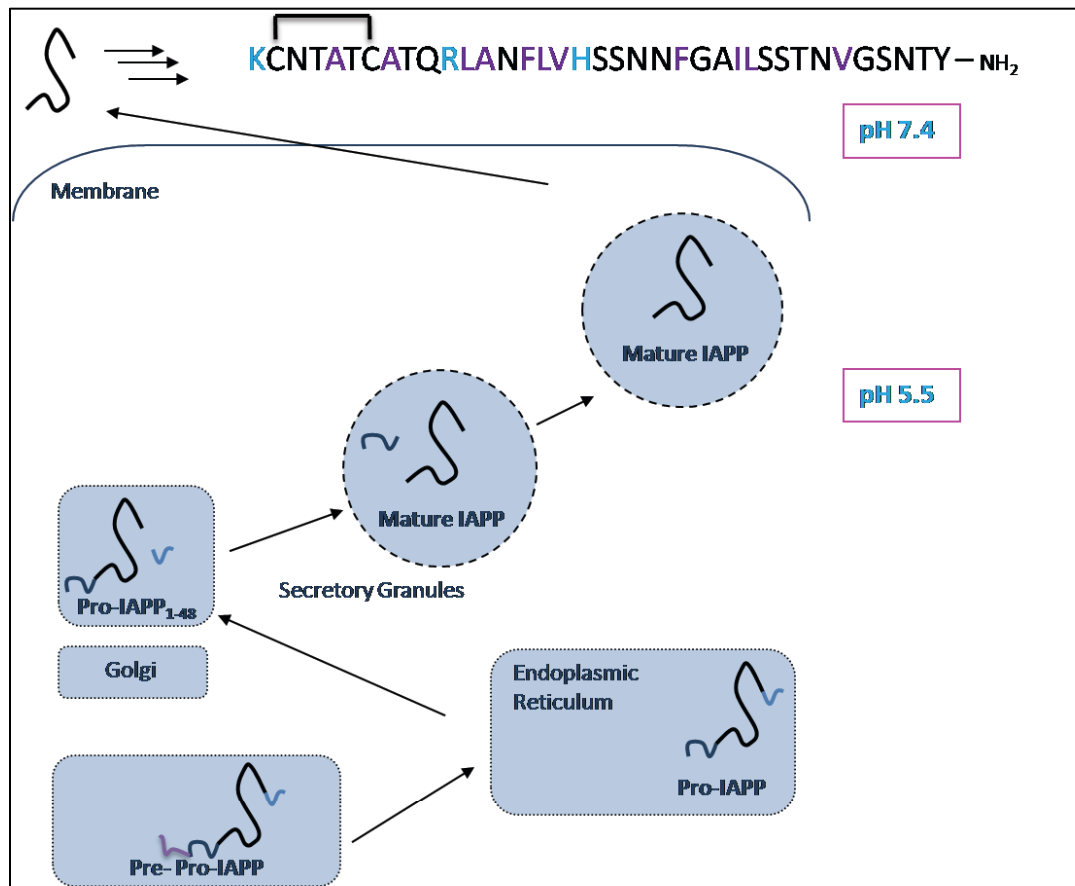


Figure 9: Biosynthesis of hIAPP.

After the secretion and processing of PreProIAPP to mature IAPP, the peptide is released from the intracellular medium (pH 5.5) to the extracellular medium (pH7.4) IAPP sequence: basic residues appear in light blue, non polar/hydrophobic residues in purple

## b) Development of type 2 diabetes mellitus

The development of type 2 diabetes mellitus can find its origin from two different pathways, one of extracellular origin, linked to the formation of IAPP amyloid fibrils on the surface of the cells and the other of intracellular origin, related to the biosynthesis of IAPP in the endoplasmic reticulum.

### i. Extracellular origin

Type 2 diabetes mellitus is a disease that is triggered by a resistance to insulin. In order to maintain the normal glucose tolerance, the pancreatic  $\beta$ -cells secrete a higher level of insulin, which leads to a higher secretion of hIAPP. As the concentration of hIAPP released into the extracellular medium increases, it triggers the auto-assembly of the peptide leading to amyloid fibrils. As the process of hIAPP fibrillization is known to be cytotoxic to the cell

membranes as the peptide interacts with the lipids, the high concentration of hIAPP leads to  $\beta$ -cells death. To compensate, the remaining pancreatic  $\beta$ -cells will secrete insulin, along with hIAPP at an even higher concentration. As the process renews itself, this leads to a vicious circle of overproduction and  $\beta$ -cells death, maintaining the disease.<sup>27,28</sup>

### *ii. Intracellular origin*

A second pathway to the development of the disease is the intracellular pathway. Although amyloid fibrils are mostly localized on the surface of the  $\beta$ -cells, evidence suggested that oligomerization could also occur in intracellular compartment. Several studies on transgenic mice capable of secreting hIAPP have shown that fibrils or prefibrillar aggregates could be found in the endoplasmic reticulum (ER), Golgi or secretory granules of the  $\beta$ -cells where hIAPP is processed. This implies a second mechanism of apoptosis linked to ER stress.

The ER serves many different functions in the cell, including ensuring the correct native folding and post-translational modification of peptides and proteins synthesized within the cell but also, transportation of those molecules to the Golgi and secretory granules and release into the extracellular space. The properties of ER are well balanced and regulated to avoid any misfolding of the secreted proteins. The accumulation of misfolded protein in the cells along with ER stress cascades into the unfolded protein response (UPR). This regulation process involves simultaneously the production of chaperones to both assist the folding of proteins and limit their aggregation; reducing ER workload by inhibiting the protein synthesis triggering the UPR; enhancing the transportation of misfolded protein to the ubiquitin-proteasome system for degradation and, as a last resort, triggering of the apoptosis process. In the context of insulin resistance, the following overproduction of insulin and hIAPP contributes to ER stress, as the processing of peptide/protein reaches its overcapacity. This further triggers a malfunction in the folding process of both hormones. In spite of the various responses of the cell in order to limit the formation of misfolded peptides, the accumulation of hIAPP leads to its intracellular aggregation, as fibrillar species could be observed inside the cell. This result shows that the prevention mechanism of misfolding is rendered non-effective as it reaches a saturation level. As the cell is unable to eliminate the formed cytotoxic oligomers, it triggers the activation of « cell-death receptors », leading to apoptosis, and further decrease of  $\beta$ -cells mass in the pancreas (figure 10).



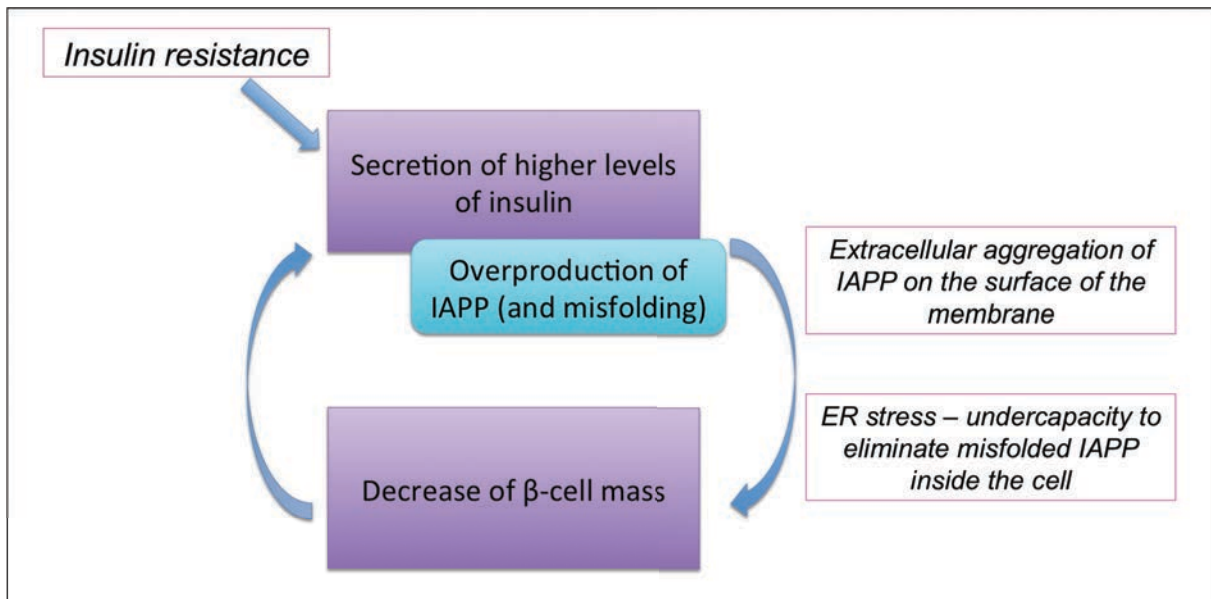


**Figure 10: Schematic illustration of the type two diabetes mellitus vicious circle.**  
 The insulin resistance induces an overproduction of IAPP in the system. IAPP can accumulate in the intra or extracellular medium leading to cell death.

c) Elongation and structure of the fibrils

The structure of the hIAPP fibrils is still not completely known, due to the insoluble and non-crystalline nature of the fibrils. However, two structural models, that present many similarities, have been based on solid-state NMR spectroscopy combined to molecular modeling and X-Ray crystallography. The first model was obtained by Tycko's group from solid state NMR. It shows that the backbone of the peptide adopts a hairpin conformation, with two  $\beta$ -strands segments, composed of residues 8-18 and 28-37 separated by a loop formed by residues 18-27. Each monomer interacts with another, forming an initial building block consisting of four  $\beta$ -sheet layers (figure 11).<sup>29</sup>

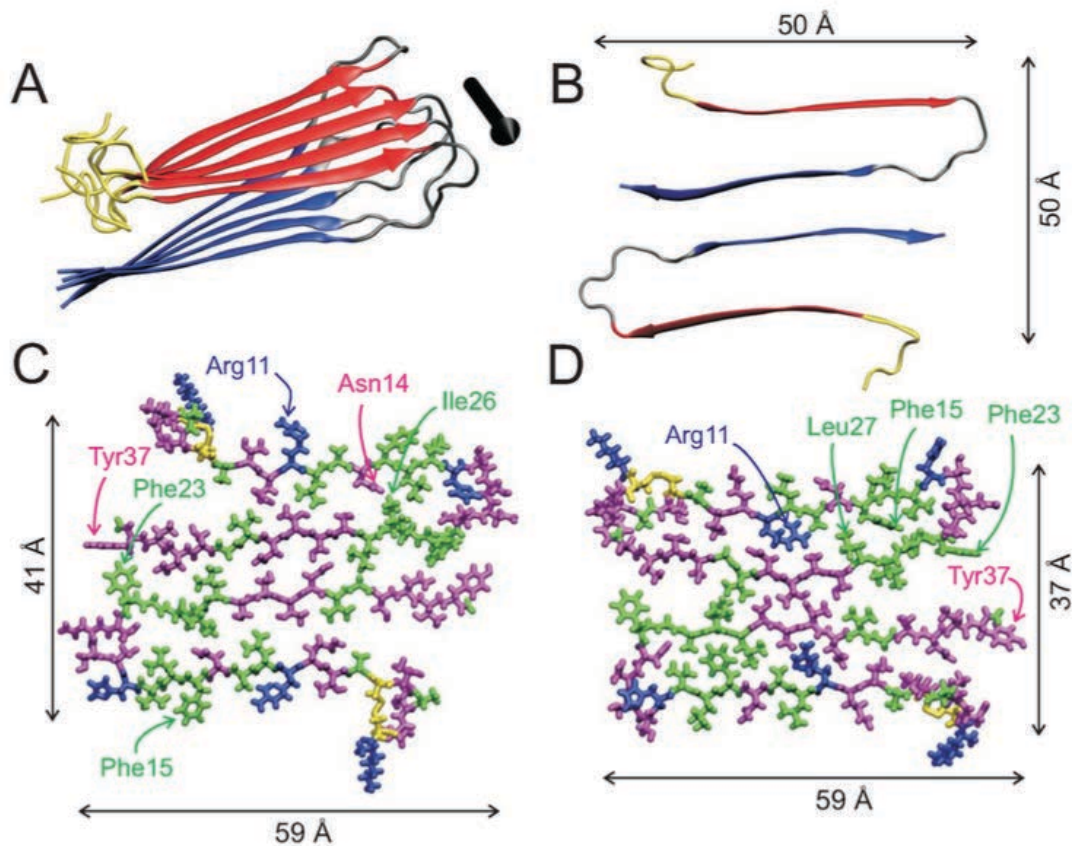


Figure 11: Molecular structural models for the protofilament in amylin fibrils with striated ribbon morphologies based on NMR combined to molecular modeling. (A) Ribbon representation of one cross- $\beta$  molecular layer, with N-terminal and C-terminal  $\beta$ -strand segments colored red and blue, respectively. The black arrow indicates the fibril axis. (B) Cross-sectional view of two amylin molecules in the protofilament. (C, D) All-atom representations of two possible models, with hydrophobic residues in green, polar residues in magenta, positively charged residues in blue and disulfide-linked cysteine residues in yellow. (From Luca *and al.* 2004)

The second model, which was inferred from X-ray crystallography of fragments NNFGAI (residues 21-26) and SSTNVG (residues 29-33), follows the structure of “steric zippers”. The monomers thus structured associate themselves as pairs, interacting one another by the residues side chains forming the protofilaments. Protofilaments then assemble on top of one another to form the amyloid fibril.<sup>30</sup> The two models are quite similar in the overall topology of the  $\beta$ -sheet but slightly differ in the packing of side chains between  $\beta$ -strands. A particularity of both structure models resides in the fact that the 20-29 segment, which is known to be the nucleation site of the peptide is not involved in the  $\beta$ -strand, showing that the bend may impact the amyloid formation (Figure 12).

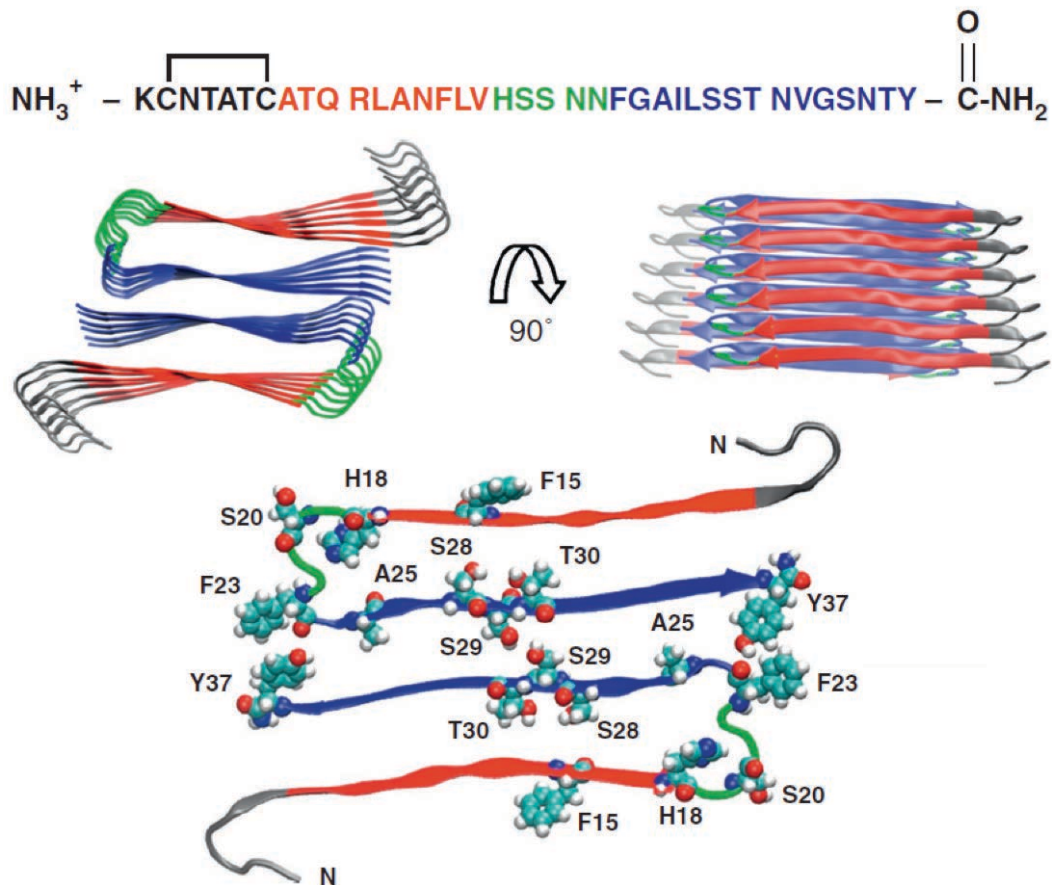


Figure 12: Structure of IAPP in fibrils.

IAPP monomers adopt a hairpin conformation separated by a short loop. Pairs of monomer interact with one another forming the building block of the fibrils. Building blocks then associate on top of another to form the fibrils. From Cao *and al.* 2012<sup>31</sup>

d) Key residues of hIAPP in the amyloidogenesis

It has been shown that the conservation of hIAPP sequence is essential for the fibrillization to occur. Many structural and fibrillization properties comparisons have been made between rat IAPP (rIAPP) and hIAPP. The particularity of rIAPP is that it only differs from hIAPP by 6 residues out of 37 but exhibits different properties, as it is non-amyloidogenic and non-toxic to  $\beta$  cells even at high concentration. This particularity has been linked to the presence of proline residues in the amyloidogenic region of the peptide (namely the 20-29 region). The substitution of serine residues in position 28 and 29 has shown to induce changes in the structuration of the peptide by promoting a  $\alpha$ -helix conformation over a  $\beta$ -sheet structure.<sup>32</sup>

Another particularity of rIAPP is the substitution of the histidine residue, present in the sequence of hIAPP by an arginine. Indeed, a study on rIAPP has been made by substituting Arg18, Leu23 and Val26 of the rIAPP sequence by His18, Phe23 and Ile26, residues present

in hIAPP. Results have shown that modified rIAPP was able to form fibrillar aggregates although it failed to form on of mature fibrils.<sup>33</sup>

These substitution studies have provided evidence that key residues in hIAPP that influence its structure and induce the mature fibril formation. The effect of substitution will be further discussed in chapter 4.

#### 4. Alzheimer's disease (AD) and formation of $\beta$ -Amyloid ( $A\beta$ ) peptide

Dementia is a category of brain diseases that affects about 35.6 million people in the world. The most common type of dementia is Alzheimer's disease, which makes up 70% of the cases (WHO, 2012). Associated with ageing, AD begins in people over 65 of age, but 4 or 5% of the patients are known to have declared an early form of the disease (early onset AD) before this age. Common symptoms for Alzheimer's disease are short-term memory loss, and, as the disease advances, impairment of the language, disorientation, and behavioral issues are observed. Ultimately, the bodily functions are lost, leading to death of the patient. Examinations of brain tissues of Alzheimer's disease patients have indicated the presence of senile plaques and neurofibrillary tangles that were therefore linked to the disease. The isolation of the amyloid fibrils has shown that they were composed of a 4 kDa subunit peptide, named amyloid- $\beta$  ( $A\beta$ ) peptide.

##### a) Formation of $\beta$ -Amyloid ( $A\beta$ ) peptide

$A\beta$  is generated by the proteolytic processing of the Amyloid Precursor Protein (APP), a single transmembrane protein that is expressed in neural and non-neural cells. This process involves a first cleavage of APP by the  $\beta$ -site cleaving enzyme (BACE), then, a second cleavage by  $\gamma$ -secretase occurs in the transmembrane domain of the protein and leads to the release of  $A\beta$  peptide and the APP intracellular domain (AICD). The  $\gamma$ -site of cleavage is variable and can occur after  $A\beta$  residues 38, 40 and 42 (figure 13). This site is of great influence on the oligomerization properties and pathogenicity as  $A\beta_{42}$ , being more hydrophobic than the two other forms of  $A\beta$ , is more likely to form fibrils *in vivo*.

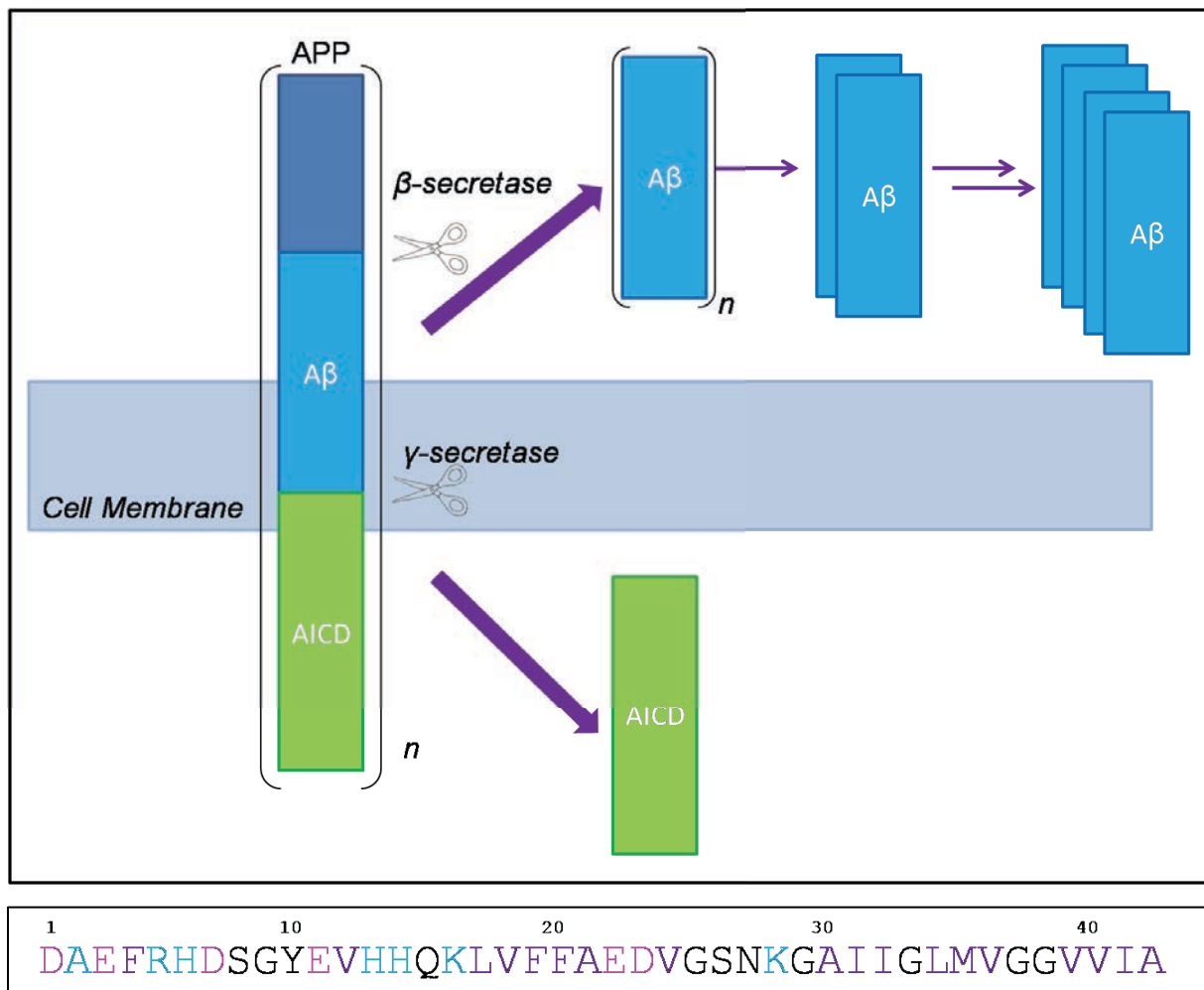


**Figure 13: (Top) Illustration of the proteolytic cleavage of APP by  $\beta$ - and  $\gamma$ -secretases. The cleavage results in the release of amyloidogenic  $A\beta_{40/42}$  depending on the  $\gamma$ -secretase cleavage site and AICD. (Bottom) Sequence of  $A\beta_{42}$ . Blue: basic amino acids, purple: hydrophobic amino acids, pink: acidic amino acids**

The increase in the level of  $A\beta_{40/42}$  in the organism, because of overexpression or reduced clearance, triggers the amyloid cascade leading to clinical Alzheimer's disease. The cascade is associated with the accumulation of  $A\beta_{40/42}$  as a result of the deregulation of the cleavage of APP. The peptide then aggregates, causing changes in the synaptic functions of the neurons. As oligomerization evolves to fibrillization, insoluble fibrils are formed, which trigger biochemical changes, inflammatory responses as well as neurotic injury. The last stages of the cascade are characterized by neuronal dysfunction, cell death, and extensive dementia.<sup>34,35</sup>

#### b) Factors to the development of AD

As the frequency of the disease increases, especially in the context of ageing of the population and the public costs involved for the treatment and caretaking of the patients,

Alzheimer’s disease constitutes a major health concern. In this light, it is critical to understand the pathologic mechanism of the disease, in order to develop further treatments for the patients. Genetic analysis suggested that many genes could contribute to the development of AD by increasing the overproduction of A $\beta$ , especially the cytotoxic A $\beta$  in the organism.<sup>36,37,38,39</sup>

*i. Mutation of APP gene*

Although AD is a neurodegenerative disease associated with late age, some genotypes have been reported to develop AD at an early onset (40-50 years old). (source: alz.org) Five mutations of the APP gene have been reported to cause early onset of AD. Biochemical studies of these APP mutations show that they influence the cleavage of APP, leading to the release of the longer form of A $\beta$ , therefore promoting the amyloidogenesis (table 2).

A $\beta$ “phenotype”	Mutation
Flemish	Ala21 to Gly21
Dutch	Glu22 to Gln22
Italian	Glu22 to Gly22
Iowa	Asp23 to Asn23
Tottori	Asp7 to Asn7

Table 2: Mutations of A $\beta$  peptide associated with early onset Alzheimer's disease

*ii. Presenilins*

A $\beta$  is released by the successive cleavage of APP by BACE and  $\gamma$ -secretase. In particular,  $\gamma$ -secretase is a complex that involves four different proteins, presenilin (PS1 and PS2), nicastrin, anterior pharynx defective 1 (Aph-1) and presenilin enhancer 2 (Pen-2) for the cleavage of APP in the transmembrane region.<sup>40</sup> Studies of the complex have shown that mutation of the genes PSEN1 and PSEN2 coding for the presenilin proteins PS1 and PS2 respectively were likely to promote the production of the pathological A $\beta$ 42 in the organism.<sup>41</sup>

### iii. ApolipoproteinE (APOE)

Apolipoprotein E (APOE4) is a 299 residue protein that is involved in the transport of the lipids in the lymph system and into the blood. The gene *APOE*, located on the chromosome 19 is polymorphic and possesses 3 different alleles: *APOE2*, *APOE3* and *APOE4* that differ by each other from one or two amino acids in position 112 and 158 (*ApoE2*: Cys112, Cys158, *ApoE3*: Cys112, Arg158, and *ApoE4*: Arg112, Arg158). Evidence has shown that the APOE4 variant is a genetic risk factor to late-onset Alzheimer's disease.<sup>42,43</sup>

Although it is still unclear how APOE4 participates in the development of AD, the protein was linked with the regulation of deposition of A $\beta$  in the brain either by promoting the amyloidogenesis and/or by having an influence on the clearance of the amyloid peptide by proteolytic cleavage. In particular, APOE4 variant was shown to be less effective in the removal of A $\beta$  than its other isoforms, which leads to high levels of amyloid peptides, thus promoting the fibrillization.<sup>44</sup>

#### c) Structure of A $\beta$ 42 in solution

##### i. A $\beta$ 42 fibrils

A $\beta$  fibrils adopt a cross- $\beta$  structure that consists of parallel  $\beta$ -sheets oriented perpendicular to the fibril axis. Structural analysis of the fibrils by solid state NMR has shown that fibrils are formed from A $\beta$ 42 units that adopt a hairpin conformation between residues 11 to 40 separated of a loop consisting of residues 23-28 (inner salt bridge between Asp23 and Lys28). A $\beta$ 42 peptide possesses two highly hydrophobic regions: from residues 16 to 21 (LVFFA) and from residues 30-36 (AIIGLMV) that adopt a highly ordered  $\beta$ -sheet conformation and interact with one another in an intra- and inter-molecular way to form the mature fibrils (figure 14).<sup>45,46</sup>



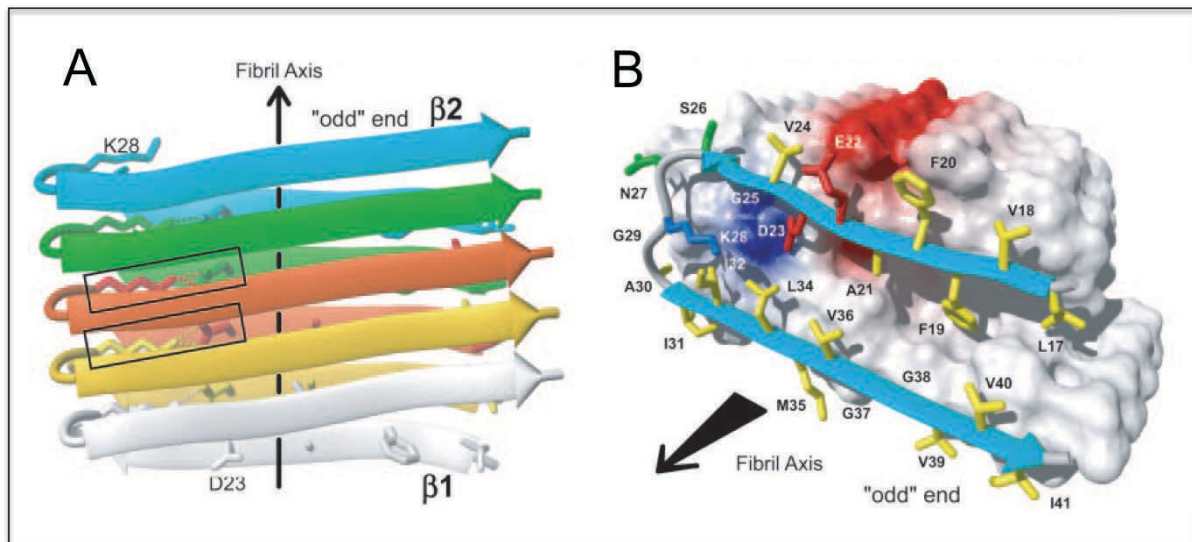


Figure 14: (A) Ribbon diagrams of the core structure of residues 17–42 illustrating the intermolecular nature of the inter- $\beta$ -strand interactions. Individual molecules are colored. The  $\beta$ -strands are indicated by arrows, nonregular secondary structure is indicated by spline curves, and side chains that constitute the core of the protofilament are shown. The intermolecular salt bridge between residues D23 and K28 is indicated by dotted lines, and the two salt bridges formed by the central  $A\beta(1-42)$  molecule are highlighted by rectangles. (B) van der Waals contact surface polarity and ribbon diagram of the  $A\beta(1-42)$  protofilament comprising residues 17–42. The  $\beta$ -sheets are indicated by cyan arrows, and nonregular secondary structure is indicated by gray spline curves. The hydrophobic, polar, negatively charged, and positively charged amino acid side chains are shown in yellow, green, red, and blue, respectively. Positively and negatively charged surface patches are shown in blue and red, respectively, and all others are shown in white. The direction of the fibril axis is indicated by an arrow pointing from even to odd. (adapted from Luhrs *et al* 2005<sup>28</sup>)

## ii. $A\beta$ intermediates

Less is known about the molecular structure of  $A\beta$  as a monomer or as oligomers, as those species are difficult to isolate and stabilize. However, studies have shown that  $A\beta$  could follow different pathways of oligomerization forming oligomers of multiple shape and size.

The fibrillar pathway involves the formation of  $A\beta$ -Derived Diffusible Ligands (ADDLs), forming globular oligomers that are mainly disordered and were shown to be highly neurotoxic.<sup>47</sup> As the aggregation occurs, the ligands then misfold and adopt an ordered parallel  $\beta$ -sheet conformation leading to the formation of protofibrils that further aggregate to form amyloid fibrils. Once formed, the amyloid fibrils can further elongate by addition of monomers or small oligomers, at the extremity of the fibril.

The oligomerization of  $A\beta$  can also lead to « off-pathway » species, which consist of oligomers that are stabilized and do not convert and elongate into fibrils. Among those species, are the annular shaped oligomers, that were mentioned in paragraph 2, and that create the pore-like structure affecting the integrity of the membrane, therefore contributing to the cell-death.<sup>48</sup> Studies have also shown the existence of low stable oligomers, with a globular shape. Those “globulomers” are composed of peptides in a  $\beta$ -sheet conformation, which



stabilizes the structure, but do not elongate into fibrils. Those oligomers were shown to bind to hippocampal neurons and are involved in memory loss, although their mechanism of interaction with the neurons is unknown (figure 15).<sup>49</sup>

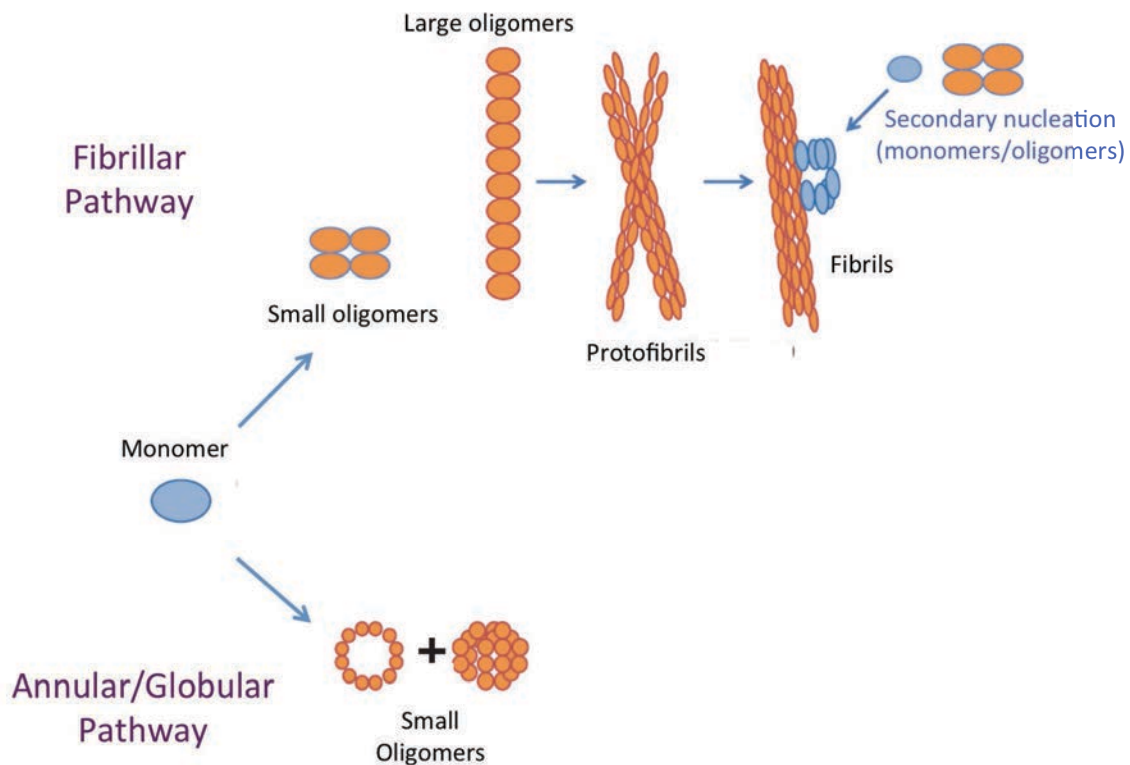


Figure 15: Model of Aβ42 assembly

**Fibrillar pathway** Monomers rapidly oligomerize into small then large unstructured oligomers. Large oligomers then convert to protofibrils involving a conformational rearrangement, during which unstructured aggregates transform into predominately β-sheet structures. Protofibrils then self-associate to form large mature fibrils. Direct addition of monomers or small oligomers (dotted arrows) to protofibrils or fibrils can contribute to the further elongation of the fibril.

**Oligomer pathway:** monomers aggregate into annular or globular species that do not evolve into protofibril or fibrils. Adapted from Taneja *and al.*<sup>50</sup>

Structural studies of the different aggregate intermediates have been hampered by their heterogeneity and instability. Recently Lendel et al. published the solid-state NMR structure of an hexameric aggregate forming a β-barrel.<sup>51</sup> This oligomer was stabilized by making an Aβ42 variant (Aβcc) where alanines were replaced by cysteines, therefore forming an engineered disulfide bond that locks the peptide in a conformation incompatible with fibril formation, stopping the aggregation in a stable protofibril state. The conformation of Aβcc was then observed by solid-state NMR spectroscopy. Results have shown that the regions 17-20 and 31-42 both adopted a β-strand conformation, which was separated by a region with a less defined structure. Observation of correlations between the side chains of

phenylalanine (Phe 19, Phe20) and isoleucines (Ile 31, Ile 32 or Ile 41) indicated that the peptides adopted a  $\beta$ -hairpin conformation.

Modelisation of the hexameric peptide, which forms the building block of the protofibrils showed a barrel structure composed of a hydrophobic core formed by the packing of the six constitutive monomers on one end and of the  $\beta$ -hairpin loops. The core involves all non-polar residues hydrophobic C-terminus and parts of the side chains in the central KLVFF motif.

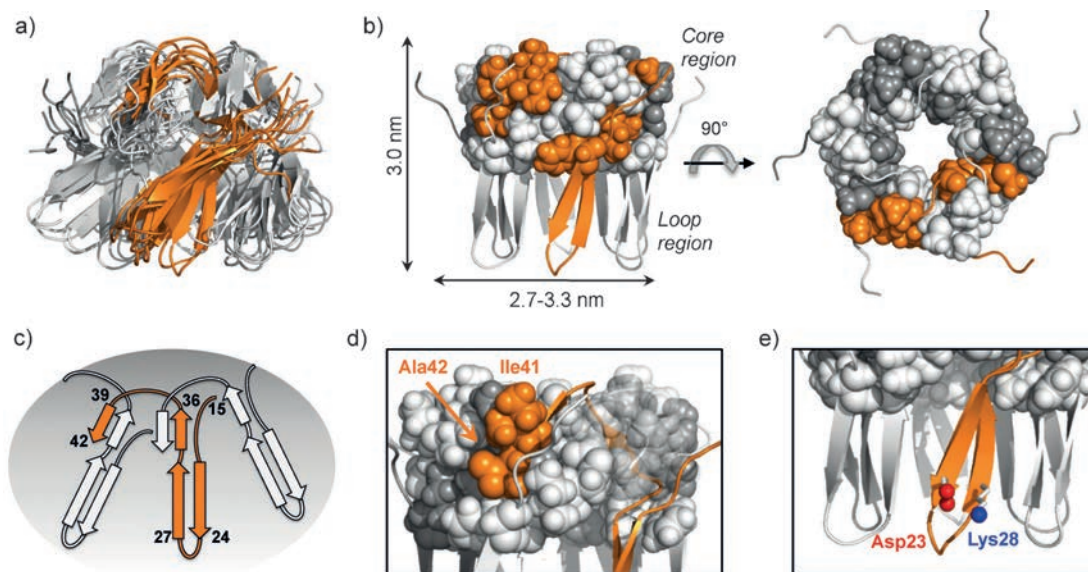


**Figure 16: Models of hexameric A $\beta$ 42cc building blocks of protofibrils.** a) Superposition of the ten models with the lowest Rosetta scores. b) Dimensions of the hexamer barrel with the loop and core regions indicated. Side chains of the hydrophobic core (those with the largest change in accessible surface area upon hexamer formation) are shown as spheres. The image to the right is rotated by 90° relative to the left image. c) Simplified representation of the hexamer topology. The numbers refer to the residue positions in the orange protomer. d) The backbone and side chains of the C-terminal residues Ile41 and Ala42 (orange spheres) are packed into the hydrophobic core of the hexamer. e) Asp23-Lys28 salt bridge. From Lendel et al.<sup>54</sup>

## 5. Interactions between amyloid peptides and the cell membrane

As shown in paragraph 2, the cytotoxicity of amyloid peptides is correlated with their interaction with the cell membranes as the fibrillization is known to disrupt the membrane integrity. However it was also shown that the structural perturbation between the membrane and the peptide is mutual. Indeed, the presence of a biological interface promotes the conversion of non-pathological protein/peptides into an amyloidogenic entity, therefore promoting their association.<sup>17</sup>

a) Influence of the cell membrane on the oligomerization

The cell membrane is a selective, semi-permeable barrier, dividing the intracellular and extracellular media, thus protecting the inside of the cell and ensuring the transportation of proteins, substrates, water, ions and other metabolites. The major components of the eukaryotic cell membranes are phospholipids and proteins. Phospholipids are amphipathic molecules that consist of two hydrophobic fatty acid chains (« tails ») of a hydrophilic phosphate group (« head »). The composition of plasma membrane can vary, depending on the cell, with hydrophobic chains of various length ( $C_{16}$  to  $C_{22}$ ) and insaturation (0 to 6), and phosphoester head groups of different charge and nature (figure 17). Mammalian plasma membranes contain four major phospholipids, that constitute approximately 60% of the cell membrane lipids: phosphatidylcholine (PC), phosphatidylserine (PS), phosphatidylethanolamine (PE), and sphingomyelin. In addition to the 60% of phospholipids, the plasma membrane also contains glycolipids and cholesterol, which constitute the remaining 40% of lipids.<sup>52,53</sup>

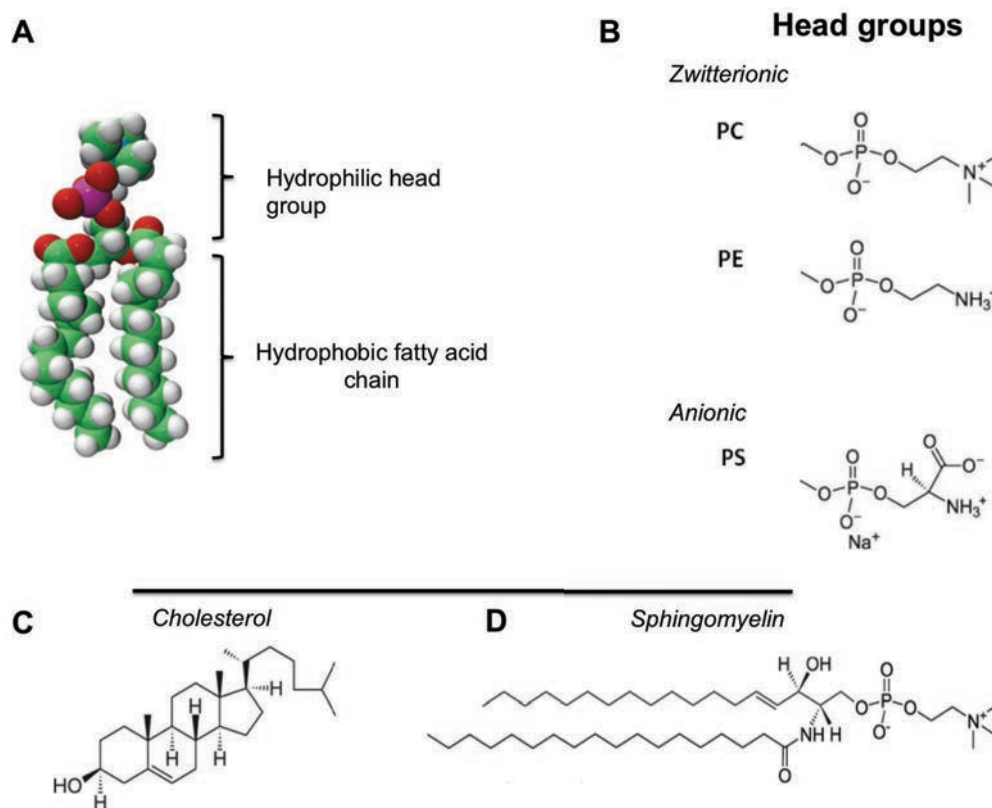
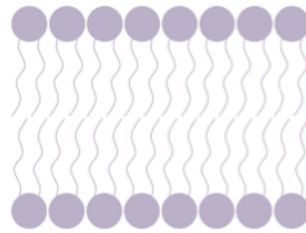


Figure 17: A) Schematic representation of a phospholipid, Chemical structures of phospho head groups (B), cholesterol (C), and sphingomyelin (D)

Since the hydrophobic tails are poorly soluble in water, phospholipids spontaneously assemble in a bilayer in aqueous solution, with fatty acid chains oriented to the inside of the bilayer and phosphate groups on both side, exposed to the solution (figure 18).



**Figure 18: Schematic representation of a lipid bilayer**

Thus formed, the lipid bilayer is a critical target for amyloid peptides as monomers or oligomers. Indeed, amyloid proteins/peptides are amphipathic and therefore are likely to associate to the cell surface, the hydrophobic regions of the peptides/proteins interacting with the buried acyl chains of the bilayer and charged side chains binding electrostatically to the headgroups. Those interactions, driven by the membrane composition, lead to a significant increase of protein or peptide concentration locally, accelerating the oligomerization process. Additionally, the membrane surface was also shown to facilitate the structuration and therefore misfolding of amyloid peptides, therefore providing a significant aggregation matrix, promoting the fibrillization.

Many factors can affect the binding capacity of the peptides on the membrane. One of the primary factors is the lipid composition of the membrane. The presence of anionic lipids and therefore a negative net charge triggers higher binding of the peptide monomers or low molecular weight oligomers to the membrane surface, especially for cationic peptides such as hIAPP but a similar effect has been observed for A $\beta$ . The introduction of lipids with an anionic headgroup such as PS was therefore shown to enhance the kinetics of fibrillization of the peptides.<sup>54</sup> The cell membrane is also composed of glycolipids and cholesterol that could form rigid microdomains known as lipid rafts. These clusters also contribute to the enhanced binding of amyloid peptides to the membrane and fibrillization.<sup>55</sup>

#### b) Structure of membrane bound amyloid peptides

In the presence of a membrane, amyloid peptides follow a different pathway to oligomerization than in solution. Indeed, the interaction of the peptides with a membrane surface can affect the structural ordering of the peptide, promoting the formation of a secondary structure. Upon binding to the membrane surface, the peptides tend to

self-associate, increasing the local concentration of peptides. This molecular crowding was shown to facilitate the transition to a  $\beta$ -sheet conformation thus promoting the fibrillization.<sup>56</sup> Studies have shown that, depending on the peptide to lipid ratio, several amyloid peptides (A $\beta$ , IAPP,  $\alpha$ -synuclein) adopted an  $\alpha$ -helical structure when adsorbed to a membrane.<sup>57</sup> Although the  $\alpha$ -helical structure is detrimental to the fibrillization, the binding to the membrane allows the stabilization of the peptides, at a high local concentration, promoting the interaction between the amyloidogenic regions of the peptides and subsequent switch to  $\beta$ -sheet conformation prone to oligomerization.<sup>58,59</sup>

### c) Membrane models

As cell membranes constitute a complex system, given the diversity of its constitution and the presence of many proteins on its surface, we simplified the system by using membrane models for our studies of amyloid peptides. The simplified model allowed us to control the composition of the lipid bilayer and determine the most relevant factors depending on the studied peptide. Thus, the use of a membrane model gives an insight on the interactions between the lipid bilayer and the peptides in order to formulate mechanistic models hypothesis that can further be developed on more complex models.

During my thesis and depending on the technique that was used, the chosen membrane models were either small (50 nm) or large (200 nm) unilamellar vesicles (SUV/LUV) or lipid monolayers.

Unilamellar vesicles (or liposomes) were made out of the hydration of a lipidic film followed by a freeze/thaw and extrusion process (see Chapter 2). The vesicles are spherically shaped, with a single lipid bilayer that separates the outside and inside aqueous media (figure 20). Unilamellar vesicles represent a relevant model for biological membranes and allow the observation of interactions with the amyloid peptides and effect of a lipid bilayer on oligomerization and fibrillization. In particular, the separation between inside and outside aqueous solution allows the observation of membrane permeabilization process by encapsulation of fluorescent dyes inside the vesicle (as calcein leakage experiment showed in chapter 2). Other than the lipid composition, the sizes of the liposomes can be controlled during the extrusion process, which allows the formation of homogeneous solutions and adaptability to the biophysical techniques that is used. Indeed, if fluorescence or dichroism experiments can be carried out in presence of large unilamellar vesicles they are not suitable for NMR experiments as the signal of the peptide or vesicles would be broadened beyond

detection. Therefore, NMR experiments required the use of small unilamellar vesicles that allowed the observation of the signals of amyloid peptides.

Lipid monolayer, which is a model that consists in the mimic of the outer leaflet of the membrane, is formed by addition of the lipids onto an aqueous solution. At the contact with the buffer, the lipids, dissolved in an organic solvent, will orient themselves at the water/air interphase with the head groups in contact with the solution and hydrophobic tails exposed to air (figure 19). The measurement of the surface pressure of the monolayer gives an indication of the lipid packing that can be disturbed upon addition of a peptide that would insert between the head groups.

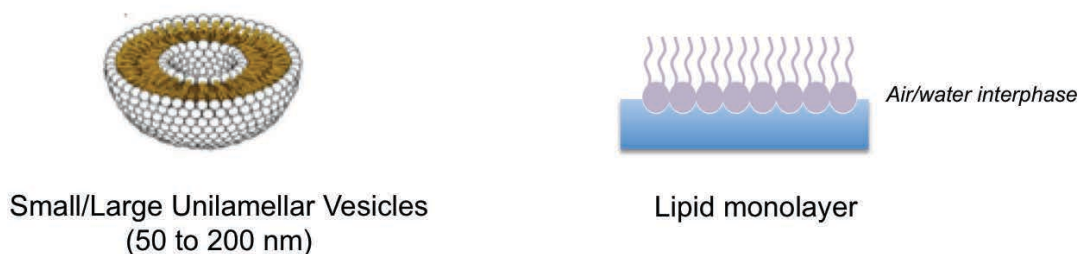


Figure 19: Schematic representation of small and large unilamellar vesicles (left) and lipid monolayer (right)

## 6. Interaction with inhibitors

Given their affinity to the cell membranes and their involvement in cell death, amyloid intermediates have become the main targets for the investigation and development of therapeutic compounds. Synthetic compounds developed as inhibitors were developed along different strategies. One of the strategies target the oligomers and aim to stabilize the monomeric precursors, disrupt the structural integrity of the toxic oligomers or redirect the formation of oligomers to a less toxic pathway. A second strategy is to enhance the formation of non-toxic fibrils, in order to reduce the lifetime of toxic oligomers. Different inhibitors were designed to interact with the amyloid peptides. They consist in small peptides or peptidomimetics that mimic the nucleation site of the amyloid peptides. As they interact with the peptides, these molecules either promote fibrillation or disturb the regular interstrand hydrogen bonds of the fibrils by the introduction of specific moieties and  $\beta$ -sheet blockers.<sup>60,61,62</sup>

In parallel with the development of synthetic compounds, investigation of natural based inhibitors was also carried out, in particular numerous polyphenols such as curcumin<sup>63</sup>, resveratrol<sup>64</sup>,  $\epsilon$ -Viniferin glucoside (EVG)<sup>65</sup> and (-)-epigallocatechin gallate (EGCG). EGCG,

which is extracted from green tea, was showed to redirect the pathway of oligomerization to less or non-toxic aggregates and to have a protective activity on cells against amyloid disorders.<sup>66,67</sup>

The development and effects of inhibiting compounds will be further discussed in chapter 5.

## 7. Objectives of the thesis

The objective of this thesis was to get an insight into the oligomerization and fibrillization of two amyloid peptides, A $\beta$  and hIAPP, and see how it could be modulated by the mutation of a residue, the pH or the addition of potential inhibitors.

The first part of my project fits in the hypothesis of “toxic oligomers”. As it was identified that soluble oligomers were more pathogenic than the fibrils during the fibrillization, my work focused on the early stages of oligomerization. The study mostly focused on hIAPP, as the peptide does not seem to form small oligomers but rather large aggregates following a mechanism that remains unclear. For this study we used different biophysical techniques such as fluorescence assay, circular dichroism, microscopy and nuclear magnetic resonance spectroscopy, which allowed us to observe different stages of aggregation and interaction between species in solution. This work will be exposed in chapter 3.

The second part of my thesis focused on the effect of pH and substitution of residue 18 of hIAPP. Indeed, residue 18, a histidine was suggested to play a key role in the fibrillization process of hIAPP as its state of protonation varies within the physiological pH range and, and its position is critical for the elongation of the fibrils. For this project, lead at pH 5.5 to pH 7.4, I investigated the oligomerization of four hIAPP mutants, in which His18 was substituted by Lys, Arg, Glu or Ala. This work will be shown in chapter 4.

As oligomeric species represent an interesting target for the development of therapeutic compounds, the last part of my project focused on the interaction of amyloid peptides with potential inhibitors. Different compounds and their respective influence on the kinetics of fibrillization of the peptides were studied: sugar-based or fluor-containing inhibitors, and epigallocatechin gallate (EGCG). This will be the subject of chapter 5.



- 
- <sup>1</sup> Rather, L. J., and Rudolf Ludwig Karl Virchow. *A Commentary on the Medical Writings of Rudolf Virchow: Based on Schwalbe's Virchow-Bibliographie, 1843-1901*. Norman Publishing, 1990. *on Schwalbe's Virchow-Bibliographie, 1843-1901*. Norman Publishing, 1990.
- <sup>2</sup> Sipe, Jean D., and Alan S. Cohen. "Review: History of the Amyloid Fibril." *Journal of Structural Biology* 130, no. 2–3 (June 2000): 88–98. doi:10.1006/jsbi.2000.4221.
- <sup>3</sup> Buxbaum, Joel N., and Reinhold P. Linke. "A Molecular History of the Amyloidoses." *Journal of Molecular Biology* 421, no. 2–3 (August 2012): 142–59. doi:10.1016/j.jmb.2012.01.024.
- <sup>4</sup> Knowles, Tuomas P. J., Michele Vendruscolo, and Christopher M. Dobson. "The Amyloid State and Its Association with Protein Misfolding Diseases." *Nature Reviews Molecular Cell Biology* 15, no. 6 (June 2014): 384–96. doi:10.1038/nrm3810.
- <sup>5</sup> Wilson, Mark R., Justin J. Yerbury, and Stephen Poon. "Potential Roles of Abundant Extracellular Chaperones in the Control of Amyloid Formation and Toxicity." *Molecular BioSystems* 4, no. 1 (December 13, 2007): 42–52. doi:10.1039/B712728F.
- <sup>6</sup> Petkova, Aneta T., Yoshitaka Ishii, John J. Balbach, Oleg N. Antzutkin, Richard D. Leapman, Frank Delaglio, and Robert Tycko. "A Structural Model for Alzheimer's  $\beta$ -Amyloid Fibrils Based on Experimental Constraints from Solid State NMR." *Proceedings of the National Academy of Sciences of the United States of America* 99, no. 26 (December 24, 2002): 16742–47. doi:10.1073/pnas.262663499.
- <sup>7</sup> Fändrich, Marcus. "Oligomeric Intermediates in Amyloid Formation: Structure Determination and Mechanisms of Toxicity." *Journal of Molecular Biology* 421, no. 4–5 (August 2012): 427–40. doi:10.1016/j.jmb.2012.01.006.
- <sup>8</sup> Kaye, Rakez, Yuri Sokolov, Brian Edmonds, Theresa M. McIntire, Saskia C. Milton, James E. Hall, and Charles G. Glabe. "Permeabilization of Lipid Bilayers Is a Common Conformation-Dependent Activity of Soluble Amyloid Oligomers in Protein Misfolding Diseases." *Journal of Biological Chemistry* 279, no. 45 (November 5, 2004): 46363–66. doi:10.1074/jbc.C400260200.
- <sup>9</sup> Arispe, N, E Rojas, and H B Pollard. "Alzheimer Disease Amyloid Beta Protein Forms Calcium Channels in Bilayer Membranes: Blockade by Tromethamine and Aluminum." *Proceedings of the National Academy of Sciences of the United States of America* 90, no. 2 (January 15, 1993): 567–71.
- <sup>10</sup> Shirwany, Najeeb A, Daniel Payette, Jun Xie, and Qing Guo. "The Amyloid Beta Ion Channel Hypothesis of Alzheimer's Disease." *Neuropsychiatric Disease and Treatment* 3, no. 5 (October 2007): 597–612.
- <sup>11</sup> Mirzabekov, Tajib A., Meng-chin Lin, and Bruce L. Kagan. "Pore Formation by the Cytotoxic Islet Amyloid Peptide Amylin." *Journal of Biological Chemistry* 271, no. 4 (January 26, 1996): 1988–92. doi:10.1074/jbc.271.4.1988.
- <sup>12</sup> Quist, Arjan, Ivo Doudevski, Hai Lin, Rushana Azimova, Douglas Ng, Blas Frangione, Bruce Kagan, Jorge Ghiso, and Ratnesh Lal. "Amyloid Ion Channels: A Common Structural Link for Protein-Misfolding Disease." *Proceedings of the National Academy of Sciences of the United States of America* 102, no. 30 (July 26, 2005): 10427–32. doi:10.1073/pnas.0502066102.



- 
- <sup>13</sup> Last, N. B., and A. D. Miranker. "Common Mechanism Unites Membrane Poration by Amyloid and Antimicrobial Peptides." *Proceedings of the National Academy of Sciences* 110, no. 16 (April 16, 2013): 6382–87. doi:10.1073/pnas.1219059110.
- <sup>14</sup> Hacker, Miles, William S. Messer II, and Kenneth A. Bachmann. *Pharmacology: Principles and Practice*. Academic Press, 2009.
- <sup>15</sup> Yang, L, T A Harroun, T M Weiss, L Ding, and H W Huang. "Barrel-Stave Model or Toroidal Model? A Case Study on Melittin Pores." *Biophysical Journal* 81, no. 3 (September 2001): 1475–85.
- <sup>16</sup> Bechinger, Burkhard, and Karl Lohner. "Detergent-like Actions of Linear Amphipathic Cationic Antimicrobial Peptides." *Biochimica et Biophysica Acta (BBA) - Biomembranes, Membrane Biophysics of Antimicrobial Peptides*, 1758, no. 9 (September 2006): 1529–39. doi:10.1016/j.bbamem.2006.07.001.
- <sup>17</sup> Butterfield, Sara M., and Hilal A. Lashuel. "Amyloidogenic Protein-Membrane Interactions: Mechanistic Insight from Model Systems." *Angewandte Chemie International Edition* 49, no. 33 (July 12, 2010): 5628–54. doi:10.1002/anie.200906670.
- <sup>18</sup> Engel, Maarten F. M., Lucie Khemtémourian, Cécile C. Kleijer, Hans J. D. Meeldijk, Jet Jacobs, Arie J. Verkleij, Ben de Kruijff, J. Antoinette Killian, and Jo W. M. Höppener. "Membrane Damage by Human Islet Amyloid Polypeptide through Fibril Growth at the Membrane." *Proceedings of the National Academy of Sciences of the United States of America* 105, no. 16 (April 22, 2008): 6033–38. doi:10.1073/pnas.0708354105.
- <sup>19</sup> Sparr, Emma, Maarten F.M. Engel, Dmitri V. Sakharov, Mariette Sprong, Jet Jacobs, Ben de Kruijff, Jo W.M. Höppener, and J. Antoinette Killian. "Islet Amyloid Polypeptide-Induced Membrane Leakage Involves Uptake of Lipids by Forming Amyloid Fibers." *FEBS Letters* 577, no. 1–2 (November 2004): 117–20. doi:10.1016/j.febslet.2004.09.075.
- <sup>20</sup> Cooper, G J, A C Willis, A Clark, R C Turner, R B Sim, and K B Reid. "Purification and Characterization of a Peptide from Amyloid-Rich Pancreases of Type 2 Diabetic Patients." *Proceedings of the National Academy of Sciences of the United States of America* 84, no. 23 (December 1987): 8628–32.
- <sup>21</sup> Lorenzo, A, and B A Yankner. "Beta-Amyloid Neurotoxicity Requires Fibril Formation and Is Inhibited by Congo Red." *Proceedings of the National Academy of Sciences of the United States of America* 91, no. 25 (December 6, 1994): 12243–47.
- <sup>22</sup> Höppener, Jo W. M., and Cees J. M. Lips. "Role of Islet Amyloid in Type 2 Diabetes Mellitus." *The International Journal of Biochemistry & Cell Biology, Diabetes: New Research and Novel Therapies*, 38, no. 5–6 (May 2006): 726–36. doi:10.1016/j.biocel.2005.12.009.
- <sup>23</sup> Lukinius, A., E. Wilander, G. T. Westermark, U. Engström, and P. Westermark. "Co-Localization of Islet Amyloid Polypeptide and Insulin in the B Cell Secretory Granules of the Human Pancreatic Islets." *Diabetologia* 32, no. 4 (1989): 240–44.
- <sup>24</sup> Sanke, T., G. I. Bell, C. Sample, A. H. Rubenstein, and D. F. Steiner. "An Islet Amyloid Peptide Is Derived from an 89-Amino Acid Precursor by Proteolytic Processing." *Journal of Biological Chemistry* 263, no. 33 (November 25, 1988): 17243–46.

- 
- <sup>25</sup> Mosselman, S., J. W. M. Höppener, C. J. M. Lips, and H. S. Jansz. "The Complete Islet Amyloid Polypeptide Precursor Is Encoded by Two Exons." *FEBS Letters* 247, no. 1 (April 10, 1989): 154–58. doi:10.1016/0014-5793(89)81260-8.
- <sup>26</sup> Westermark, Per, Ulla Engström, Kenneth H. Johnson, Gunilla T. Westermark, and Christer Betsholtz. "Islet Amyloid Polypeptide: Pinpointing Amino Acid Residues Linked to Amyloid Fibril Formation." *Proceedings of the National Academy of Sciences* 87, no. 13 (1990): 5036–40.
- <sup>27</sup> Gupta, Dhananjay, and Jack L. Leahy. "Islet Amyloid and Type 2 Diabetes: Overproduction or Inadequate Clearance and Detoxification?" *The Journal of Clinical Investigation* 124, no. 8 (August 1, 2014): 3292–94. doi:10.1172/JCI77506.
- <sup>28</sup> Kahn, Steven E., Mark E. Cooper, and Stefano Del Prato. "PATHOPHYSIOLOGY AND TREATMENT OF TYPE 2 DIABETES: PERSPECTIVES ON THE PAST, PRESENT AND FUTURE." *Lancet* 383, no. 9922 (March 22, 2014): 1068–83. doi:10.1016/S0140-6736(13)62154-6.
- <sup>29</sup> Luca, Sorin, Wai-Ming Yau, Richard Leapman, and Robert Tycko. "Peptide Conformation and Supramolecular Organization in Amylin Fibrils: Constraints from Solid State NMR." *Biochemistry* 46, no. 47 (November 27, 2007): 13505–22. doi:10.1021/bi701427q.
- <sup>30</sup> Wiltzius, Jed J.W., Stuart A. Sievers, Michael R. Sawaya, Duilio Cascio, Dmitriy Popov, Christian Riek, and David Eisenberg. "Atomic Structure of the Cross-B Spine of Islet Amyloid Polypeptide (amylin)." *Protein Science* 17, no. 9 (September 2008): 1467–74. doi:10.1110/ps.036509.108.
- <sup>31</sup> Cao, Ping, Andisheh Abedini, and Daniel P Raleigh. "Aggregation of Islet Amyloid Polypeptide: From Physical Chemistry to Cell Biology." *Current Opinion in Structural Biology* 23, no. 1 (February 2013): 82–89. doi:10.1016/j.sbi.2012.11.003.
- <sup>32</sup> Dupuis, Nicholas F., Chun Wu, Joan-Emma Shea, and Michael T. Bowers. "Human Islet Amyloid Polypeptide Monomers Form Ordered B-Hairpins: A Possible Direct Amyloidogenic Precursor." *Journal of the American Chemical Society* 131, no. 51 (December 30, 2009): 18283–92. doi:10.1021/ja903814q.
- <sup>33</sup> Green, Janelle, Claire Goldsbury, Thierry Mini, Shabir Sunderji, Peter Frey, Joerg Kistler, Garth Cooper, and Ueli Aebi. "Full-Length Rat Amylin Forms Fibrils Following Substitution of Single Residues from Human Amylin." *Journal of Molecular Biology* 326, no. 4 (February 2003): 1147–56. doi:10.1016/S0022-2836(02)01377-3.
- <sup>34</sup> Selkoe, Dennis J. "The Molecular Pathology of Alzheimer's Disease." *Neuron* 6, no. 4 (January 4, 1991): 487–98. doi:10.1016/0896-6273(91)90052-2.
- <sup>35</sup> Haass, Christian, and Dennis J. Selkoe. "Soluble Protein Oligomers in Neurodegeneration: Lessons from the Alzheimer's Amyloid B-Peptide." *Nature Reviews Molecular Cell Biology* 8, no. 2 (February 2007): 101–12. doi:10.1038/nrm2101.
- <sup>36</sup> Mattson, Mark P. "Pathways towards and Away from Alzheimer's Disease." *Nature* 430, no. 7000 (August 5, 2004): 631–39. doi:10.1038/nature02621.
- <sup>37</sup> Ballard, Clive, Serge Gauthier, Anne Corbett, Carol Brayne, Dag Aarsland, and Emma Jones. "Alzheimer's Disease." *The Lancet* 377, no. 9770 (March 25, 2011): 1019–31. doi:10.1016/S0140-6736(10)61349-9.

- 
- <sup>38</sup> Hardy, John. "Amyloid, the Presenilins and Alzheimer's Disease." *Trends in Neurosciences* 20, no. 4 (1997): 154–59.
- <sup>39</sup> Hardy, John. "Has the Amyloid Cascade Hypothesis for Alzheimer's Disease Been Proved?" *Current Alzheimer Research* 3, no. 1 (2006): 71–73.
- <sup>40</sup> Zhang, Xian, Yanfang Li, Huaxi Xu, and Yun-wu Zhang. "The  $\Gamma$ -Secretase Complex: From Structure to Function." *Frontiers in Cellular Neuroscience* 8 (December 11, 2014). doi:10.3389/fncel.2014.00427.
- <sup>41</sup> Scheuner, D., C. Eckman, M. Jensen, X. Song, M. Citron, N. Suzuki, T. D. Bird, et al. "Secreted Amyloid  $\beta$ -protein Similar to That in the Senile Plaques of Alzheimer's Disease Is Increased in Vivo by the Presenilin 1 and 2 and APP Mutations Linked to Familial Alzheimer's Disease." *Nature Medicine* 2, no. 8 (August 1996): 864–70. doi:10.1038/nm0896-864.
- <sup>42</sup> Strittmatter, W J, A M Saunders, D Schmechel, M Pericak-Vance, J Enghild, G S Salvesen, and A D Roses. "Apolipoprotein E: High-Avidity Binding to Beta-Amyloid and Increased Frequency of Type 4 Allele in Late-Onset Familial Alzheimer Disease." *Proceedings of the National Academy of Sciences of the United States of America* 90, no. 5 (March 1, 1993): 1977–81.
- <sup>43</sup> Roses, Allen D. "The Alzheimer Diseases." *Current Opinion in Neurobiology* 6, no. 5 (October 1996): 644–50. doi:10.1016/S0959-4388(96)80098-5.
- <sup>44</sup> Jiang, Qingguang, C.Y. Daniel Lee, Shweta Mandrekar, Brandy Wilkinson, Paige Cramer, Noam Zelcer, Karen Mann, et al. "ApoE Promotes the Proteolytic Degradation of A $\beta$ ." *Neuron* 58, no. 5 (June 12, 2008): 681–93. doi:10.1016/j.neuron.2008.04.010.
- <sup>45</sup> Petkova, A.T., G. Buntkowsky, F. Dyda, R.D. Leapman, W.-M. Yau, and R. Tycko. "Solid State NMR Reveals a pH-Dependent Antiparallel B-Sheet Registry in Fibrils Formed by a B-Amyloid Peptide." *Journal of Molecular Biology* 335, no. 1 (January 2004): 247–60. doi:10.1016/j.jmb.2003.10.044.
- <sup>46</sup> Lührs, Thorsten, Christiane Ritter, Marc Adrian, Dominique Riek-Loher, Bernd Bohrmann, Heinz Döbeli, David Schubert, and Roland Riek. "3D Structure of Alzheimer's Amyloid- $\beta$ (1–42) Fibrils." *Proceedings of the National Academy of Sciences of the United States of America* 102, no. 48 (November 29, 2005): 17342–47. doi:10.1073/pnas.0506723102.
- <sup>47</sup> Lambert, M. P., A. K. Barlow, B. A. Chromy, C. Edwards, R. Freed, M. Liosatos, T. E. Morgan, et al. "Diffusible, Nonfibrillar Ligands Derived from A $\beta$ 1–42 Are Potent Central Nervous System Neurotoxins." *Proceedings of the National Academy of Sciences of the United States of America* 95, no. 11 (May 26, 1998): 6448–53.
- <sup>48</sup> Lasagna-Reeves, Cristian A., Charles G. Glabe, and Rakez Kaye. "Amyloid- $\beta$  Annular Protofibrils Evade Fibrillar Fate in Alzheimer Disease Brain." *The Journal of Biological Chemistry* 286, no. 25 (June 24, 2011): 22122–30. doi:10.1074/jbc.M111.236257.
- <sup>49</sup> Barghorn, Stefan, Volker Nimmrich, Andreas Striebinger, Carsten Krantz, Patrick Keller, Bodo Janson, Michael Bahr, et al. "Globular Amyloid Beta-peptide1-42 Oligomer - a Homogenous and Stable Neuropathological Protein in Alzheimer's Disease." *Journal of Neurochemistry* 95, no. 3 (November 2005): 834–47. doi:10.1111/j.1471-4159.2005.03407.x.

- 
- <sup>50</sup> Taneja, Vibha, Meenakshi Verma, and Abhishek Vats. "Toxic Species in Amyloid Disorders: Oligomers or Mature Fibrils." *Annals of Indian Academy of Neurology* 18, no. 2 (2015): 138. doi:10.4103/0972-2327.144284.
- <sup>51</sup> Lendel, Christofer, Morten Bjerring, Anatoly Dubnovitsky, Robert T. Kelly, Andrei Filippov, Oleg N. Antzutkin, Niels Chr. Nielsen, and Torleif Härd. "A Hexameric Peptide Barrel as Building Block of Amyloid- $\beta$  Protofibrils." *Angewandte Chemie International Edition* 53, no. 47 (November 17, 2014): 12756–60. doi:10.1002/anie.201406357.
- <sup>52</sup> Cooper, G M. *The Cell, 2nd Edition. A Molecular Approach*. Sinauer Associates, Inc., 2000.
- <sup>53</sup> Vance, Dennis E., and J. E. Vance. *Biochemistry of Lipids, Lipoproteins and Membranes*. Elsevier, 1996.
- <sup>54</sup> Jayasinghe, Sajith A., and Ralf Langen. "Membrane Interaction of Islet Amyloid Polypeptide." *Biochimica et Biophysica Acta (BBA) - Biomembranes* 1768, no. 8 (August 2007): 2002–9. doi:10.1016/j.bbamem.2007.01.022.
- <sup>55</sup> Fukunaga, Saori, Hiroshi Ueno, Takahiro Yamaguchi, Yoshiaki Yano, Masaru Hoshino, and Katsumi Matsuzaki. "GM1 Cluster Mediates Formation of Toxic A $\beta$  Fibrils by Providing Hydrophobic Environments." *Biochemistry* 51, no. 41 (October 16, 2012): 8125–31. doi:10.1021/bi300839u.
- <sup>56</sup> Bokvist, Marcus, and Gerhard Gröbner. "Misfolding of Amyloidogenic Proteins at Membrane Surfaces: The Impact of Macromolecular Crowding." *Journal of the American Chemical Society* 129, no. 48 (December 1, 2007): 14848–49. doi:10.1021/ja076059o.
- <sup>57</sup> Wong, Pamela T., Joseph A. Schauerte, Kathleen C. Wisser, Hao Ding, Edgar L. Lee, Duncan G. Steel, and Ari Gafni. "Amyloid- $\beta$  Membrane Binding and Permeabilization Are Distinct Processes Influenced Separately by Membrane Charge and Fluidity." *Journal of Molecular Biology* 386, no. 1 (February 13, 2009): 81–96. doi:10.1016/j.jmb.2008.11.060.
- <sup>58</sup> Abedini, Andisheh, and Daniel P. Raleigh. "A Role For Helical Intermediates in Amyloid Formation By Natively Unfolded Polypeptides?" *Physical Biology* 6, no. 1 (February 10, 2009): 015005. doi:10.1088/1478-3975/6/1/015005.
- <sup>59</sup> Knight, Jefferson D., James A. Hebda, and Andrew D. Miranker. "Conserved and Cooperative Assembly of Membrane-Bound  $\alpha$ -Helical States of Islet Amyloid Polypeptide <sup>†</sup>." *Biochemistry* 45, no. 31 (August 2006): 9496–9508. doi:10.1021/bi060579z.
- <sup>60</sup> Takahashi, Tsuyoshi, and Hisakazu Mihara. "Peptide and Protein Mimetics Inhibiting Amyloid  $\beta$ -Peptide Aggregation." *Accounts of Chemical Research* 41, no. 10 (October 21, 2008): 1309–18. doi:10.1021/ar8000475.
- <sup>61</sup> Dorgeret, Bertrand, Lucie Khemtémourian, Isabelle Correia, Jean-Louis Soulier, Olivier Lequin, and Sandrine Onger. "Sugar-Based Peptidomimetics Inhibit Amyloid  $\beta$ -Peptide Aggregation." *European Journal of Medicinal Chemistry* 46, no. 12 (December 2011): 5959–69. doi:10.1016/j.ejmech.2011.10.008.
- <sup>62</sup> Soto, Claudio, Einar M. Sigurdsson, Laura Morelli, R. Asok Kumar, Eduardo M. Castaño, and Blas Frangione. " $\beta$ -Sheet Breaker Peptides Inhibit Fibrillogenesis in a Rat Brain Model of Amyloidosis: Implications for Alzheimer's Therapy." *Nature Medicine* 4, no. 7 (July 1998): 822–26. doi:10.1038/nm0798-822.
- <sup>63</sup> Yang, Fusheng, Giselle P. Lim, Aynun N. Begum, Oliver J. Ubeda, Mychica R. Simmons, Surendra S. Ambegaokar, Pingping P. Chen, et al. "Curcumin Inhibits Formation of Amyloid  $\beta$  Oligomers and Fibrils, Binds

---

Plaques, and Reduces Amyloid in Vivo.” *Journal of Biological Chemistry* 280, no. 7 (February 18, 2005): 5892–5901. doi:10.1074/jbc.M404751200.

- <sup>64</sup> Sun, Albert Y., Qun Wang, Agnes Simonyi, and Grace Y. Sun. “Resveratrol as a Therapeutic Agent for Neurodegenerative Diseases.” *Molecular Neurobiology* 41, no. 2–3 (June 2010): 375–83. doi:10.1007/s12035-010-8111-y.
- <sup>65</sup> Richard, Tristan, Pascal Poupard, Merian Nassra, Yorgos Papastamoulis, Marie-Laure Iglésias, Stéphanie Krisa, Pierre Waffo-Teguo, Jean-Michel Méryllon, and Jean-Pierre Monti. “Protective Effect of  $\epsilon$ -Viniferin on  $\beta$ -Amyloid Peptide Aggregation Investigated by Electrospray Ionization Mass Spectrometry.” *Bioorganic & Medicinal Chemistry* 19, no. 10 (May 2011): 3152–55. doi:10.1016/j.bmc.2011.04.001.
- <sup>66</sup> Ehrnhoefer, Dagmar E., Jan Bieschke, Annett Boeddrich, Martin Herbst, Laura Masino, Rudi Lurz, Sabine Engemann, Annalisa Pastore, and Erich E. Wanker. “EGCG Redirects Amyloidogenic Polypeptides into Unstructured, off-Pathway Oligomers.” *Nature Structural & Molecular Biology* 15, no. 6 (June 2008): 558–66. doi:10.1038/nsmb.1437.
- <sup>67</sup> Meng, Fanling, Andisheh Abedini, Annette Plesner, C. Bruce Verchere, and Daniel P. Raleigh. “The Flavanol (–)-Epigallocatechin 3-Gallate Inhibits Amyloid Formation by Islet Amyloid Polypeptide, Disaggregates Amyloid Fibrils and Protects Cultured Cells Against IAPP Induced Toxicity.” *Biochemistry* 49, no. 37 (September 21, 2010): 8127–33. doi:10.1021/bi100939a.

## **Chapter 2:**

**Investigating the fibrillization mechanisms,  
the structure of amyloid peptides and the  
interactions between species**



The study of amyloid peptides can be done by an association of different and complementary techniques that allow us to follow different stages of the fibrillization and characteristics of the monomers, oligomers and fibrils (structure, morphology, interactions between different species or between the peptides and membrane models).

Fluorescence assays using two probes, Thioflavin T and Tryptophanol that bind to either fibrils or small oligomeric species, allowed us to follow the kinetics of kinetics of oligomerization and fibrillization. Circular dichroism (CD) allowed us to probe the secondary structure of the peptides as, while they are mainly disordered in solution, they adopt a  $\beta$ -sheet conformation that promotes their fibrillation. Nuclear Magnetic Resonance (NMR) spectroscopy was a useful technique as different set of experiments allowed us to observe the kinetics of depletion of the monomer as well as the interactions between different oligomers and amyloid peptides and potential inhibitors. The morphologies of the mature fibrils were observed using transmission electron microscopy (TEM). Gel electrophoresis allowed us to observe the presence of multiple sized oligomers, mainly in the early stages of oligomerization. Finally, the interactions between the amyloid peptides and membrane models were followed by monolayer experiments (insertion of the peptide in a monolayer and calcein leakage (permeabilization of the membrane)).

This chapter will describe the different techniques that I used during my thesis. Each paragraph will be divided in a description of the technique, the advantages and inconvenient of each, the experimental protocol used during this thesis and the troubleshooting I may have encountered during my thesis. Part of this chapter will also focus on the peptides preparation, as we had to ensure that the peptides were mainly monomeric for each experiments, lipid vesicles preparation and bacterial expression of the double  $^{15}\text{N}$ ,  $^{13}\text{C}$ -labelled peptide A $\beta$ 42 that we used for NMR experiments.

## **1. Monitoring the kinetics of fibrillation and oligomer formation by fluorescence**

### a) Fluorescent probes

Molecular probes are useful in order to detect the formation of oligomers and amyloid fibrils in different media. During my thesis, I used two different fluorescent probes,



Thioflavin T and Tryptophanol, in order to follow the kinetics of fibrillation or the formation of oligomers over time.

*i. Thioflavin T*

Introduced in 1959 by Vassar as a molecule able to bind to amyloid fibrils, the Thioflavin T dye (figure 20) has since become the standard probe for amyloid detection and for monitoring the fibrillation process.

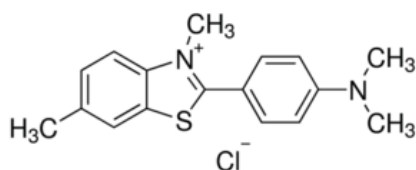
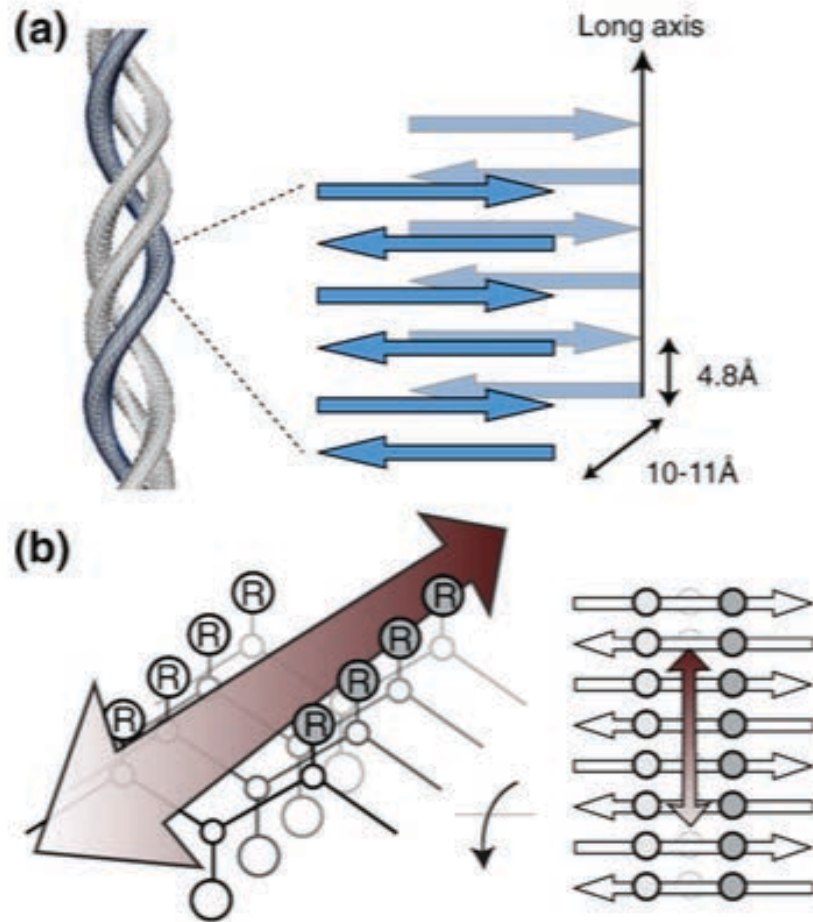


Figure 20: Chemical structure of Thioflavin T

ThT has been shown to bind to the amyloid fibrils in a groove parallel to the long axis of the fibrils and perpendicular to the  $\beta$  sheets (figure 21). As the ThT molecule binds to the  $\beta$ -structures of amyloid fibrils or oligomers, it undergoes a change in conformational freedom as the free rotation over the benzothiazole and aniline rings around the C-C bond is restricted, thus leading to an observed increase in fluorescence intensity.<sup>1</sup>



**Figure 21: The common structure of fibrils and a structural rationale for fibril–ThT interactions.**  
 (a) Cross- $\beta$  structure of amyloid fibrils, formed from layers of laminated  $\beta$ -sheets. (b) “Channel” model of ThT binding to fibril-like  $\beta$ -sheets. ThT is proposed to bind along surface side-chain grooves running parallel to the long axis of the  $\beta$ -sheet. From Biancalana *and al.*<sup>1</sup>

The resulting fluorescence signal obtained over time is mainly sigmoidal, with a prime lag time associated with the presence of monomers and slowly forming small oligomeric species in the nucleation step. As the elongation phase occurs, the fluorescence signal increases before reaching a plateau, which is linked to the presence of mature fibrils (Figure 22).

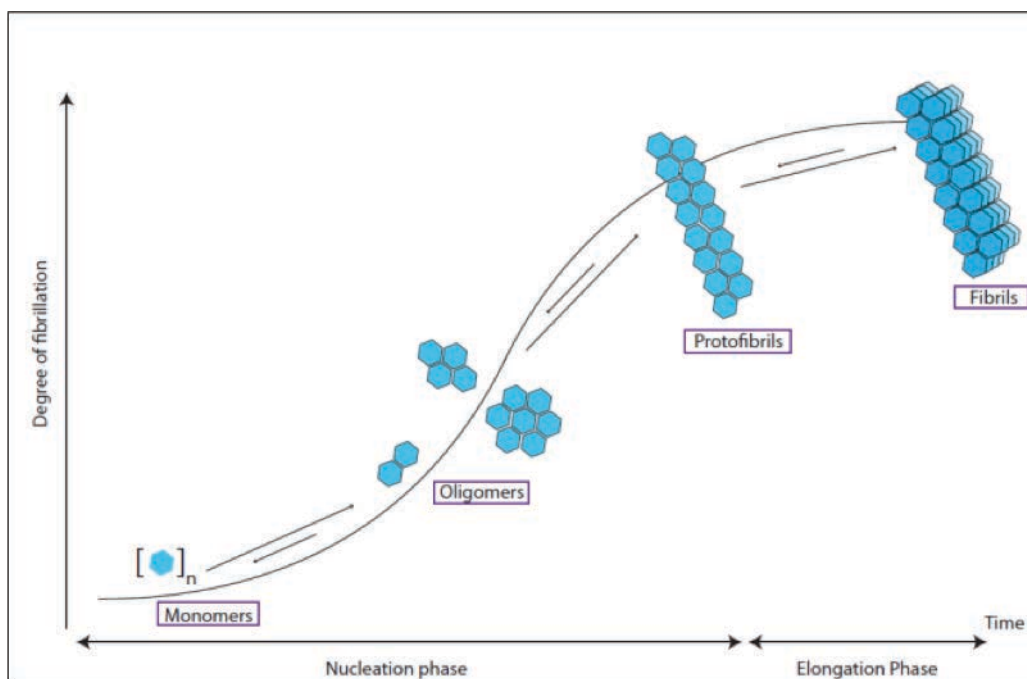


Figure 22: Representation of the ThT fluorescence sigmoidal curve typically obtained for amyloid peptides, enabling to follow the fibrillation process over time.

## ii. Tryptophanol

As it has lately been suggested that the cytotoxicity of some amyloid peptides results from the oligomers formed in the early stages of the fibrillation process, investigations have been made in order to find small fluorescent molecules that would preferentially interact and bind to the small oligomers or prefibrillar species rather than fibrillar aggregates. Identifying such molecules is of great interest, as it would give us more insight about the mechanisms of oligomerization and production of cytotoxic species.

A screening of many molecules was done by Reinke et al<sup>1</sup>, for their capacity to interact with oligomers of A $\beta$ , which was the targeted peptide, in association with a modification of their fluorescence properties. In this screening, it was shown that compounds that contained an indole moiety had their fluorescence modified whether they interacted with oligomers/prefibrils or with fibrils. From these results, a « ThT like » compound, tryptophanol (TROL) was developed for the detection of small oligomers and prefibrillar aggregates.<sup>2,3,4</sup>

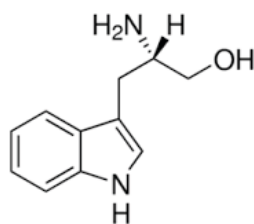


Figure 23: Chemical structure of tryptophanol

In solution and in the presence of monomers or small oligomers, TROL emits a fluorescent signal that is quenched over time as the molecule binds to larger oligomers and prefibrils. In contrast with ThT, TROL does not recognize fibrillar A $\beta$ . TROL molecule is likely to bind to specific sites within oligomers and prefibrillar aggregates, which become inaccessible or conformationally altered in fibrils. So far, TROL has been shown to bind to the oligomeric species of different amyloid peptides or proteins such as A $\beta$  and IAPP (but not  $\alpha$ -synuclein) (Figure 24).

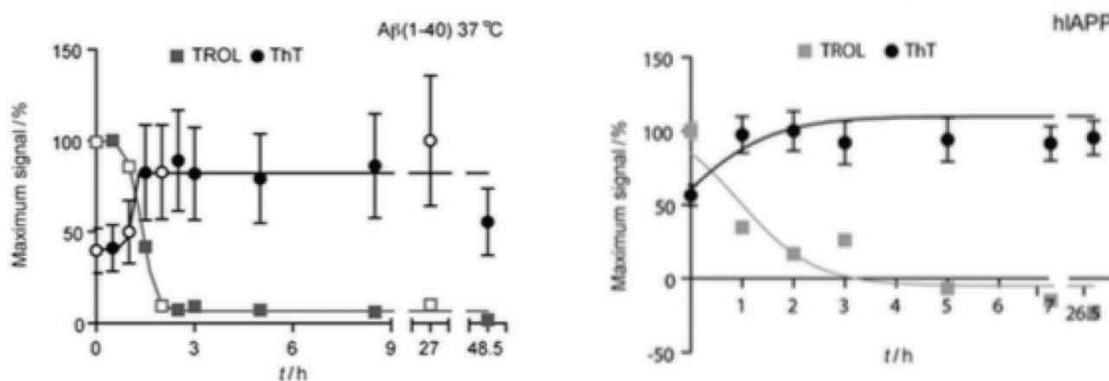


Figure 24: Kinetics of fibrillation of amyloid peptides (left: A $\beta$ 40, right, human IAPP) over time, followed by ThT and TROL fluorescence assays (Reinke *and al.* 2010).  
As the aggregation occurs, the fluorescence of ThT increases as the probe binds to prefibrils and fibrils whereas the TROL fluorescence decreases in the presence of oligomers and prefibrils.

## b) Experimental protocol

As a standard dye, ThT fluorescence experiments have been done on a 96 well black plate using a Fluostar Optima, BMG Labtech plate reader with an excitation filter at 440 nm and an emission filter at 485 nm. For TROL fluorescence assays, a 280 nm excitation filter and 340 nm emission filter were used. The samples were prepared directly in the wells with a peptide/probe ratio of 1:1. Samples were then inserted in the plate reader and mixed for 10

seconds before the first measurement. The measurements were done at regular intervals (10 or 15 minutes).

Once the data processed, the resulting curves can be processed by a sigmoidal Boltzmann equation (figure 25). This fitting allows the estimation of kinetic parameters such as the time for which the fluorescence reaches 50% of its maximal intensity ( $t_{1/2}$ ) and  $\tau$  the rate of elongation linked to the slope of the curve.

$$F_t = \frac{F_i - F_f}{1 + e^{\left(\frac{t-t_1}{\tau}\right)}} + F_f$$

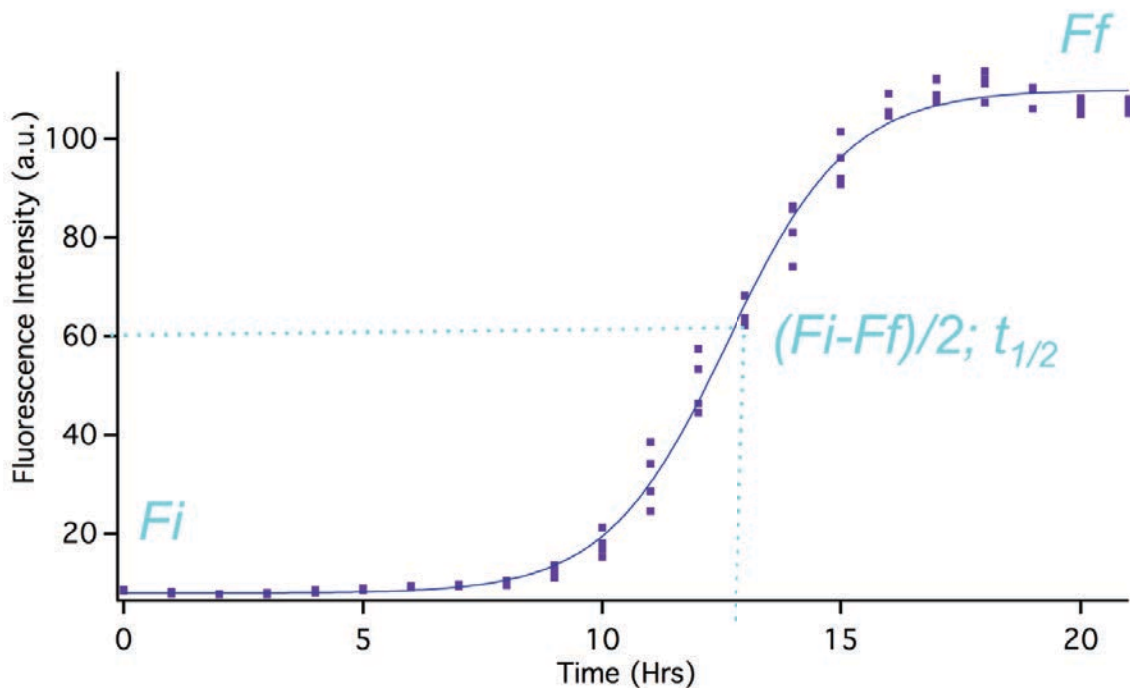


Figure 25: (Top) Boltzmann equation for the fitting of fluorescence data. (Bottom) ThT Fluorescence intensity over time (dots), fitted by a Boltzmann function.

### c) Advantages, drawbacks and troubleshooting

The advantages of those fluorescence assays are that both system and experiment are easy to run and require only small amounts of peptide.

However, as small molecules with similar structures as thioflavin T (aromatic rings) where known to affect to a different extent (e.g. inhibition, aggregation) the fibril formation<sup>5,6</sup>, it is of great importance to assess the influence of our two fluorescent probes on the kinetics of fibrillization of amyloid peptides. The same goes for tryptophanol, as it is a newly

described probe and its effects on the kinetics of fibrillation have not been widely studied. Therefore at the described concentration, especially in chapter 3 where probes are used at a high concentration of 75  $\mu\text{M}$ , the probes may have an influence on the kinetics of fibrillation of our peptides. This subject will further be discussed in chapter 3.

Another point is that, for long experiments (above 48 hours), we encountered an evaporation phenomenon in the plate wells, leading to higher concentrations of soluble peptides in the wells, probably affecting the kinetics of fibrillation.

## 2. Study of the membrane permeabilization by calcein leakage experiments

### a) Calcein

Calcein leakage experiments were carried out in order to observe the permeabilization of lipid vesicles induced by an amyloid peptide.

This method is based on the fluorescence of the calcein molecule (figure 26) depending on its concentration. Indeed, at a high concentration (above 70 mM), calcein self quenches whereas it is fluorescent at a lower concentration.

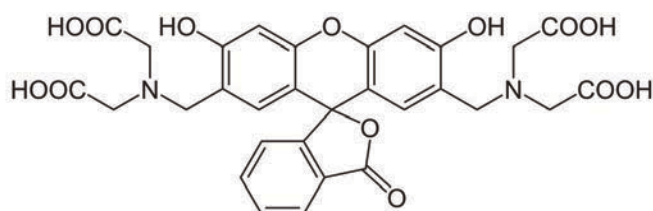


Figure 26: Structure of the calcein molecule

The calcein dye is encapsulated into lipid vesicles (as described in paragraph 8) at a high concentration leading to its self-quenching. Once the peptide is added in the calcein vesicle sample, two different observations can be made. Either the peptide does not permeabilize the membrane, in which case calcein leakage does not occur, leading to a low fluorescence intensity that is stable over time. Otherwise, if the peptide permeabilizes the membrane, the dye leaks out of the vesicles from the formed pores and is diluted in the buffer, leading to an increase in the fluorescence.

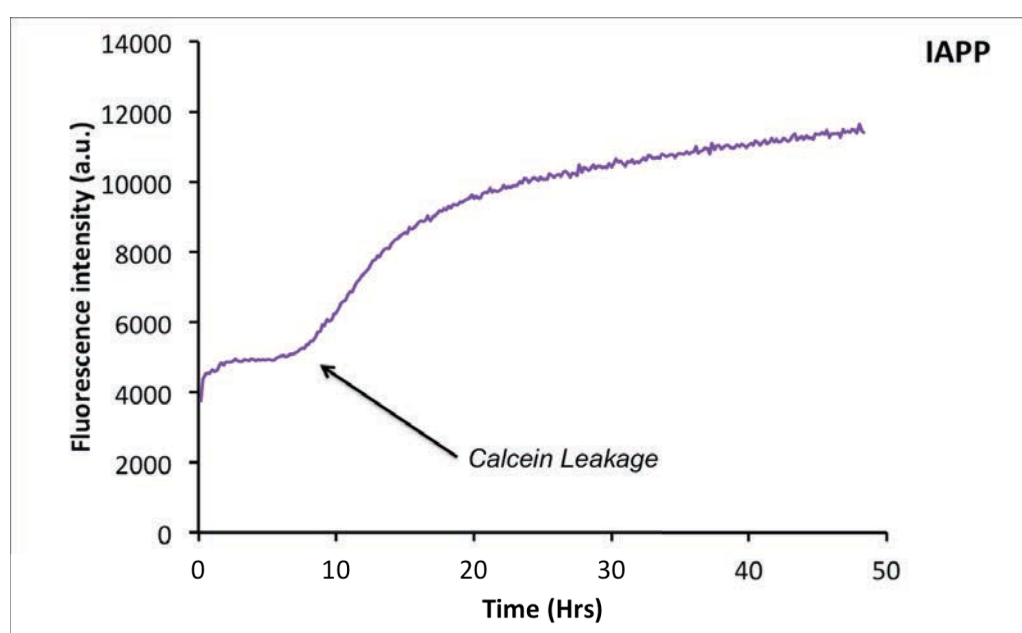
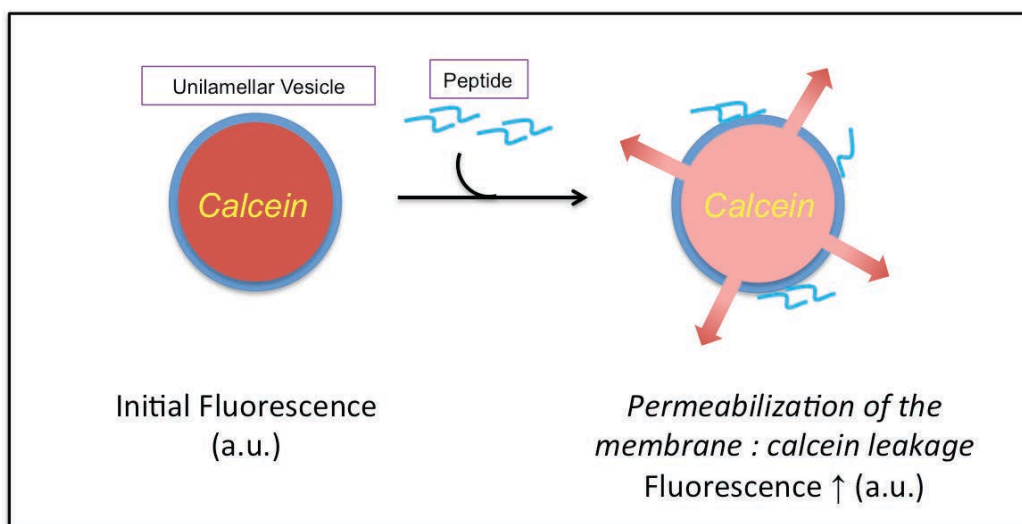


Figure 27: Illustration of the calcein leakage induced by a pore-forming peptide. As the peptide permeabilizes the membrane, a leakage occurs leading to an increase of fluorescence intensity

#### b) Experimental protocol

Calcein leakage experiments are done in a clear 96-well plate using a Fluostar Optima, BMG Labtech plate reader with an excitation filter at 480 nm and an emission filter at 530 nm. Peptides were added to the lipids (Ratio 1:10) just before the measurement, at a concentration of 10  $\mu\text{M}$  in a 50 mM Tris/HCl, 100 mM NaCl buffer at pH 7.4 or 5.5. Optimal gain is measured by the addition of 1  $\mu\text{L}$  of Triton-X-100 10% to three wells containing 200  $\mu\text{L}$  LUV/buffer mixture with the required concentration of lipids. The addition of the detergent to the medium induces 100% leakage and maximum fluorescence intensity. The plate was inserted in the plate reader and measurement is done immediately after a 10 second

shaking of the plate. Measurements are done at a regular interval (5-10 minutes). After the experiment, plate is removed and 1  $\mu\text{L}$  of Triton-X-100 10% is added in every well. After shaking, an additional measurement is done (end point measurement).

#### c) Advantages, drawbacks and troubleshooting

One of the major troubleshooting of the calcein leakage experiment is due to the fragility of the calcein containing vesicles. Indeed, if a great difference of osmolarity between the inside buffer of the vesicles containing a high concentration of calcein and the outside buffer is observed, then the vesicles tend to burst prior to the addition of the peptide. This phenomenon induces a leakage in all wells or an increase of the fluorescence even before the first measurement as the peptide is added in the wells. To avoid this problem and ensure the stability of the vesicles, the quantity of salts is measured and a control of the osmolarity of the inside and outside buffers of the vesicle is done with an osmometer. If the measurement shows an imbalance of osmolarity between the inside and outside buffers, the salts concentrations are adjusted accordingly to homogenise the system.

### 3. Analysis of the secondary structure of the peptides with circular dichroism (CD)

#### a) Principle

Plane polarized light can be described as two circular polarized components of equal magnitude: the left-handed (L) component, rotating counter clock-wise, and the right handed (R) component rotating clock-wise. As the polarized light passes through an optically active sample, the right and left component may not be absorbed at the same extent, resulting, as the two components recombine, in an elliptically polarized radiation deviating from the original plane. Spectropolarimeters (CD instruments), measure the ellipticity ( $\theta$  in degrees), corresponding to  $\theta = \tan^{-1}(b/a)$  where b and a are the minor and major axes of the resulting ellipse (Figure 28).



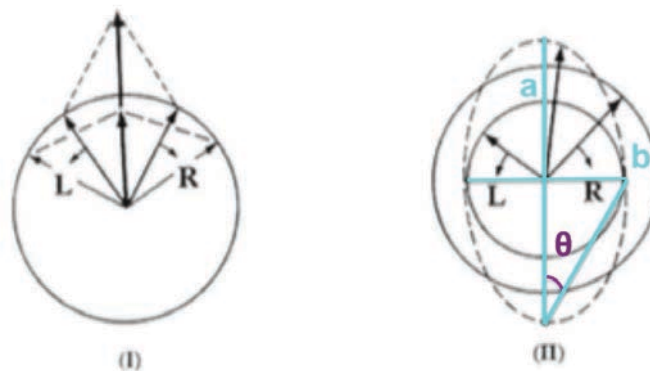


Figure 28: Origin of the CD effect.

(I) : the left (L) and right (R) components have the same amplitude, resulting in a plane polarized radiation. (II) After absorption by a chiral molecule, the components have different amplitudes leading to elliptically polarized radiation (dashed line), a and b being the major and minor axes of the ellipse.

The ellipticity can be linked to the difference of absorbance ( $\Delta A$ ) of the left and right components of the polarized light, depending on the wavelength at which the measurement is done.

$$\theta = 32.98 \times \Delta A = 32.98 \times (A_L - A_R)$$

$\theta$  is the ellipticity in degrees

$\Delta A$  the difference of absorbance

$A_{L/R}$  is the absorbance of the left and right components

The study of peptides/proteins by CD allows us to access information concerning their secondary structure composition in different media, by observation of the far UV signal between 190 and 240 nm. The absorption of the light, in this region, is mainly due to the peptidic bond chromophore, with the contribution of the  $n \rightarrow \pi^*$  transition around 220 nm and the  $\pi \rightarrow \pi^*$  transition around 190 nm. The resulting data is expressed by the molar ellipticity per residue, after normalization, by scaling the measured ellipticity to the molar concentration as well as the number of repeating units, here, the peptidic bonds, of the peptide/protein.

The resulting molar ellipticity per residue is given by the following equation:

$$[\theta] = \frac{\theta}{10 * n * l * c}$$

$[\theta]$  is the molar ellipticity per residues in  $\text{deg cm}^2 \text{dmol}^{-1} \text{residue}^{-1}$

$\theta$  the ellipticity in degrees  
 $n$  is the number of residues  
 $l$  the cuvette length  
 $c$  the molar concentration

Depending on the secondary structure of the peptide/protein, some characteristic CD spectra can be observed<sup>7</sup> (Figure 29).

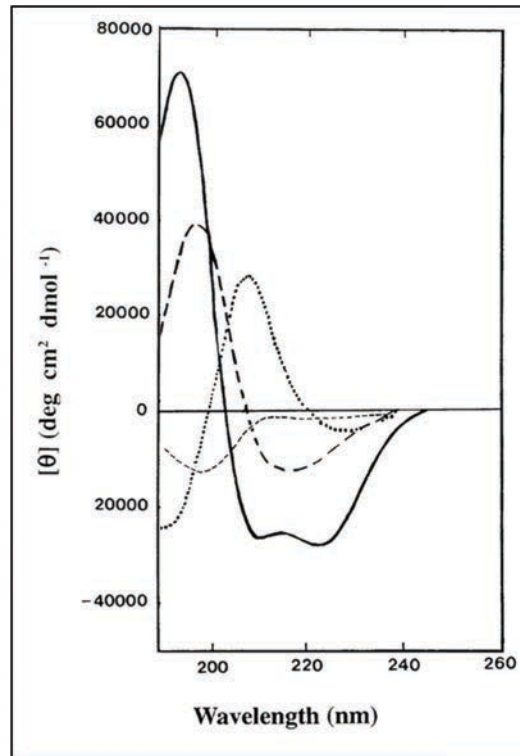


Figure 29: CD spectra associated with various secondary structures.  
Solid line:  $\alpha$ -helix, long dashed line : anti-parallel  $\beta$ -sheet, dotted line, type I  $\alpha$ -turn, short dashed line : random coil.

An estimation of the proportion of the different secondary structure elements composing a sample can be made by using specific algorithms that deconvolute the signal.

#### b) Experimental protocol

During my thesis, all CD data were acquired on a J815 CD Spectrometer – JASCO equipped with a Peltier temperature-controlled cell holder over the wavelength range 190-260 nm. Measurements were carried out in cells of 0.1 cm path in aqueous solution (details of the buffer compositions will be given in each chapter). For each sample, measurements were taken every 0.2 nm at a scan rate of 10 nm/min. Spectra were acquired every 30 minutes over

a period of 7 to 48 hours. Data were then collected with the Spectra Manager Software for treatment. If needed, the estimation of the secondary structure of the peptides was done by deconvolution of the spectra with CDfriend software.

Values at a characteristic wavelength can also be plotted over time and fitted to the following Boltzmann equation (figure 30).

$$\theta_t = \frac{\theta_i - \theta_f}{1 + e^{\left(\frac{t-t_{1/2}}{\tau}\right)}} + \theta_f$$

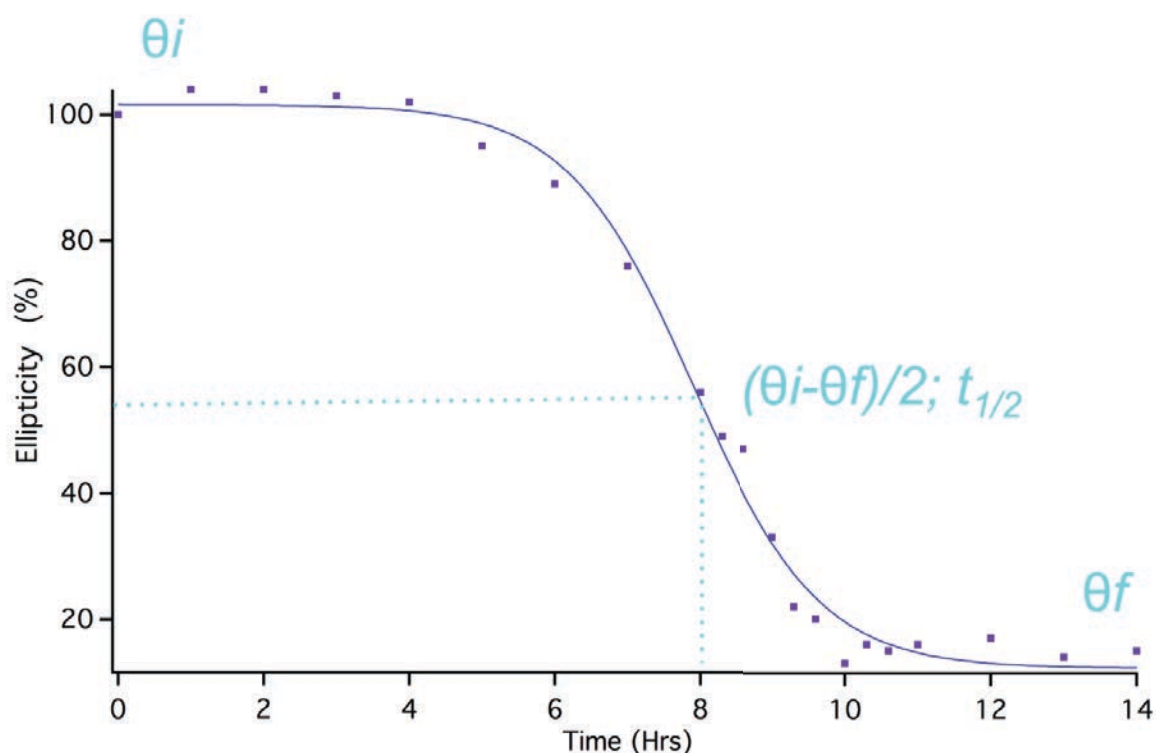


Figure 30: (Top) Boltzmann equation for the fitting of CD data. (Bottom) Ellipticity at 200 nm of circular dichroic spectra over time (dots), fitted by a Boltzmann function.

### c) Advantages, drawbacks and troubleshooting

The inconvenient of this technique in our study came from the aggregating nature of amyloid fibrils. As the oligomerization occurs, large oligomers are formed in solution over time. Those insoluble oligomers either are too large to allow the light to pass through the sample leading to light scattering and a flat line or a low signal difficult to interpret, or they sediment in the bottom of the cuvette leading to the sole observation of residual monomer and small oligomers. Another point is that as the CD signal results from the contribution of all

peptidic chromophores, CD experiments do not give any information about the secondary structure of a local part of the peptide.

The CD technique is thereby privileged for the observation of the global secondary structure of the peptides in their early stages of fibrillation (monomers, small oligomers) and to follow the structuration of the peptide into a  $\beta$ -sheet.

#### 4. Nuclear Magnetic Resonance (NMR) spectroscopy

Liquid-state Nuclear Magnetic Resonance (NMR) spectroscopy is widely used in the study of peptides and proteins. Depending on the set of experiments that is used, it allows us to observe the monomeric peptide or small oligomers and to study their structure and their interaction with other molecules.

##### a) Principle

NMR spectroscopy is based on the observation of nuclei that possess a non-zero spin quantum number. These nuclei can be considered as charged moving particles resulting in a nuclear magnetic moment  $\mu$ . In the absence of a magnetic field, the nuclei are randomly oriented. The application of a magnetic field  $B_0$ , causes all nuclei to align along the magnetic field direction, commonly expressed as the  $z$  axis, with 2 orientations, either spin aligned or spin opposed, for spin  $\frac{1}{2}$  nuclei. As a result, a net macroscopic magnetization  $M_0$ , is formed along the  $z$  axis, parallel to the magnetic field  $B_0$ .

At their equilibrium, the nuclei precess around the  $B_0$  axis at a speed called the Larmor frequency, which depends on  $B_0$ . Upon application of a small magnetic field, the radiofrequency field  $B_1$ , oscillating at or near the Larmor frequency the net magnetization is flipped from the  $z$  axis to the  $xy$  plane. After the pulse has finished, the magnetization precesses generating a *free induction decay* (FID), which is a function that decays exponentially with time, with a characteristic transverse relaxation time  $T_2$ . The FID is recorded by a coil detector placed in the  $xy$  plane (figure 31).<sup>8</sup> The data is then processed by a Fourier transform, which converts the signal from a time domain function (the FID) into a frequency domain function (figure 32)

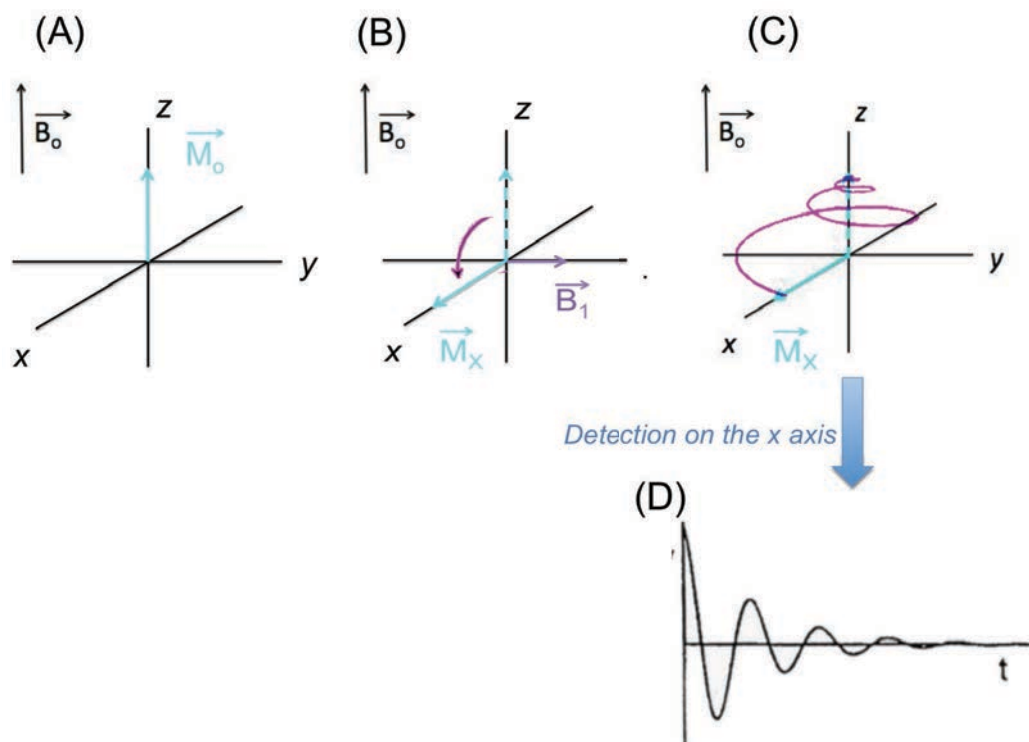


Figure 31: One pulse NMR experiment (A) Net magnetization along the z axis. (B) Upon application of the oscillating radiofrequency  $B_1$  along the y axis of a rotating reference frame, the magnetization flips into the xy plane. (C) After suppression of  $B_1$ , the net magnetization precesses until reaching its equilibrium. (D) The signal is detected along the x axis.

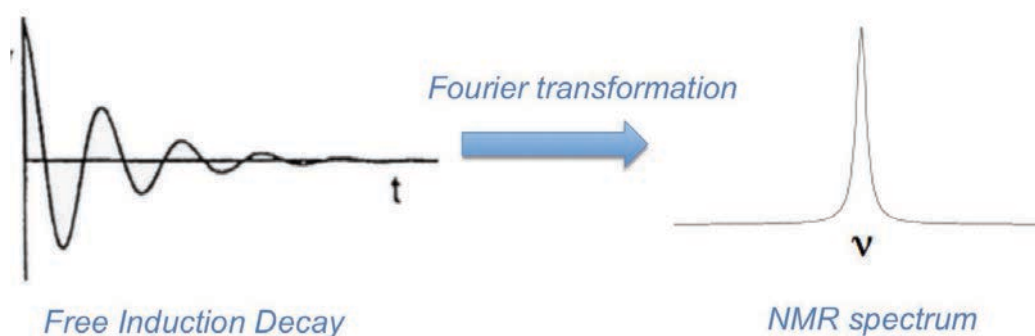


Figure 32: Conversion of the FID (time domain function) to a frequency domain function (NMR spectrum) using the Fourier transformation

### b) 1D spectrum acquisition

The linewidth of a resonance is inversely proportional to the transverse relaxation time  $T_2$ , which is also approximately inversely proportional to the overall rotational correlation time  $t_c$  of the molecule. Therefore the resonance linewidth is approximately proportional to  $t_c$  and thus depends on the molecular mass and shape of the molecule. As a consequence, large oligomers are not detectable by liquid state NMR spectroscopy since their resonances will be broadened beyond detection.

We took advantage of this effect to quantify the monomer population of amyloid peptides. A series of acquisition of 1D  $^1\text{H}$  NMR spectrum of the peptides allow us to observe monomer depletion over time. As the peptide aggregates, the signal of the monomer decreases (figure 33).

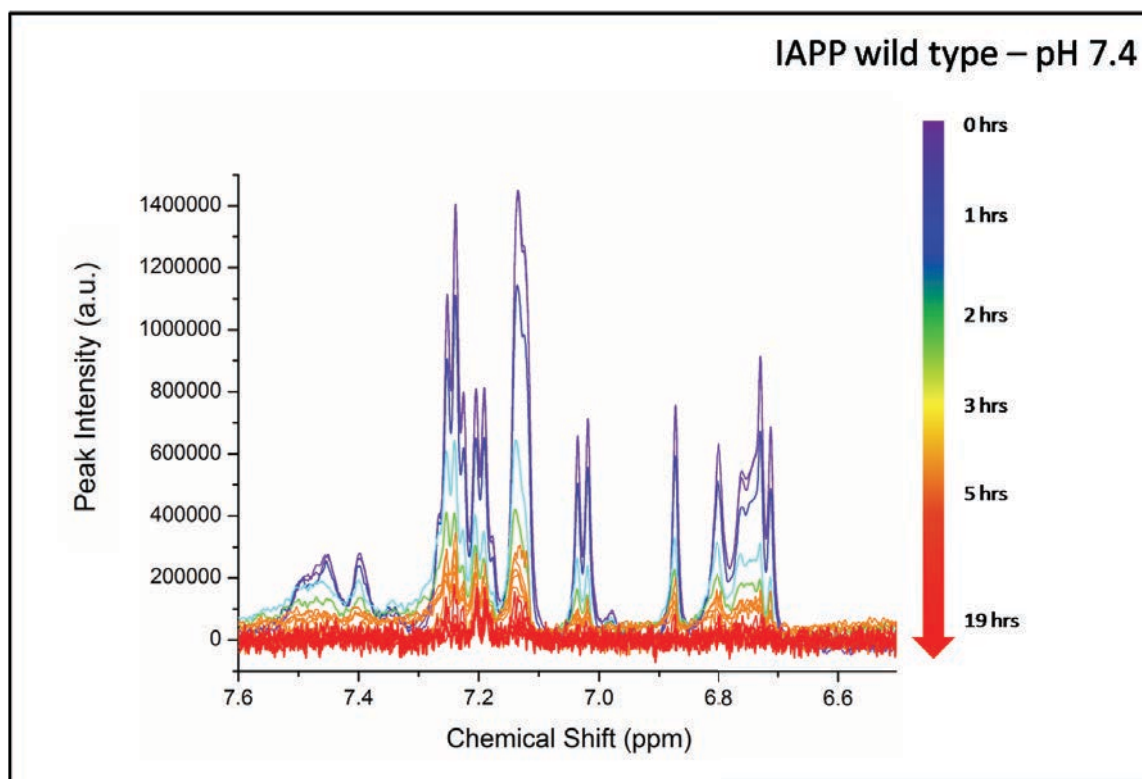


Figure 33: Depletion of the signal of A $\beta$ 42 monomer over time, followed by liquid-state NMR spectroscopy

The peak area of the spectra can be measured and plotted over time. Depending on the shape of the curve, the sigmoid can be fitted either by a sigmoidal Boltzmann function (figure 34) or a Richards function (figure 35), which fits with a more flexible S-shape curve, with plateaus replaced by linear functions of the kind of  $y = ax+b$ .

Fitting allowed us to determine kinetics parameters such as the half-time ( $t_{1/2}$ ) linked to the monomer depletion.

Boltzmann equation:

$$I_t = \frac{I_i - I_f}{1 + e^{\left(\frac{t-t_{1/2}}{\tau}\right)}} + I_f$$

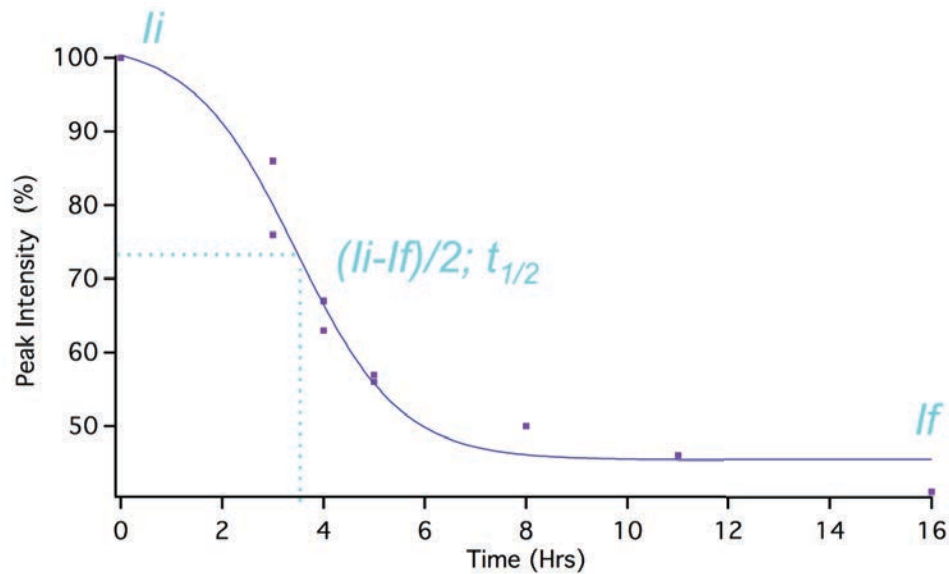


Figure 34: (Top) Boltzmann equation for the fitting of NMR data. (Bottom) Peak intensity of IAPP monomer over time (dots), fitted by a Boltzmann function.

Richards equation:

$$I_t = \frac{(a_i t + b_i) + (a_f t + b_f)}{1 + \exp\left(\frac{t - t_{1/2}}{t}\right)}$$

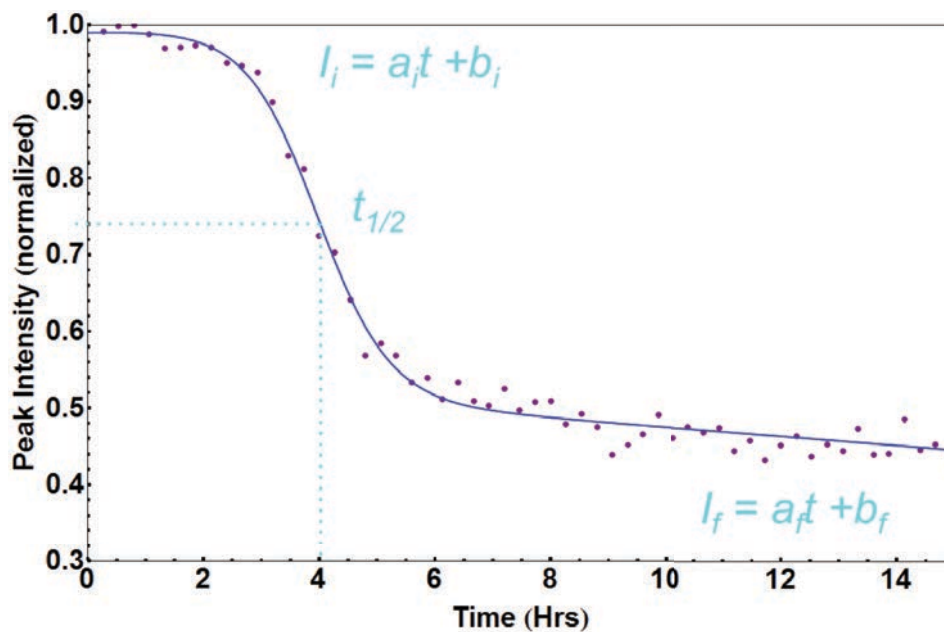


Figure 35: (Top) Richards equation for the fitting of NMR data. (Bottom) Peak intensity of IAPP monomer over time (dots), fitted by a Richards function.

c) Diffusion Ordered NMR-Spectroscopy (DOSY) / Pulse Field Gradient (PFG) experiment

Diffusion Ordered NMR-Spectroscopy (DOSY) is based on the application of Pulse Field Gradient (PFG) to the system and is used to determine hydrodynamic parameters such as diffusion coefficients of the peptides in solution. The principle of the experiment is to apply a dephasing gradient to the sample then a refocusing gradient after a delay that is called the diffusion time. Diffusion causes the molecules to move from their initial position inside the NMR tube, which means that the signal will not be completely refocused after application of the refocusing gradient (figure 36)

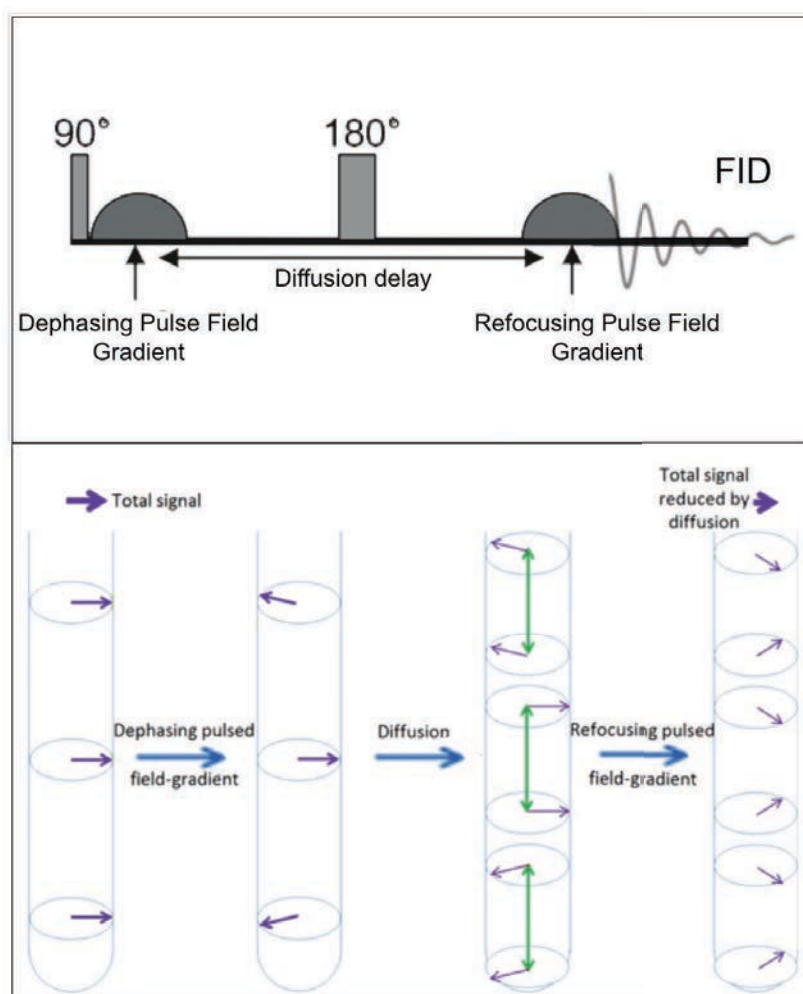


Figure 36: (Top) Carr Purcell spin echo sequence. (Bottom) Schematic representation of the Effect of diffusion combined with field gradient pulses on the spins. The diffusion of the nuclei inside the tube leads to a decrease of the signal as it is not completely refocused by the application of the refocusing pulsed field gradient.



This results in a decrease of the signal intensity, which appears as a decaying exponential curve (figure 37). The intensity of the signal can be given by the following equation:

$$I = I_0 e^{-D\gamma^2 g^2 \delta^2 (\Delta - \frac{\delta}{3})}$$

$I_0$  is the reference intensity

$D$  is the diffusion coefficient in  $\text{m}^2\text{s}^{-1}$

$\gamma$  the gyromagnetic ration of the observed nucleus in  $\text{rad}\cdot\text{s}^{-1}\cdot\text{T}^{-1}$

$g$  the gradient strength in  $\text{T}\cdot\text{m}^{-1}$

$\delta$  the length of the gradient in s

$\Delta$  the diffusion time in s

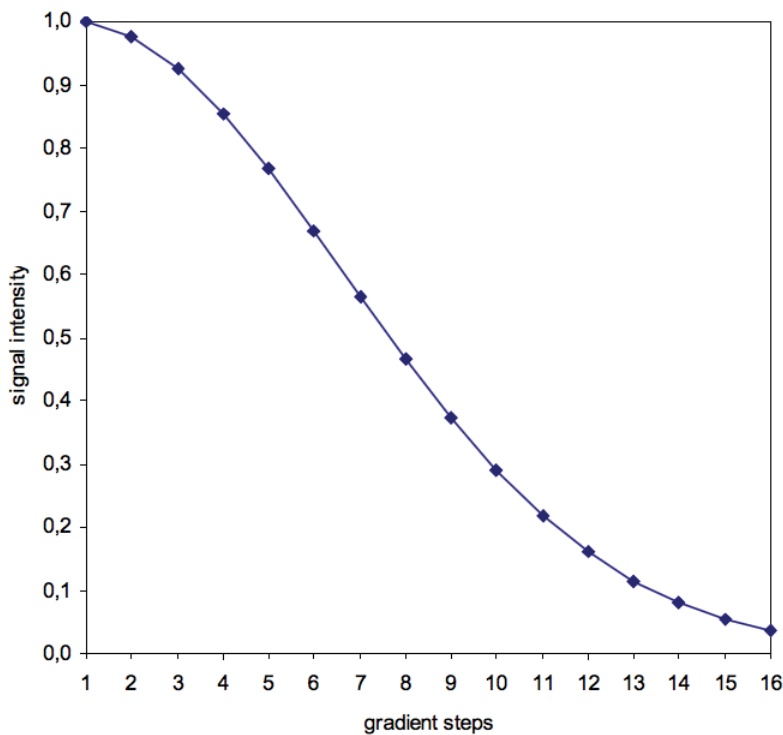


**Figure 37: Simulated diffusion decay curves by varying the gradient strength from 2 to 95 % in 16 steps for the same diffusion constant.**

**Data points are sampled along the whole decay curve. From DOSY and Diffusion by NMR, Bruker.**

The estimation of the decrease of intensity as a function of the gradient strength allows us to obtain the diffusion coefficient  $D$  (in  $\text{m}^2\text{s}^{-1}$ ).

The diffusion coefficient is linked to the hydrodynamic radius  $r$ , which depends on the folding and association of the peptides in solution and obtained following the equation below.

$$D = \frac{k_B T}{6\pi\eta r}$$

$k_B$  is the Boltzmann constant in  $\text{m}^2\text{kg}\cdot\text{s}^{-2}\cdot\text{K}^{-1}$

$T$  the temperature in K  
 $r$  the hydrodynamic radius in m  
 $\eta$  the viscosity of the fluid in Pa·s<sup>-1</sup>

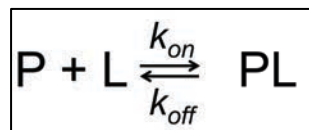
Therefore, the measurement of the diffusion coefficient on aggregating amyloid peptides allows us to obtain some information on the species that are present at a given time in solution (monomers, oligomers, fibrils)

#### d) Saturation Transfer Difference (STD) experiments

Saturation Transfer Difference (STD) experiments allows the observation of possible interactions between large molecules (oligomers, protofibrils or mature fibrils) and their ligands (monomers or low molecular weight oligomers).

As the formation of a Protein/Ligand complex occurs, it induces changes in the magnetic environment, thus in the chemical shifts of the two species, showing differences between the spectra of the complex form and the un-bound/free form. Given the size of the large molecule, it is not observed by liquid state NMR spectroscopy as the signals are too broad to appear on the spectrum. Therefore, only the signals attributed to the small molecules can be observed and, when bound to the large species, the signal broadens and leads to its disappearance over time.

The association of a protein with a ligand can be given by the following expression, where P is the protein, L the ligand and  $k_{on}$  and  $k_{off}$  the association and dissociation rate constants.



Depending on the exchange rates between the protein and the ligands, three different regimes can be observed.

In the case of a fast exchange rate on the chemical shift scale, the value of  $k_{off}$  is higher than the value of  $\Delta\omega$ , which is the resonance frequency difference of the signals in the bound and free state ( $\Delta\omega=2\pi\Delta\nu$ ). The resulting signal appears as a weighted average of the chemical shifts from the bound and the free ligands. On the contrary, in the case of a slow exchange

rate on the chemical shift scale, the value of  $k_{off}$  is lower than the value of  $\Delta\omega$ . Two distinct signals from the bound and free ligands will be observed on the spectrum. The intermediate exchange regime corresponds to the situation where  $k_{off}$  is close to  $\Delta\omega$ , corresponding to the coalescence of signals that are often broadened beyond detection (figure 38).

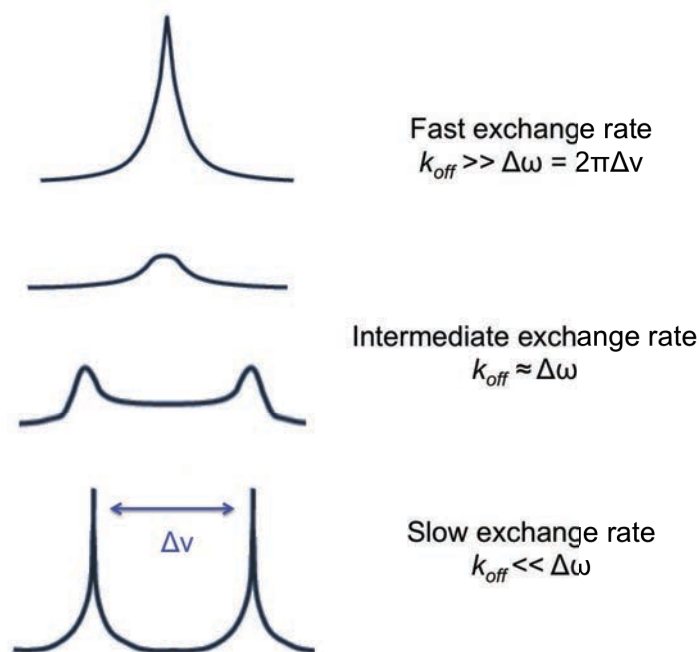
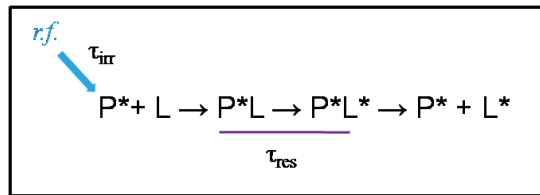


**Figure 38: Appearance of the NMR spectrum of bound and free ligands depending on the exchange rates. At a fast exchange rate, the signal appears as a weighted average of the chemical shifts of bound and free ligands. At a slow exchange rate, two distinct signals can be observed. At an intermediate exchange rate, we can observe a broadening and coalescence of both signals.**

The STD experiment consists into different 1D spectra. The first spectrum, “on resonance” is recorded after the irradiation, at a given chemical shift (here around -1 ppm) in a region where the signals of the macromolecule are expected to be found (due to large linewidths), but where no signals of the free ligand can be observed. The second is an off resonance spectrum, meaning that the irradiation is made at a frequency (here, 30 ppm) where no signal of either the macromolecule or the ligand can be observed. This consists in our reference spectrum.

When the large molecule and its ligand interact, at a fast exchange rate, the irradiation passes from the macromolecule to the ligand, which successively binds to the macromolecule then goes back in solution.



*r.f.* is the radiofrequency signal of the saturation

$P/P^*$  is the unsaturated/saturated protein

$L/L^*$  is the unsaturated/saturated ligand

$\tau_{\text{irr}}$  the irradiation time

$\tau_{\text{res}}$  the residence time in the occupied binding site

When irradiated, part of the signal of the ligand that is in interaction with the large molecule, is decreased in regards of the off resonance spectrum because of the saturation transfer. A difference between the on resonance and off resonance spectra allows us to detect small molecules exhibiting association equilibrium with macromolecules and also to map the residues or part of the ligand that are in close contact with the large molecule.

#### e) Sequential assignment of hIAPP

Sequential assignment was done on hIAPP full length and fragment hIAPP<sub>1-19</sub> in chapter 5, in order to observe the interaction between hIAPP/ hIAPP<sub>1-19</sub> and epigallocatechin gallate (EGCG), which was studied as an inhibitor compound of the fibrillization.

The sequential assignment strategy involves the use of two homonuclear 2D NMR experiments that allows us to observe the connectivities through-bond and through-space of the residues of the observed peptide (figure 39).

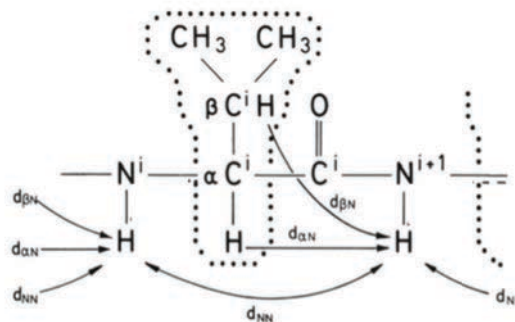


**Figure 39: Polypeptide segment with indication of the spin systems of non-labile protons in the individual residues (inside the dotted lines) and the sequential NOE connectivities.**

The first step of the assignment strategy was the identification of each amino acids spin systems, by a 2D  $^1\text{H}$ - $^1\text{H}$  TOCSY (TOtal Correlation SpectroscopY) experiment. 2D  $^1\text{H}$ - $^1\text{H}$  TOCSY experiments are used to correlate J-coupled spins with each other (*i.e.* nuclei that are connected through  $^2\text{J}$  and  $^3\text{J}$  homonuclear scalar coupling). This allows the identification of amino acids types through characteristic patterns of cross signals (figure 40).

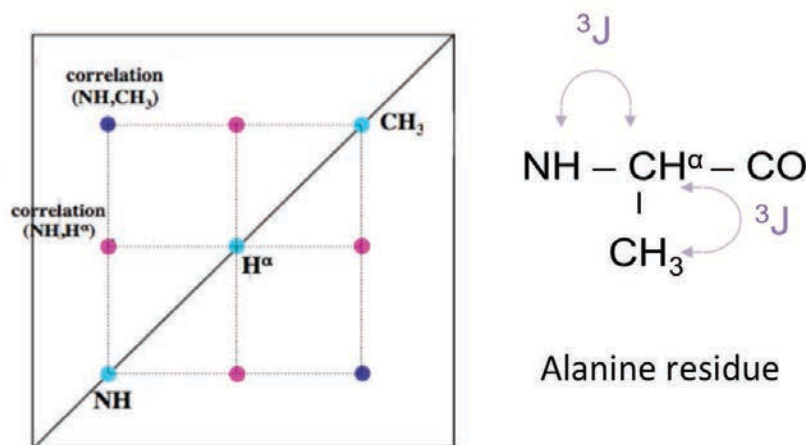
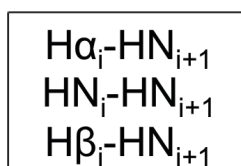


Figure 40: Schematic representation of the characteristic pattern of the alanine observed on a 2D  $^1\text{H}$ - $^1\text{H}$  TOCSY spectrum

The second step was the identification of the neighboring amino acids of the assigned residues by observation of the sequential NOE (Nuclear Overhauser Effect) correlations. Nuclear Overhauser Effect is the transfer of magnetization from one spin to another by cross relaxation induced by the dipolar interaction between the two spins. The magnitudes of the NOE cross peaks gives information on the distance between the two nuclei. Typical sequential NOE observed therefore indicates the connectivities between the following protons:



The two steps described above are repeated until the whole sequential assignment is completed

#### f) Experimental protocol

Given the numerous NMR parameters inherent to the multiple pulses sequences and samples that were used during my thesis, experimental protocols and parameters of NMR experiments will be described in the material and methods sections of following chapters 3, 4 and 5.

g) Advantages and drawbacks

NMR spectroscopy is a very powerful technique to investigate the early stages of amyloid peptides, as well as their dynamics and interaction with other molecules such as potential inhibitors. However, NMR spectroscopy is not a very sensitive technique and requires high concentration of peptides or long acquisition times, which are unfavorable in the case of amyloid peptides as it promotes aggregation.

## 5. Monolayer experiment

a) Principle

The principle of the experiment is to measure the surface pressure of a specific lipid monolayer due to its compression as it interacts with a peptide.

Once the peptide is introduced in the buffer, either it does not insert into the monolayer and the surface pressure remains stable over time, or the peptide inserts into the monolayer leading to an increase in the surface pressure (figure 41).

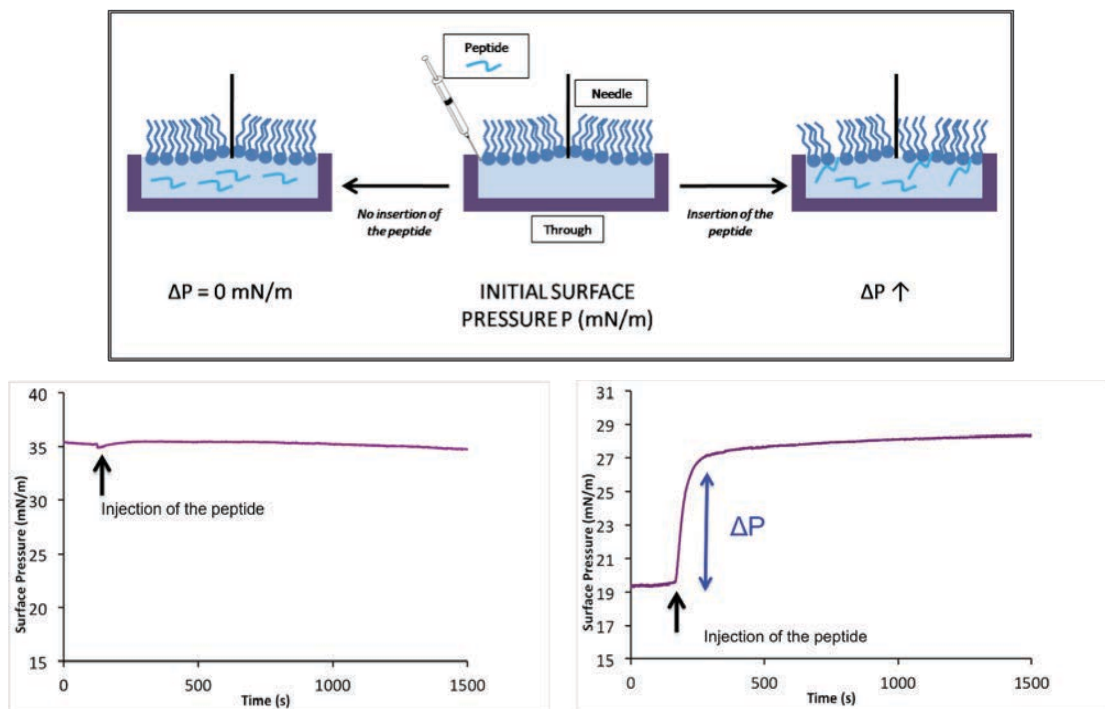


**Figure 41: Illustration of the monolayer experiment principle.**  
If the peptide does not insert into the monolayer no variation in surface pressure is observed (bottom left). Peptide insertion leads to an increase in the measured surface pressure (bottom right)

The experimental data to estimate the ability of the peptide to insert into a monolayer is the difference in surface pressure  $\Delta P$ . A monolayer experiment is a set of at least five different measurements with different initial surface pressures. The obtained  $\Delta P$  values from the measurements can then be plotted versus the initial surface pressure. Drawing a trend line of the plot can then allow the calculation of the maximum surface pressure, which is the pressure under which the studied peptide is able to insert into the membrane (figure 42). The higher the value, the easier the peptide can insert into the monolayer.

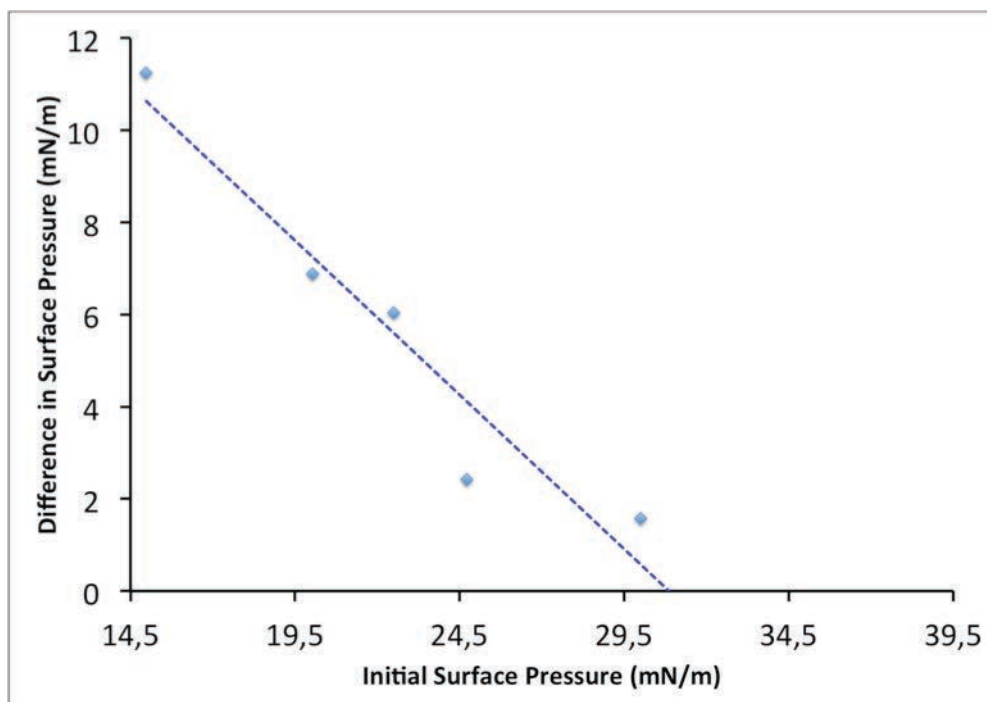


Figure 42: Plot of the difference in surface pressure depending on the initial surface pressure and associated trend line

#### b) Experimental protocol

The experiment was done in the laboratory of the group of Membrane Biochemistry and Biophysics in Utrecht, in the Netherlands. The apparatus is a Langmuir-Blodgett trough containing 18 mL of buffer. The measure of the surface pressure is done over time with a surface pressure sensor (the needle) after calibration of the surface tension of the air/water interphase. The DOPC/DOPS (7:3) monolayer is then deposited upon the buffer with a Hamilton® syringe until the desired surface pressure is reached. If needed, the surface pressure can be adjusted with a barrier, which compresses the monolayer on the surface of the

buffer. Once the monolayer is stabilized, the peptide is injected into the buffer with a Hamilton® syringe.

The experiment is repeated five times, with different initial surface pressures ranging from 15 to 35 mN/m depending on the studied peptide.

#### c) Advantages, drawbacks and troubleshooting

Since the through requires a volume of 18 mL for every measure, a high amount of peptide is necessary (roughly 400 µg of IAPP for one experiment at five different initial surface pressures). Moreover, the experiment gives information about the insertion of the peptide in a lipid monolayer, which may differ from a true membrane bilayer.

## 6. Transmission Electron Microscopy

#### a) Principle

Transmission Electron Microscopy is a technique in which a beam of electron is transmitted through a very thin sample. The interaction between the electrons and the sample leads to a transmitted image that is magnified and focused by different lenses, onto a fluorescent screen where it can be observed (figure 43).



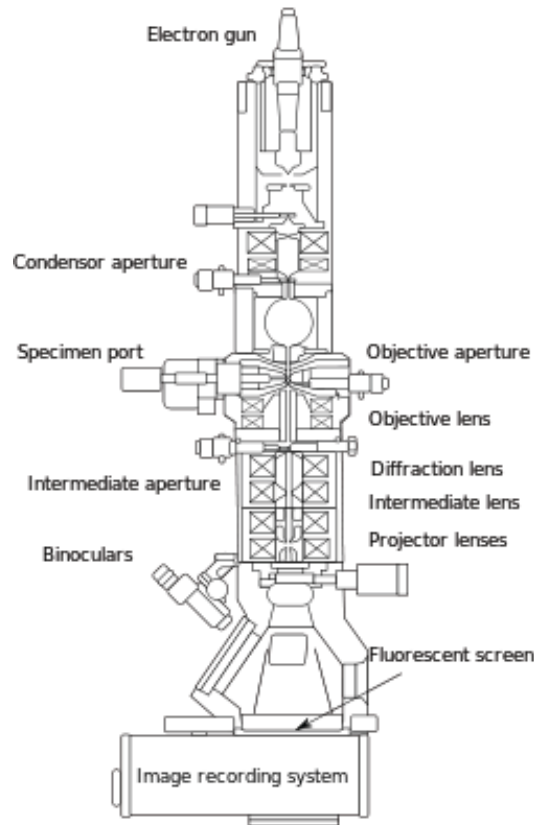


Figure 43: Schematic representation of a transmission electron microscope

TEM is a useful technique to observe the morphology of amyloid fibrils *in vitro*. The observation of the samples at a nanometer scale allows us to identify and characterize the morphologies of the fibrils and aggregates. For the observation of amyloid fibrils we use a negative staining which will provide a contrast as well as a protection of the sample. The electron beam passes through the sample but is absorbed by the stain (here, uranyl acetate 2%), leading to an image where the fibrils appear light and the background dark.<sup>9</sup>

#### b) Experimental protocol

Peptides are incubated during a specific time at room temperature, at a concentration of 75  $\mu\text{M}$  in a 10 mM Phosphate buffer pH 7.4 in the presence or absence of fluorescent probes (Chapter 3) or 10  $\mu\text{M}$  in a 50 mM Tris/HCl 100 NaCl buffer pH 7.4 or pH 5.5 (Chapter 4). The carbon layer of the grid is laid down on 25  $\mu\text{L}$  of the sample for 2 minutes before being dried by touching a filter paper with the edge of the grid. The grid is then laid down on 25  $\mu\text{L}$  of uranyl acetate 2.5% for 45 s. The grid is once again dried on a filter paper.

The observation of the grids was done on three different microscopes:

- Zeiss 912 Omega electron microscope operating at 80 kV (Institut de Biologie Intégrative IFR83, Université Pierre et Marie Curie)
- JEOL 1010 electron microscope operating at 80 kV (Faculté de Médecine Xavier Bichat)
- Technai 12 electron microscope operating at 120 kV (Biology Imaging Center – cell biology and microscopy department, Utrecht University, the Netherlands)

#### c) Drawbacks and troubleshooting

TEM is an efficient method to have access to the morphology of the amyloid fibrils at a high resolution and only requires small volumes and low concentration of peptide. However, negative staining might involve the presence of artifacts, which can hamper the observation of the fibrils on the surface of the grid as they can be mistaken for peptide's aggregates. TEM also does not provide information on the atomic or 3D structure of the fibrils, as atomic force microscopy (AFM) would do.

## 7. Polyacrylamide gel electrophoresis

#### a) Principle

Polyacrylamide gel electrophoresis is a useful technique to separate proteins or peptides as a function of their size and charge.

Gels are usually composed of two parts: an upper stacking gel with a low percentage of polyacrylamide, which allows proteins to move through quickly and “stack” into a tight band over the resolving gel, with a higher percentage of polyacrylamide, which allows the separation of the molecules. Experiments are carried out in electrophoresis chambers, filled with buffer, where the gel in which the samples were loaded, is placed. Upon application of an electric field, through a power source, molecules contained in the analyzed sample move through the gel. The particles will then migrate depending on their charge, (cations towards the cathode, anions towards the anode), and on their size. Larger molecules will move more slowly through the gel than the smaller ones as they are retained by the acrylamide matrix. Different type of acrylamide gels and electrophoresis conditions can be used, depending on the nature and stability of the sample we want to observe.

For peptide and proteins, gel electrophoresis can be done in non-denaturing (native) conditions, maintaining the structural integrity of the molecule. The migration through the gel then occurs depending on the size and charge of the peptides/proteins as described above. Electrophoresis can also be done in denaturing conditions (SDS-PAGE) employing detergent and reducing agents to disrupt the natural structure of the peptides/proteins. SDS-PAGE (Sodium Dodecyl Sulfate PolyAcrylamide Gel Electrophoresis) is useful for the separation of molecules depending on their charge. SDS is a detergent that denatures secondary and non-disulfide linked tertiary structures and coats the proteins with a negative charge allowing a separation depending on their size only.<sup>10</sup>

During my thesis, I made use of gel electrophoresis for different aim using accordingly denaturing or non-denaturing conditions. On the first hand, the technique allowed me to follow the different steps of expression and purification of A $\beta$ 42 peptide (see paragraph 9). On the second hand, gel electrophoresis was used to observe the presence of monomeric and oligomeric species in incubated samples of A $\beta$ 42 and hIAPP (chapter 3).

#### b) Gel composition and electrophoresis conditions

Gels were either cast in the lab (Tris-Tricine and Bis-Tris gels), or were commercial gradient Tris-Glycine gels.

Tris Tricine gels (Tricine-SDS-PAGE) are used to separate peptides and proteins within the mass range of 1 to 100 kDa. As they resolution is more precise for lower molecular weights, those gels were used for the observation of A $\beta$ 42 monomer during the expression and purification steps of the peptide. Bis-Tris gels are run at a pH of 7.2, which is lower than the pH of Tris-Glycine gels (pH 9.5). The neutral pH minimizes the protein modification and degradation during the electrophoresis than can occur during the use of the tris-glycine gels.<sup>11</sup>

Some experiments, also required the use of gradient gels (4-20%) that allowed a greater range of separation if large and small molecules have to be separated simultaneously.

*Gel composition :*

<b>Tris Tricine Gel</b>	<b>Bis Tris gel</b>
<p><b>Stacking gel:</b>            800 µL of Acrylamid/Bisacrylamid solution (30%)            3.7 mL of milliQ water            1.5 mL of separating gel buffer 3X (3M Tris, 1mL HCl, 0.3% SDS, pH 8.45)            50 µL Ammonium persulfate 10%            5 µL TEMED            (N, N, N', N'-tetramethylethylenediamine)</p> <p><b>Resolving gel:</b>            6.4 mL of Acrylamid/Bisacrylamid solution (30%)            4 mL of separating gel buffer 3X (3M Tris, 1mL HCl, 0.3% SDS, pH 8.45)            600 µL milliQ water            952 µL glycerol            45 µL Ammonium persulfate 10%            5 µL TEMED            -</p> <p>Pour the resolving gel between the glass plates and let the polymerization occur. Pour the stacking gel and add the comb.</p>	<p><b>Stacking gel:</b>            0.67 mL Acrylamid/Bisacrylamid (29:1)            1.42 mL Bis Tris 1.25 M pH 6.8            2.9 mL H<sub>2</sub>O milliQ            40 µL Ammonium persulfate 10%            20 µL TEMED</p> <p><b>Resolving gel:</b>            4 mL Acrylamid/Bisacrylamid (29:1)            2.86 mL Bis Tris 1.25 M pH 6.8            3.14 mL H<sub>2</sub>O milliQ            67 µL Ammonium persulfate 10%            18.7 µL TEMED            -</p> <p>Pour the resolving gel between the glass plates and let the polymerization occur. Pour the stacking gel and add the comb.</p>

*Sample buffers composition :*

<b>Native Tris Glycine Sample buffer (2X)</b>	<b>Tris Glycine gel Tris-Tricine gel Sample Buffer (2X)</b>	<b>Bis Tris gel Sample Buffer (4X)</b>
0.187 M Tris/HCl 30% glycerol (v/v) 0.08% Bromophenol Blue (w/v)	250 mM Tris-HCl pH 6.8 8 % SDS (w/v) 0.05 % Bromophenol Blue (w/v) 10 % glycerol (v/v) (20% β- mercaptoethanol)	0.12 M Tris 4% SDS (w/v) 20% glycerol (v/v) 0.08% Bromophenol Blue (w/v)

*Running buffers composition :*

<b>Native Tris Glycine (4X)</b>	<b>Tris Glycine (4X)</b>	<b>Tris Tricine (10X)</b>	<b>Bis Tris (5X)</b>
100 mM Tris 75 mM Glycine	100 mM Tris 75 mM Glycine 0.004% SDS (w/v)	Anode buffer : 1 M Tris 0.225 M HCl pH 8.9  Cathode buffer : 1 M Tris 1 M Tricine 0.5% SDS pH 8.25	50 mM MES 50 mM Tris 1 mM EDTA 0.1% SDS (w/v) 1 mM Na <sub>2</sub> S <sub>2</sub> O <sub>3</sub>

The gels can be stained either by Coomassie blue staining or by Silver staining, depending on the concentration of the peptides on the gels and the sensitivity for detection.

**Coomassie Blue staining protocol:**

Fixing: fix the gel by incubating it in a destaining solution (10% acetic acid (v/v), 20% isopropanol (v/v)) for 10 minutes.

Staining: Pour the staining solution (0.4 g/L Coomassie blue R-250, 10% acet acid (v/v), 10% isopropanol (v/v)) on the gel, and heat the gel for 1 min at 450 W in a microwave oven. Remove from oven and place on a platform rotator for 1 hour.

Destaining: Pour the destaining solution on the gel and let it destain until the background of the gel is clear.

**Silver staining protocol (buffers described table 3):**

Washing: incubate the gel in ethanol 35% for 20 minutes.

Pre-treatment: incubate the gel in the “pre-treatment buffer” (see table for the buffer composition) for 1 minute then replace buffer with milliQ water to wash the gel.

Staining: incubate the gel in the “staining buffer” for 20 minutes.

Washing: wash two times (about 20 seconds for each washing) with milliQ water.

Revelation: incubate the gel in the “revelation buffer” until the desired staining intensity of the bands. Once the bands are observable, eliminate the buffer, wash the gel with milliQ water and incubate the gel for 10 minutes in the “stop buffer”.

Washing and conservation: Incubate the gel for 10 minutes in ethanol 35%. The gel can then be dried or conserved in milliQ water.

Pre-treatment buffer	127,5 mg Na <sub>2</sub> S <sub>2</sub> O <sub>3</sub> in 1 L milliQ water
Coloration buffer	1 g AgNO <sub>3</sub> 376 µL HCO <sub>2</sub> H 37% Add milliQ water until volume is 500 mL
Revelation buffer	60 g Na <sub>2</sub> CO <sub>3</sub> 500 µL HCO <sub>2</sub> H 37% 20 mL Pre-treatment buffer Add milliQ water until volume is 500 mL
Stop buffer	50% methanol (or isopropanol) 12 % acetic acid Fill to 1L with milliQ water

**Table 3: Composition of buffers for silver staining protocol**

### c) Advantages and drawbacks

Native gel electrophoresis is an interesting technique as it allows us to native gels have the advantage of not using any detergent that may stabilize or dissolve amyloid oligomers. However, as the amyloid oligomers shape, size and charge are unknown, it is difficult, to predict their mobility and how they will migrate through the gel.

## 8. Sample preparation

### a) Materials

hIAPP and IAPP mutants with an amidated C-terminus and disulfide bridge (chapter 3 and 4) were synthesized using Fmoc chemistry at the Institut de Biologie Intégrative (IFR83) at the University Pierre et Marie Curie. The peptide was purified by reverse phase high-performance liquid chromatography (HPLC). The purity of the peptide was higher than 95%, as determined by analytical HPLC and the mass of the peptide was confirmed with MALDI-TOF mass spectrometry.

hIAPP (chapter 5) was purchased from Bachem (Batch #2500067).

Aβ<sub>42</sub> was obtained from American Peptide Company, Inc. (Batch #1207090T)

DOPC, and DOPS were obtained from Avanti® Polar Lipids, Inc., were used without further purification.

Sequence-verified plasmid for Aβ<sub>42</sub> with the additional methionine at N-terminus was obtained from the Department of Biochemistry, Chemical Centre of Lund University (Sweden).

Thioflavin T (ThT), Calcein, SDS and acrylamid/bisacrylamid solution, were obtained from Sigma.

b) Preparation of the peptides

*hIAPP*: Peptide stock solution was obtained by dissolving the peptide at a concentration of 1 mM in hexafluoroisopropanol (HFIP) and one hour incubation. Then, HFIP was evaporated and the sample was dried by vacuum dessication for at least 30 min. Depending on the experiment and project, the resulting peptide film was dissolved in different buffers.

- Chapter 3: peptide film was dissolved at a concentration of 1 mM in either DMSO (fluorescence experiments) or in a 10 mM sodium phosphate buffer, pH 7.4 (Circular Dichroism, NMR experiments).
- Chapter 4: peptide film was dissolved at a concentration of 1 mM in either DMSO (fluorescence experiments) or in a 50 mM sodium phosphate, 100 fluoride at pH 7.4 or pH 5.5, or in a 50 mM Tris, 100 mM sodium fluoride buffer pH 7.4 or pH 5.5

*Aβ42*: Peptide stock solution was obtained by dissolving the peptide at a concentration of 1 mM in a 1% NH<sub>4</sub>OH aqueous solution and was then adjusted in the required concentration in a 10 mM phosphate buffer pH 7.4.

c) Preparation of the vesicles

*i. Choice of the lipids*

Membrane models were used in chapter 4, for the study of the effect of charge and substitution of residue 18 on the fibrillation properties of IAPP. For this study, the membrane model we used was a mixture of DOPC/DOPS (7:3) (figure 44) as the presence of anionic lipids (DOPS) is known to enhance the interactions between IAPP and the membrane, the fibrillation, and as the composition of the membrane model is a good mimetic for the pancreatic islet of Langerhans.<sup>12</sup>

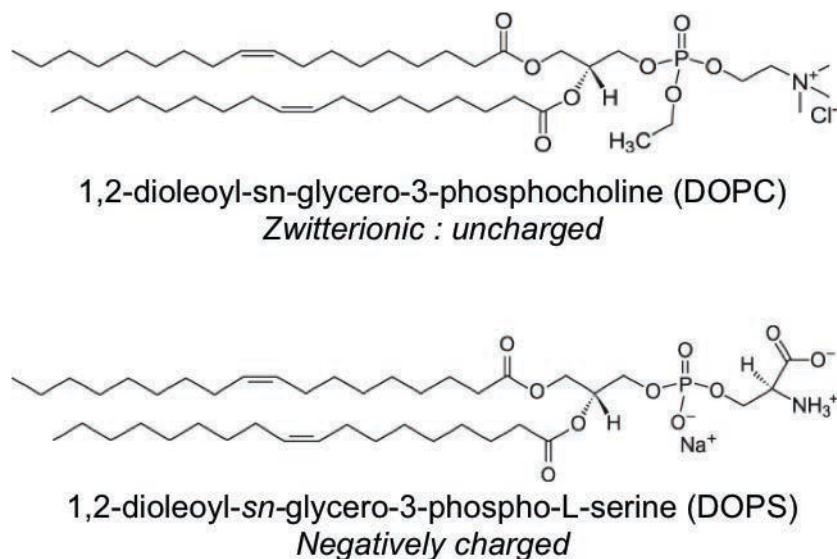


Figure 44: Chemical structures of DOPC and DOPS

Many different techniques were used for the study of IAPP wild type and mutants. Depending on the experiments, we used either monolayers or small or large unilamellar vesicles which preparation will be described below.

*ii. Preparation of Small/Large Unilamellar Vesicles (S/LUV)*

The lipids, as a stock solution in chloroform, are mixed at a 7:3 ratio in a glass tube. Then, chloroform is successively evaporated under nitrogen gas and put in a vacuum dessicator for at least 30 minutes. The dry mixture is then hydrated with a buffer for at least 30 minutes, in order to solubilize the lipids in the buffer. The mixture, composed of multilamellar vesicles is submitted to ten freeze/thaw cycles. This step will allow the disruption of the phospholipid layers and separating the lamellae of the vesicles thus leading to unilamellar vesicles of different sizes.<sup>13</sup>

In order to have the most homogeneous mixture, the formed unilamellar vesicles are ten times filtered (21 passes through the membrane) at 50 nm (formation of SUV) or 200 nm (formation of LUV) with a mini-extruder (Avanti Polar Lipids).

*iii. Preparation of calcein vesicles (LUV 200 nm)*

The lipid preparation for calcein vesicles is identical as described in paragraph *ii*. The dry mixture is however hydrated by a buffer containing 50 mM of calcein. Calcein is difficult to dissolve and acidifies the buffer, so pH has to be measured and adjusted before addition to



the lipids. The lipid mixture, once hydrated undergoes ten freeze/thaw cycles before being extruded 10 times with a mini extruder (Avanti Polar Lipids). To remove calcein outside the loaded LUVs, a size exclusion column (Sephadex G-50, fine) was used. The column was equilibrated with the buffer with outside buffer. The elution was performed by centrifugation (1 min at 3000g) using buffer without calcein.

*iv. Quantification of the phospholipid concentration*

The concentration of phospholipids in the lipid stock solutions and in the samples of prepared vesicles was quantified by the Rouser method.<sup>14</sup>

For this quantification, a solution of  $\text{KH}_2\text{PO}_4$  at a known concentration of 0.5 mM was used as a standard, in order to build a calibration curve. This standard solution as well as 20 to 40 nmol of our vesicles samples are introduced into glass tubes and placed in an oven at 150°C for about one hour for evaporation of the solvent. Once the tubes are completely dry, 0.3 mL of perchloric acid are added on the lipid film and tubes, closed with glass beads, and placed in a heating block for 2 hours. Then, the tubes are cooled down and successively 1 mL of  $\text{H}_2\text{O}$ , 0.4 mL of ammonium molybdate 1.25% (w/v) and 0.4 mL of freshly prepared solution of ascorbic acid 0.5% (w/v) are added into the tubes. After mixing the solution, the tubes are placed in boiling water for 6 minutes then cooled down.

The phosphate groups react with the ammonium molybdate in an acidic medium to form a phosphomolybdic acid complex according to the following reaction:



The complex, initially yellow (oxidation degree: +VI) is reduced by the addition of ascorbic acid in the solution (oxidation degree of the complex: +V) leading to a blue coloration. The absorbance of the samples is then measured at a wavelength of 797 nm. The final concentration of the phospholipids in our samples is calculated out of the calibration curve with the Beer-Lambert law.

The quantification of phospholipids is done on every preparation of unilamellar vesicles. For LUV, the quantification is usually carried out prior to the experiments (fluorescence, circular dichroism). SUV are less stable, therefore, an estimation of the concentration is done, and precise quantification of phospholipids are done after the NMR experiments.

## 9. Expression of A $\beta$ 42

Expression of the peptide was done following the protocol of Walsh et al. 2011<sup>15</sup> using a plasmid construction of A $\beta$ 42 containing an exogenous methionine residue at its N-terminus.

### *i. Experimental protocol*

#### **Bacterial expression (non labeled peptide):**

An overnight culture containing 40 mL of LB broth (10 g/L Casein Peptone, 5 g/L Yeast Extract, 10 g/L NaCl, pH 7.2) was inoculated with an A $\beta$ 42 stock solution BL21(DE3) pLysS *Escherichia coli* bacteria in the presence of 100  $\mu$ g/mL ampicillin and 30  $\mu$ g/mL chloramphenicol. After cell growth in an incubator at 37°C and agitation at 220 rpm, the culture was transferred in a 500 mL day culture (LB broth, 100  $\mu$ g/mL ampicillin, 30  $\mu$ g/mL chloramphenicol) such as the starting optical density (OD) of the medium at 600 nm was 0.05. When the density of cells reached an OD<sub>600nm</sub> of 0.6, peptide expression was induced by adding 1 mM of Isopropyl- $\beta$ -D-thiogalactoside. Cell growth continued for 3 more hours before the cells were harvested. Medium was then centrifuged at 2800 g for 20 minutes at 4°C and cell pellets were resuspended in a 10 mM Tris, 1 mM EDTA, pH 8 buffer (« buffer A »).

#### **Bacterial expression (double labeled peptide <sup>13</sup>C, <sup>15</sup>N):**

The double-labeled peptide was expressed and purified following the Marley protocol.<sup>16</sup> Overnight cell culture was set up as for the non-labeled peptide. This culture was then transferred in 8 flasks of 500 mL day culture (LB broth, 100  $\mu$ g/mL ampicillin, 30  $\mu$ g/mL chloramphenicol) such as the optical density (OD) of the medium at 600 nm was 0.05. When the density of cells reached an OD<sub>600nm</sub> of 0.6, the culture was centrifuged at 2,800 g for 15 minutes at 20°C. Supernatant was removed and cell pellets were resuspended in 2\*500 mL of M9 minimal medium without nutriment (Na<sub>2</sub>HPO<sub>4</sub>, 7 H<sub>2</sub>O 12.8 g/L, KH<sub>2</sub>PO<sub>4</sub> 3g/L, NaCl 0.5 g/L, MgSO<sub>4</sub> 1 mM, CaCl<sub>2</sub> 0.1 mM, thiamine 10mg/L, ampicillin 100 mg/L, chloramphenicol 30 mg/L, yeast nitrogen base 1.7 g/L). Cultures were replaced at 37°C/220 rpm in the agitator-incubator for about 45 minutes for clearance of LB broth nutriment inside the bacteria. Then, labeled <sup>13</sup>C glucose (4 g/L) and <sup>15</sup>N ammonium chloride (1 g/L) were added to the cultures. After another incubation of 45 minutes, peptide expression was induced by adding 1 mM of Isopropyl- $\beta$ -D-thiogalactoside. After 3 hours, cells were harvested and

culture was then centrifuged at 2800 g for 20 minutes at 4°C. Cell pellets were resuspended in a 10 mM Tris, 1 mM EDTA, pH 8 buffer (« buffer A »).

### **Purification:**

Cell pellets were sonicated 5 times during 10 seconds on ice then centrifuged at 15,000 g for 20 minutes at 4°C. Supernatant was discarded and pellets were resuspended in 20 mL of Buffer A. This cycle of sonication-centrifugation was repeated twice more before the pellets were resuspended in 10 mL of 10 mM Tris, 1 mM EDTA, 8 M Urea, pH 8 buffer and sonicated as described previously until the obtained solution was clear. This solution was then diluted 5 times in buffer A and mixed with 20 mL of DEAE cellulose resin for purification.

The fractions “B1” and “B2” were then purified on a Hypersep C18 column. After the column was washed with 5 mL of acetonitrile 10%, elution was done with 6 x 5 mL acetonitrile 35%, NH<sub>4</sub>OH 0.1%, then the column was washed again with 5 mL acetonitrile 100%

#### *ii. Troubleshooting and protocol optimization*

The main problem I encountered during the expression and purification of Aβ42 was the desalting and the concentration of the peptide.

#### ➤ Cut-off membranes

Following the protocol of Walsh *and al.*, we first tried to concentrate and eliminate the salt in our samples using cut off membranes.

#### Purification and concentration of B1 fraction:

Cut-off 30 kDa (Volume: 40 mL)	3 x centrifugation at 3000 g, 4°C, 15 minutes
Cut-off 3 kDa (Volume solution: 35 mL, volume of the falcon: 15 mL, 2 falcons were used)	Centrifugation at 5000 g, 4°C for (1) 40 minutes, (2) 50 minutes, (3) 40 minutes

### Change of buffer:

As we wanted to eliminate the presence of Tris/HCl and NaCl in the solution, we used two different buffers. The first buffer was a 10 mM Phosphate buffer as it was used for the studies of A $\beta$ 42 (chapter 3) or milliQ water. Centrifugation was done at 5000 g for 60 minutes at 4°C. After centrifugation, less than 1 mL was left above the membranes in both falcons. The solutions were retrieved, placed in two eppendorfs and lyophilized. Before lyophilization, 50  $\mu$ L of each solution was taken for gel electrophoresis analysis. The gel electrophoresis showed that a band corresponding to the peptide (4 kDa) was observed in the flow through of the 30 kDa membrane as expected. However, no bands associated with A $\beta$ 42 could be seen in the samples that were taken above 3 kDa after concentration and change of buffer. This result showed that either the peptide had aggregated during the centrifugation process or, that A $\beta$ 42 was stuck to the cut-off membrane, leading to a very small yield of purified peptide.

#### ➤ Dialysis

In order to obtain higher amount of purified peptide, and to avoid the use of membranes on which the peptide could stick, we tried another technique, dialysis to desalt the peptide and change our buffer. Different set ups were carried out, changing either the length of the dialysis or the number of baths.

### Fraction “B1”:

*Length of dialysis: overnight*

Gel electrophoresis on the samples taken before and after dialysis showed bands corresponding to the peptide in its monomeric form. The bands, although very clear, have about the same intensity, suggesting that there was no loss of material during the dialysis (figure 45).

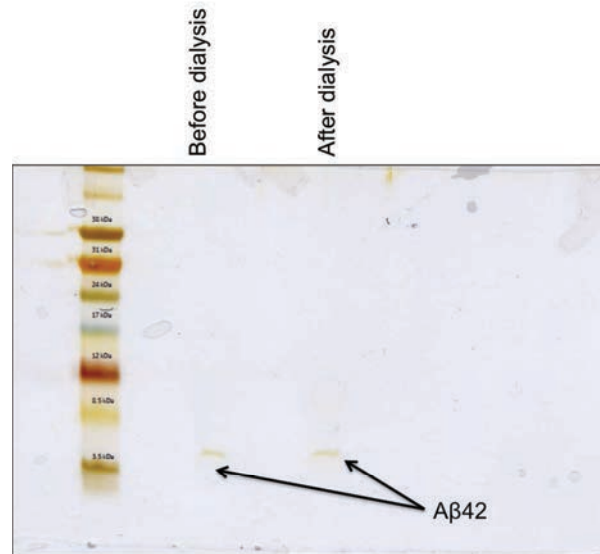


**Figure 45: Results of gel electrophoresis after dialysis of fraction B1.**

Bands corresponding to the peptide in its monomeric form can be observed on the gel. Revelation was done by silver staining.

Fraction “B2”:

*Length of dialysis:* 2 x 3h, changing the solution in between

*Quantity of material weighed in the eppendorf:* 8 mg

As previously, gel electrophoresis showed bands corresponding to the monomeric peptides in the samples taken before and after dialysis. Peptide concentration was high enough to be detected by Coomassie blue staining (figure 46).

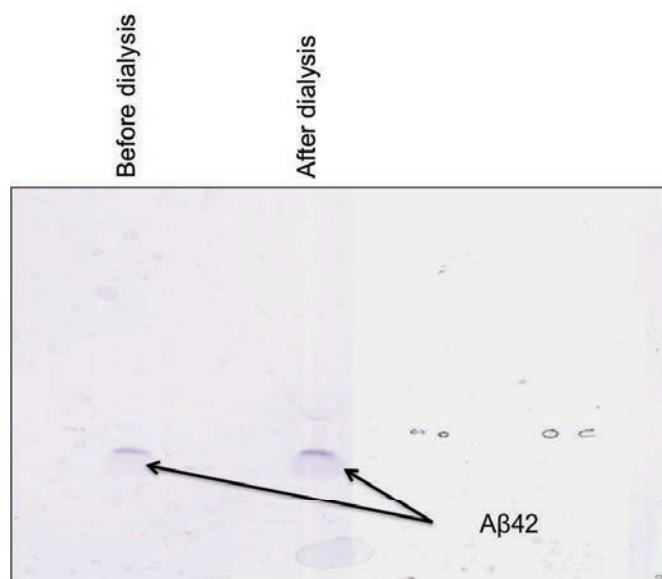


**Figure 46: Results of gel electrophoresis after dialysis of fraction B2.**

Bands corresponding to the peptide in its monomeric form can be observed on the gel. Revelation was done by Coomassie blue staining

NMR analysis: the presence of Tris and EDTA was observable on the spectrum as well as the peaks that were attributed to A $\beta$ 42. A series of  $^1\text{H}$  NMR experiments was recorded in order to observe any evolution of the signal overtime. Results have shown that the signal of the peptide decreased over time, as observed with the synthetic peptide (figure 47).

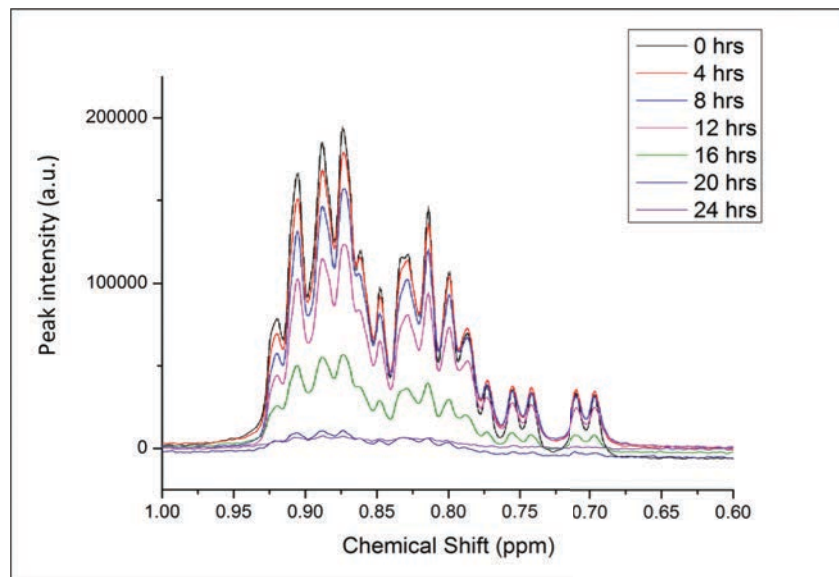


Figure 47:  $^1\text{H}$  NMR experiments on A $\beta$ 42 peptide after dialysis.

A signal corresponding to the monomer was observed. Peak intensity decreased over time, suggesting the aggregation of the peptide.

### Conclusion, advantages and drawbacks:

Dialysis turned out to be a better way of purification for our peptide than the cut-off system as A $\beta$ 42 could be retrieved after the process. MALDI-TOF analysis and NMR experiments showed that the peptide had a satisfying level of purity and was mainly monomeric, as the signal on the NMR spectra is quite narrow. The technique showed nevertheless some drawbacks. The attempted estimation of the peptide concentration by measurement of the absorbance with a NanoDrop spectrophotometer ( $\lambda = 275$  nm, absorbance of the tyrosine) showed that the concentration of the peptide was very low and was difficultly detected in reason of the broad peak associated with the peptide bond at 240 nm. Dialysis also dealt with large volumes of samples (about 20 mL) and does not allow us to concentrate the sample prior or during the process. Moreover, NMR spectra also showed the presence of remaining salts, mainly Tris and Urea, which explains the excessive mass in comparison to the peptide concentration that was weighted after lyophilization. Given these drawbacks, the protocol was further optimized as we wanted to find a technique that would allow us to desalt and concentrate our peptide.

➤ Liquid chromatography – C18, Batch mode.

Given the many hydrophobic regions of A $\beta$ 42, chromatography using a C18 apolar column seemed to be a good option for the desalting of the peptide. In addition, the use of chromatography allowed an elution with low volumes of solvent, hence the concentration of the peptide.

#### Test on Sep-Pak® C18 (Waters):

Given the low concentration of the peptides we charged about 10 mL of fraction “B1” and “B2” on the column. The elution was done roughly by 2x1 mL Acetonitrile 80%, NH<sub>4</sub>OH 0.1%. The collected fractions were then lyophilized and the material was then characterized by mass spectrometry and gel electrophoresis. Although, no bands corresponding to the peptide could be observed by electrophoresis, analysis by mass spectrometry showed a peak at 4645 Da, corresponding to A $\beta$ 42 with the addition of the methionine N-terminal residue.

#### Hypersep™ C18 – Cartridge (Thermo scientific):

As the previous step with the Sep-Pak gave promising results, we set up the same experiments using Hypersep® C18 columns (5 mL, Thermo Scientific). Again, fractions “B1” and “B2” were charged on the column before elution

#### **First protocol of elution:**

- 5 x 5mL of ACN 80%, NH<sub>4</sub>OH 0.1%
- 1 x ACN 100%

#### **Analysis of the fractions:**

Gel electrophoresis showed the presence of monomeric peptide as well as impurities after elution. This suggested that the concentration of acetonitrile was too high for the elution of pure peptide (figure 48).

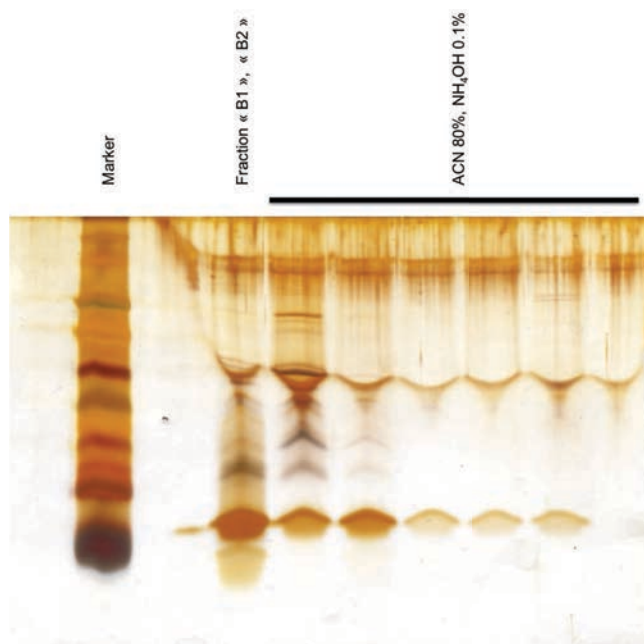


Figure 48: Gel electrophoresis of purified fractions of A $\beta$ 42, elution with 80% ACN, 0.1% NH<sub>4</sub>OH

Considering those results, we changed our protocol of purification, including washing steps and elution with a lower percentage of acetonitrile in the buffer.

### Second protocol of elution:

- 5 mL ACN 10% (washing step)
- 4 x ACN 35% NH<sub>4</sub>OH 0.1% (collected in the same falcon)
- 5 mL ACN 80% NH<sub>4</sub>OH 0.1%
- 5 mL ACN 100%

### Analysis of the fractions:

Gel electrophoresis showed that after purification, the peptide was found in its highest concentration in the fractions of 35% acetonitrile, 0.1%NH<sub>4</sub>OH. Mass spectrometry showed a peak at 4647 Da corresponding to the peptide A $\beta$ 42 with the addition of methionine on N-terminus. Although it was difficult to estimate the exact concentration of the peptide in solution, amounts of materials were weighed and samples were prepared following the same protocol as the synthetic peptide for further experiments. ThT fluorescence assay showed sigmoidal curves, consistent with the fibrillation of the peptide. The observation of the peptide after incubation for a week in a phosphate buffer at pH 7.4 showed the presence of large fibrillar mats (figure 49 to 51).



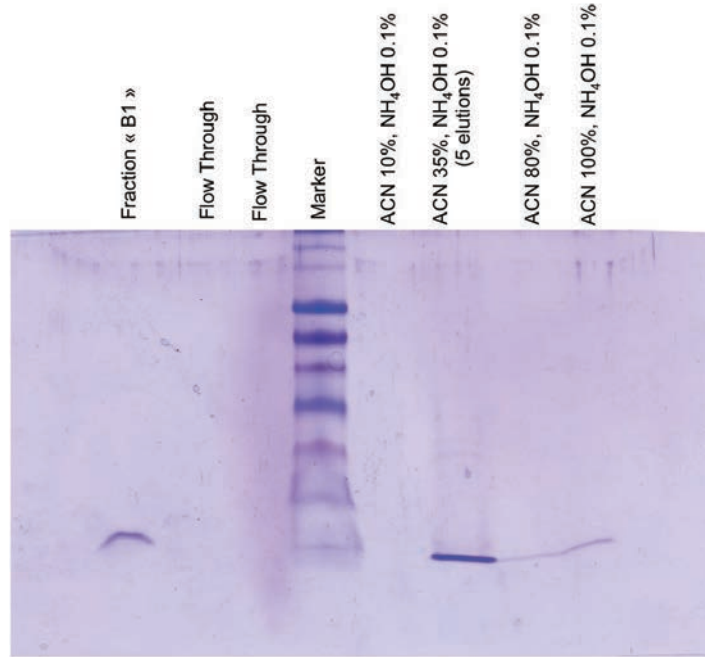


Figure 49: Gel electrophoresis on the different fractions of the purified peptide.

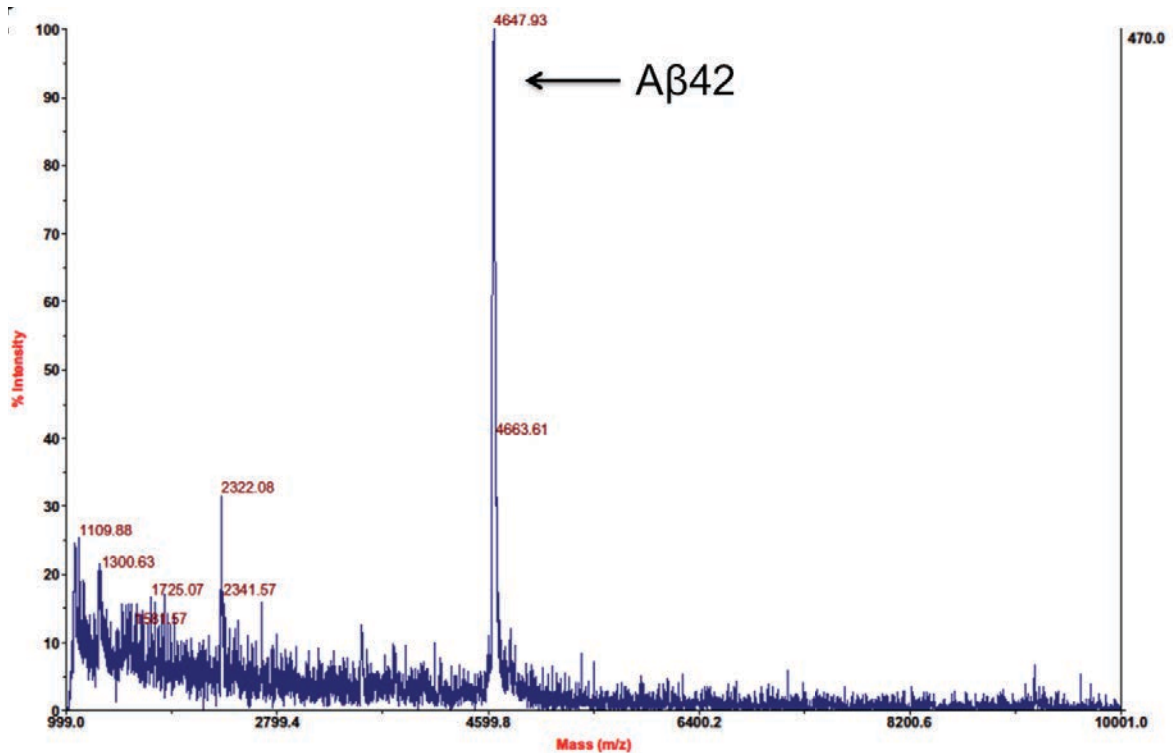


Figure 50: Mass spectrometry of purified A $\beta$ 42.

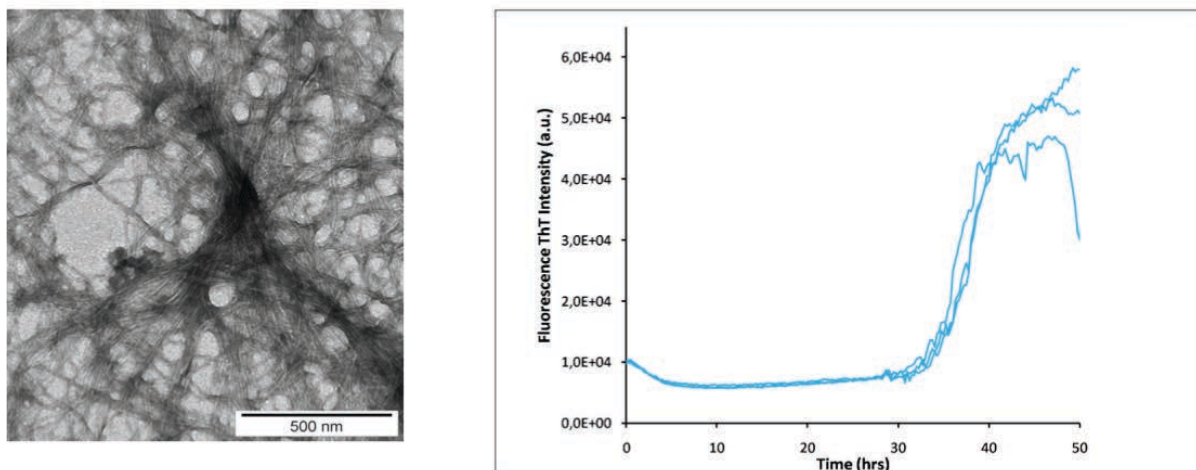


Figure 51: MET observation of purified A $\beta$ 42 after 7 days of incubation (left), ThT fluorescence assay on purified peptide (right).

### Conclusion, advantages and drawbacks:

The obtained peptide is mainly monomeric, and no major impurities (proteins or peptides) are detected by MALDI-TOF spectrometry. NMR and fluorescence experiments showed that the peptide tended to aggregate over time in a time range that was similar to synthetic A $\beta$ 42 (i.e. within the time course of a single ThT fluorescence experiments, which is of 48 to 60 hours depending on the peptide concentration) forming dense mats of amyloid fibrils. This method was quick and efficient to obtain the monomeric peptide, and was therefore the chosen protocol for further purifications of A $\beta$ 42. However, NMR spectra on the peptide showed the presence of remaining salts (Tris, EDTA, Urea) in the sample. This leads to two drawbacks: 1/ the salts may influence the kinetics of oligomerization of the peptide, 2/ it induces a bias in the estimation of the quantity of peptide obtained after purification and lyophilisation as we do not know the exact quantity of remaining salts in the sample. Therefore, estimation of the concentration of the peptide for further experiments remains a critical point.

<sup>1</sup> Biancalana, Matthew, and Shohei Koide. "Molecular Mechanism of Thioflavin-T Binding to Amyloid Fibrils." *Biochimica et Biophysica Acta (BBA) - Proteins and Proteomics* 1804, no. 7 (July 2010): 1405–12. doi:10.1016/j.bbapap.2010.04.001.

<sup>2</sup> Reinke, Ashley A., Han Yiau Seh, and Jason E. Gestwicki. "A Chemical Screening Approach Reveals That Indole Fluorescence Is Quenched by Pre-Fibrillar But Not Fibrillar Amyloid-B." *Bioorganic & Medicinal Chemistry Letters* 19, no. 17 (September 1, 2009): 4952–57. doi:10.1016/j.bmcl.2009.07.08

- 
- <sup>3</sup> Reinke, Ashley A., and Jason E. Gestwicki. "Insight into Amyloid Structure Using Chemical Probes: Amyloid Structure Using Chemical Probes." *Chemical Biology & Drug Design* 77, no. 6 (June 2011): 399–411. doi:10.1111/j.1747-0285.2011.01110.x.
- <sup>4</sup> Reinke, Ashley A., Gelareh A. Abulwerdi, and Jason E. Gestwicki. "Quantifying Prefibrillar Amyloids in Vitro by Using a 'Thioflavin-Like' Spectroscopic Method." *Chembiochem: A European Journal of Chemical Biology* 11, no. 13 (September 3, 2010): 1889–95. doi:10.1002/cbic.201000358.
- <sup>5</sup> Lorenzo, A., and B A Yankner. "Beta-Amyloid Neurotoxicity Requires Fibril Formation and Is Inhibited by Congo Red." *Proceedings of the National Academy of Sciences of the United States of America* 91, no. 25 (December 6, 1994): 12243–47.
- <sup>6</sup> Kim, Yong-Sung, Theodore W. Randolph, Mark C. Manning, Fred J. Stevens, and John F. Carpenter. "Congo Red Populates Partially Unfolded States of an Amyloidogenic Protein to Enhance Aggregation and Amyloid Fibril Formation." *Journal of Biological Chemistry* 278, no. 12 (March 21, 2003): 10842–50. doi:10.1074/jbc.M212540200.
- <sup>7</sup> Kelly, Sharon M., Thomas J. Jess, and Nicholas C. Price. "How to Study Proteins by Circular Dichroism." *Biochimica et Biophysica Acta (BBA) - Proteins and Proteomics* 1751, no. 2 (August 2005): 119–39. doi:10.1016/j.bbapap.2005.06.005.
- <sup>8</sup> Evans, Jeremy N. S. *Biomolecular NMR Spectroscopy / Jeremy N.S. Evans*. Oxford ; New York : Oxford University Press, 1995., 1995.
- <sup>9</sup> Gras, Sally L., Lynne J. Waddington, and Kenneth N. Goldie. "Transmission Electron Microscopy of Amyloid Fibrils." In *Protein Folding, Misfolding, and Disease*, edited by Andrew F. Hill, Kevin J. Barnham, Stephen P. Bottomley, and Roberto Cappai, 752:197–214. Totowa, NJ: Humana Press, 2011. [http://link.springer.com/10.1007/978-1-60327-223-0\\_13](http://link.springer.com/10.1007/978-1-60327-223-0_13).
- <sup>10</sup> Brunelle, Julie L., and Rachel Green. "One-Dimensional SDS-Polyacrylamide Gel Electrophoresis (1D SDS-PAGE)." In *Methods in Enzymology*, 541:151–59. Elsevier, 2014. <http://linkinghub.elsevier.com/retrieve/pii/B9780124201194000124>.
- <sup>11</sup> Hachmann, John P., and Joseph W. Amshey. "Models of Protein Modification in Tris–glycine and Neutral pH Bis–Tris Gels during Electrophoresis: Effect of Gel pH." *Analytical Biochemistry* 342, no. 2 (July 2005): 237–45. doi:10.1016/j.ab.2005.04.015.
- <sup>12</sup> Díaz, Graciela B., Ana Maria Cortizo, María Elisa García, and Juan José Gagliardino. "Lipid Composition of Normal Male Rat Islets." *Lipids* 23, no. 12 (1988): 1125–28.
- <sup>13</sup> Castile, Jonathan D., and Kevin MG Taylor. "Factors Affecting the Size Distribution of Liposomes Produced by Freeze–thaw Extrusion." *International Journal of Pharmaceutics* 188, no. 1 (1999): 87–95.
- <sup>14</sup> Rouser, George, Sidney Fleischer, and Akira Yamamoto. "Two Dimensional Thin Layer Chromatographic Separation of Polar Lipids and Determination of Phospholipids by Phosphorus Analysis of Spots." *Lipids* 5, no. 5 (1970): 494–96.
- <sup>15</sup> Walsh, Dominic M., Eva Thulin, Aedín M. Minogue, Niklas Gustavsson, Eric Pang, David B. Teplow, and Sara Linse. "A Facile Method for Expression and Purification of the Alzheimer's Disease-Associated Amyloid B-

---

Peptide: Expression and Purification of the Amyloid B-Peptide.” *FEBS Journal* 276, no. 5 (March 2009): 1266–81. doi:10.1111/j.1742-4658.2008.06862.x.

<sup>16</sup> Marley, Jonathan, Min Lu, and Clay Bracken. “A Method for Efficient Isotopic Labeling of Recombinant Proteins.” *Journal of Biomolecular NMR* 20, no. 1 (2001): 71–75.



# **Chapter 3:**

**Insights into the kinetics and mechanism of fibrillization of hIAPP in solution**



Understanding the pathways that lead to the formation of toxic amyloid species and especially pinpointing which species and what mechanism are associated to cell death are of great interest in the further development of therapeutic agents in order to prevent and/or delay the progression of amyloid diseases. Although widely studied, the mechanisms involved in the amyloid fibril formation are yet to be completely understood. Such mechanistic studies are hampered by the fast kinetics of fibrillization and the formation of many intermediate species that are transient in nature and structurally heterogeneous. As the diseases have always been linked to the accumulation of large insoluble amyloid fibrils, it was initially believed that cell death was induced by these mature fibrils. Recently, however, increasing evidence has shown that the toxicity of amyloid peptides is more likely mediated by oligomeric species or the ongoing oligomerization process rather than by the fibrils<sup>1,2,3</sup>. In this regard, it is of great importance to identify the nature of the formed species and the mechanisms involved in the early stages of oligomerization of amyloid peptides, as they would be critical targets in the prospect to disrupt the amyloidogenic process or reorient it into a non-toxic off-pathway, so as to reduce the cytotoxicity of the peptide.

A general common pathway for fibril formation is believed to characterize all amyloid peptides and proteins. Initially soluble in solution, they undergo a conformational change, associated with a misfolding of the peptide/protein, which leads to oligomerization and insoluble  $\beta$ -sheet amyloid fibril formation. In addition to this, it has been shown that an anti-oligomer specific antibody, obtained by immunization of rabbits with A $\beta$  oligomers mimetics, was able to recognize peptides oligomers of not only A $\beta$  peptide, but also hIAPP and  $\alpha$ -synuclein. This suggests a common morphology of oligomers and putatively, similar mechanisms of fibrillization<sup>4,5</sup>. This hypothesis can be reinforced by a careful sequence comparison of hIAPP and A $\beta$ 42. Despite the lack of homology relationship, both peptides share close amino acid sequences (24% in identity and about 40% in similarity, Figure 52) and length (37 vs 42 residues). In addition to the sequence similarity, hIAPP and A $\beta$ 42 also share overlapping binding sites that trigger the formation of toxic aggregates residues 20-29 (SSNFGAIL) for IAPP and residues 28-35 for A $\beta$ 42 (GAIIGLM).

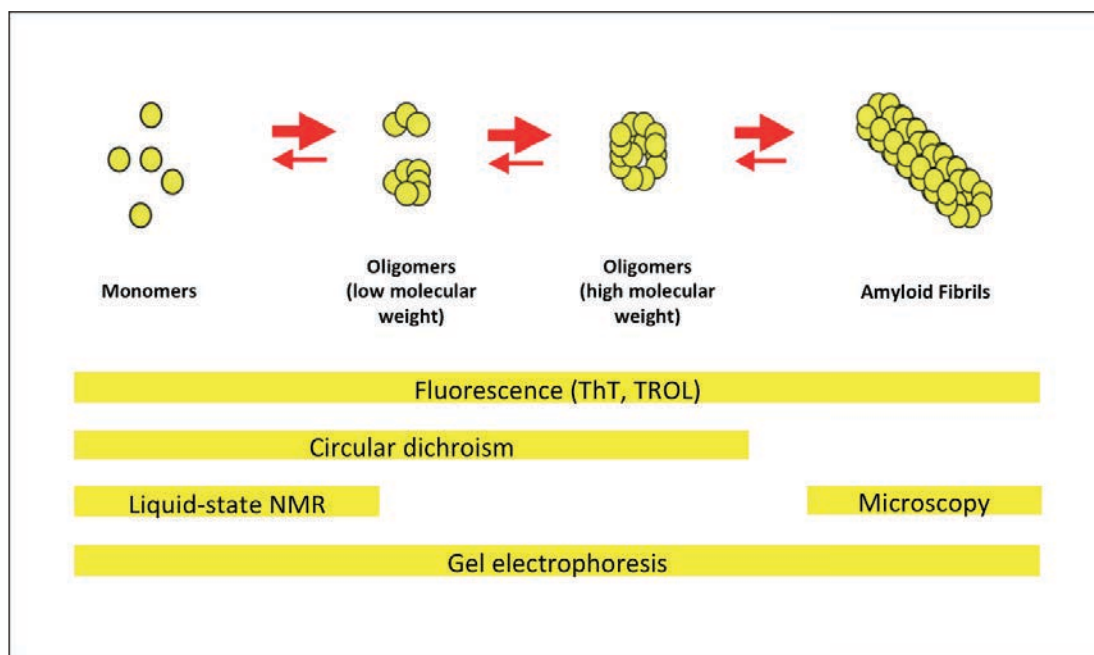
<b>A<math>\beta</math>42</b>	DAEFRHDSGYEVHHQKLVFFAEDVGSNKGAIIGLM VGGVVIA
<b>IAPP</b>	KCNTATCATQRLANFLVHSSNNFGAILSSSTNVGSNTY

Figure 52: Sequence alignment of A $\beta$ 42 and hIAPP. Blue: residues with similar physicochemical properties (charge, polarity), Green: identical residues



However, in spite of sequence similarities, diverging results have been reported in the literature regarding the oligomeric species for A $\beta$ 42 and hIAPP. Low molecular weight oligomers as well as protofibrils have been observed and characterized in the case of A $\beta$ 42 and for other amyloid peptides<sup>6,7</sup>. In contrast, hIAPP does not seem to form stable low molecular weight oligomers under comparable conditions<sup>8,9</sup>. In this context, our study here was to focus on the early stages of the oligomerization process of hIAPP in terms of mechanism of fibrillization and formation of oligomers.

A large number of biophysical and biochemical data have accumulated in the literature but it is not always easy to compare results obtained by different groups owing to the variability in peptide samples (peptide lots with different synthesis, purification and solubilization protocols) and the diversity of experimental conditions often imposed by technique limitations. For the sake of consistency and in order to compare results obtained by different spectroscopic techniques, we have paid much attention in this study to design experimental protocols using conditions as close as possible in terms of buffer compositions, physicochemical parameters (temperature, pH, ionic strength) and peptide concentration. We have carried out a panel of complementary biophysical experiments, each focusing on different stages of fibril formation in order to better characterize the oligomerization and fibrillization of hIAPP. Thioflavin T fluorescence (ThT) experiments are compulsory so as to observe the global fibrillization process over time. Circular dichroism (CD) experiments allowed us to monitor the secondary structure of different peptide species over time. Tryptophanol (TROL) fluorescence together with liquid state NMR experiments focus on the early stages of the process. TROL fluorescence is expected to yield details on the formation of small oligomeric species as this fluorescent probe was described to bind to prefibrillar species but not fibrils. Finally, the depletion of the monomer in solution as the peptide oligomerizes could be readily monitored by <sup>1</sup>H NMR. Gel electrophoresis have also been done on incubated samples of hIAPP and A $\beta$ 42 in an attempt to visualize oligomeric species, especially those of low molecular weight. Finally, electron microscopy (TEM) focuses on the final stage of fibrillization, as it allows us to observe large oligomers and particularly the fibrils morphology (Figure 53).



**Figure 53: Biophysical strategy for the study of hIAPP and A $\beta$ 42 oligomers and fibrils.**  
Each technique targets different species along the fibrillization pathway.

In addition, since we used fluorescent probes, ThT and TROL, at a high concentration of 75  $\mu$ M, it was a critical point to check whether these probes would not have any influence on the kinetics of fibrillization resulting from their interaction with the peptides. For this part of the study, we performed further NMR and CD experiments on our peptides in the presence and in the absence of ThT and TROL to observe the effects of probes on the fibrillization.

## 1. Results

### a) Study of the early stages of fibrillization

#### i. *ThT and TROL fluorescence assays*

The curves obtained by using ThT fluorescence were S-shaped, which is a well-known characteristic of amyloid fibril formation<sup>10</sup>. Data for hIAPP exhibited a lag phase of approximately 2 hours followed by an exponential growth phase over 1 hour using a peptide concentration of 75  $\mu$ M at room temperature. ( $t_{0.5} = 3.1 \pm 0.1$  hrs;  $\tau = 0.7 \pm 0.1$  hrs<sup>-1</sup>). These results show that the kinetics of fibrillization of hIAPP is very fast and that, given the steep of the sigmoid, it tends to stabilize large aggregates (protofibrils and fibrils) that bind to ThT dye over the small oligomeric species. Under the same conditions, fluorescence measurements for

A $\beta$ 42 at 75  $\mu$ M indicated that the kinetics of fibrillization were slower than those of hIAPP with a lag phase of approximately 4 hours followed by a growth phase of 10 hours ( $t_{0.5} = 9.8 \pm 0.1$  hrs;  $\tau = 2.9 \pm 0.1$  hrs<sup>-1</sup>). The longer elongation phase of A $\beta$ 42 could be explained by, first, the lower kinetics of oligomerization, but also by a progressive growth of fibrils, mediated by the formation of small oligomeric species, thus leading to a gradual binding to ThT probe (Figure 54A). We also observed that the signal at the plateau did not reach the same intensity for hIAPP and A $\beta$ 42. Indeed, after normalizing the curves (values for hIAPP being the 100% reference intensity) the plateau for A $\beta$ 42 reached only 45% of the maximum intensity of that of hIAPP. These results could first reflect differences regarding ThT binding properties for the two peptides. Indeed, ThT probe could have less affinity or fewer binding sites to A $\beta$ 42 or display different fluorescence properties (quantum yield) in the binding states. Alternatively, the amount and the morphologies of the mature fibrils may be different for both peptides. This is the reason why TEM studies were carried out in parallel to analyze the final formed species (see below).

Although ThT probe binds to large aggregates and allows us to observe the global kinetics of oligomerization process, it provides us no information about the formation of the species involved in nucleation stages. Therefore, we chose to use a recently described Thioflavin-like fluorescent probe, the tryptophanol (TROL), which exhibits opposite properties with respect to ThT. Indeed, TROL fluorescence turns out to be quenched when the probe binds amyloid peptides while ThT fluorescence is enhanced upon binding to amyloid species. Furthermore TROL binds to prefibrillar forms of amyloid peptides but not to mature fibrils<sup>11</sup> whereas ThT binds to both prefibrillar and fibrillar species.

We set up the TROL fluorescence assay in the laboratory using parameters described by Reinke et al. As expected, for both peptides TROL assays lead to decreasing fluorescence curves over time before reaching a plateau, indicating that the probe has bound to monomers or small oligomeric species that has formed in solution (Figure 54B). Interestingly, TROL fluorescence decay showed no apparent lag phase in the case of A $\beta$ 42 while a short lag phase of about 2 hours was observed for hIAPP.

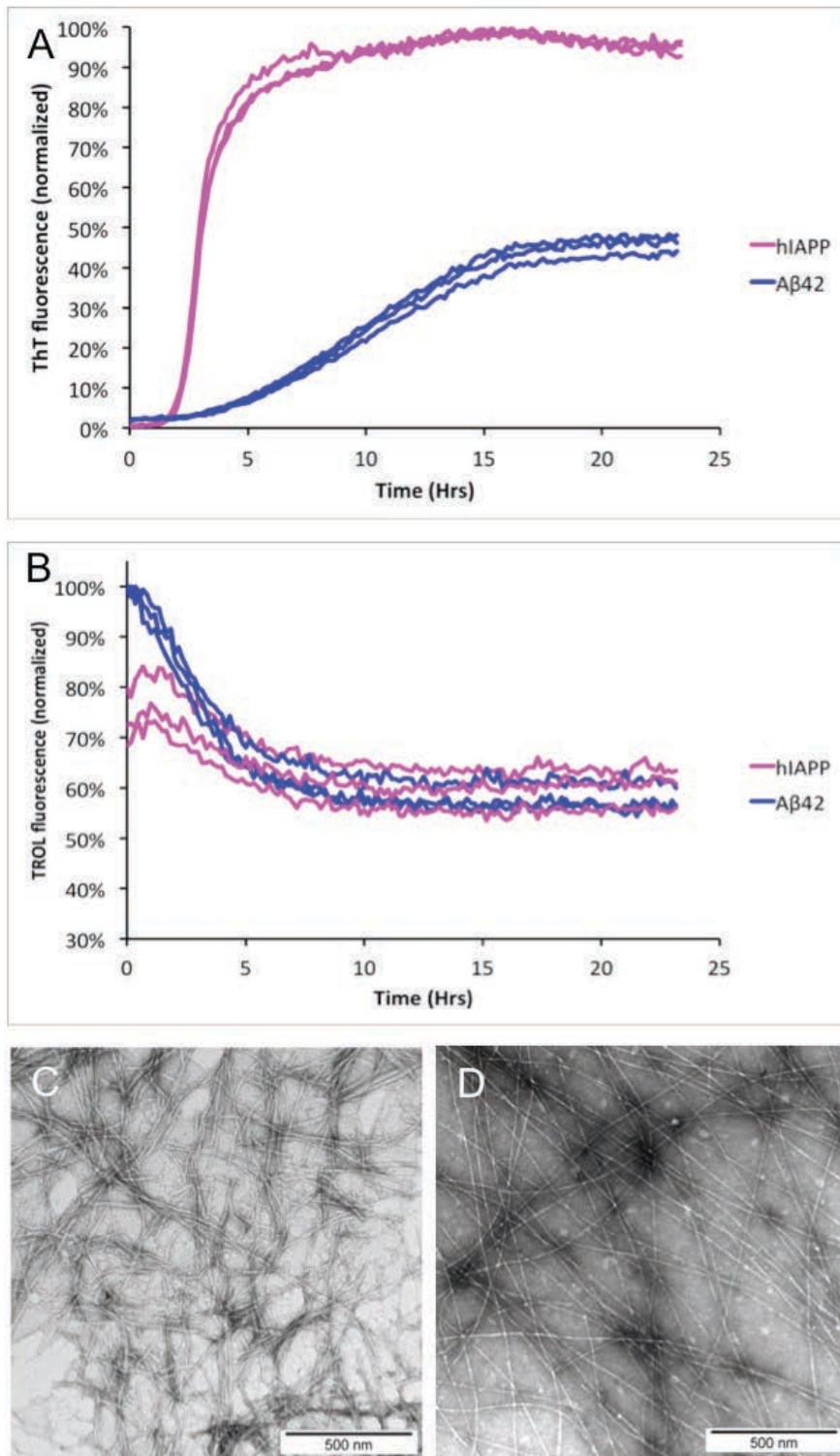


**Figure 54:** (A,B) Kinetics of fibrillization of hIAPP (magenta) and Aβ42 (blue) probed by ThT (A) and TROL (B) , fluorescence. ThT and TROL fluorescences were normalized to the highest value observed for hIAPP and Aβ42, respectively. (C, D) TEM of hIAPP (C) and Aβ42 fibrils (D) after 4 days of incubation.

Nevertheless, we noticed that curves drawn for hIAPP and Aβ42 were very similar as much for the decrease of the values as the stationary phase that was reached at the same time, approximately 10 hours for both peptides

From the ThT and TROL experiments, we observed a roughly inverse relationship between the signals. At early time, the TROL assay showed maximum monomeric or oligomeric content while ThT indicated low amounts of total aggregated hIAPP and A $\beta$ . Then, the TROL signal decreased for both peptides, while ThT signal, after a lag time, increased, showing that oligomerization and formation of large aggregates occurred.

Interestingly, the comparison of the times necessary to reach the fluorescence plateaus suggests mechanistic differences in fibrillization for the two peptides. In the case of hIAPP, the TROL signal was still decreasing after the plateau was reached in the ThT fluorescence experiment, which could indicate the coexistence, during a short time before the TROL fluorescence reaches a plateau, of either monomer or very small oligomers with large species and fibrils that are formed at a very fast rate but with no intermediates. A different trend is observed for A $\beta$ 42, the ThT signal was still increasing after the TROL signal reached equilibrium, which correlates with the fact that A $\beta$ 42 peptide undergoes different stages of oligomerization before forming large mature fibrils. This clearly suggested that hIAPP has a different mechanism of fibril formation than the one of A $\beta$ 42.

In addition to the fluorescence experiments and in order to investigate the contents of our samples, we carried out transmission electron microscopy (TEM) to detect the presence of amyloid fibrils and characterize the morphology of aggregated species that formed in our peptides samples. Observations of the samples that were incubated for 4 days at room temperature showed smooth and long fibrils about 10-12 nm wide for A $\beta$ 42 whereas hIAPP samples showed large and dense mats of fibrils that were about 5 to 8 nm wide, revealing that not only the two peptides had different kinetics of fibrillization but that they also have a distinct fibril morphology (Figure 54C et D).

## *ii. CD spectroscopy*

We next carried out CD experiments in order to evaluate the conformational changes of the peptide over time. CD spectrum of hIAPP, freshly dissolved in 10 mM phosphate buffer at 75  $\mu$ M concentration and pH 7.4, showed a curve with a negative minimum at 200 nm, thus revealing a prevailing unordered conformation, which is characteristic of the structure of the peptide in solution.<sup>12</sup> Upon a few hours of incubation, we were able to observe the disappearance of the minimum at 200 nm in favor of a negative peak at 220 nm and the apparition of a positive peak around 190 nm, indicative of a  $\beta$ -sheet structure. Kinetics measurements showed a lag time of 2 hours followed by the transition towards  $\beta$ -sheet

structure after 4 hours for hIAPP (Figure 55A). Deconvolution of the spectra allowed us to obtain the contribution of  $\beta$ -sheet conformation and random coil to the signal. At initial time, the deconvolution indeed indicates that the peptide is mainly disordered (78.7% random coil). Although the increase of  $\beta$ -sheet conformation can be observed over time (3.5 to 25%) can be observed, deconvolution of the final spectra still indicated a large amount of random coil signal, which was surprising given the characteristic signal for  $\beta$ -sheet that we observed. This result might be explained by the weak intensity of the dichroic signal, that can skew the deconvolution values (table 4)

	Random coil	$\beta$ -sheet	$\alpha$ -helix
hIAPP (initial time)	78.7 %	3.5 %	10.6 %
hIAPP (final time)	68.1 %	25%	6.2 %

**Table 4: Contribution of disordered state,  $\beta$ -sheet and  $\alpha$ -helical conformation to the structure of hIAPP at initial and final times.**

Deconvolution of the CD spectrum was done with CDfriend software.

As for A $\beta$ 42, the freshly dissolved peptide gave the same type of signal than hIAPP, with a minimum around 200 nm, showing that the peptide was mainly disordered in solution. Over time, a gradual transition is observed with the presence of an isodichroic point. The random coil state is predominant at the beginning of the experiment and gradually converts into a  $\beta$ -sheet conformation, with a minimum at 220 nm, which is observed after 14 hours (Figure 55B, table 5).

	Random coil	$\beta$ -sheet	$\alpha$ -helix
A $\beta$ 42 (initial time)	76.2 %	11.3 %	2.8 %
A $\beta$ 42 (final time)	67.2 %	22.1 %	10.8 %

**Table 5: Contribution of disordered state,  $\beta$ -sheet and  $\alpha$ -helical conformation to the structure of A $\beta$ 42 at initial and final times.**

Deconvolution of the CD spectrum was done with CDfriend software.

The differences between the evolutions of the spectra over time can be observed by plotting the ellipticity at 200 nm over time for hIAPP and A $\beta$ 42. The plotted data show a sigmoidal curve for hIAPP, showing the presence of two different states (the prevalent disordered species vs. the structured  $\beta$ -sheet species) while data for A $\beta$ 42 show a linear curve showing a gradual transition with a coexistence of the ordered and disordered state for the peptide (figure 55C).

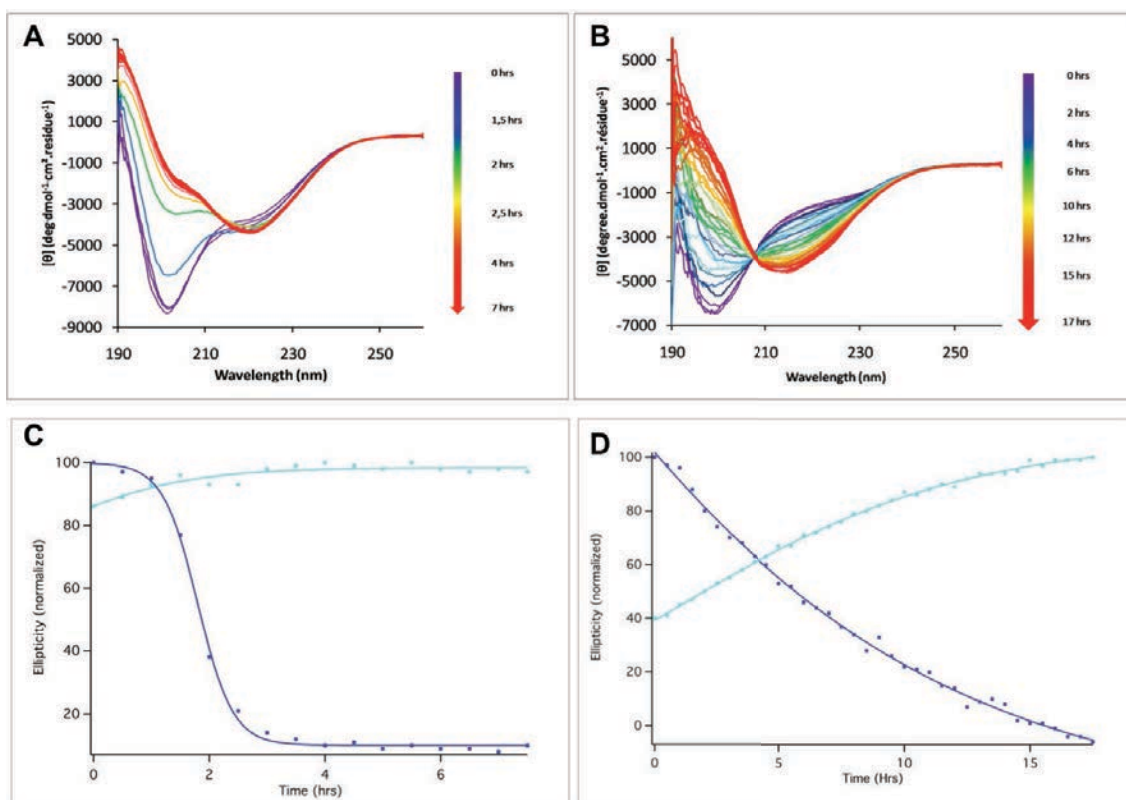


**Figure 55:** CD spectra of hIAPP (A) and A $\beta$ 42 (B) over time. Both peptides adopt a  $\beta$ -sheet conformation over time. The apparition of the  $\beta$ -sheet conformation prevalence is faster for hIAPP than for A $\beta$ 42 where it is more gradual with a distinctive isodichroic point (Peptide concentration: 75  $\mu$ M, Temperature: 30°C). (C) Ellipticity at 200 nm (pink) and 220 nm (green) of hIAPP (magenta). (D) Ellipticity at 200 nm (cyan) and 220 nm (blue) of A $\beta$ 42 at 30°C.

Our results were found in agreement with data that were obtained by fluorescence of ThT, once again presenting a faster kinetics of fibrillization for hIAPP in comparison with A $\beta$ 42. Further information can be inferred from the different shapes for the time evolution of CD ellipticities (Fig. 4C and 4D). The weak increase in the negative ellipticity for hIAPP at 220 nm while the negative peak at 200 nm decreases suggests that a fraction of  $\beta$ -sheet species is not visible in the CD spectrum. Indeed, the shape of the curve can be best explained by a conversion of random coil monomers (or small oligomers) into  $\beta$ -sheet oligomers in parallel with a conversion of  $\beta$ -sheet species into higher molecular weight species that do not contribute to the CD signal (presumably owing to precipitation or scattering).

The accumulation of kinetics data correlated to the actual presence of fibrils in our different samples led us to investigate the presence and dynamics of oligomeric species of our peptides in solution, thus, performing more complete experiments.

### *iii. NMR spectroscopy*

Cross results of fluorescence and circular dichroism have shown that hIAPP has different kinetics of aggregation than A $\beta$ 42 and may have a different pathway of fibrillization, but only little information can be inferred about the early stages of the oligomerization process and the species that are formed during this phase with those techniques. In order to get more insight on these initial steps, we used liquid state NMR spectroscopy. Our goal was to measure the kinetics of depletion of peptide monomers as well as to obtain indirect information on oligomeric species in solution that may interconvert with the monomer fraction.

One dimensional  $^1\text{H}$  NMR spectra were recorded at a peptide concentration of 75  $\mu\text{M}$  to be consistent with the results obtained with aforementioned techniques. On the first hand,  $^1\text{H}$  spectra allowed us to observe the soluble fraction of peptides corresponding to the monomer (or weakly oligomerized states), as inferred from the narrow linewidths, especially in the methyl region, and from diffusion coefficient measurements (see below). NMR signals from large oligomeric species, which tumble slowly on the NMR time-scale and behave like a solid, are expected to be very broad and therefore invisible to detection by liquid-state NMR experiments. Therefore, any variation over time of the peptide signal intensities was a source of information concerning the oligomerization kinetics of hIAPP and A $\beta$ 42. Figures 56 and 57 show that the methyl resonances intensity of hIAPP decreased dramatically within the first 3 hours of experiments, subsequently reaching a stationary state during the rest of the experiment with a weak residual signal. In the meantime, we can notice the apparition of a very broad signal around 0.7 ppm that can be ascribed to oligomeric hIAPP species of high molecular weight that have appeared in solution, allowing us to observe the aggregation of the peptide. In contrast, A $\beta$ 42 methyl signals intensity gradually decreased over time, starting in the first 3 hours of experiments until reaching a nearly stationary state, where the signal still persists, after more than 40 hours of incubation.



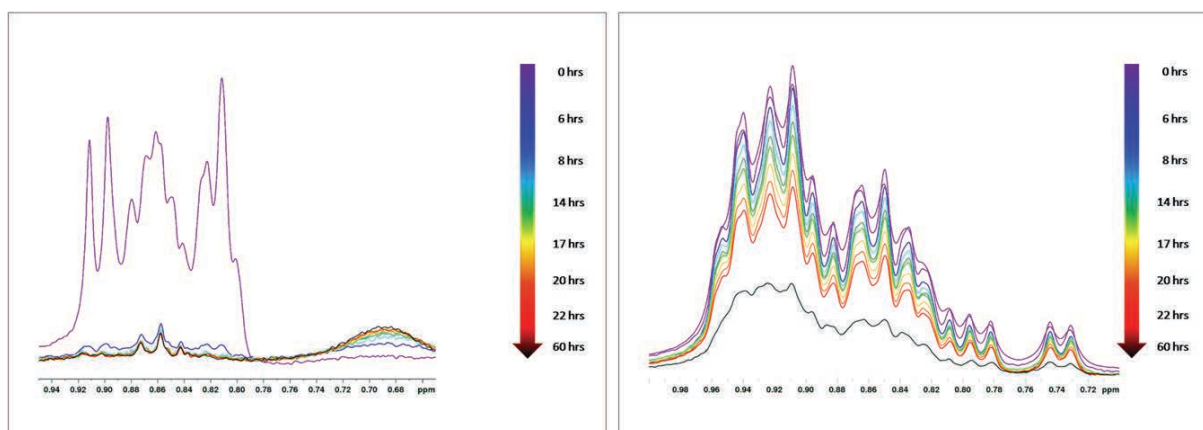


Figure 56: Methyl region of  $^1\text{H}$  NMR spectra of hIAPP (left) and  $\text{A}\beta_{42}$  (right) over time. hIAPP peak intensity decreases in less than 6 hours, showing no more monomer. A broad peak, indicative of high molecular weight oligomers appears in the meantime. Monomeric  $\text{A}\beta_{42}$  can still be observed after a gradual decrease and appearance of a plateau after more than 40 hours of experiment.

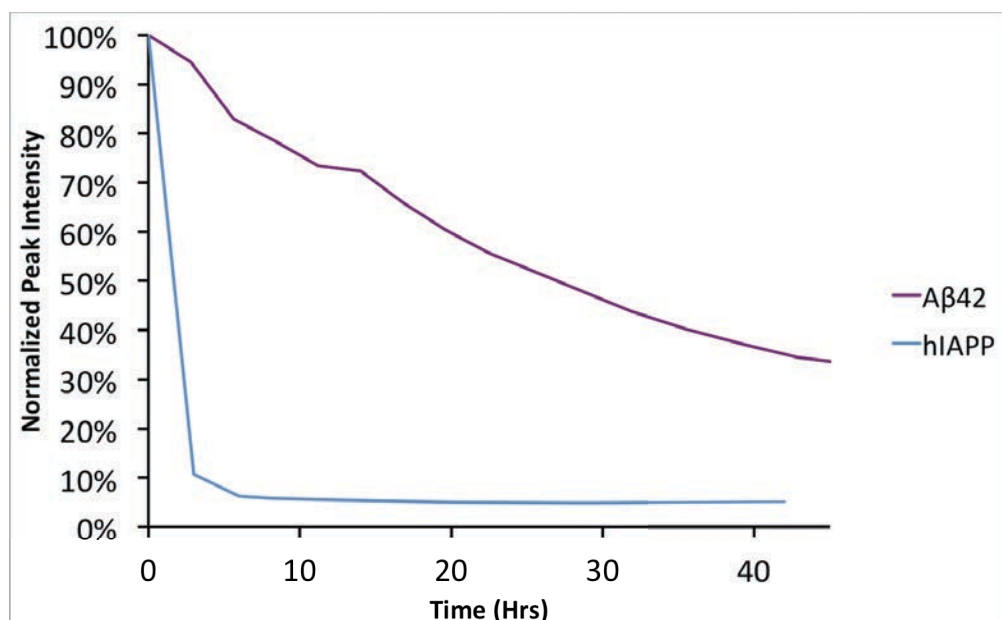


Figure 57: Time evolution of  $^1\text{H}$  resonance intensities for hIAPP and  $\text{A}\beta_{42}$  at  $30^\circ\text{C}$ . NMR signals were integrated between 0.7 and 1 ppm.

We also used magnetization transfer experiments in order to detect putative equilibria between the monomeric peptides and oligomeric states, which could be possible provided that the oligomerization equilibria occur in fast exchange on the NMR time scale. Saturation Transfer Difference (STD) experiments consist in the irradiation of large unobserved species in solution, *i.e.* the high molecular weight oligomers or fibrils. In the case of a fast exchange conversion between those species and monomers, the irradiation is transferred from the large oligomers to the smaller ones or to the monomer, leading to a decrease of signal intensity of the NMR visible low molecular weight species. As a part of this study, STD experiments

could show whether IAPP or A $\beta$ 42 species of different molecular weights coexist and interact with one another.

STD experiments were carried out by irradiating, for the on resonance experiment, the upfield region at  $-0.5$  ppm, which is devoid of signals for both IAPP and A $\beta$ 42 monomers. The STD experiments on A $\beta$ 42 shows the appearance of weak STD signals, as can be seen in the aromatic region (Figure 58D). Interestingly these STD signals increase over time, underlying an interaction in fast exchange between peptide monomer and oligomers whose concentration increases over time. For IAPP peptide, weak STD signals can be detected at the very beginning of the experiments before disappearing. In this latter case, the very fast peptide aggregation, which nearly consumes all the monomer in solution, prevents the observation of aggregation equilibria involving the residual monomer fraction.

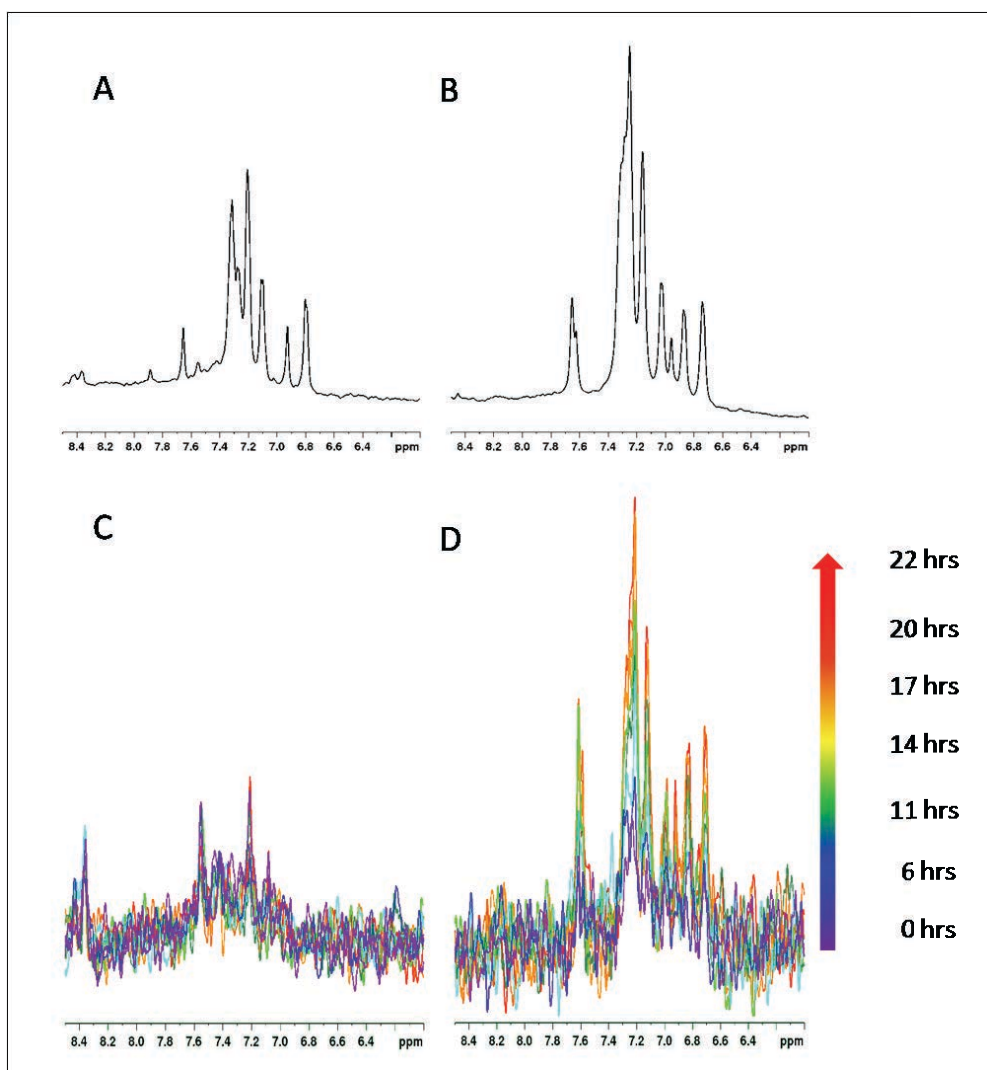


Figure 58: (A, B) Aromatic region of 1D  $^1\text{H}$  spectra of hIAPP (A) and A $\beta$ 42 (B) at  $t=0$ hr, (C, D) STD signal of hIAPP (C) and A $\beta$ 42 (D) over time at  $30^\circ\text{C}$ .

hIAPP shows a very weak signal close to the noise level, even at  $t=0$  hr where it could still be detected due to the presence of monomer in solution whereas A $\beta$ 42 shows an apparition of STD signal at  $t=0$ hr that increases over time.

Finally, to get information on the shape and size of aggregates, we determined the diffusion coefficients using PFG NMR experiments for hIAPP and A $\beta$ 42 at 30°C. The diffusion coefficient is inversely related to the hydrodynamic radius of the particle, which in turn is determined by the peptide compactness and also the degree of self-association. Table 7 exhibits the hydrodynamics parameters relative to the aggregation of hIAPP and A $\beta$ 42. The diffusion coefficient measured for A $\beta$ 42 at time  $t_0$  is close to values reported in the literature and is compatible with a peptide being mainly monomeric. An evolution of the diffusion coefficient is observed over time, decreasing from  $1.88 \cdot 10^{10} \text{ m}^2/\text{s}$  to  $1.47 \cdot 10^{10} \text{ m}^2/\text{s}$  in less than 24 hours. In the case of hIAPP, the fast kinetics of fibrillization made it very difficult to determine the diffusion coefficient of the monomer since its signal tended to disappear during the first 6 hours of incubation.

	A $\beta$ 42 (30°C)		hIAPP (30°C)	
	Ds ( $10^{10} \text{ m}^2/\text{s}$ )	$\Delta$ Ds ( $10^{10} \text{ m}^2/\text{s}$ )	Ds ( $10^{10} \text{ m}^2/\text{s}$ )	$\Delta$ Ds ( $10^{10} \text{ m}^2/\text{s}$ )
0 hrs	<b>1.88</b>	0.05	<b>1.11</b>	0.05
3 hrs	<b>1.87</b>	0.05	<b>1.06</b>	0.58
6 hrs	<b>1.83</b>	0.05	-	-
8 hrs	<b>1.73</b>	0.05	-	-
11 hrs	<b>1.60</b>	0.05	-	-
14 hrs	<b>1.51</b>	0.05	-	-
17 hrs	<b>1.48</b>	0.05	-	-
20 hrs	<b>1.47</b>	0.06	-	-
22 hrs	<b>1.47</b>	0.01	-	-

**Table 6: Diffusion coefficient for A $\beta$ 42 and hIAPP over time.**  
**The formation of high molecular weight species of hIAPP over time hampers the determination of the hydrodynamic parameter as the signal of the monomer disappears during the experimental time**

In light of these results and taking account that the kinetics of fibrillization of hIAPP was very fast at 30°C thus preventing us from observing any intermediate forms in the time of NMR experiments, we decided to perform further studies at lower temperatures, namely 20°C, 15°C and 10°C. At 20°C, we found that signals on  $^1\text{H}$  NMR spectra tended to decrease during the 6 first hours of experiment before reaching a stationary state further on (Figure 59A). Nevertheless, studies at 15°C and 10°C showed a very slow depletion rate over

time and high intensity, well resolved signals even after 48 hours of incubation (Figure 59B and C). The signals were integrated and plotted depending on the time (figure 60).

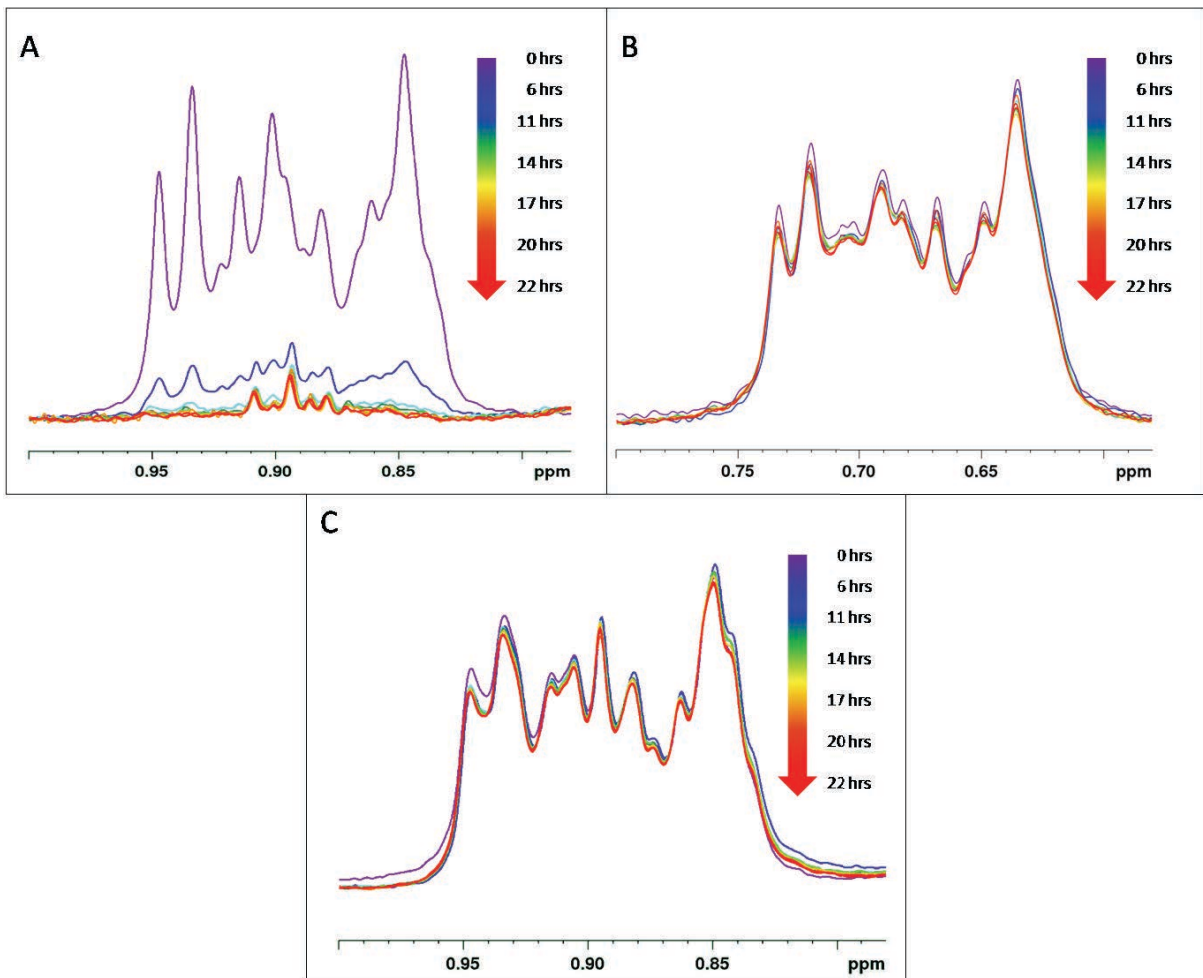


Figure 59: Monomer depletion of hIAPP at 20°C (A), 15°C (B) and 10°C (C) observed by NMR spectroscopy. At 20°C the signal disappears in the first 6 hours of experiment. At 10 and 15°C the signal remains stable over 22 hours.

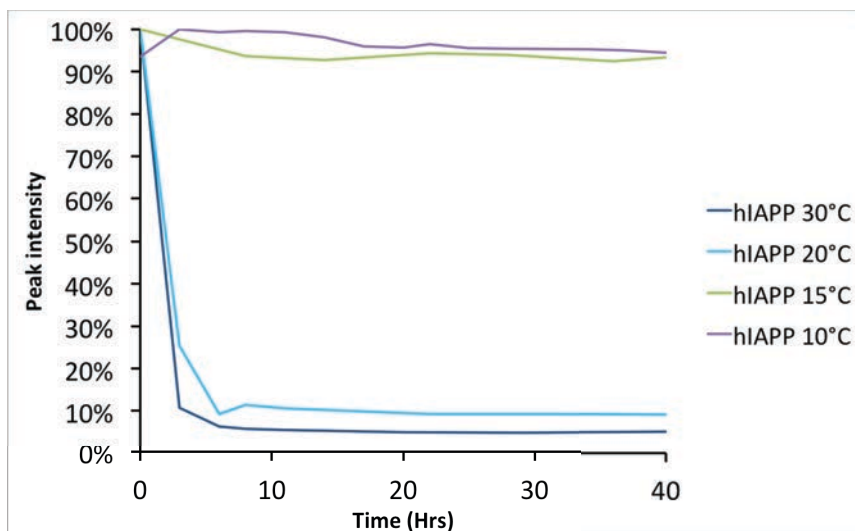


Figure 60: Peak intensity of hIAPP monomer over time at 30, 20, 15 and 10°C.

Measurements of hydrodynamic parameters of hIAPP have also been made at different temperatures (table 8). Data showed that at 20°C, as at 30°C, the loss of the signal made it difficult to obtain exploitable values of the diffusion coefficient as the signal/noise ratio was very low and led to large error bars. At 10 and 15°C, the coefficient of diffusion was stable over the duration of the experiment ( $0.79 \pm 0.01 \cdot 10^{10} \text{ m}^2/\text{s}$  at 10°C;  $0.96 \pm 0.01 \cdot 10^{10} \text{ m}^2/\text{s}$  at 15°C). These results show that at low temperature the monomeric form is stabilized and the oligomerization is slowed down.

	IAPP 20°C	IAPP 15°C	IAPP 10°C
	Ds ( $10^{10} \text{ m}^2/\text{s}$ )	Ds ( $10^{10} \text{ m}^2/\text{s}$ )	Ds ( $10^{10} \text{ m}^2/\text{s}$ )
0 Hrs	1.12± 0.03	0.95 ± 0.01	0.79± 0.01
5 Hrs	1.45± 0.19	0.96± 0.01	0.78± 0.01
11 Hrs	1.54± 0.41	0.95± 0.01	0.79± 0.01
16 Hrs	2.10± 0.67	0.95± 0.01	0.79± 0.01
21 Hrs	1.56± 0.67	0.96± 0.01	0.79± 0.01
27 Hrs	1.91± 0.71	0.98± 0.02	0.79± 0.01
28 Hrs	1.86± 0.80	0.99± 0.02	0.79± 0.01
48 Hrs	2.23± 0.84	1.21± 0.10	0.80± 0.01

Table 7: Hydrodynamic parameters of hIAPP at 20, 15 and 10°C.

At 20°C, the measurements become inconsistent after the first few hours of incubation because of the loss of signal. The values in grey are therefore not reliable.

At 10°C, a STD signal can be observed showing the coexistence of unobserved species and monomers in solution over time, but with a persistence of the monomer over time, which correlates with the slow rate of oligomerization. This signal tends to weakly decrease over time. This observation suggests that the larger species that were present at initial time evolved to larger aggregates, which are not in fast exchange with the monomer. The loss of this exchange between species therefore leads to the decrease of the observed signal (figure 61).

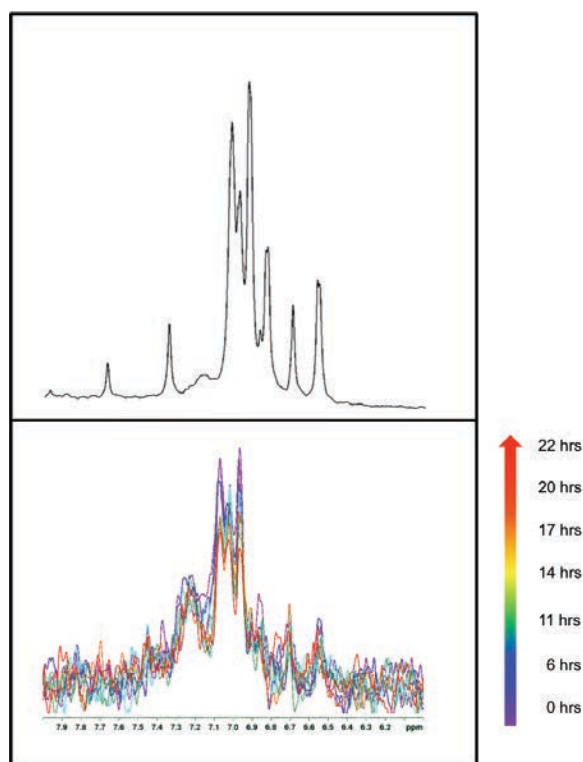


Figure 61: (top) Aromatic region of 1D  $^1\text{H}$  spectra of hIAPP. (Bottom) STD signal of hIAPP over time at  $10^\circ\text{C}$ .

Experiments on hIAPP at  $15^\circ\text{C}$  and higher showed a weak STD signal at initial time that could not be detected on the following experiments, despite the persisting signal of the monomer. This result, as those at  $10^\circ\text{C}$ , suggests that transient oligomeric species that interact with the monomer are present at initial time then rapidly evolves to larger aggregates, leading to a loss of STD signal during the first hours of incubation.

Our results are consistent with previous studies on hIAPP where much lower temperature was used ( $4^\circ\text{C}$ )<sup>8</sup>. However, since the oligomerization happens at a very slow rate at 10 and  $15^\circ\text{C}$ , with little information about the formation of any small oligomers, it seems more appropriate to work at a higher temperature in order to trigger the oligomerization. Additionally, in regard of the fact that the kinetics of hIAPP fibril formation are close at 20 and  $30^\circ\text{C}$ , the experiments that are shown here have all been done at  $30^\circ\text{C}$ , in order to be compared to those obtained with A $\beta$ 42.

#### *iv. Gel electrophoresis*

Gel electrophoresis experiments have been run in addition to the previous experiments in order to observe with more details which species were formed in solution for hIAPP as

well as for A $\beta$ 42. The principle of the experiments was to incubate the peptides at different times, to allow the oligomerization to take place and to run gel electrophoresis. As electrophoresis separates the different species in solution depending on their charge/weight ratio, it allows the monomers, oligomers to fibrils to be separated through the length of the gel provided that the different species are largely represented in the mixture and have sufficient stability. Gel electrophoresis under native conditions or on amyloid peptides had never been done in our laboratory previously. In this light, we started to run gels using protocols that could be found in the literature and tried to optimize them for our study.<sup>13,14,15</sup>

It was at first decided to run gel electrophoresis under native conditions, therefore without detergents or reducing agents ( $\beta$ -mercaptoethanol), as the SDS contained in the common SDS-PAGE gels could interact and possibly dissociate the oligomers. As the detection of oligomeric species of A $\beta$ 40/42 in solution has previously been described by several groups, the optimization process was done using incubated samples of A $\beta$ 42 in solution. Results for native gels showed the presence of what is likely the A $\beta$ 42 monomer, at all incubation times, indicating that the monomer is still present even after many hours in solution at room temperature. However, no other bands testifying of the presence of any possible oligomers could be seen on the gel, even after a silver staining, which is more sensitive than the Coomassie blue staining (Figure 62). The limitation of native gel electrophoresis is that the separation between the species depends of the size and the shape of the oligomers rather than only their weight, as it is for SDS-PAGE. Also, the conservation of the native state implies that the structure of the species is conserved. This parameter has to be taken into account as the shape and available surface of the oligomers may impact the electrophoretic mobility of the different species<sup>16</sup>. It was shown that A $\beta$ 42 could aggregate into oligomers of different size and shape, following different pathways. Therefore, oligomers of similar weight and charge could either adopt an ordered  $\beta$ -sheet structure or a globular conformation, which would lead to different speeds of migration through the gel. In this light, given the fact that we did not know which A $\beta$ 42 assemblies would be present in solution, it was quite difficult to predict the possible positions of the bands on the gel, or identify the nature of the observed species, after migration.

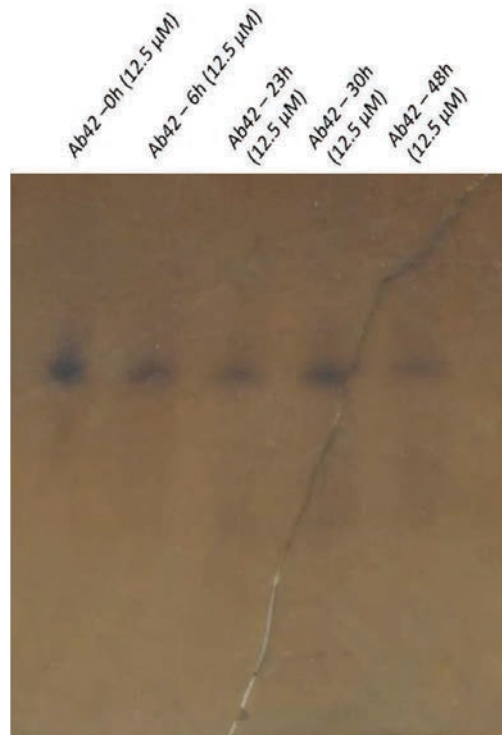


**Figure 62: Native Tris Glycine gel - A $\beta$ 42 at 0,6,23,30 and 48 hours of incubation. Only the band of the monomer was observed**

Another set of experiments was done using Bis Tris 12% gels. SDS is present in the running buffer (0.01% SDS) as well as in the sample buffer (1% SDS), allowing the oligomers to be separated according to their respective weight. In order to limit the denaturation of peptides, the samples were mixed with a bromophenol blue sample buffer containing no reducing agent (that would lead to the reduction of IAPP disulfide bridge) and were not heated. The samples were immediately pooled into the wells and the gel was run at 200 mV.

Results showed that in all wells containing A $\beta$ 42 samples, a large band corresponding to the monomer was present. The band being more intense at initial time, showing that the monomer was at a higher concentration than in the other wells, where oligomers had likely formed. In wells containing hIAPP samples, a light band corresponding to the monomer was observed at initial time but was not present at longer incubation time, showing that it was likely consumed to form oligomers even though no other bands at higher molecular weights could be observed (Figure 63).



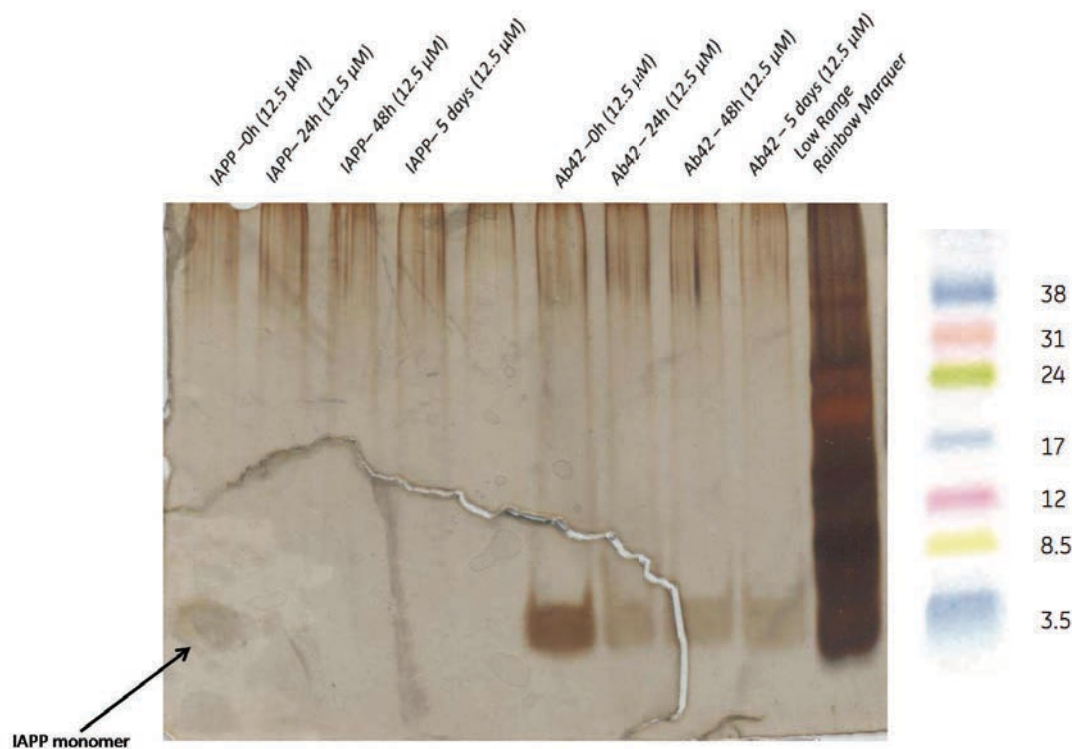
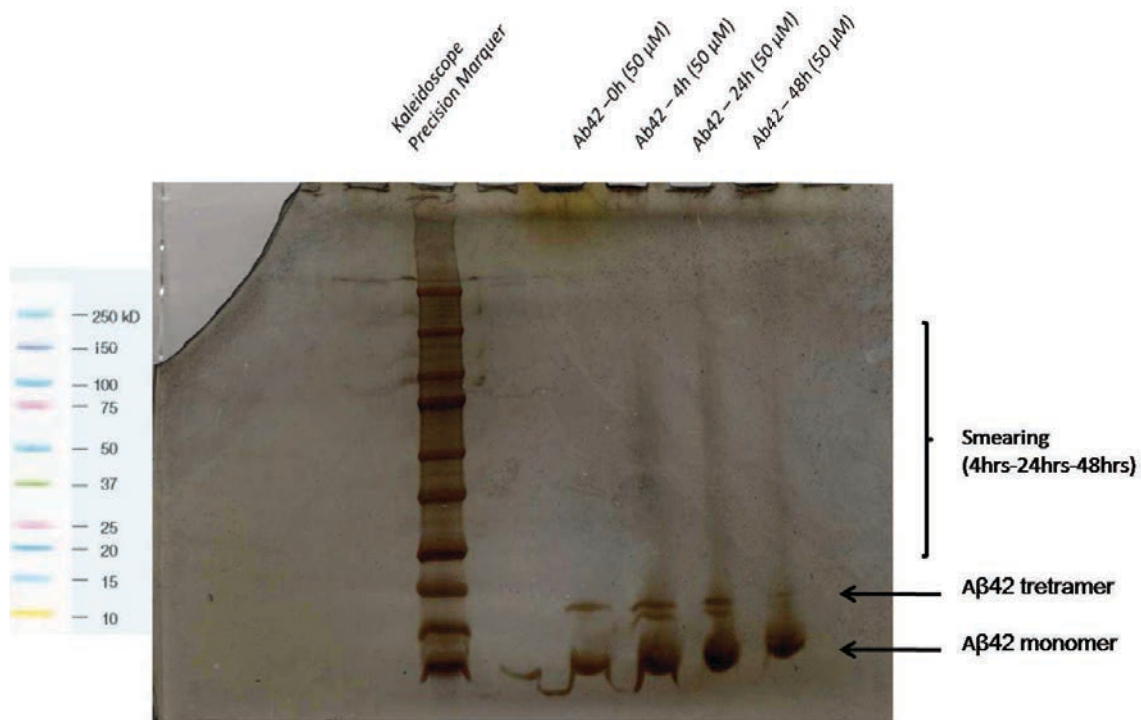


Figure 63: Bis Tris 12% acrylamide gel for IAPP and A $\beta$ 42 at different incubation times

If Bis-Tris gels have given some results regarding the detection of the peptides as monomers could be observed, it had the inconvenient of having a low concentration of acrylamide/bisacrylamide. This leads to large bands, as observed on Figure 63, making it difficult to determine if other low molecular weight species were formed as their bands could be overlapping because of their width.

Finally for the last set of experiments, we chose a compromise between the full native gel without SDS and the SDS-PAGE gel, which is done under denaturing conditions. Therefore, the experiment consisted on a 4-20% Tris-Glycine gel containing no SDS. The gradient gel is here ideal for the simultaneous observation of the different species, from monomer to large oligomers, and the absence of SDS in the gel buffer should limit the denaturation of the oligomers. Still, to be able to discriminate the different species depending on their weight and regardless of the charge, the samples were mixed with a Bromophenol blue sample buffer containing SDS and no  $\beta$ -mercaptoethanol to avoid the reduction of the disulfide bridges (hIAPP). The samples were immediately pooled in the gel wells, without being heated at 95°C to avoid any possible dissociation of the oligomers by a heat denaturation. Result of the first experiments on A $\beta$ 42 showed, as it was seen previously for the other experiments, that the band corresponding to the monomer was present regardless of the incubation time. Another band, around 15 kDa, which could correspond to A $\beta$ 42 tetramer,

was also observed for every other incubation time, showing that this oligomeric form was very stable in solution. At 4, 24 and 48 hours of incubation, a smearing could be observed on the gel. This could be linked to the presence of many heterogeneous oligomeric species present at low concentration in solution (Figure 64).



**Figure 64: Tris Glycine gel of Aβ42 at 0, 4, 24 and 48 hours of incubation.**  
Bands of the monomer, tetramer as well as smearings at higher molecular weight could be observed

Samples of hIAPP, incubated at different times and prepared under the same conditions were run on the 4-20% Tris Glycine gels. Results for hIAPP showed that a light band corresponding to the monomer was observed at initial time but disappeared quickly as it was not observed after 2 hours of incubation and was not present in other wells (Figure 65). Silver staining of the gel was also carried out after initial Coomassie blue staining, as we wanted to detect possible supplementary bands that required more sensitivity. The results of the staining showed no additional bands, and the gel became too dark to be able to discriminate any eventual species. The absence of the IAPP monomer band in the wells containing the peptide after a few hours of incubation is consistent with the previous results showing that the monomer is fully consumed during the oligomerization process.

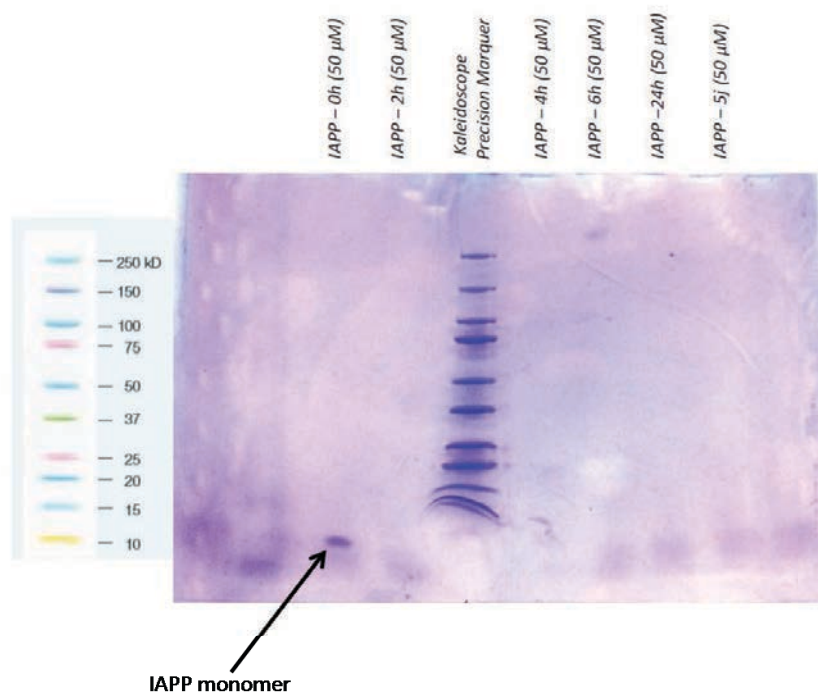


**Figure 65: Tris Glycine gel of hIAPP at different incubation times.**  
**Band of the monomer could be observed at initial time but not for higher incubation times**

Gel electrophoresis results can be correlated with NMR and CD experiments as it shows that hIAPP monomer is consumed at a very fast rate once in solution and assembles to form large species, although not observed on the gels. As for A $\beta$ 42, results of the electrophoresis have shown a persistence of the monomer even after 48 hours of incubation, which indicates a coexistence of different species in solution. The lack of detection of bands of higher molecular weight oligomers on the gel could be either because the species are too large and do not penetrate the gel, or, that they are present in a very low concentration that is beneath the limit of detection by Coomassie blue or silver staining.

b) Interaction with fluorescent probes

i. *Influence on A $\beta$ 42 kinetics of fibrillization*

The comparison of  $^1\text{H}$  experiment on A $\beta$ 42 was based on the integration of the NMR signal between 0.5 and 1.5 ppm in order to monitor the depletion of the peptide in the monomeric state. For all samples (A $\beta$ 42 alone, A $\beta$ 42+ThT and A $\beta$ 42+TROL), the intensity of the methyl signals decreased over time with comparable rates, suggesting that the probes

had little to no effect on the kinetics of depletion of the peptide monomer. However, for the one containing ThT, depletion of the signal was slower than the two others, suggesting that ThT binding slightly inhibited the oligomerization process (Figure 66A). The curves from the PFG experiments showed a decrease of the translational diffusion coefficient over time in a similar way for the three samples (Table 9), indicating that the presence of probes had not a strong influence on the equilibrium between monomers and aggregated species detected by PFG NMR. This conclusion was strengthened by TEM experiments, which exhibited identical fibrils for the three samples, *i.e.* long, smooth and un-branched fibrils (Figure 66B,C).

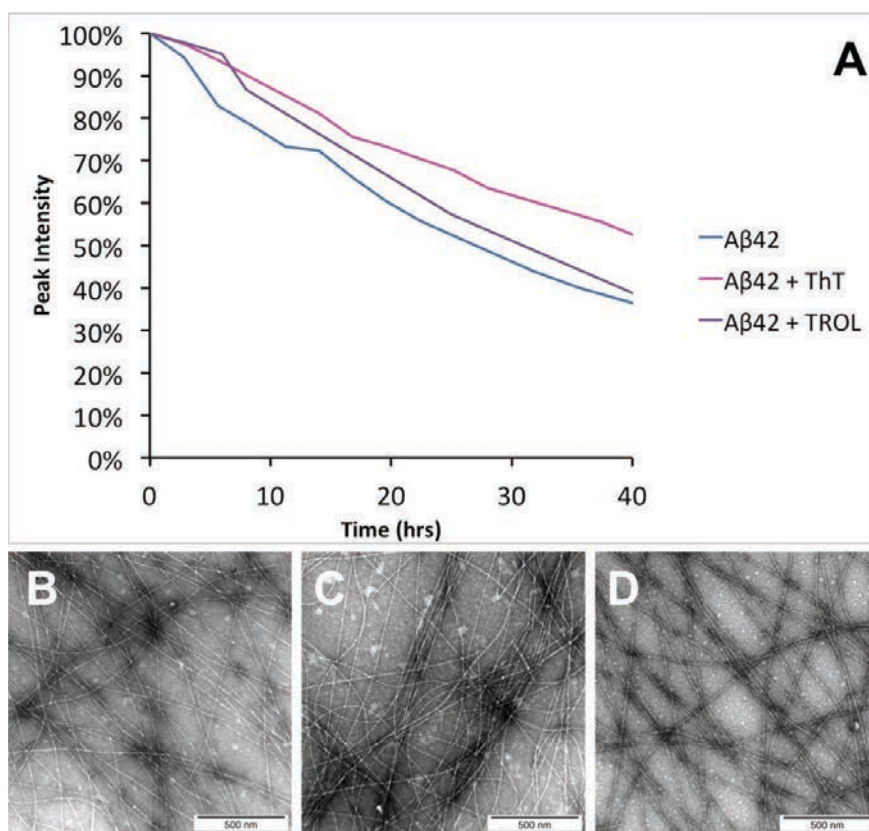


Figure 66: A) evolution of peak area of Aβ42 in absence and presence of ThT and TROL over time (B, C, D) TEM of Aβ42 in absence of probes and in presence of TROL and ThT respectively,

	Time (hrs)	Ds ( $10^{10}$ m <sup>2</sup> /s)	$\Delta$ Ds ( $10^{10}$ m <sup>2</sup> /s)
A $\beta$ 42	0	1.87	0.05
	3	1.87	0.05
	24	1.46	0.06
	40	1.56	0.12
A $\beta$ 42 and ThT	0	1.73	0.04
	3	1.70	0.05
	24	1.40	0.07
	40	1.52	0.06
A $\beta$ 42 and TROL	0	1.85	0.04
	3	1.78	0.06
	24	1.46	0.06
	40	1.44	0.11

**Table 8 : Diffusion coefficient of A $\beta$ 42 in the absence and in the presence of ThT or TROL**

Next, CD experiments showed in presence of ThT and TROL, a shift from random coil to  $\beta$ -sheet structure within the same time-range than A $\beta$ 42 alone (Figure 67). In presence of ThT, as we did not know if the peptide had reached a stable state, an additional spectrum was acquired after 48 hours of incubation, showing a prevalence of  $\beta$ -sheet conformation. The ellipticity over time was also plotted out for A $\beta$ 42 in absence and presence of fluorescent dyes (figure 67A,B). The results showed that all curves were linear, showing a gradual transition for the disordered state to a  $\beta$ -sheet structure. We can observe a lesser steep for the curves of A $\beta$ 42 in presence of ThT and TROL compared to A $\beta$ 42 in absence of dyes, which might suggest that the fibrillization might be slowed down, to a small extent, by the presence of fluorescent probes.

Altogether, our results indicate that the fluorescent probes have little influence on the structuration and kinetics of fibrillization of the A $\beta$ 42.

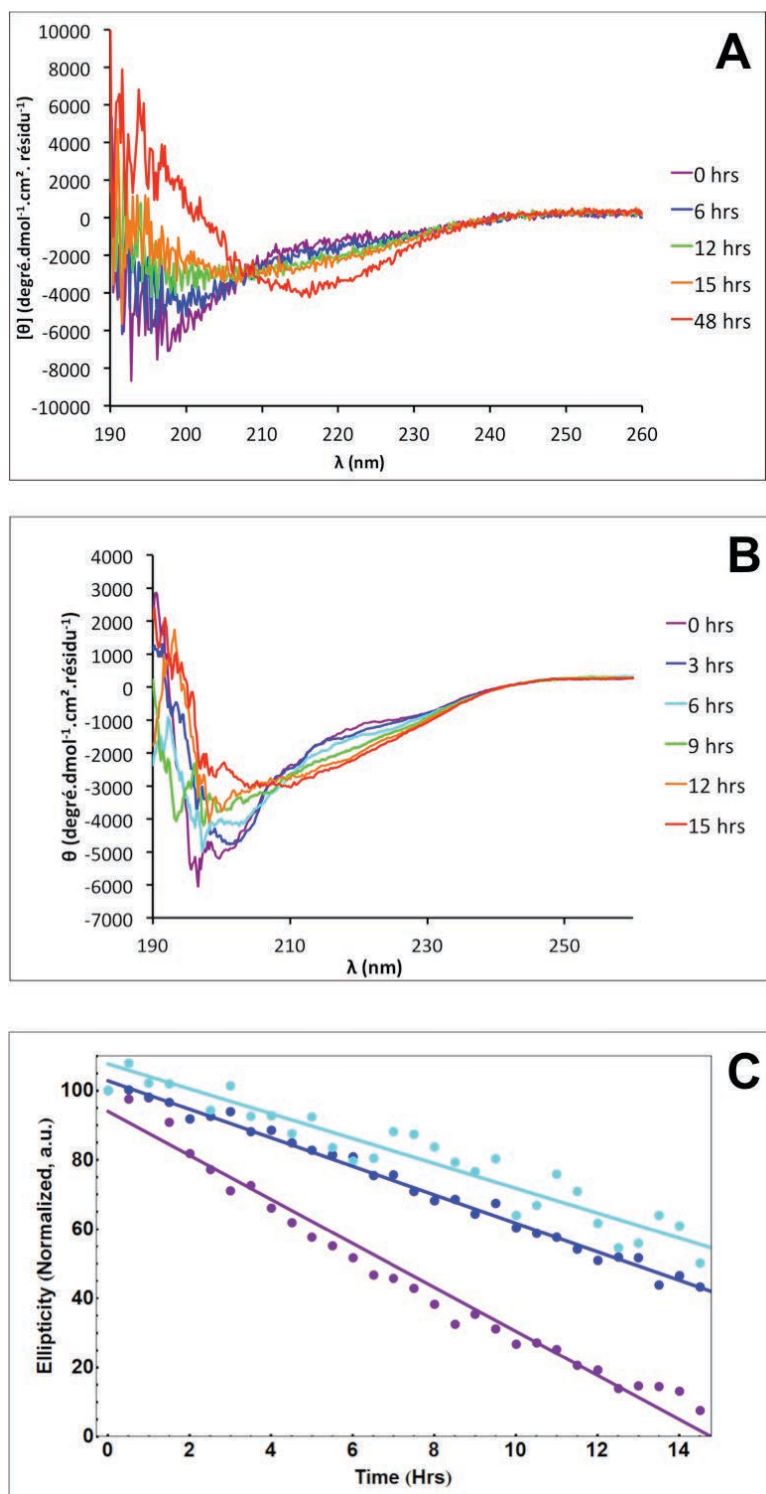


Figure 67: (A), CD experiments on Aβ42 in presence of ThT (B) CD experiments on Aβ42 in presence of TROL. Spectra were smoothed (adjacent-averaging 25 points) to optimize the signal/noise ratio as TROL absorbs around 190 nm, (C) ellipticity at 205 nm for Aβ42 (purple), Aβ42 and ThT (blue), Aβ42 with TROL (cyan) over time.

*ii. Influence on hIAPP kinetics of fibrillization*

We performed TEM, CD and NMR experiments in the absence and in the presence of the fluorescent probes in order to investigate if the probes could have an effect on the fibrillization and on the morphology of hIAPP fibrils. In each experiments, the peptide and the probe were held at a concentration of 75  $\mu\text{M}$  (peptide:probe ratio of 1:1). Given the results of NMR and CD experiments on the peptide alone at 30°C showing faster kinetics of aggregation than at 20°C, we decided to carry out these experiments in the presence of fluorescent dyes at a temperature of 20°C.

$^1\text{H}$  experiments performed on hIAPP in the presence of fluorescent dyes exhibited a weak decrease of the peptide's peaks over time with a signal still evolving after more than 24 hours of experiment and a stationary state reached after at least 40 hours of incubation in the NMR tube. Peak intensities between 0.6 and 0.9 ppm, in the methyl region of the peptide could be measured and plotted over time for the different experiments (Figure 68A). This enabled us to measure the diffusion coefficient in the methyl zone, which showed almost no variation and remained quite stable with small error bars over the time of the experiment (table 10). Therefore NMR experiments tended to indicate that the aggregation of hIAPP is slower when in presence the two fluorescent probes. However, TEM revealed fibrils with an identical morphology, i.e. large and dense mats of twisted and tangled fibrils that are about 5 to 8 nm wide, as those of the probe-less peptide, (Figure 68B, C).



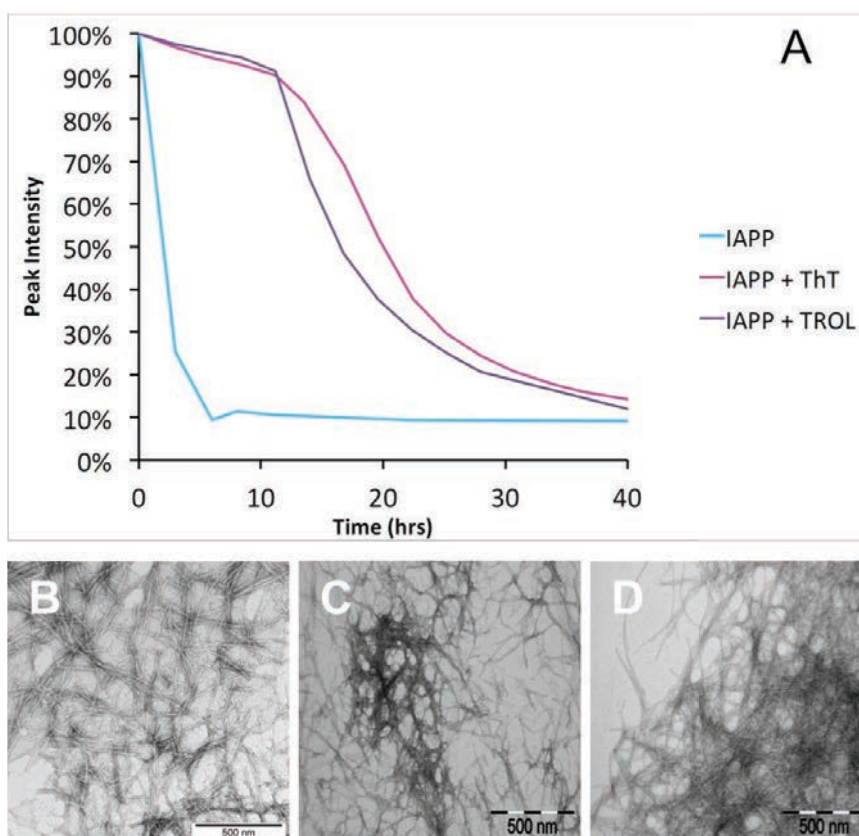


Figure 68: (A) Evolution of peak intensity over time for IAPP in the absence and in presence of ThT and TROL obtained by  $^1\text{H}$  NMR experiments at  $20^\circ\text{C}$  (B, C,D) TEM for IAPP in absence and in presence of TROL and ThT, respectively.

	Time (hrs)	Ds ( $10^{10}$ m <sup>2</sup> /s)	$\Delta$ Ds ( $10^{10}$ m <sup>2</sup> /s)
hIAPP	0	1.15	0.03
	3	1.45	0.35
	24	0.78	0.81
	40	0.51	0.07
hIAPP and ThT	0	1.14	0.07
	3	1.13	0.07
	24	1.12	0.02
	40	1.37	0.04
hIAPP and TROL	0	1.14	0.04
	3	1.14	0.04
	24	1.23	0.99

Table 9: Hydrodynamic parameters for IAPP and IAPP in presence of ThT and TROL. The values highlighted are not reliable given the loss of signal and large error bars.

In parallel, we also recorded CD experiments to analyze the evolution of the secondary structure of hIAPP in the absence and in the presence of the probes. The CD experiment on hIAPP in presence of ThT was done two times. For the first measurement, no evolution of the



spectrum could be observed after 15 hours of incubation, although macroscopic aggregates could clearly be seen in the cuvette. We gently shook the cuvette and then started another set of acquisition. The obtained spectra (17-20 hours) showed a decrease of both minima at 200 nm and 225 nm. This suggested that either a transition had occurred during the two hours between the two sets of acquisition or, that the large aggregates that bound to ThT had sunk in the bottom of the cuvette and were not detected before the shaking (Figure 69A). Given the two different signals obtained for the same sample (0-15 hours then 17-20 hours), and lack of data between 15 and 17 hours, the experiment was repeated. Results for the second set of experiments showed that after 20 hours of incubation, the signal of ThT was constant. On the second CD experiment in presence of ThT an additional spectrum obtained after 48 hours of incubation and without shaking indicated that the signal had shifted from random coil to  $\beta$ -sheet (Figure 69B). This result showed that the kinetics of loss of signal in presence of ThT was slower than for hIAPP alone, with a transition appearing after over 20 hours of incubation. This result also shows that the shaking in the first CD experiment with ThT had likely dispersed species that induced light scattering in solution. CD experience in presence of TROL also showed that the kinetics of oligomerization were slowed down, with a signal that was constant in the first 7 hours of incubation. An additional spectrum acquired after 48 hours of incubation showed a loss of signal at 200 nm, showing that large aggregates had formed in the meantime (Figure 69C). The ellipticity of hIAPP over time was also plotted out in absence and in the presence of fluorescent dyes. The results showed a very small linear decrease, showing only little evolution of the ellipticity over time. On the contrary, the curve obtained for hIAPP in absence of probes was sigmoidal, showing the transition to the structured  $\beta$  sheet (figure 69D).

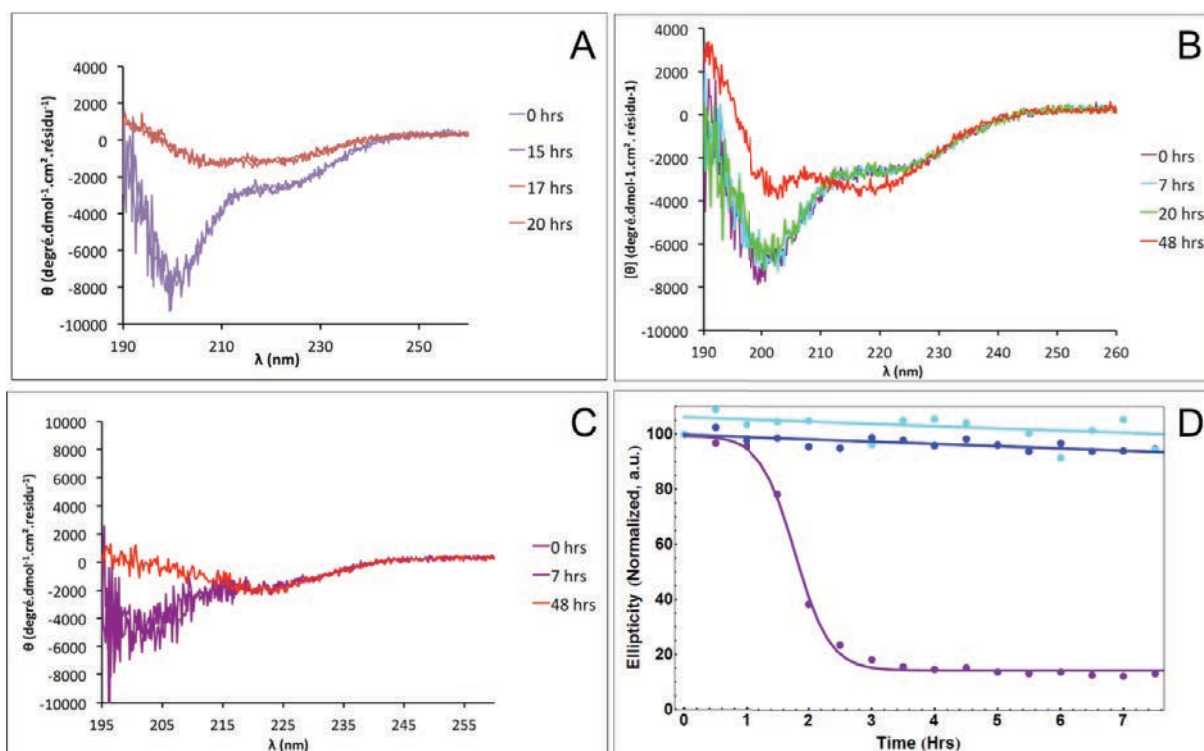
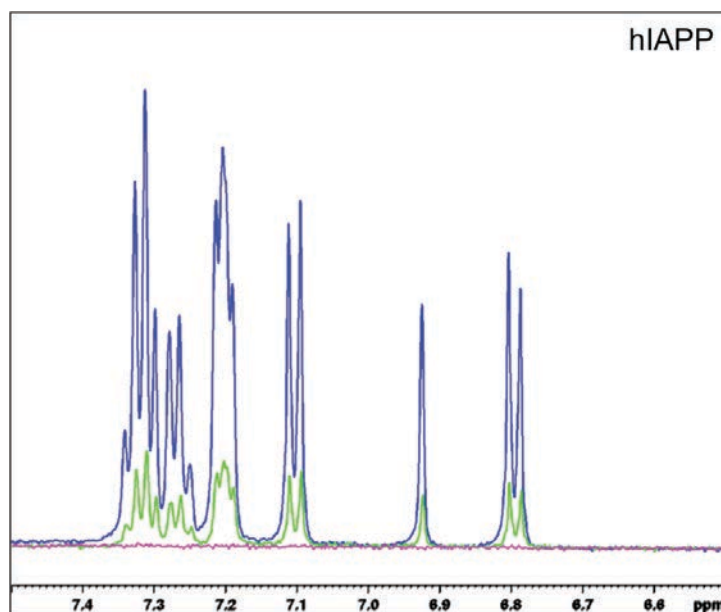


Figure 69: (A) CD experiment on IAPP in the presence of ThT, spectra in red were acquired after shaking the cuvette, (B) Second CD experiment on IAPP in the presence of ThT, without shaking the sample. A transition was observed after acquisition of an additional spectrum after 48 hours of incubation, (C) CD experiment on IAPP in the presence of TROL. A transition was observed after acquisition of an additional spectrum after 48 hours of incubation, (D) ellipticity at 205 nm for hIAPP (purple), hIAPP and ThT, second CD experiment (blue), hIAPP with TROL (cyan) over time.

The results for NMR and CD experiments on IAPP in presence of ThT and TROL showed that the fluorescent probes had a dramatic effect on the kinetics of oligomerization of the peptide, by slowing down monomer depletion as well as  $\beta$ -sheet conformational transition and aggregation of the peptide.

A new set of NMR and CD experiments have been carried out on another batch of IAPP in absence and presence of new probes. In order to minimize the variability and ensure the reproducibility of experiments, IAPP aliquots were prepared in the same conditions, peptide was dissolved in a sodium phosphate buffer at pH 7.4, prepared in  $D_2O$  for both NMR and CD experiments and the temperature was set at  $30^\circ C$ , which also allowed us a better comparison with A $\beta$ 42 results.

NMR experiments carried out on hIAPP in the absence of fluorescent probes showed a decrease of the monomer signal within the two first hours of experiments, which was consistent with the results that were obtained previously with another hIAPP sample. However, the broad signal that could be detected with the previous batch of hIAPP did not appear on our spectra over the time course of experiments (figure 70).



**Figure 70: Monomer depletion of hIAPP at 30°C observed by NMR spectroscopy (Methy region). Spectra were recorded at t = 0 hrs (blue), t = 1 hr (green) and t = 2 hrs (magenta)**

In the presence of ThT and TROL, a decrease of the signal could be observed shortly after initial time, without any lag time, which differed with the results that we obtained with our first set of experiments on IAPP at 20°C in presence of fluorescent probes (figure 71).

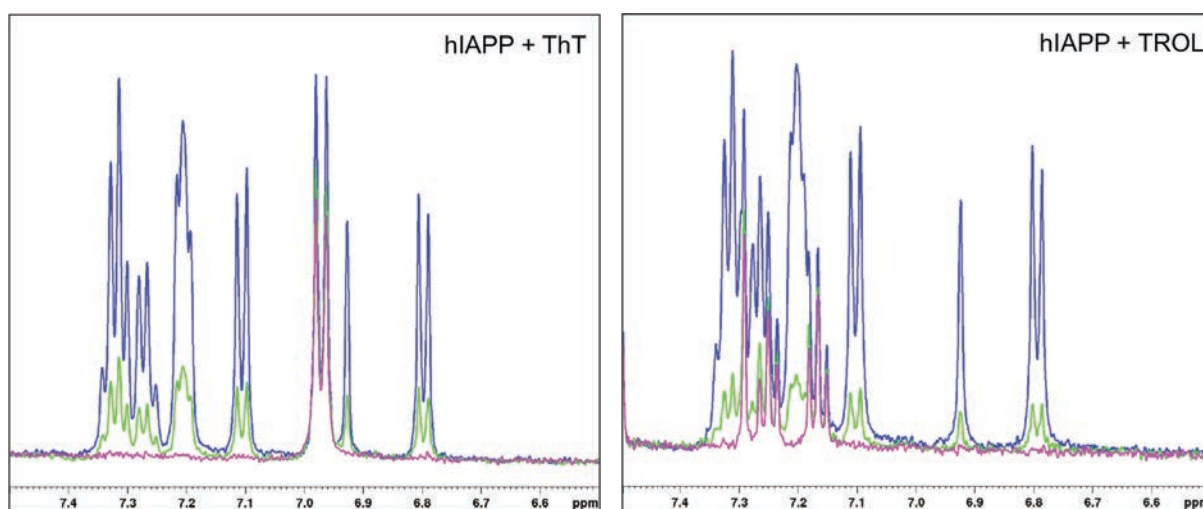


**Figure 71: Monomer depletion of hIAPP in the presence of ThT (left) and TROL (right) at 30°C observed by NMR spectroscopy (Methy region). Spectra were recorded at t = 0 hrs (blue), t = 1 hr (green) and t = 2 hrs (magenta)**

The values of peak intensity for the three samples were measured and plotted over time. The result showed that intensity of the methyl signals decreased linearly over time with similar rates, showing that the fluorescent probes had no or little effect on the aggregation of this batch of hAPP (figure 72).

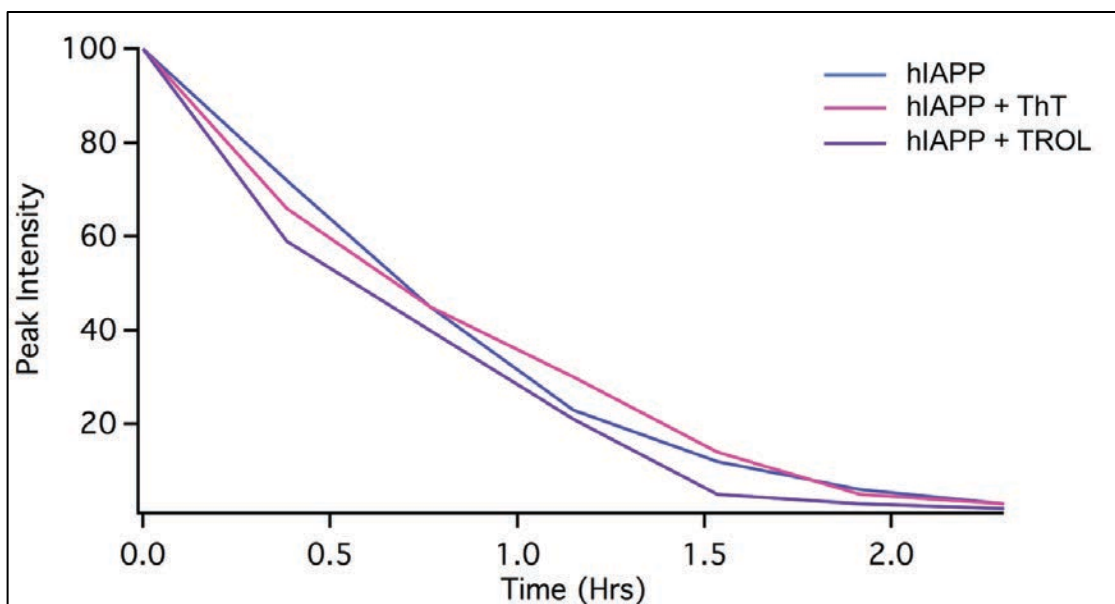


Figure 72: Time evolution of  $^1\text{H}$  resonance intensities for hIAPP and hIAPP in the absence or in the presence of fluorescent dyes at  $30^\circ\text{C}$ . NMR signals were integrated between 0.7 and 1 ppm.

CD experiments showed that the freshly dissolved hIAPP showed a mainly disordered conformation, which was consistent with our previous observations. The signal for the peptide stable over the first hour of incubation and then rapidly evolved to a signal characteristic of a  $\beta$ -sheet structure, with the disappearance of the minimum at 200 nm, and presence of a maximum at 190 nm and minimum at 220 nm (figure 73A, table 11).

	Random coil	$\beta$ -sheet	$\alpha$ -helix
hIAPP (initial time)	81.4 %	10.9 %	7.7 %
hIAPP (final time)	69.2%	18.1%	12.8 %

Table 10: Contribution of disordered state,  $\beta$ -sheet and  $\alpha$ -helical conformation to the structure of hIAPP at initial and final times.

Deconvolution of the CD spectrum was done with CDfriend software.

This result was expected, as the transition is inherent to the fibrillization of the peptide and was consistent with our previous results. However, the transition here is also characterized by an augmentation of the absolute value of the minimum at 220 nm, showing an increase of  $\beta$ -sheet population, which was not observed in our first set of experiments. The conformational shift and concomitant decrease of the signal at 200 nm and increase of signal at 205 nm can be plotted over time (figure 73B). The resulting curves appear to be a sigmoid and an inverted sigmoid, characterized by two plateaus: at initial phase showing the prevalence of random coil signal and at the final stage, where the stable signal shows a prevalence of  $\beta$ -sheet structure.

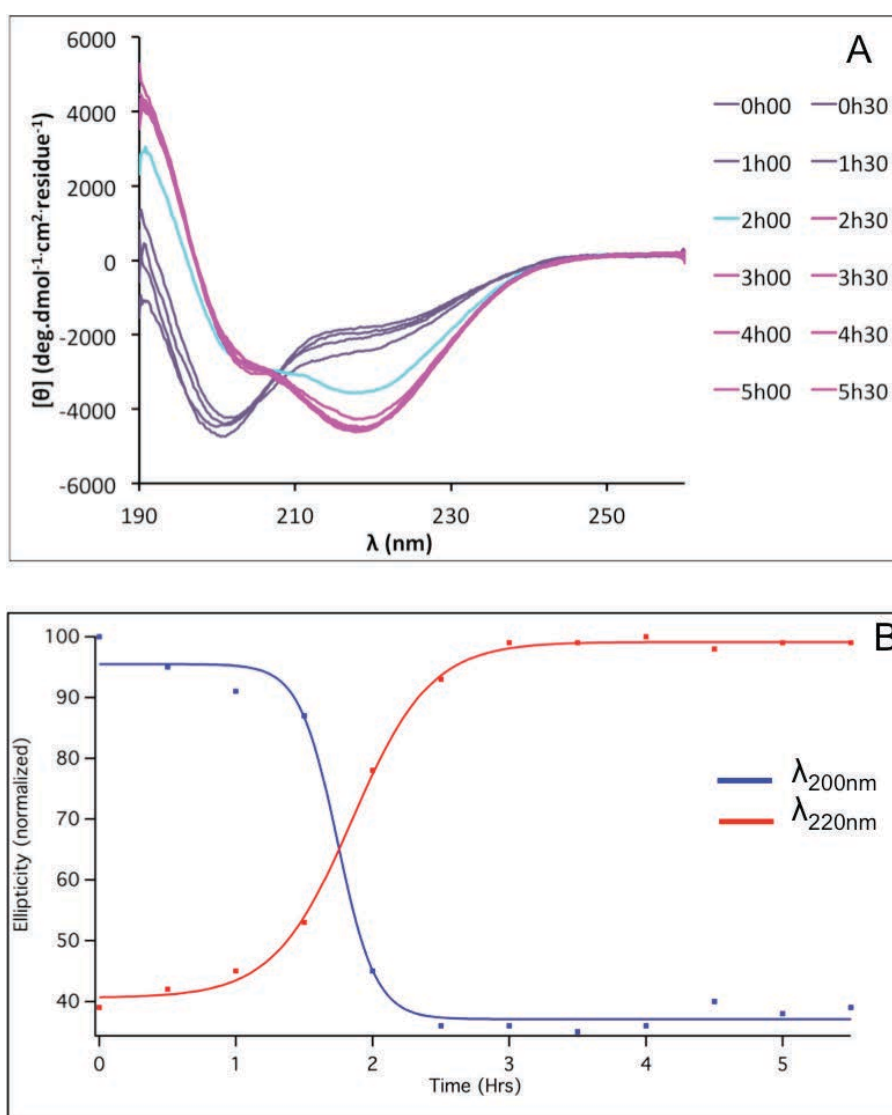


**Figure 73:** (A) CD spectra of hIAPP over time. The peptide gradually adopts a  $\beta$ -sheet conformation over time with an apparition of a characteristic isodichroic point (Peptide concentration: 75  $\mu$ M, Temperature: 30°C). (B) Measured ellipticities at 200 nm (blue) and 220 nm (red) as a function of time.

In presence of fluorescent dyes, the result that we obtained for CD experiments were strikingly different from what we had observed during our first set of experiments. Indeed, the allures of the spectra in presence of ThT or TROL were very similar to the ones of hIAPP alone with an initial random coil signal switching to a  $\beta$ -sheet signal on a similar time scale as in the absence of fluorescent probes (figure 74A,C). Likewise the transition is here characterized by the disappearance of the minimum at 200 nm in favor of a minimum at 220 nm and a increase of signal at 190 nm. The values of ellipticity for the two minima can also be plotted over time, showing S-shaped or inverted S-shaped curves that are characteristic of the shift between the two conformational states (figure 74B,D).

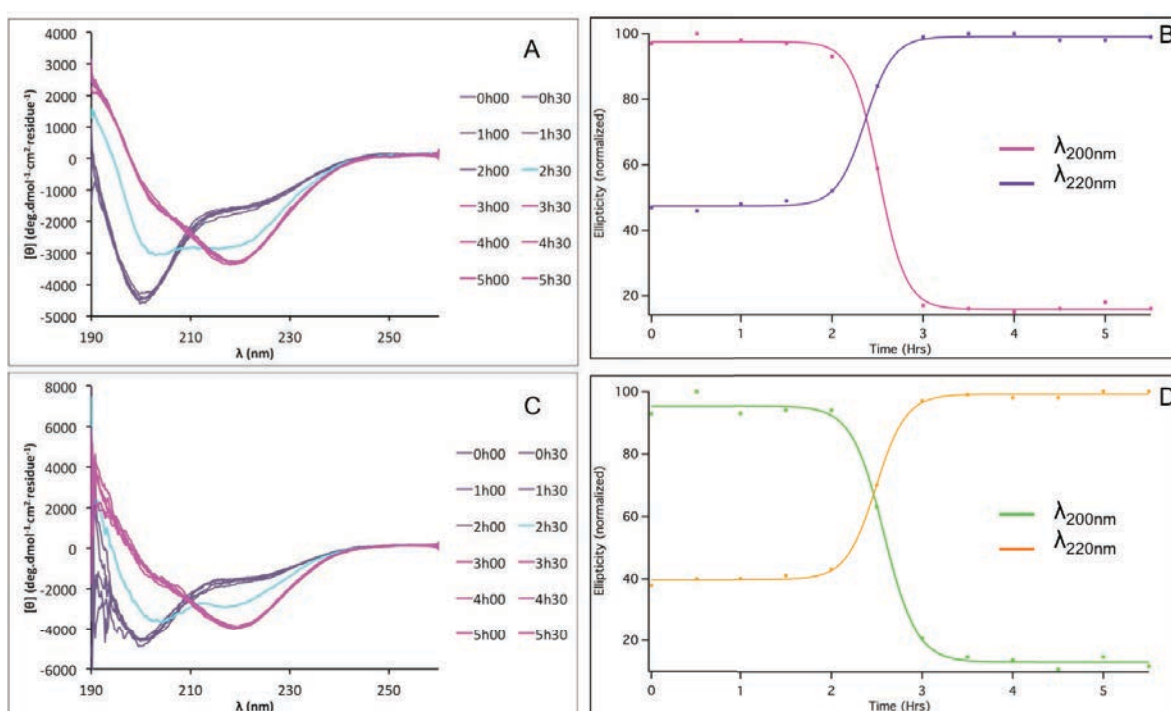


**Figure 74:** CD spectra of hIAPP in presence of ThT (A) and TROL (B) over time. (C,D) Ellipticities at 200 and 220 nm as a function of time measured for hIAPP in presence of ThT and TROL, respectively.

In order to compare the results between the three samples, the measured values of the ellipticity at 200 nm over time were plotted on the same graph. The result showed that the loss of signal was slower in presence of fluorescent dyes than in their absence ( $t_{1/2} = 2.51 \pm 0.02$  hrs in presence of ThT,  $t_{1/2} = 2.59 \pm 0.03$  hrs in presence of TROL vs.  $t_{1/2} = 1.73 \pm 0.05$  hours in absence of dyes), but the effect is less pronounced than what was previously observed (figure 75).

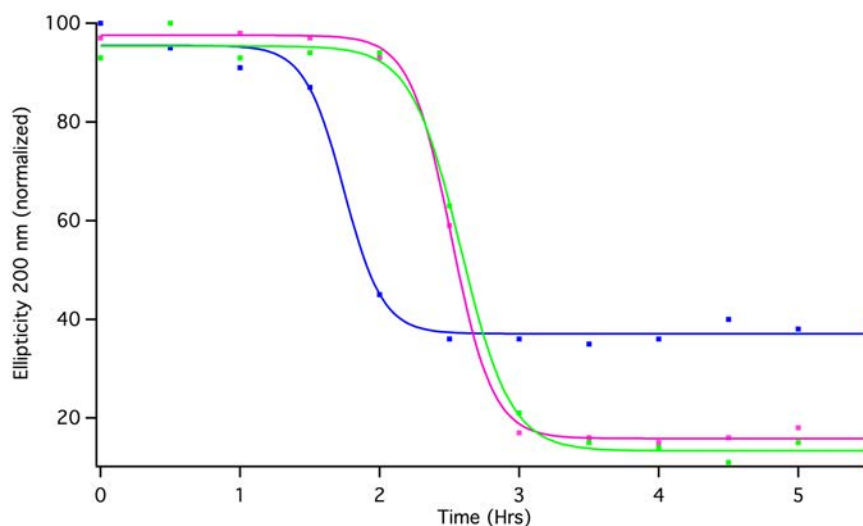


Figure 75: Ellipticity at 200 nm over time of hIAPP (blue), IAPP in presence of ThT (magenta) and IAPP in presence of TROL (green)

## 2. Discussion

This study was focused on the early stages of fibrillization of the human Islet Amyloid PolyPeptide (hIAPP), especially on the oligomers that are formed and the possible interaction that could exist between those species and the monomer or the fibrils in solution. As the mechanism of fibrillization is still unclear, and that only little information exists on the transient oligomeric states of hIAPP, the experiments on the peptide were made in parallel with another amyloid peptide, A $\beta$ 42, which is known to form more stable oligomers in solution. Characterized by a high sequence similarity, those two peptides have shown very intricate mechanisms of self-association that are yet to be explained. The results show that hIAPP had fast kinetics of fibrillization, rapidly aggregating to form large oligomers and fibrils. This process is characterized by an absence of stable low oligomeric species and no or slow exchanges between the monomer or small oligomers and fibrils in solution.

This study involved the use of different biophysical techniques in order to observe the different stages of the fibrillization process. We performed fluorescence and circular dichroism under the same conditions in order to evaluate the kinetics of aggregation for the peptides in our experimental conditions. Then, NMR experiments, from  $^1\text{H}$  spectra, Saturation Transfer Difference and Pulse Field Gradient experiments were recorded in order to gain more information about the monomer depletion and the dynamics of fibrillization in solution, by gathering data about oligomers that could be formed. Gel electrophoresis experiments

were carried out in order to observe the possible oligomeric species. Finally, transmission electron microscopy was done in order to observe the morphologies of the formed fibrils.

During this study, we encountered many difficulties that we had to overcome. First, it appeared that the experiments were batch-dependent as what could be observed on the two hIAPP batches that we used for the experiments. Both batches displayed fast kinetics of aggregations but some differences were observed on the NMR spectra. Indeed, the first batch showed the appearance of a broad peak around 0.6 ppm, which could be attributed to the appearance of large species in solution. This peak could not be observed on NMR experiments with the second batch of peptides.

We also observed that the presence of fluorescent probes could interfere with the oligomerization of the peptide. If this effect was quite limited for A $\beta$ 42, the experiments on our first batch of hIAPP showed that the presence of the probes induces a high inhibition of the oligomerization that was not observed during the experiments on our second hIAPP batch at a higher temperature. These results implied that comparisons between experiments had to be done on the same batch of peptides, and that the kinetics of fibrillization could not finely be compared between fluorescence experiments, that involved fluorescent probes and NMR/CD experiments, that were done on the peptide in the absence of probes.

Moreover, even in the absence of fluorescent probes, the results for NMR and CD experiments were to be interpreted with caution. The use of NMR tubes and CD cuvettes might indeed lead to slight differences, as they do not have the same shape, the same glass composition, the same surface of contact between the tube/cuvette and the solution, different air/water interface etc.

However, if the encountered difficulties have made the interpretation of the data from a kinetics point of view complex, the study of the oligomerization and the fibrillization of hIAPP and A $\beta$  by different biophysical techniques have allowed us to obtain mechanistic information of the process that are distinct for the two peptides.

First, the use of two different but complementary probes as well as different sets of experiments, was interesting as it made it possible for us to highlight some differences in the mechanism of fibrillization of the two peptides by cross analyzing the results showing the depletion of the monomer as well as the formation of fibrils in solution. ThT experiments on hIAPP showed that regardless of the batch of peptide used, hIAPP displayed fast kinetics of fibrillization with short lag times, and small steps suggesting the quick formation of large



aggregates in a cooperative way. Fluorescence experiments with the two fluorescent probes also revealed that the plateau for hIAPP for the ThT curve was reached earlier than the plateau for TROL (4 hours vs. 10 hours), while for A $\beta$ 42, ThT curve reached a plateau around 16 hours of experiments while TROL curve reached a plateau around 10 hours. The fact that ThT and TROL curves lack of a symmetrical aspect, particularly during fluorescence assays with A $\beta$ 42 also highlights a particular time zone where small species as well as pre-fibrillar species are present in solution. However, the decrease of TROL fluorescence intensity at the very beginning of the experiment showed TROL binds very quickly to the monomeric or small oligomeric peptides that were not detected by ThT, before reaching a plateau. This decrease and lack of lag time means that, although the probe allows us to have access to oligomers that does not interact with ThT dye, the use of TROL lead to results that are difficult to interpret as it is still not specific enough to determine which specific oligomers are formed, or to determine their lifetime.

NMR experiments allowed us to further the investigation of the presence of small oligomers and especially the existence of a possible exchange between the fibrils and rather small oligomeric species or monomer. NMR experiments allowed us to quantify the quantity of monomer in solution as well as dynamic exchanges between species. We observed very significant differences between hIAPP and A $\beta$ 42. Experiments on hIAPP showed a drastic depletion followed by the disappearance of the hIAPP monomer's signal over time, showing that the peptide had quickly aggregated to large species, consuming all the monomer. On the contrary,  $^1\text{H}$  spectra of A $\beta$ 42 showed the persisting presence of the peptide in a monomeric state over time, even as large oligomers and fibrils have already formed, according to ThT fluorescence, PFG experiments and TEM. The fact that the monomer signal of A $\beta$ 42 persists over time while it disappears completely for hIAPP could also explain the differences of values of the plateau observed at final stages of ThT fluorescence experiments. Indeed, if the fluorescence intensity was 100% for hIAPP, it only reached 50% for A $\beta$ 42 perhaps due to the existence of monomeric and small oligomeric species that are not detected by ThT probe and therefore lessens the fluorescence intensity.

PFG experiments showed that the diffusion coefficient measured on A $\beta$ 42 over time was slowly decreasing, which was consistent with the gradual formation of aggregates in solution. In addition to that, STD experiments and appearance of a persisting signal over time in the aromatic region of the peptide indicates that, as the peptide aggregates, the formed oligomers interact at a fast exchange rate with the monomer that is still present. We also

noticed that the STD signal was increasing over time, which showed that the concentration of aggregated species increased over time, while the monomer concentration was consumed. Thus, the overall results indicates that A $\beta$ 42 peptide mechanism of fibrillization is likely to present a fast exchange between different species *i.e.* small oligomers and monomers and high molecular weight species.

On the contrary, the same experiments on hIAPP did not allow us to observe any specific exchanges between hIAPP aggregates as the fast kinetics of fibrillization lead to a disappearance of the signal in the 3 first hours of experiment. In an attempt to observe early stages of oligomerization and possible exchanges between different hIAPP species, we carried out the experiments at lower temperatures of 10, 15 and 20 °C. The results have shown that at 10 or 15°C, the kinetics of fibrillization were slowed down, with no monomer depletion that could be observed over time. On the contrary, the experiments at 20°C displayed fast kinetics of oligomerization that did not allow us to observe any possible exchange between the monomer and aggregated species in solution. This indicated that only a small temperature window between 15 and 20°C at which the coexistence of species in interaction with each other could exist.

Gel electrophoresis also supports this conclusion as, in different protocols, no hIAPP oligomers could be observed on the gels whereas stable small aggregates (tetramers or pentamers) were detected in the wells for A $\beta$ 42. Gel electrophoresis failed to detect the presence of small stable aggregates for hIAPP, even with a sensitive detection such as silver staining. Moreover, results showed that the monomer band was only present in the well of the freshly dissolved peptide but not in the wells with longer incubation times, which meant that there was no coexistence between small oligomers and prefibrillar aggregates. This shows that hIAPP oligomerizes very quickly after being dissolved in the buffer promoting the formation of large oligomers instead of smaller species. These results are consistent with the NMR experiments results, where we could see a complete disappearance of the monomer signal only after a few hours of incubation. NMR and gel electrophoresis therefore show consistent results with the literature, suggesting the no formation of IAPP oligomers.

CD experiments on hIAPP showed a change of conformation from random coil to  $\beta$ -sheet within the first few hours of incubation with little transitory states and no observation of an isodichroic point. If we can observe a decrease of signal at 200 nm, consistent with structuration of the peptide, results have also shown that the signal at 225 nm is quite stable. This could suggest that the peptide undergoes, a conformational switch concomitant with a

quick oligomerization and formation of large oligomers that would lead to light scattering, therefore inducing a global loss of signal over time. The transition from random coil to  $\beta$ -sheet is much faster for hIAPP than for A $\beta$ 42 for which we observe a gradual shift of the signal with the presence of an isodichroic point at 208 nm. This point, which is likely to indicate the presence of an exchange between large and small oligomeric species or monomer tends to indicate that the oligomerization process of hIAPP and A $\beta$ 42 follows a different pattern.

In this study we tried to be as consistent as possible, in order to be able to compare results obtained by different spectroscopic techniques. However fluorescence experiments required the use of molecular probes at a high concentration 75  $\mu$ M. Therefore we investigated the effect of the probes on the kinetics of fibrillization since the probes could interfere with the oligomerization process as they bind to specific sites of the peptides and hamper the elongation phase. Previous research has showed that fluorescent probes, for example Congo Red could interfere with the processes of misfolding and protein aggregation, promoting or inhibiting the fibril formation.<sup>17,18</sup> ThT was reported to have no or little effect on the kinetics of aggregation of amyloid peptides, but studies are usually done at a lower concentration than the one we used for this project (5 to 10  $\mu$ M).<sup>19,20</sup> Studies about the influence of the TROL on the fibrillization has not been done yet.

If the experiments on A $\beta$ 42 showed only little effect of the fluorescent probes on the fibrillization of the peptide, the results of the experiment on hIAPP with fluorescent probes showed striking differences compared to the results that were obtained for the peptide alone and were shown to be batch-dependent.

With the first batch of the peptide that we used, NMR experiments, both <sup>1</sup>H spectra and PFG experiments, on hIAPP with fluorescent probes showed striking differences compared to the results that were obtained for the peptide alone. Indeed, when with ThT and TROL, the depletion rate of the monomer slowed down considerably suggesting that amyloidogenic propensity of hIAPP was lessened in presence of fluorescent probes. CD spectra, although difficult to interpret showed that hIAPP adopted a  $\beta$ -sheet conformation over time in the presence of fluorescent probes but at a lower rate than in their absence. We also seemed to encounter another inconvenience as the formed aggregates were likely to sink at the bottom of the CD cuvette, as it may have been observed with our first CD experiment on hIAPP in presence of ThT (figure 69A). In spite of NMR and CD results that showed that, although the oligomerization kinetics seemed hampered by the presence of fluorescent probes, observation

of those samples by TEM showed that the peptide had formed several fibrils, in their mature state, *i.e.* dense mats of twisted fibrils, with a width and a morphology that could easily be compared to the fibrils that could be seen for the hIAPP sample that was devoid of fluorescent probes. Given this first set of results, the same experiments were carried out on another batch of hIAPP and at a higher temperature. The results showed that the fluorescent probes still influenced the kinetics of oligomerization of the peptide, but to a much lesser extent.

### 3. Conclusion

The results of all experiments that were performed in identical experimental conditions showed that the fibrillization mechanism of hIAPP seemed to be a mostly cooperative process. The kinetics of oligomerization are very fast and characterized by the quick aggregation of the monomer into large insoluble fibrils with no or short-lived, unstable, small oligomers that could not be detected by the described techniques. The mechanism also presents an absence of exchange process between all different species or, they do interact at a very slow exchange rate, still promoting the existence of large oligomers and fibrils over time. On the contrary, A $\beta$ 42 peptide, presents a more stepwise mechanism, with the persisting presence of the monomer over time that exchanges at a fast rate with the larger oligomers that are undetected by NMR spectroscopy.

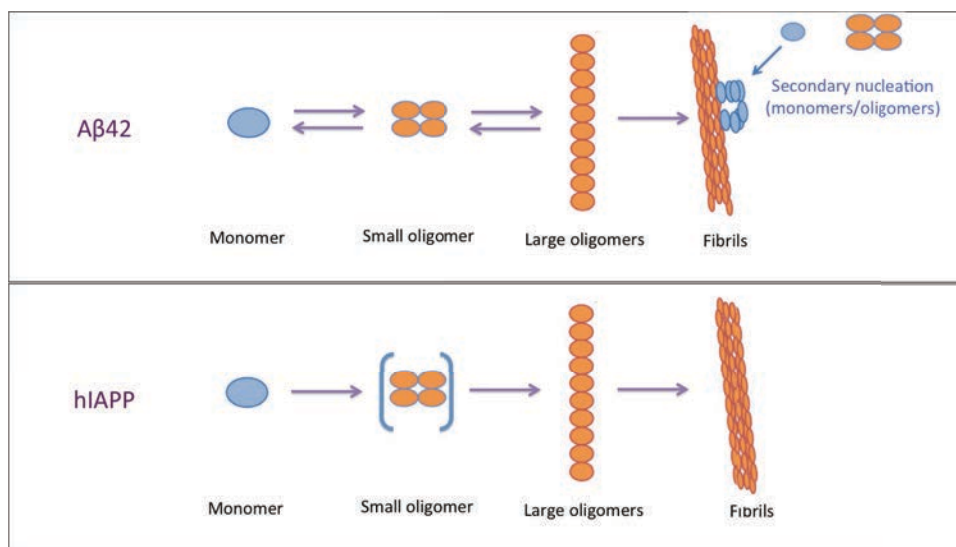


**Figure 76: Schematic representation of the mechanisms models oligomerization and fibrillization for A $\beta$ 42 and hIAPP.**

**(Top) The mechanism for A $\beta$ 42 is gradual, involving reversible states and exchanges between monomeric/small oligomeric with larger species, as shown by the secondary nucleation. (Bottom) hIAPP displays a cooperative mechanism with the existence of small oligomers that are short lived and were not detected by our techniques. The mechanism is shown to be irreversible, with no specific exchanges between small oligomers and larger species.**

As for the interaction with the fluorescent probes, it was shown that ThT and TROL affect the kinetics of fibrillization of the amyloid peptides, slowing them down, especially when they interact with hIAPP, and only little effect was observed with A $\beta$ 42. This suggests that, at this concentration, the presence of ThT or TROL may induce a bias in our fluorescence results, which has to be taken into account.

#### 4. Materials and Methods

The syntheses of hIAPP and A $\beta$ 40/42 were performed at the Institut de Biologie Intégrative (IFR83) at the University Pierre et Marie Curie. A $\beta$ 42 and hIAPP with an amidated C-terminus and disulfide bridge were synthesized using Fmoc chemistry. The peptides were then purified by HPLC and characterized by MALDI-TOF mass spectrometry.

hIAPP used for the second set of experiments with fluorescent probes was purchased from Bachem.

##### Sample preparation

*hIAPP*: Peptide stock solution was obtained by dissolving the peptide at a concentration of 1 mM in hexafluoroisopropanol (HFIP) for one hour. Then, HFIP was evaporated and the sample was dried by vacuum dessication for at least 30 min. The resulting peptide film was dissolved at a concentration of 1 mM in either DMSO (fluorescence experiments) or in a 10 mM sodium phosphate buffer, pH 7.4 (Circular Dichroism, TEM and gel electrophoresis) or 10 mM sodium phosphate buffer pH 7.4 prepared in D<sub>2</sub>O (NMR experiments)

For the second set of NMR and CD experiments at 30°C: IAPP was dissolved in HFIP, and divided in six aliquots. HFIP was then evaporated under nitrogen gas then were dried in a vacuum dessicator for at least 30°C. The resulting peptidic film was dissolved at a concentration of 75  $\mu$ M in 10 mM sodium phosphate buffer prepared in D<sub>2</sub>O.

*A $\beta$ 40/A $\beta$ 42 preparation*: Peptide stock solution was obtained by dissolving the peptide at a concentration of 1 mM in a 1% NH<sub>4</sub>OH aqueous solution.

*Fluorescent dyes*: ThT was dissolved at a concentration of 1 mM in either milliQ water (for ThT, CD, TEM experiments) or D<sub>2</sub>O (NMR experiments). TROL was dissolved at a

concentration of 1 mM in either milliQ water containing 1% DMSO for solubilization of the dye (for ThT, CD, TEM experiments) or D<sub>2</sub>O containing 1% DMSO (NMR experiments)

### **Fluorescence assays**

The kinetics of fibril formation was measured using the fluorescence intensity increase upon binding of the fluorescent probes Thioflavin T (ThT) to fibrils and Tryptophanol (TROL) to oligomers. A plate reader (Fluostar Optima, BMG LabTech, Offenburg, Germany) and a standard 96 well black microtiter plate were used. Prior to the first measurement, the plate was shaken at 600 rpm for 10s. The fluorescence was measured at room temperature from the top of the plate every 10 minutes with excitation filter at 440 nm and emission filter at 480 nm for ThT and with excitation filter at 280 nm and emission filter at 340 nm for TROL.

The fluorescence assay was started by adding 15  $\mu$ L of a 1 mM hIAPP in DMSO or 1 mM A $\beta$ 42 in NH<sub>4</sub>OH (1%) solution to 185  $\mu$ L of a mixture of 75  $\mu$ L ThT/TROL and 10 mM sodium phosphate buffer pH 7.4.

Experiments were carried out once, for each fluorescent probe. Each sample was done in triplicate wells in the plate.

### **Circular dichroism**

The changes in secondary structure for hIAPP and A $\beta$ 42 were measured using a Jasco J-815 CD spectropolarimeter with a Peltier temperature-controlled cell holder over the wavelength range 190-260 nm.

Measurements were carried out in cells of 0.1 cm path length at 20°C for hIAPP and 30°C for A $\beta$ 42 in aqueous solution (10 mM phosphate buffer, pH 7.4). For each sample, measurements were taken every 0.2 nm at a scan rate of 10 nm/min. Spectra were acquired every 30 minutes over a period of 7 to 16 hours. Peptide concentration was 75  $\mu$ M.

### **NMR experiments**

NMR experiments were recorded on a Bruker Avance III 500 MHz spectrometer equipped with a <sup>1</sup>H/<sup>13</sup>C/<sup>15</sup>N TCI cryoprobe with Z-axis gradient. NMR spectra were processed and analysed with TopSpin software (Bruker).

One-dimensional spectra were acquired over 8000 points using a spectral width of 6000 Hz. Solvent resonance was suppressed using presaturation during the relaxation delay. The experiments were done at a temperature of 10, 15, 20 and 30°C for hIAPP and 30°C for A $\beta$ 42.

<sup>1</sup>H NMR diffusion measurements were carried out at 500 MHz using a LED experiment using bipolar gradients and Watergate pulse sequence with squared gradient pulses of constant duration and variable gradient amplitude along the longitudinal axis.

1D <sup>1</sup>H STD experiments were acquired using a cascade of Gaussian shaped pulses (50 ms pulse, B<sub>1</sub> field of 0.1 kHz, total duration of 3 s) applied on resonance (-0.7 ppm) and off resonance (+30 ppm), alternatively. The number of scans was set to 320, corresponding to an experiment duration of 50 min.

### **Electron Microscopy**

TEM was performed on each sample after a 4 day incubation at room temperature, at Faculté de Médecine Xavier Bichat, in order to describe fibrils morphology. 25  $\mu$ L of each sample were adsorbed onto glow-discharged carbon coated 200 mesh copper grids. After the grids have dried off, the grids were negatively stained during 45 s with a 2.5% uranyl acetate solution in 1:1 ethanol/water. The grids were then blotted and dried. Grids were examined using a JEOL 1010 electron microscope operating at 80 kV.

### **Gel Electrophoresis**

Acrylamid gels were either prepared in the lab, following the protocole described thereafter (table 11) or we used commercial Tris-Glycine gels (Mini- Protean® TGX™ pre-cast gels, BioRad) 4-20%.

<b>Composition of Bis Tris gel</b>
<b>Stacking gel:</b> 0.67 mL Acrylamid/Bis (29:1) 1.42 mL Bis Tris 1,25 M pH 6.8 2.9 mL H <sub>2</sub> O milliQ 40 µL Ammonium persulfate 10% 20 µL TEMED
<b>Resolving gel:</b> 4 mL Acrylamid/Bis (29:1) 2.86 mL Bis Tris 1,25 M pH 6.8 3.14 mL H <sub>2</sub> O milliQ 67 µL Ammonium persulfate 10% 18.7 µL TEMED

**Table 11: composition of Bis-Tris 12% gel**

Peptide concentration during the incubation was 50 µM (Native Tris Glycine 4-20% gel and Bis Tris 12% gel) or 100 µM (Tris Glycine 4-20% gel). Peptide samples were mixed with a bromophenol blue sample buffer (table 12).

*Sample buffers composition:*

<b>Native Tris Glycine Sample buffer (2X)</b>	<b>Tris Glycine gel Sample Buffer (2X)</b>	<b>Bis Tris gel Sample Buffer (4X)</b>
0.187 M Tris/HCl 30% glycerol 0.08% Bromophenol Blue	250 mM Tris-HCl pH 6.8 8 % SDS 0.05 % Bromophenol Blue 10 % glycerol	0.12 M Tris 4% SDS (w/v) 20% glycerol (v/v) 0.08% Bromophenol Blue (w/v)

**Table 12: Sample buffer composition**



*Running buffers composition:*

<b>Native Tris Glycine (4X)</b>	<b>Tris Glycine</b>	<b>Bis Tris (5X)</b>
100 mM Tris 75 mM Glycine	100 mM Tris 75 mM Glycine 0.004% SDS (w/v)	50 mM MES 50 mM Tris 1 mM EDTA 0.1% SDS (w/v) 1 mM Na <sub>2</sub> S <sub>2</sub> O <sub>3</sub>

**Table 13: Sample buffer composition**

Migration of the samples was done in the appropriate buffer (table 13) under a voltage of 200 mV at room temperature.

- 
- <sup>1</sup>Meier, J. J., R. Kaye, C.-Y. Lin, T. Gurlo, L. Haataja, S. Jayasinghe, R. Langen, C. G. Glabe, and P. C. Butler. "Inhibition of Human IAPP Fibril Formation Does Not Prevent Beta-Cell Death: Evidence for Distinct Actions of Oligomers and Fibrils of Human IAPP." *AJP: Endocrinology and Metabolism* 291, no. 6 (July 5, 2006): E1317–24. doi:10.1152/ajpendo.00082.2006.
- <sup>2</sup>Jan, A., O. Adolfsson, I. Allaman, A.-L. Buccarello, P. J. Magistretti, A. Pfeifer, A. Muhs, and H. A. Lashuel. "A 42 Neurotoxicity Is Mediated by Ongoing Nucleated Polymerization Process Rather than by Discrete A 42 Species." *Journal of Biological Chemistry* 286, no. 10 (March 11, 2011): 8585–96. doi:10.1074/jbc.M110.172411.
- <sup>3</sup>Haataja, Leena, Tatyana Gurlo, Chang J. Huang, and Peter C. Butler. "Islet Amyloid in Type 2 Diabetes, and the Toxic Oligomer Hypothesis." *Endocrine Reviews* 29, no. 3 (May 2008): 303–16. doi:10.1210/er.2007-0037.
- <sup>4</sup>Kayed, R., E. Head, et al.. "Common structure of soluble amyloid oligomers implies common mechanism of pathogenesis." *Science* (2003) **300**(5618): 486-489.
- <sup>5</sup>Glabe, Charles G. "Common Mechanisms of Amyloid Oligomer Pathogenesis in Degenerative Disease." *Neurobiology of Aging* 27, no. 4 (April 2006): 570–75. doi:10.1016/j.neurobiolaging.2005.04.017.
- <sup>6</sup>Lashuel, Hilal A., Dean Hartley, Benjamin M. Petre, Thomas Walz, and Peter T. Lansbury. "Neurodegenerative Disease: Amyloid Pores from Pathogenic Mutations." *Nature* 418, no. 6895 (July 18, 2002): 291–291. doi:10.1038/418291a.
- <sup>7</sup>Coalier, Kelley A., Geeta S. Paranjape, Sanjib Karki, and Michael R. Nichols. "Stability of Early-Stage Amyloid-β(1–42) Aggregation Species." *Biochimica et Biophysica Acta (BBA) - Proteins and Proteomics* 1834, no. 1 (January 2013): 65–70. doi:10.1016/j.bbapap.2012.08.017.
- <sup>8</sup>Soong, Ronald, Jeffrey R. Brender, Peter M. Macdonald, and Ayyalusamy Ramamoorthy. "Association of Highly Compact Type II Diabetes Related Islet Amyloid Polypeptide Intermediate Species at Physiological Temperature Revealed by Diffusion NMR Spectroscopy." *Journal of the American Chemical Society* 131, no. 20 (May 27, 2009): 7079–85. doi:10.1021/ja900285z.

- 
- <sup>9</sup>Vaiana, Sara M., Rodolfo Ghirlando, Wai-Ming Yau, William A. Eaton, and James Hofrichter. "Sedimentation Studies on Human Amylin Fail to Detect Low-Molecular-Weight Oligomers." *Biophysical Journal* 94, no. 7 (April 1, 2008): L45–47. doi:10.1529/biophysj.107.125146.
- <sup>10</sup>Groenning, Minna. "Binding Mode of Thioflavin T and Other Molecular Probes in the Context of Amyloid Fibrils—current Status." *Journal of Chemical Biology* 3, no. 1 (March 2010): 1–18. doi:10.1007/s12154-009-0027-5.
- <sup>11</sup>Reinke, Ashley A., Gelareh A. Abulwerdi, and Jason E. Gestwicki. "Quantifying Prefibrillar Amyloids in Vitro by Using a 'Thioflavin-Like' Spectroscopic Method." *Chembiochem: A European Journal of Chemical Biology* 11, no. 13 (September 3, 2010): 1889–95. doi:10.1002/cbic.201000358.
- <sup>12</sup>Kayed, Rakez, Jürgen Bernhagen, Norma Greenfield, Khuloud Sweimeh, Herwig Brunner, Wolfgang Voelter, and Aphrodite Kapurniotu. "Conformational Transitions of Islet Amyloid Polypeptide (IAPP) in Amyloid Formation in Vitro." *Journal of Molecular Biology* 287, no. 4 (1999): 781–96.
- <sup>13</sup>Arndt, Claudia, Stefanie Koristka, Holger Bartsch, Michael Bachmann, Biji T., Editor Kurien, and R. Hal, Editor Scofield. "Native Polyacrylamide Gels." *Protein Electrophoresis: Methods and Protocols*, Methods in Molecular Biology: Methods and Protocols, 2012, 49. doi:10.1007/978-1-61779-821-4\_5.
- <sup>14</sup>Sarroukh, Rabia, Emilie Cerf, Sylvie Derclaye, Yves F. Dufrêne, Erik Goormaghtigh, Jean-Marie Ruyschaert, and Vincent Raussens. "Transformation of Amyloid  $\beta$ (1–40) Oligomers into Fibrils Is Characterized by a Major Change in Secondary Structure." *Cellular and Molecular Life Sciences* 68, no. 8 (April 2011): 1429–38. doi:10.1007/s00018-010-0529-x.
- <sup>15</sup>Stine, W. Blaine, Lisa Jungbauer, Chunjiang Yu, and Mary Jo LaDu. "Preparing Synthetic A $\beta$  in Different Aggregation States." *Methods in Molecular Biology (Clifton, N.J.)* 670 (2011): 13–32. doi:10.1007/978-1-60761-744-0\_2.
- <sup>16</sup>Garfin, David E. "[33] One-Dimensional Gel Electrophoresis." In *Methods in Enzymology*, edited by Murray P. Deutscher, 182:425–41. Guide to Protein Purification. Academic Press, 1990. <http://www.sciencedirect.com/science/article/pii/007668799082035Z>.
- <sup>17</sup>Lorenzo, A, and B A Yankner. "Beta-Amyloid Neurotoxicity Requires Fibril Formation and Is Inhibited by Congo Red." *Proceedings of the National Academy of Sciences of the United States of America* 91, no. 25 (December 6, 1994): 12243–47.
- <sup>18</sup>Kim, Yong-Sung, Theodore W. Randolph, Mark C. Manning, Fred J. Stevens, and John F. Carpenter. "Congo Red Populates Partially Unfolded States of an Amyloidogenic Protein to Enhance Aggregation and Amyloid Fibril Formation." *Journal of Biological Chemistry* 278, no. 12 (March 21, 2003): 10842–50. doi:10.1074/jbc.M212540200.
- <sup>19</sup>Foderà, Vito, Fabio Librizzi, Minna Groenning, Marco van de Weert, and Maurizio Leone. "Secondary Nucleation and Accessible Surface in Insulin Amyloid Fibril Formation." *The Journal of Physical Chemistry B* 112, no. 12 (March 2008): 3853–58. doi:10.1021/jp710131u.
- <sup>20</sup>Nielsen, Liza, Ritu Khurana, Alisa Coats, Sven Frokjaer, Jens Brange, Sandip Vyas, Vladimir N. Uversky, and Anthony L. Fink. "Effect of Environmental Factors on the Kinetics of Insulin Fibril Formation: Elucidation of the Molecular Mechanism†." *Biochemistry* 40, no. 20 (May 1, 2001): 6036–46. doi:10.1021/bi002555c.



# **Chapter 4:**

**Effect of charge and mutation of residue 18 on the aggregation properties of the Islet Amyloid PolyPeptide (IAPP) in membrane environment**



## 1. Introduction

As introduced in chapter 1, hIAPP is co-secreted with insulin in the pancreatic islets of Langerhans in secretory vesicles at a slightly acidic pH of 5.5. Once formed, the fully functional hIAPP is released in the extracellular medium at pH 7.4, where it tends to aggregate under favorable conditions. Although oligomers and fibrils can be found in the intracellular medium, it has been shown that numerous factors (pH values, ionic strength, metal ion and protein components such as insulin) prevent the misfolding and aggregation of the peptide in the  $\beta$ -cell secretory granules.<sup>1</sup> Among those factors, studies have shown a link between the slightly acidic pH of the intracellular medium and the aggregation propensity of the peptide.<sup>2</sup> Indeed, one of the particularities of hIAPP is the presence of a single histidine in position 18. In the peptide, the pKa of the histidine is expected to be around 6, which means that its protonation state should be affected by the change of pH from intracellular to extracellular compartments. At pH 5.5, in the secretory granules, the histidine is protonated, leading to a global charge of +4 (protonated Lys1, Arg11, His18 residues and N-terminus group) whereas at pH 7.4, in the extracellular medium, this residue is uncharged, which results in a global charge of +3 for the peptide (assuming that the N-terminal backbone amine group is charged). This change in the state of protonation is likely to modify the electrostatic interactions either within the monomer or between monomers and thus could interfere with the fibrillization process. Another particularity of the residue 18 is that, if a histidine is present in the human sequence of hIAPP, it can differ in the sequences of other mammalian species that are able to secrete hIAPP (Figure 77). Attention was especially drawn to the non-amyloidogenic and non-toxic rat IAPP, where among the 6 residues that differ from the human IAPP sequence, the residue 18 is an arginine instead of a histidine.

	1	10	20	30
Human :	KCNTATCAT	QRLANFLVHS	SNNFGAILSS	TNVGSNTY
Rat :	KCNTATCAT	QRLANFLVRS	SNNLGPVLPP	TNVGSNTY
Monkey :	KCNTATCAT	QRLANFLVRS	SNNFGTILSS	TNVGSNTY
Porcine :	KCNMATCAT	QHLANFLDRS	RNNLGTIFSP	TKVGSNTY
Cow :	KCGTATCET	QRLANFLAPS	SNKLGAI FSP	TKMGSNTY
Cat :	KCNTATCAT	QRLANFLIRS	SNNLGAILSP	TNVGSNTY
Dog :	KCNTATCAT	QRLANFLVRS	SNNLGAILSP	TNVGSNTY
GuineaPig :	KCNTATCAT	QRLTNFLVRS	SHNLGALLP	TDVGSNTY
Hamster :	KCNTATCAT	QRLANFLVHS	NNNLGPVLS P	TNVGSNTY
Ferret :	KCNTATCVT	QRLANFLIHS	SNNLGAILLP	TDVGSNTY
Rabbit	CNTVTCAT	QRLANFLIHS	SNNFGAFLPPS	
Hare :		T QRLANFLIHS	SNNFGAFLPPT	

Figure 77: Sequences of IAPP for several mammalian species. In red: residues that differ from the human IAPP sequence

To determine the involvement of His18 and the further effects of electrostatic interactions in the fibrillization process, four mutants of hIAPP have been synthesized. Residue 18 was substituted from a histidine to an arginine (hIAPP18R), lysine (hIAPP18K), glutamic acid (hIAPP18E) or alanine (hIAPP18A), which are either positively/negatively charged or uncharged, and therefore involving different interactions of the residue with its close environment. Lysine and arginine are both polar, basic amino acids. On the contrary, glutamic acid is an acidic amino acid, with a pKa of  $4.2 \pm 0.9$ , therefore negatively charged at pH 5.5 and 7.4. The substitution of His18 by Ala18 allowed us to observe the influence of both the charge and the side-chain, as alanine is neutral and possesses a short side chain.

The introduction of differently charged amino acids also allowed us to observe the effect of the pH on the kinetics of oligomerization and fibrillization as the substitution of His18 by differently charged amino acids induces a change in the global charge of the peptide. Indeed, at pH 7.4, the wild-type hIAPP shares the same global charge as mutant hIAPP H18A as both His18 and Ala18 residues are uncharged. At pH 5.5, the histidine residue is positively charged, leading to the same global charge of the peptide as mutants hIAPP H18K and hIAPP H18R (figure 78, table 14).

Additionally, a substitution of the residue 18 could be interesting in regards of the interaction between the peptide and the membrane, as the N-terminal part of IAPP, especially the 19 first residues, were reported to be involved in the first steps of membrane interaction.<sup>3</sup> Likewise, the study at an acidic pH could also influence the interaction between the peptide and the membrane. Indeed, the N-terminus of the peptide is more likely to be protonated at pH 5.5 rather than at pH 7.4, which could induce modifications in the orientation of the peptide on the surface of the lipid bilayer or its depth of burial in the membrane.

hIAPP Wild Type: KCNTATCAT QRLANFLV**HS** SNNFGAILSS TNVGSNTY-NH<sub>2</sub>  
 hIAPP H18K KCNTATCAT QRLANFLV**KS** SNNFGAILSS TNVGSNTY-NH<sub>2</sub>  
 hIAPP H18R KCNTATCAT QRLANFLV**RS** SNNFGAILSS TNVGSNTY-NH<sub>2</sub>  
 hIAPP H18E KCNTATCAT QRLANFLV**ES** SNNFGAILSS TNVGSNTY-NH<sub>2</sub>  
 hIAPP H18A KCNTATCAT QRLANFLV**AS** SNNFGAILSS TNVGSNTY-NH<sub>2</sub>

Figure 78: Sequences of the five synthesized peptides (wild type and mutants)

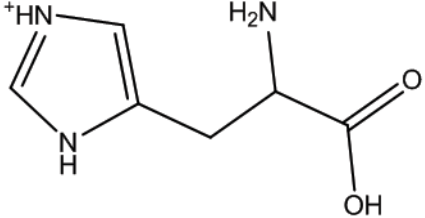
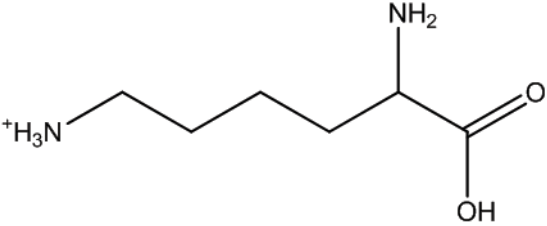
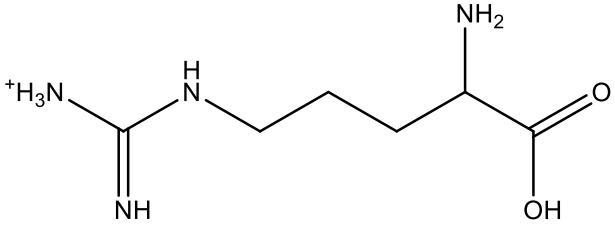
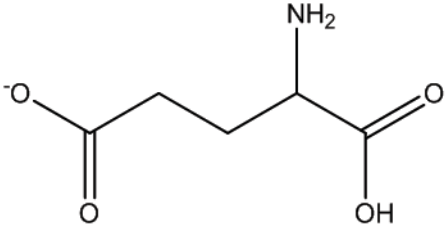
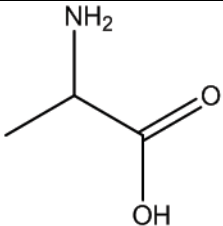
	<p><b>Histidine (H) – pKa around 6.6 ± 1.0</b></p> <p>Positively charged at pH 5.5</p> <p>Global charge +4</p> <p>Uncharged at pH 7.4</p> <p>Global charge +3</p>
	<p><b>Lysine (K) – pKa around 10.5 ± 1.1</b></p> <p>Positively charged at pH 5.5 and 7.4</p> <p>Global charge +4</p>
	<p><b>Arginine (R) – pKa around 12-12.5</b></p> <p>Positively charged at pH 5.5 and 7.4</p> <p>Global charge +4</p>
	<p><b>Glutamic Acid (E) – pKa around 4.2 ± 0.9</b></p> <p>Negatively charged at pH 5.5 and 7.4</p> <p>Global charge +2</p>
	<p><b>Alanine (A)</b></p> <p>Uncharged at pH 5.5 and 7.4</p> <p>Global charge +3</p>

Table 14: Structure of histidine, lysine, arginine, glutamic acid and alanine. Their protonation state at pH 5.5 and 7.4 and the resulting global charge of the peptides were calculated assuming typical pKa values for amino acid side chains and a protonated N-terminus (pKa around 7.7 ± 0.5). The pKa values indicated are average values determined on a set of folded proteins.<sup>4</sup>



To answer those questions, we used different techniques that focused either in the kinetics of the fibrillization or monomer depletion (ThT fluorescence and NMR experiments), the secondary structure of the peptides (circular dichroism), the interaction between the peptide and the membrane (monolayer and calcein leakage experiments) and the morphology of the oligomers or fibrils (transmission electron microscopy).

As hIAPP interacts strongly with the  $\beta$ -cell membrane, all experiments were carried out using a membrane model, with a lipid composition inspired of that of pancreatic  $\beta$ -cells that consisted in a mixture 7:3 of 1,2-dioleoyl-*sn*-glycero-3-phosphocholine (DOPC) with a zwitterionic headgroup and 1,2-dioleoyl-*sn*-glycero-3-phospho-L-serine (DOPS), which is negatively charged. Depending on the experiment, either Small Unilamellar Vesicles (SUV) of 50 nm diameter, Large Unilamellar Vesicles (LUV) of 200 nm or monolayers were used.

## 2. Results and discussion

### a) Fibrillization occurs for all mutants under both pH conditions

The fibrillization kinetics of the different peptides were first studied by ThT fluorescence in the presence of LUVs of DOPC/DOPS (7:3) with a peptide/lipid ratio of 1:10. For all peptides, an increase in the fluorescence intensity could be observed with different rates showing that the peptides formed fibrillar species. Figure 79 shows the kinetics of fibrillization for all 5 peptides. Depending on the mutation, the fibrillization rate varies, with a much higher rate of aggregation for wild type peptide ( $t_{1/2} = 10.55 \pm 0.05$  hrs at pH 5.5;  $t_{1/2} = 7.57 \pm 0.02$  at pH 7.4) and a slower rate for all the mutants, especially hIAPP H18E and hIAPP H18A which fibrillization is slowed down by a factor of 5 to 6.7 in regards of the kinetics of the wild type peptide (Table 15). Mutants hIAPP H18K and hIAPP H18R, with the positively charged substitution seem to share common fibrillization properties, as their fluorescence curves at pH 5.5 and 7.4 are similar, with close kinetics parameters of fibrillization.

The slower rates of fibrillization for all mutants in regard of the wild type peptide show that the histidine in position 18 is likely to involve in specific interactions that promote the formation of oligomers and fibrils. These results also show that the fibrillization does not only depend of the global charge of the peptide, as hIAPP H18A is the mutant with the slowest kinetics of fibrillization despite having the same global charge as the wild type peptide (+3) at pH 7.4. This also supports the fact that the nature of the side chain influences the

fibrillization, since hIAPP H18A has a short side chain. The results for hIAPP H18E, which kinetics of fibrillization are the slowest along with hIAPP H18A, also show that the introduction of a negatively charged side-chain has a negative impact on the fibrillization process.

Overall, regardless of the global charge of the peptides, the kinetics of fibrillization are slower at pH 5.5 than at pH 7.4 as it is systematically slowed down for all peptides by a factor 1.4 to 1.9. The measured slopes of the curves are less steep at pH 5.5 than at pH 7.4 showing that not only the nucleation phase but also the elongation process are slowed down at acidic pH. The results for hIAPP H18K and hIAPP H18R show that their kinetics of fibrillization are slower than those of the wild type peptide, despite having the same global charge than IAPP (+4 at pH 5.5). Mutants hIAPP H18E and hIAPP H18A, as for pH 7.4 have slower rates of fibrillization than the three other peptides. Therefore, these results also indicate that kinetics of oligomerization do not only depend on the global charge of the peptide but also of the nature of the side chain and associated properties. The results of the ThT fluorescence experiments showed that acidic pH is unfavorable to the fibrillization process, which is consistent with previously reported data.<sup>5</sup>

Another interesting fact is that the maximum fluorescence intensity depends on the peptide. At pH 7.4, the higher fluorescence intensity is observed for wild type hIAPP and hIAPP H18E (80 and 100% respectively), but is only 20% for hIAPP H18K and hIAPP H18R and 25% for hIAPP H18A. At pH 5.5, 100% of the fluorescence is obtained with wild type IAPP whereas the maximum for hIAPP H18K and hIAPP H18R reaches about 20% of fluorescence and 10% for hIAPP H18E and hIAPP H18A. This indicates that either ThT probe binds differently to the fibrils, in reason of fewer binding sites, or, that fewer fibrils are formed at final stages of aggregation.

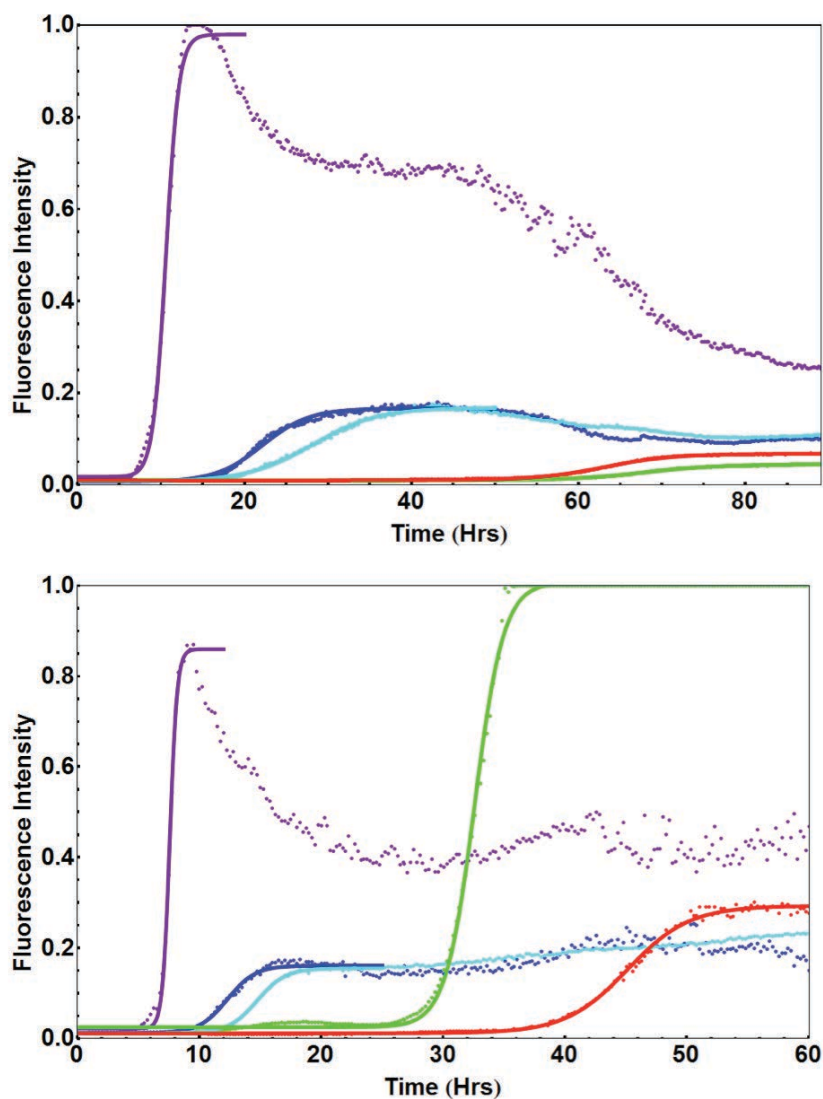


Figure 79: ThT fluorescence of hIAPP Wild Type (purple) and mutants H18K (blue), H18R (cyan), H18E (green) and H18A (red) at pH 5.5 (top) and pH 7.4 (bottom) in the presence of 200 nm Unilamellar Vesicles of DOPC/DOPS (7:3). Dots: mean of triplicates values. Fitted curves were obtained using Mathematica Program.

	pH 7.4		pH 5.5	
	$t_{1/2}$ (hrs)	$\tau$ (hrs <sup>-1</sup> )	$t_{1/2}$ (hrs)	$\tau$ (hrs <sup>-1</sup> )
<b>hIAPP Wild-Type</b>	7.59± 0.02	0.28± 0.02	10.55± 0.05	0.73± 0.04
<b>hIAPP H18K</b>	12.54 ± 0.04	1.30 ± 0.04	21.98 ± 0.09	2.61 ± 0.08
<b>hIAPP H18R</b>	14.79 ± 0.02	1.18 ± 0.02	28.50 ± 0.10	3.98 ± 0.08
<b>hIAPP H18E</b>	35.44 ± 0.28	4.59 ± 0.26	67.97 ± 0.08	4.55 ± 0.07
<b>hIAPP H18A</b>	45.15 ± 0.05	2.55 ± 0.04	63.09 ± 0.06	4.12 ± 0.05

Table 15: Kinetic parameters (half time  $t_{1/2}$  and elongation rate  $\tau$ ) of ThT fluorescence signal for IAPP and four analogs in the presence of DOPC/DOPS (7:3) vesicles

As ThT fluorescence experiments showed that the kinetics of fibrillization of the peptides differed depending on the substitution of the residue 18 and that the nature of fibrils formed at the final states of aggregation were of different nature or quantity, we wanted to focus on what happened in the early stages of the fibrillization that could lead to those differences.

b) Quantification of hIAPP wild type and mutant monomers over time by NMR

1D  $^1\text{H}$  NMR spectra have been recorded in order to observe the early stages of the oligomerization process, namely the “lag phase” observed by ThT fluorescence experiments, as it allows us to observe the signal of the monomeric state of our peptides over time. For the sake of consistency with the other experiments, which were done in presence of LUV (diameter: 200 nm), the NMR experiments were carried out in the presence of model membranes as well. However, the use of LUV in NMR would be detrimental, as their size would lead to a broadening of the NMR signal beyond detection. Therefore, NMR experiments were carried out in the presence of SUV (diameter: 50 nm), which are more appropriate for this type of experiment as their small dimension allows a fast tumbling of the vesicle and leads to a good detection of the NMR signal.<sup>6</sup>

Results on wild type peptide show that at pH 7.4 the signal of the monomeric peptides decreases, as a sign of the aggregation of the peptides (as seen on Figure 80). The signal then stabilizes as a plateau is reached showing a weak residual signal during the rest of the experiment.

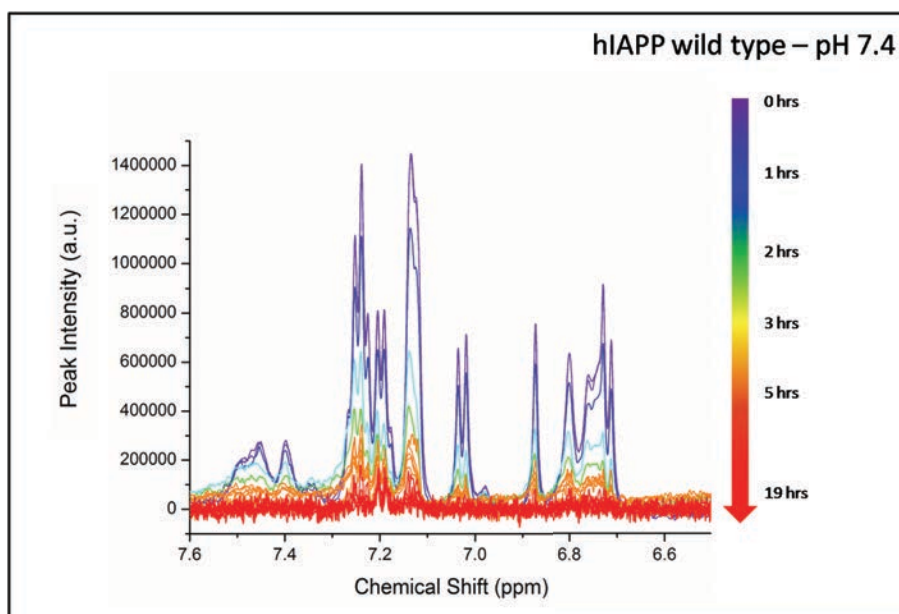


Figure 80: Signal of hiAPP wild type observed over time by liquid-state NMR spectroscopy at pH 7.4 (aromatic region of 1D  $^1\text{H}$  spectra).

Experiments on the mutants at pH 7.4 indicated similar results, with a decreasing signal of the monomer that stabilized over time as it reaches a plateau with residual signals of different intensities (figure 81).

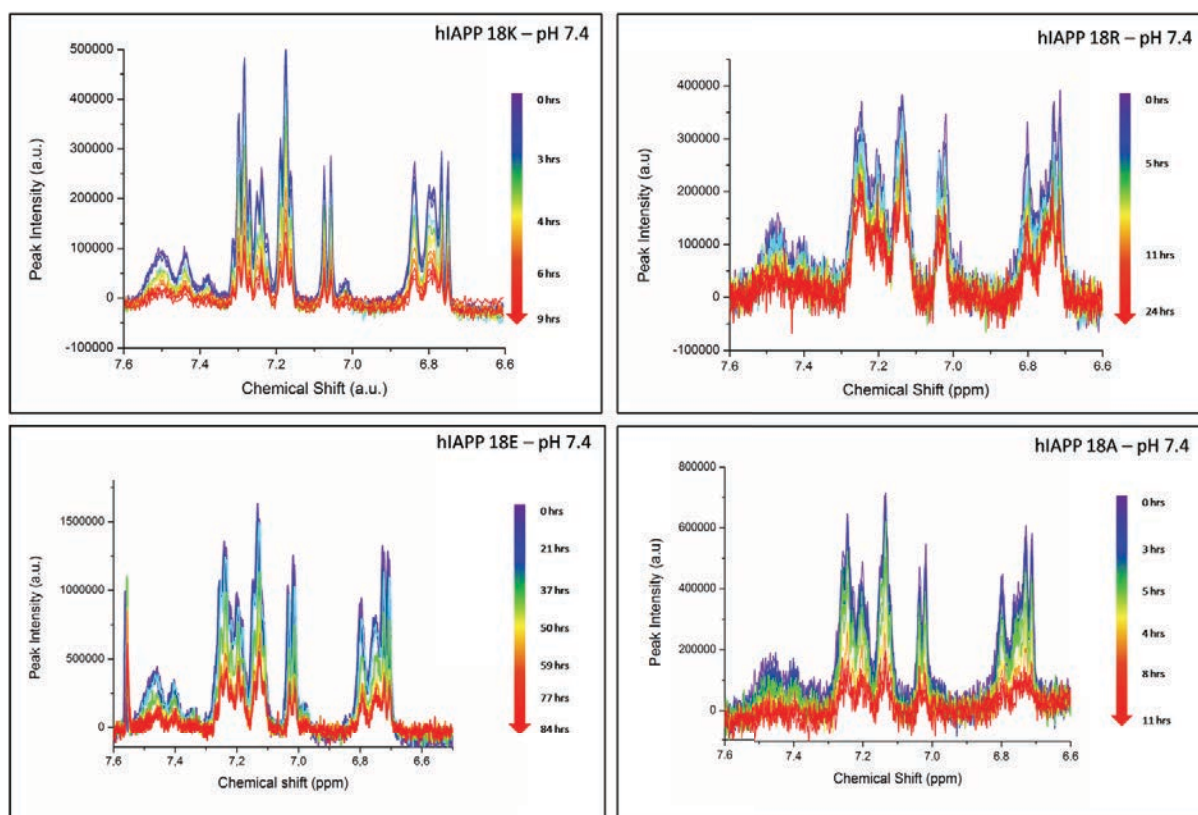


Figure 81: Signal of IAPP H18K (top left), IAPP H18R (top right), IAPP H18E (bottom left) and IAPP H18A (bottom right) observed over time by liquid-state NMR spectroscopy at pH 7.4 (aromatic region of 1D  $^1\text{H}$  spectra).

The intensity of the signal can then be calculated and plotted over time before being fitted with a Boltzmann or a Richards function in order to obtain the rates of monomer depletion and estimate the fraction of residual monomer once the signal is stabilized. Results are shown in Figure 82 and Table 16.

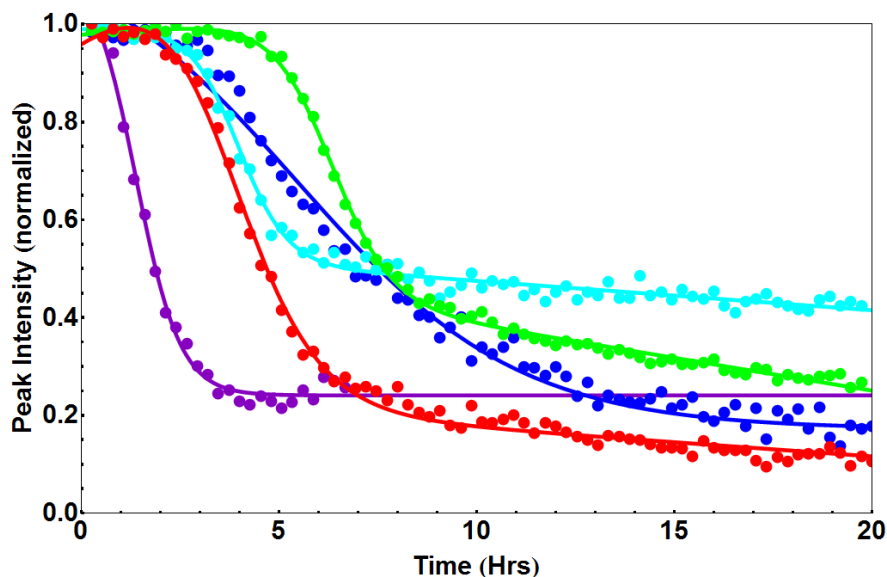


Figure 82: Peak intensity of hIAPP wild type (purple), hIAPP H18K (blue), hIAPP H18R (cyan), hIAPP H18E (green) and hIAPP H18A (red) over time at pH 7.4

	ThT Fluorescence	NMR experiments	
	peptide concentration: 10 $\mu$ M	peptide concentration: 50 $\mu$ M	
	$t_{1/2}$ (hrs)	$t_{1/2}$ (hrs)	Final monomer fraction (%)
<b>hIAPP Wild-Type</b>	7.59 $\pm$ 0.02	0.40 $\pm$ 0.23	5%
<b>hIAPP H18K</b>	12.54 $\pm$ 0.04	3.28 $\pm$ 0.06	17%
<b>hIAPP H18R</b>	14.79 $\pm$ 0.02	2.39 $\pm$ 0.09	44%
<b>hIAPP H18E</b>	35.44 $\pm$ 0.28	> 24	-
<b>hIAPP H18A</b>	45.15 $\pm$ 0.05	9.53 $\pm$ 0.05	23%

Table 16: Kinetics parameters ( $t_{1/2}$ ) of fibrillization process (ThT fluorescence), monomer depletion (NMR experiments) and final monomer fraction linked to monomer depletion for all peptides over the course of NMR experiments for all peptides in presence of DOPC/DOPS (7:3) vesicles at pH 7.4. Peptid/Lipid ratio (1:10)

The results of NMR experiments at pH 7.4 showed that the rates of monomer depletion for the peptides were consistent with the fluorescence experiments result. Indeed, the signal of the wild type peptide disappeared faster than the signal of the four other mutants. Mutants IAPP H18K and IAPP H18R showed a similar monomer depletion rate, with overlapping curves to the exception of the plateau. Finally, IAPP H18E and IAPP H18A exhibited slower

kinetics of aggregation, IAPP H18E being stable during the 24 first hours of incubation, and IAPP H18A having a half time of  $9.53 \pm 0.05$  hours that is 24 times higher than the half time of the wild type peptide and 3 to 4 times higher than those of IAPP H18K and IAPP H18R. As the concentration of the peptide was five times higher than for fluorescence experiments and given the fact that that NMR experiments only allows the observation of the early stages of oligomerization, the timescale for NMR experiments were expected shorter than for fluorescence experiments. However, although the concentrations between ThT and NMR experiments are different, it is still possible to compare the relative values obtained in the series of five peptides.

At pH 5.5, results for wild type peptide indicated that the kinetics of depletion of the monomer were slower at a lower pH than at pH 7.4 ( $t_{1/2} = 1.38 \pm 0.08$  at pH 5.5 whereas  $t_{1/2} = 0.40 \pm 0.23$  at pH 7.4), which a higher intensity of the residual signal (24% vs. 5%) which indicates that not only the oligomerization is slower but also less monomer is consumed at pH 5.5. (figure 83, table 17)

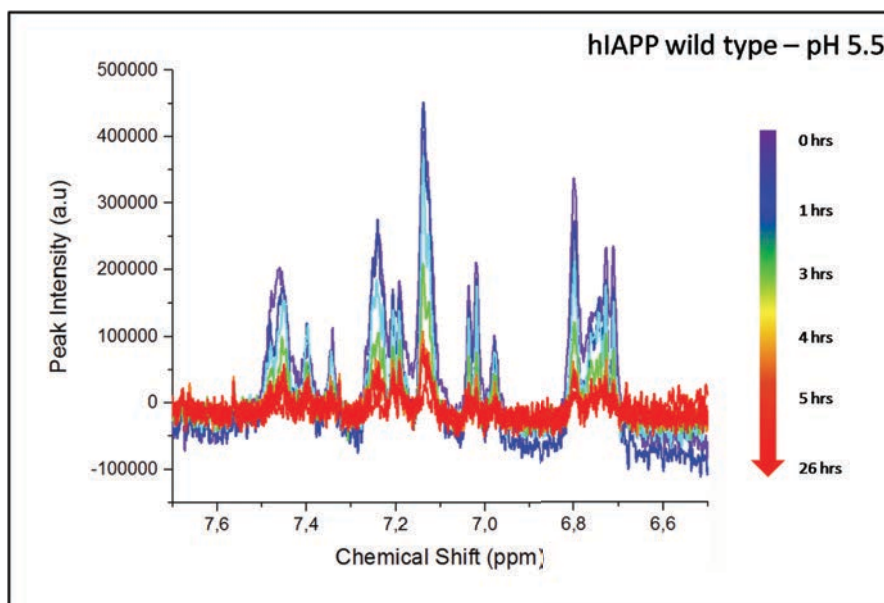
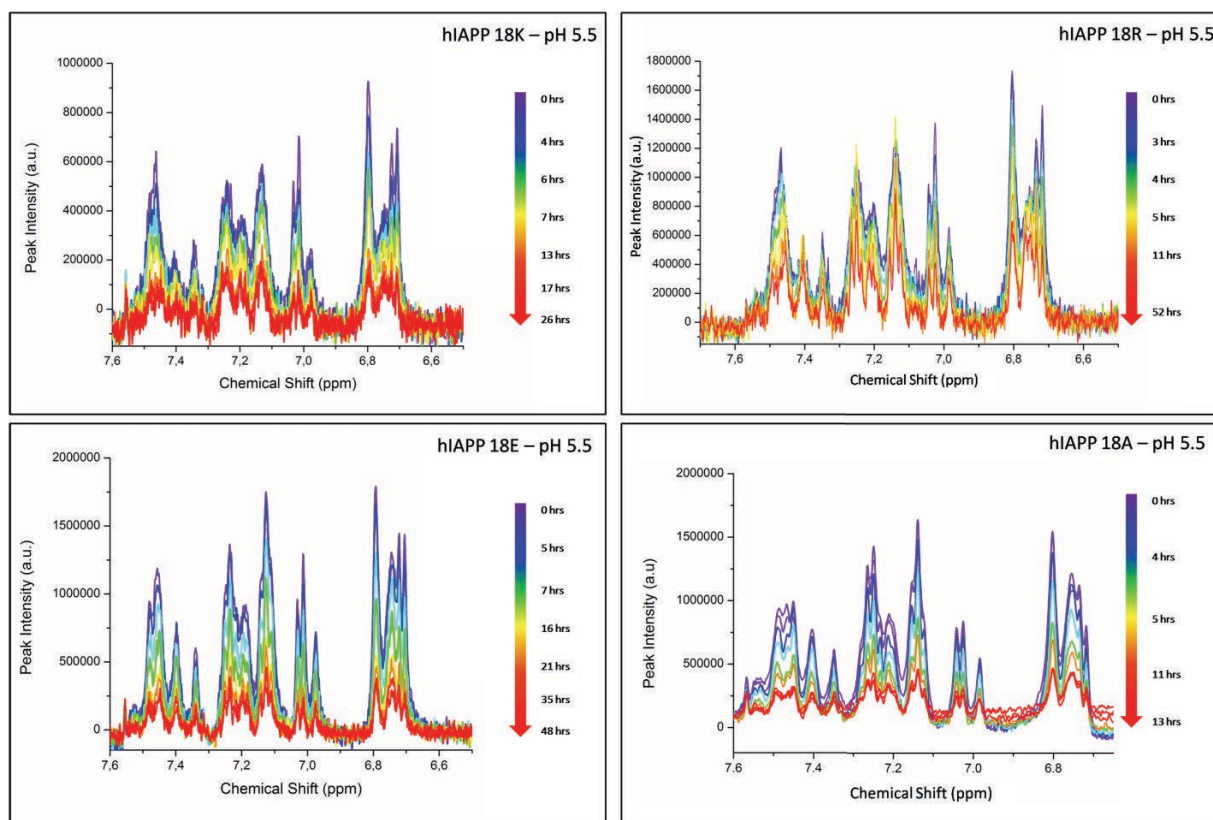


Figure 83: Signal of hIAPP wild type peptide observed over time by liquid-state NMR spectroscopy at pH 5.5 (aromatic region of 1D  $^1\text{H}$  spectra).  
The intensity of the signal decreases over time before reaching a stationary state

Experiments on the mutants showed similar spectra (figure 84).





**Figure 84:** Signal of hIAPP H18K (top left), hIAPP H18R (top right), hIAPP H18E (bottom left) and hIAPP H18A (bottom right) observed over time by liquid-state NMR spectroscopy at pH 5.5 (aromatic region of ID  $^1\text{H}$  spectra).

The measurement of the signal intensity over time showed that the kinetics of monomer depletion were about two times slower for hIAPP H18R and hIAPP H18R at pH 5.5 than at pH 7.4, which is consistent with ThT experiments. However differences are observed for peptides hIAPP H18E and hIAPP H18A. Indeed, if at pH 7.4, hIAPP H18A monomer depletion rate is consistent with what is observed by ThT fluorescence by being much slower than the wild type peptide, it is not the case at pH 5.5, where the signal disappears twice faster than at pH 7.4. A more striking difference is observed for hIAPP H18E mutant where the monomer depletion occurs after more than 24 hours of incubation at pH 7.4 but with a half time depletion of  $6.77 \pm 0.08$  hrs at pH 5.5. (figure 85, table 17) These results show that at an acidic pH, in presence of DOPC/DOPS LUV, monomer depletion occurs faster when the global charge of the peptide is lower.



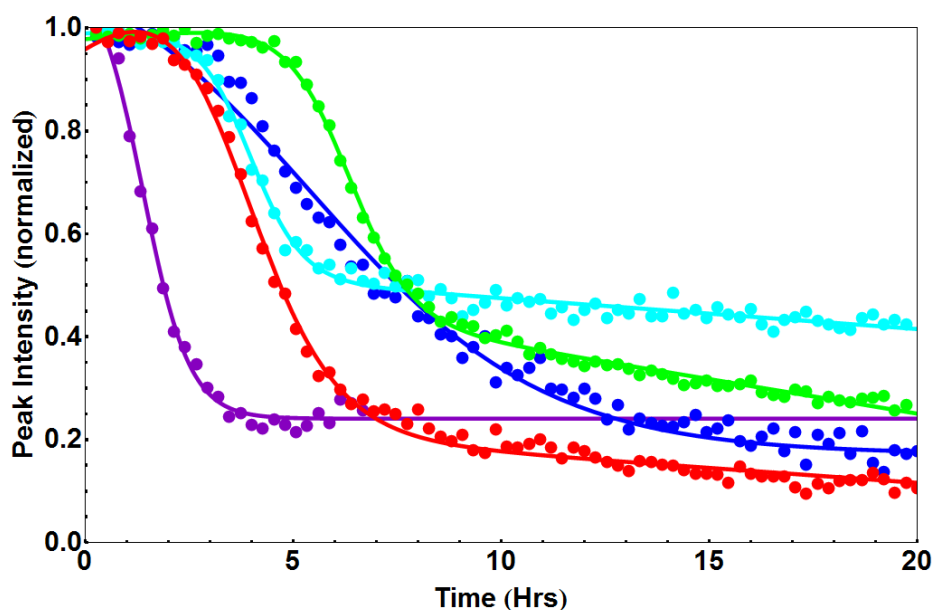


Figure 85: Peak intensity of hIAPP wild type (purple), hIAPP H18K (blue), hIAPP H18R (cyan), hIAPP H18E (green) and hIAPP H18A (red) over time at pH 5.5

	ThT Fluorescence	NMR experiments	
	peptide concentration: 10 $\mu$ M	peptide concentration: 50 $\mu$ M	
	$t_{1/2}$ (hrs)	$t_{1/2}$ (hrs)	Final monomer fraction (%)
<b>hIAPP Wild-Type</b>	10.55 $\pm$ 0.05	1.38 $\pm$ 0.08	24%
<b>hIAPP H18K</b>	21.98 $\pm$ 0.09	5.45 $\pm$ 0.27	17 %
<b>hIAPP H18R</b>	28.50 $\pm$ 0.10	4.12 $\pm$ 0.10	51%
<b>hIAPP H18E</b>	67.97 $\pm$ 0.08	6.77 $\pm$ 0.08	31%
<b>hIAPP H18A</b>	63.09 $\pm$ 0.06	4.09 $\pm$ 0.20	10%

Table 17: Kinetics parameters ( $t_{1/2}$ ) of fibrillization process (ThT fluorescence), monomer depletion (NMR experiments) and final monomer fraction linked to monomer depletion measured by NMR experiments for all peptides in presence of DOPC/DOPS (7:3) vesicles at pH 5.5. Peptid/Lipid ratio (1:10)

Another particularity is observed for mutant hIAPP H18R at both pH. Indeed, if all signals tend to reach a plateau after few hours of incubation, allowing us to estimate the percentage of signal left at the end of the process, the residual signal for hIAPP H18R monomer is much higher than for other peptides. This result shows that although the substitution of the histidine by an arginine does not prevent the oligomerization to occur, it stabilizes the monomeric form.

d) Circular dichroism show shows the formation of large  $\beta$ -sheet aggregates

Circular dichroism experiments were performed to obtain information about the secondary structure of the five peptides at both pH. Peptides were dissolved at 25  $\mu$ M in a 50 mM sodium phosphate, 100 mM NaF at pH 5.5 or pH 7.4 in the presence of 250  $\mu$ M of lipids (LUV, 200 nm), and analyzed at 25°C. At initial time, the signal of the freshly dissolved wild type hIAPP presented two minima around 205 nm and 225 nm. Although the minimum at 205 nm was shifted in regards of the characteristic minimum of the random coil signal (195-200 nm), the peptide appeared to be mainly disordered, as was shown by deconvolution of the signal (table 18).

	Random coil (%)	$\alpha$ -helix (%)	$\beta$ -sheet (%)
<b>hIAPP Wild Type</b>	73.5	6.9	11.2

Table 18 : Percentage values of random coil,  $\alpha$ -helix and  $\beta$ -sheet for IAPP wild type at initial time at pH 7.4. Values were obtained by deconvolution of the CD spectra by CDfriend program.

Over time, we observed a loss of the initial secondary structure in favor of a prevalent  $\beta$ -sheet signal characterized by a minimum around 225 nm (figure 86). We also observed that over time, the  $\beta$ -sheet signal at 225 nm decreased showing that the peptide formed large aggregates that are no longer observable by CD.

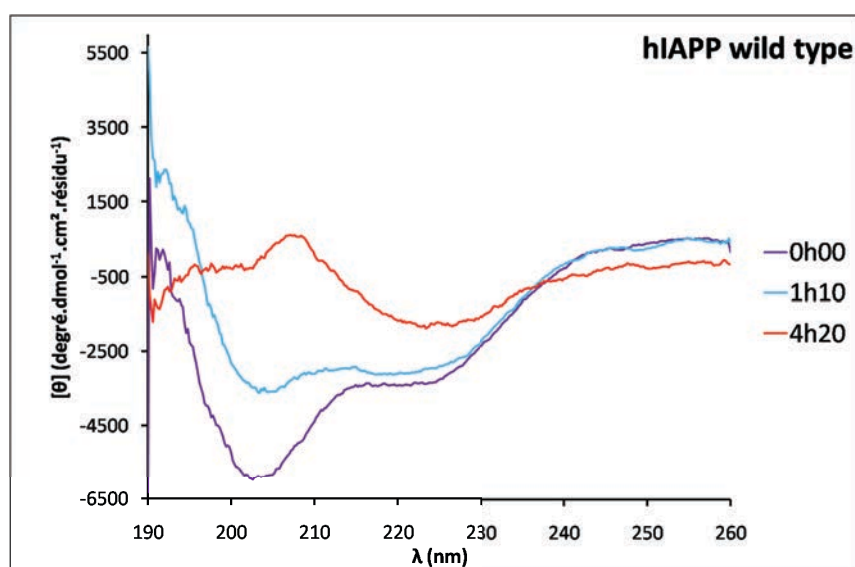
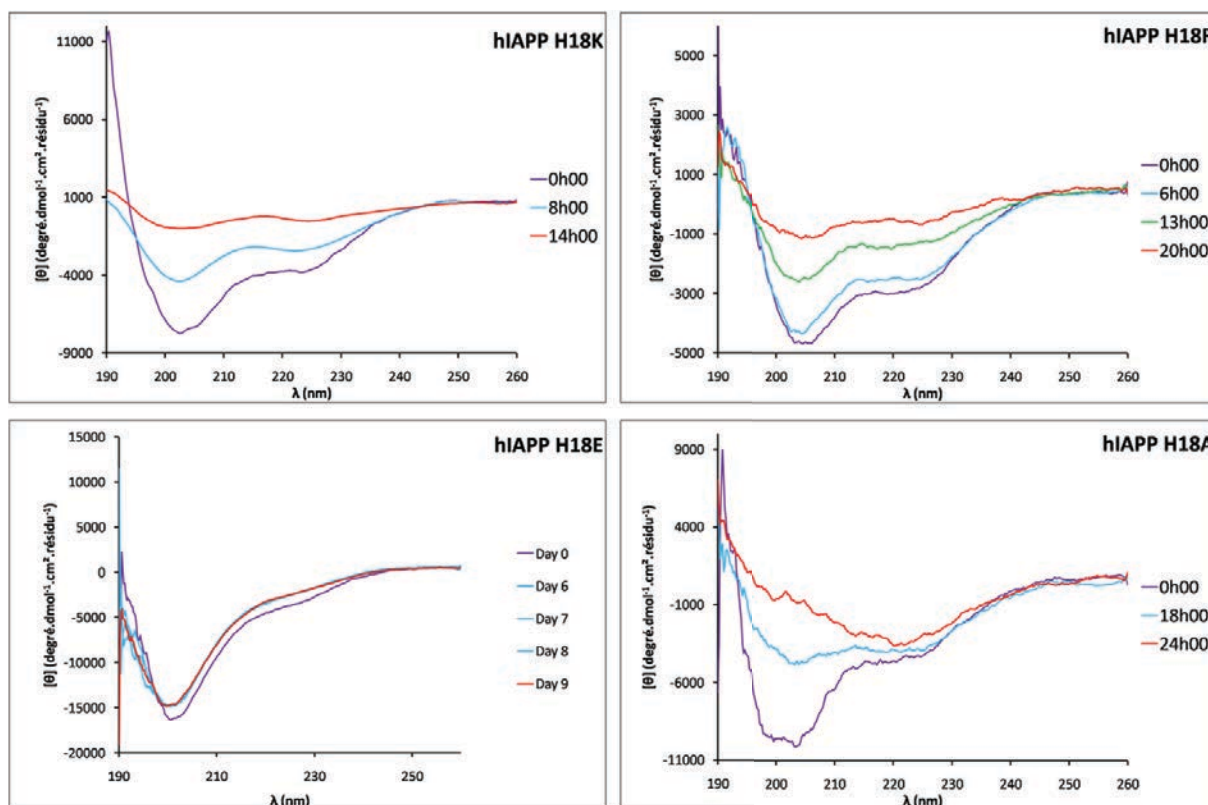


Figure 86: Evolution of the circular dichroism spectrum over time.

At initial time, the spectrum shows two minima at 200-205 and 225 nm. Over time, we can observe a loss of signal, especially at 200-205 nm.

At the same pH, all mutants gave the same initial signal as the wild type mutant, showing a prevalence of random coil. The percentage values of random coil,  $\alpha$ -helix and

$\beta$ -sheet signals were obtained by deconvolution of the signals and shown in table 19. Over time, to the exception of hIAPP H18E which was very stable, all signals evolved in the same way as wild type peptide, favoring a  $\beta$ -sheet conformation, and a complete loss of signal was observed ( $[\theta] = 0 \text{ deg cm}^2 \text{ dmol}^{-1} \text{ residue}^{-1}$ ), showing that large aggregates had formed (figure 87).



**Figure 87:** Circular dichroism spectra of hIAPP wild type and mutants over time at pH 7.4. A loss of signal is observed for all mutants with the exception of hIAPP H18E which signal is stable over the time course of the experiment (9 days). Curves were smoothed on OriginLab by the adjacent-averaging method (25 pts)

	Random coil (%)	$\alpha$ -helix (%)	$\beta$ -sheet (%)
<b>hIAPP Wild Type</b>	73.5	6.9	11.2
<b>hIAPP H18K</b>	73.1	18.3	1.5
<b>hIAPP H18R</b>	75.6	13.9	10.5
<b>hIAPP H18E</b>	60.9	6.7	0
<b>hIAPP H18A</b>	72.6	9.2	4.3

**Table 19 :** Percentage values of random coil,  $\alpha$ -helix and  $\beta$ -sheet for hIAPP wild type and mutants at initial time at pH 7.4. Values were obtained by deconvolution of the CD spectra by CDFriend program.

As showed on Figure 88, the loss of signal at 205 nm over time can be plotted, and shows that the process is characterized by 3 different phases, forming inverted sigmoid

curves. An initial lag time, linked to the initial conformation of the peptide in its monomeric form, is followed by a decrease of the signal as the peptide changes its conformation to a  $\beta$ -sheet structure and aggregates in large oligomers that lead to large scattering. The signal decreases before reaching a plateau corresponding to the formation of large aggregates in solution

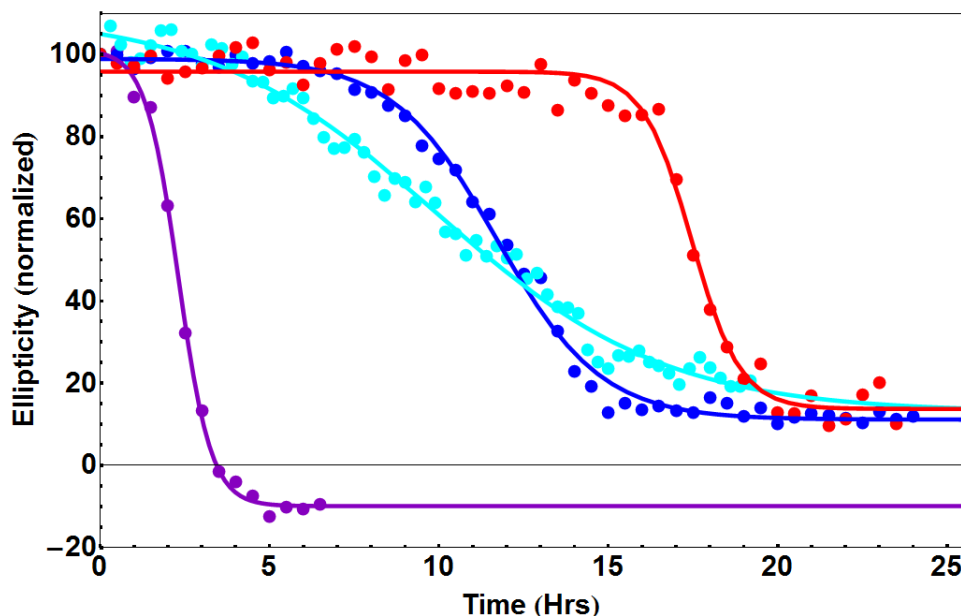


Figure 88: Ellipticity at 205 nm over time of hIAPP wild type (purple), hIAPP H18K (blue), hIAPP H18R (cyan), IAPP hH18A (red) at pH 7.4. A loss of random coil signal is observed for all peptides, except for IAPP hH18E at pH 7.4 which signal remains stable over time (as seen on figure 6)

The signals were fitted by a Boltzmann equation, which allowed us to obtain the kinetics parameters, linked to the loss of initial conformation over time as well as the formation of species, which are too large to give a dichroic signal (Table 20).

Consistent with fluorescence and NMR experiments data, the loss of signal appeared at a slower rate for mutants in comparison to the wild-type peptide, showing slower kinetics of oligomerization. Results for CD experiments indicated that mutants with the positively charged substitution have similar rates of signal-loss ( $t_{1/2} = 11.70 \pm 0.08$  hrs for hIAPP H18K,  $t_{1/2} = 9.94 \pm 0.22$  hrs for hIAPP H18R). CD experiments have also shown that substitution of His18 by Glu18 or Ala18 has the most deleterious effect, with no transition observed for over 7 days for hIAPP H18E, and with a signal-loss rate being increased by a factor 8 for hIAPP H18E in regards to the wild type peptide ( $17.46 \pm 0.089$  hrs vs  $2.30 \pm 0.04$  hrs).

	ThT Fluorescence peptide concentration: 10 $\mu$ M	NMR experiments peptide concentration: 50 $\mu$ M	CD experiments peptide concentration: 25 $\mu$ M
	$t_{1/2}$ (hrs)	$t_{1/2}$ (hrs)	$t_{1/2}$ (hrs)
<b>hIAPP Wild-Type</b>	7.59 $\pm$ 0.02	0.40 $\pm$ 0.23	2.30 $\pm$ 0.04
<b>hIAPP H18K</b>	12.54 $\pm$ 0.04	3.28 $\pm$ 0.06	11.70 $\pm$ 0.08
<b>hIAPP H18R</b>	14.79 $\pm$ 0.02	2.39 $\pm$ 0.09	9.94 $\pm$ 0.22
<b>hIAPP H18E</b>	35.44 $\pm$ 0.28	> 24	No Transition (days)
<b>hIAPP H18A</b>	45.15 $\pm$ 0.05	9.53 $\pm$ 0.05	17.46 $\pm$ 0.089

Table 20: Kinetic parameters (half time  $t_{1/2}$ ) of fibrillization (fluorescence ThT), of monomer depletion (NMR experiments) and random coil loss using the time course of CD ellipticity at 205 nm (CD experiments) at pH 7.4 for all peptides in presence of DOPC/DOPS (7:3) vesicles. Peptid/Lipid ratio (1:10)

At initial time, at pH 5.5, the spectrum of wild type peptide shows prevalence of random coil signal (table 21). Within the first hours of incubation, the signal shifts from random coil to a  $\beta$ -sheet, with the minimum at 205 nm disappearing while the signal at 225 nm increases. Over time, we can observe a loss of signal at 225 nm. This result for wild type peptide shows that the peptide adopts a  $\beta$ -sheet structure and then forms large aggregates that lead to the loss of signal over time (figure 89).

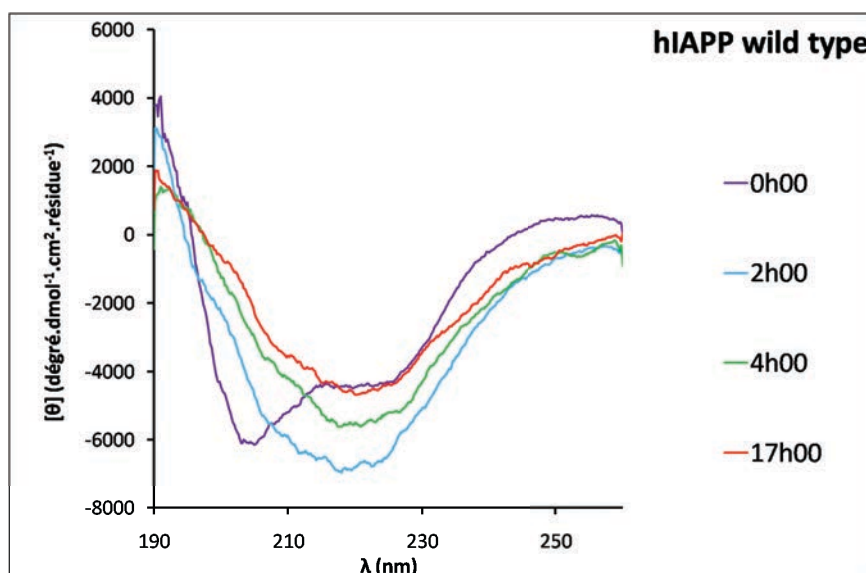


Figure 89: Circular dichroism spectra of hIAPP mutants over time at pH 5.5.

For the mutants, at pH 5.5 a loss of dichroic signal at 205 nm could be observed for all peptides, including hIAPP H18E (figure 90). The ellipticities at 205 nm could also be plotted over time and fitted by a Boltzmann equation, which allowed us to obtain the kinetics

parameters at pH 5.5 (Figure 91 and table 22). At pH 5.5, results showed that to the exception of the wild type peptide, the loss of random coil signal appears faster than at pH 7.4, especially for the hIAPP H18E mutant where the normalized ellipticity at 205 nm decreases within the first 7 hours of experiments ( $t_{1/2} = 3.52 \pm 0.11$  hours) whereas the signal at pH 7.4 remains stable for at least 9 days.

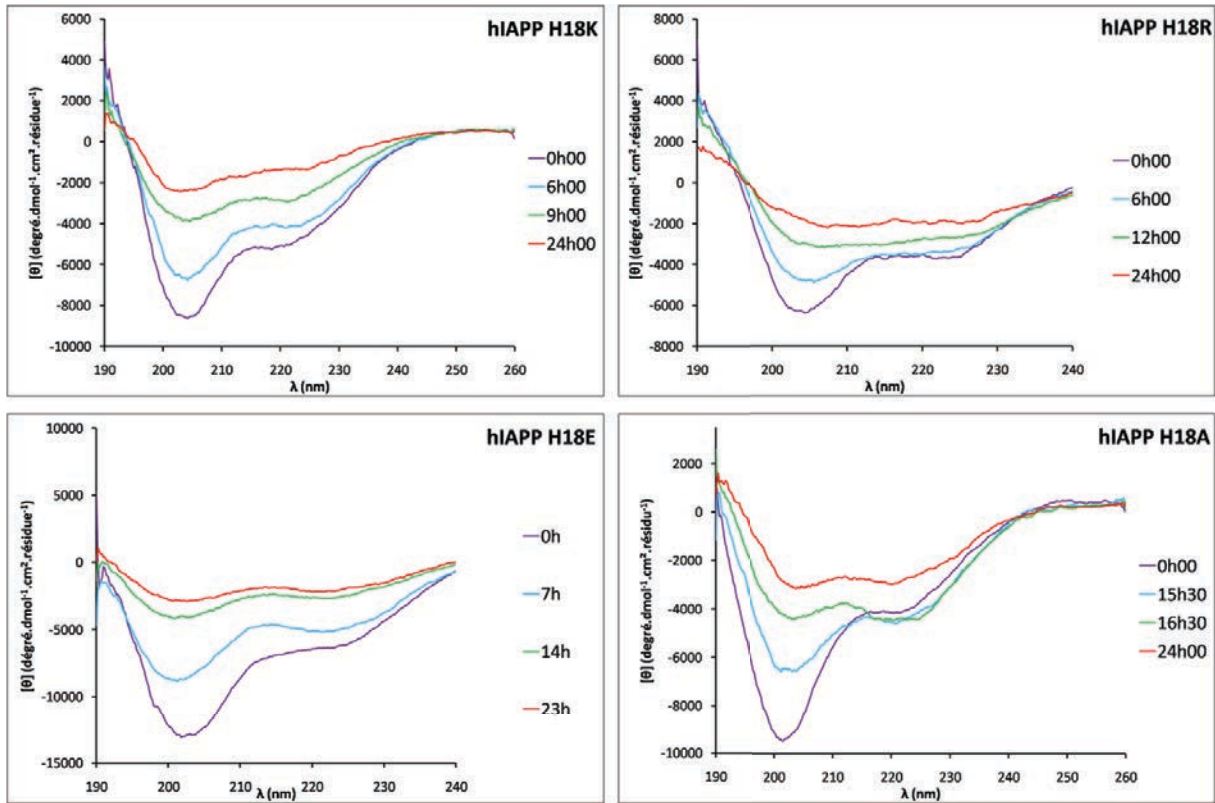


Figure 90: Circular dichroism spectra of hIAPP mutants over time at pH 5.5.

A loss of signal is observed for all mutants. Curves were smoothed on OriginLab by the adjacent-averaging method (25 pts)

	Random coil (%)	$\alpha$ -helix (%)	$\beta$ -sheet (%)
<b>IAPP Wild Type</b>	75.2	19.1	5.7
<b>hIAPP H18K</b>	73.1	18.2	1.5
<b>hIAPP H18R</b>	74.8	19	6.2
<b>hIAPP H18E</b>	62.4	16.5	0
<b>hIAPP H18A</b>	77	12.7	9.8

Table 21: Percentage values of random coil,  $\alpha$ -helix and  $\beta$ -sheet for IAPP wild type and mutants at initial time at pH 5.5. Values were obtained by deconvolution of the CD spectra by CDFriend program.

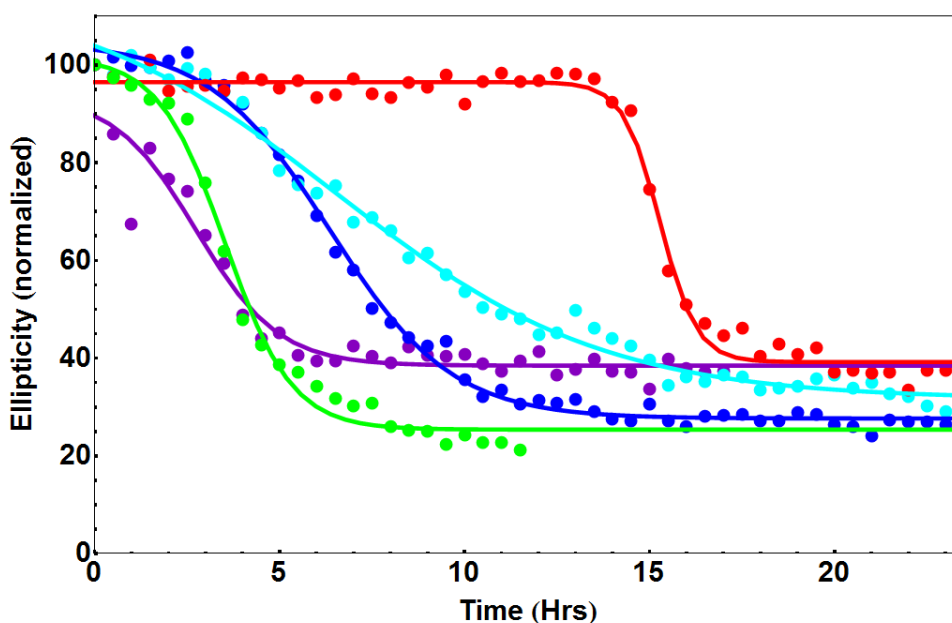


Figure 91: Ellipticity at 205 nm over time of hIAPP wild type (purple), hIAPP H18K (blue), hIAPP H18R (cyan), hIAPP H18E (green), hIAPP H18A (red) at pH 5.5.

	ThT Fluorescence peptide concentration: 10 $\mu$ M	NMR experiments peptide concentration: 50 $\mu$ M	CD experiments peptide concentration: 25 $\mu$ M
	$t_{1/2}$ (hrs)	$t_{1/2}$ (hrs)	$t_{1/2}$ (hrs)
<b>hIAPP Wild-Type</b>	10.55 $\pm$ 0.05	1.38 $\pm$ 0.08	2.74 $\pm$ 0.35
<b>hIAPP H18K</b>	21.98 $\pm$ 0.09	5.45 $\pm$ 0.27	6.36 $\pm$ 0.09
<b>hIAPP H18R</b>	28.50 $\pm$ 0.10	4.12 $\pm$ 0.10	6.55 $\pm$ 0.45
<b>hIAPP H18E</b>	67.97 $\pm$ 0.08	6.77 $\pm$ 0.08	3.52 $\pm$ 0.11
<b>hIAPP H18A</b>	63.09 $\pm$ 0.06	4.09 $\pm$ 0.20	15.28 $\pm$ 0.06

Table 22: Kinetic parameters (half time  $t_{1/2}$ ) of fibrillization (fluorescence ThT), of monomer depletion (NMR experiments) and random coil loss using the time course of CD ellipticity at 205 nm (CD experiments) at pH 5.5 for all peptides in presence DOPC/DOPS (7:3) vesicles. Peptid/Lipid ratio (1:10)

A peculiar fact with the CD experiments was that, at initial time, we could observe that the peptides did not adopt an  $\alpha$ -helical conformation upon interaction with the membrane models but showed a prevalence of random coil signal, as showed previously by the deconvolution of the spectra in tables 19 and 21.

This observation differed from previous description in the literature, which characterized the  $\alpha$ -helix structure as an intermediate between the disordered peptide and the  $\beta$ -sheet structure.

This observation can be linked to different factors such as the peptide-to-lipid ratio (P/L), which is here of 1:10, or interaction of the peptide with the membrane. On the first hand, a high P/L could implicate fewer anionic binding sites for the peptides on the membrane surface, which might not be sufficient for the conversion of the disordered peptide to an  $\alpha$ -helical structure.<sup>7</sup> Also, a few binding sites on the membrane surface would lead to a significant amount of mainly disordered monomer left in solution.<sup>8</sup> This could explain the high proportion of random coil population that we obtained compared to the  $\alpha$ -helical structure that could be observed for wild type hIAPP at the same concentration in the presence of DOPC/DOPS LUV but at a ratio 1:20.<sup>2</sup> In the second hand, it has been shown the  $\alpha$ -helical conformation was induced by anchoring and incorporation of the peptide in the lipid bilayer. Therefore, the addition of the peptides in the preformed vesicle solution, would mainly locate them on the surface of the membrane model, not inserting enough to stabilize the peptide and induce the structuration into a  $\alpha$ -helix.<sup>9</sup>

However, despite the lack of observation of an  $\alpha$ -helical structure, the CD signal for all the peptides at pH 5.5 or pH 7.4 was very similar, showing that wild type peptide and mutants share a same global conformation. At pH 7.4, the differences of kinetics of oligomerization between the peptides could be explained by an effect of the substitution of residue 18 on the local structure of the peptide hindering the oligomerization and further elongation of fibrils. The results show that the side-chain of histidine significantly contributes to the aggregation as an acidic or small side chain turn out to slow down the oligomerization. CD results at pH 5.5 have also shown the higher aggregation rate for the wild-type peptide, but showed inconsistency with fluorescence and NMR experiments. Indeed the estimated kinetics parameters showed that the loss of signal was faster at pH 5.5 than at pH 7.4 suggesting that the lower pH and an influence on the aggregation of the peptide. This could be an effect of the state of protonation of the N-terminus of the peptide. The addition of a positive charge would indeed enhance the binding of the peptides to the membranes, leading to large complexes and further disappearance of the dichroic signal.



- e) Mutation and change of pH does not influence the peptide insertion into the membrane

As we wanted to see if the difference in the kinetics of fibrillization depended on the interaction between the peptides and the membrane models, we carried out monolayer experiments.

Monolayer experiments were performed in order to probe the insertion of the peptides in a DOPC/DOPS (7:3) monolayer, by measurement of the increase in surface pressure of the lipid layer after injection of the peptide in solution. The difference in the surface pressure that was measured was plotted as a function of time, which allowed us to estimate the maximum surface pressure for the two peptides at pH 5.5 and pH 7.4 (figure 92, table 22).

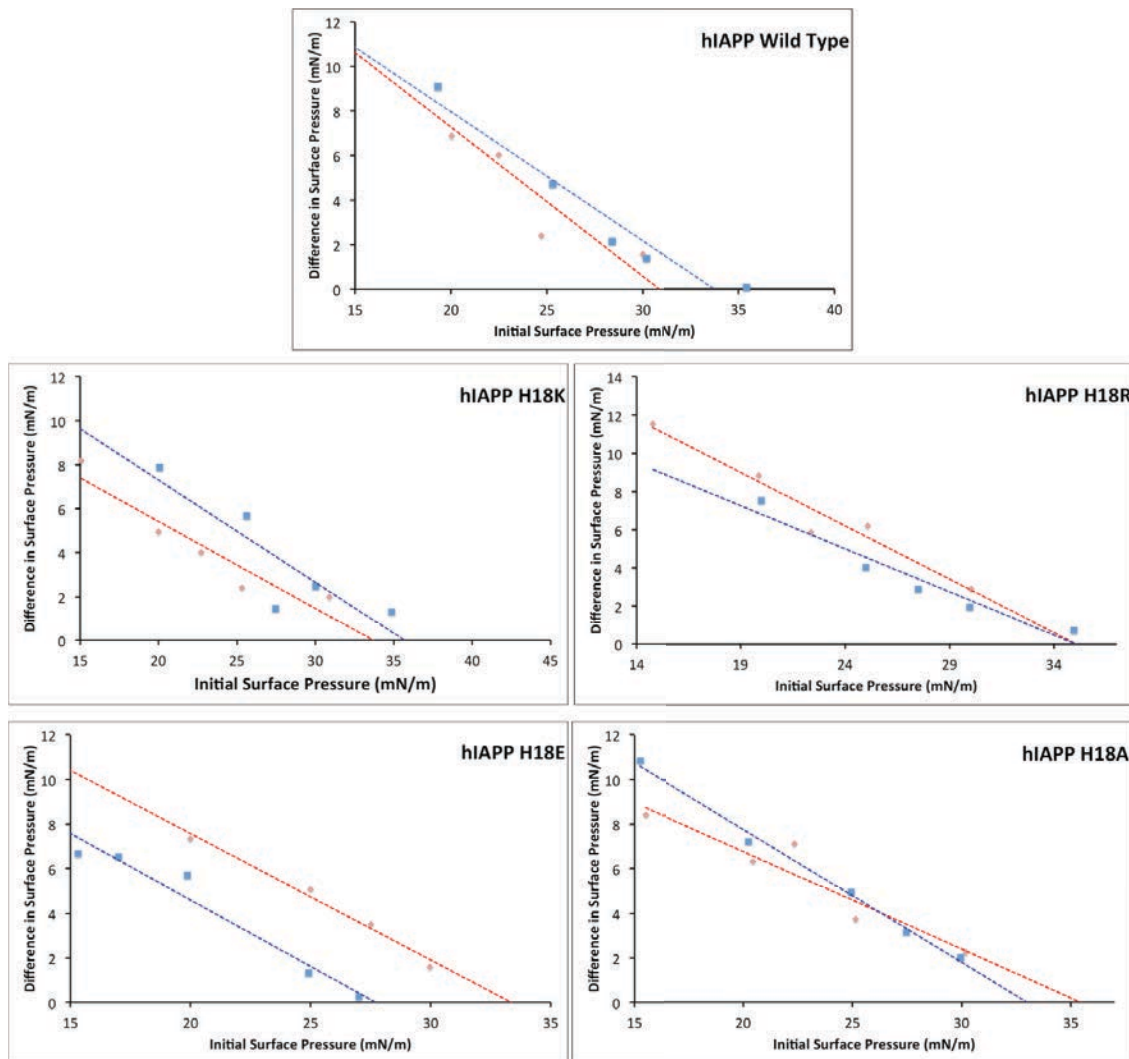


Figure 92: Difference in surface pressure depending on the initial surface pressure of the PC/PS monolayer for all five peptides at pH 5.5 (red) and 7.4 (blue)

At pH 7.4, wild type peptide and mutants to the exception of hIAPP H18E showed similar maximum surface pressure that was estimated between 30 and 35 mN/m, showing that the peptides interact with the membrane in a similar way. hIAPP H18E showed the lowest surface pressure, which can be explained by the presence of electrostatic repulsion between the anionic lipid head groups and negatively charged glutamic acid residue.

At pH 5.5, the obtained values were estimated between 30 and 35 mN/m for all peptides, including hIAPP H18E, suggesting that the electrostatic repulsion between this mutant and the membrane was lessened at acidic pH, which can be explained by the fact that the N-terminus of the peptide might be charged at pH 5.5.

	pH 7.4	pH 5.5
	Maximum insertion pressure (mN/m)	Maximum insertion pressure (mN/m)
<b>hIAPP Wild-Type</b>	33.74	30.86
<b>IAPP H18K</b>	35.69	33.68
<b>IAPP H18R</b>	33.64	35.07
<b>IAPP H18E</b>	27.71	33.36
<b>IAPP H18A</b>	32.99	32.99

**Table 23 : Maximal insertion surface pressure of wild type IAPP and IAPP H18K, H18R, H18E, H18A mutants into DOPC/DOPS (7:3) monolayer**

f) Calcein leakage experiment

Calcein leakage experiments were carried out in order to assess the capacity of the peptide to permeabilize the membrane. Results for wild type IAPP showed that after an initial lag time, an increase in fluorescence signal was observed at both pH showing that a calcein leakage, thus a permeabilization of the vesicle was occurring over time (figure 93). Results of the calcein leakage experiments were consistent with those of ThT experiments and showed the half time at pH 7.4 was shorter than at pH 5.5 ( $t_{1/2} = 16.49 \pm 0.30$  hours at pH 7.4,  $t_{1/2} = 26.92 \pm 0.22$  hours at pH 5.5). This result therefore shows that pore formation, due to the peptide or oligomers, occurred at both pHs but took a longer time to appear at a lower pH.

At pH 7.4, data showed that a leakage occurred after interaction of every mutant with the membrane, to the exception of hIAPP H18K for which no increase in fluorescence intensity was observed after 2 days. Consistent again with the ThT fluorescence results, the

lag time is longer for hIAPP H18R ( $t_{1/2} = 47.97 \pm 0.30$  hours) and hIAPP H18E and hIAPP H18A ( $t_{1/2} = 71.37 \pm 1.08$  hours and  $t_{1/2} = 65.53 \pm 0.46$  hours respectively) than for the wild type peptide. At pH 5.5, except for wild type peptide and in one of the wells of hIAPP H18A, no increase in the fluorescence intensity was observed, showing that although the peptides interact with the membrane model, at it was seen with monolayer experiments, they do not necessarily induce a subsequent leakage from the vesicle. This observation suggests that at pH 5.5, the mutants are located on the surface of the membrane, instead of in the hydrophobic core of the lipid bilayer. The possible aggregation of the peptides would then occur preferably on the surface of the lipid bilayer or in solution, thus minimizing the catalytic effect of the membrane to the oligomerization.

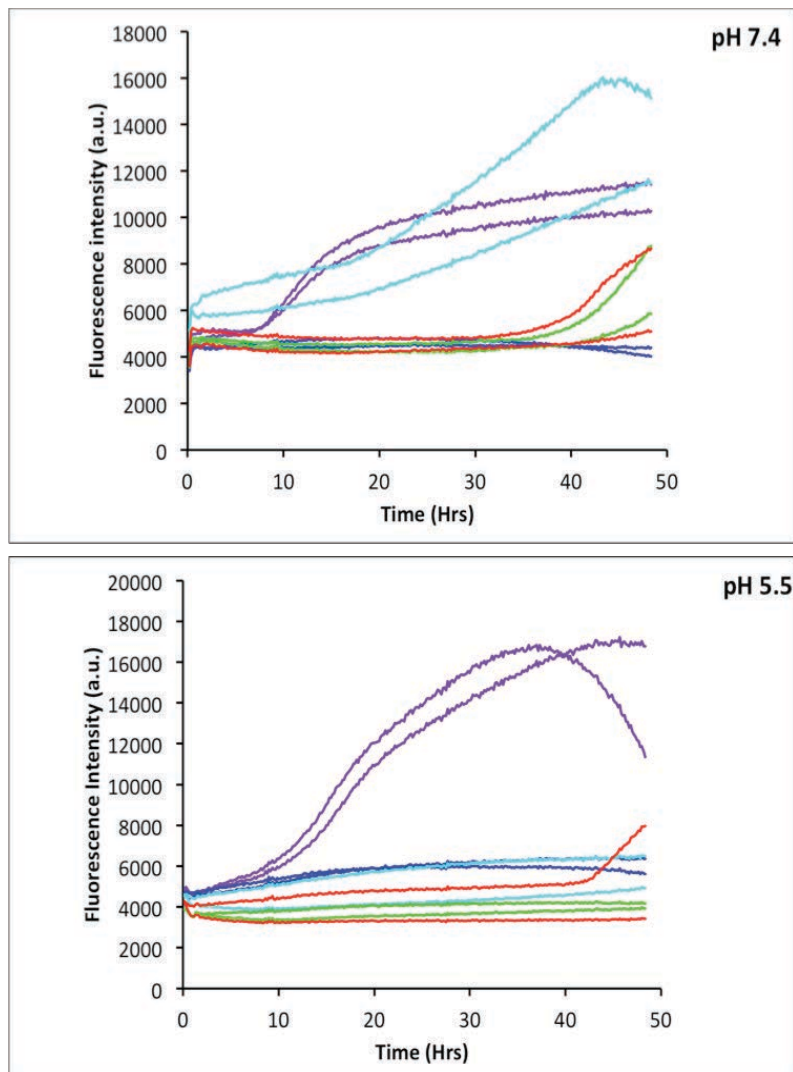


**Figure 93: Calcein leakage experiment of IAPP Wild Type (purple) and mutants H18K (blue), H18R (cyan), H18E (green) and H18A (red) at pH 7.4 (top) and pH 5.5 (bottom) in presence of 200 nm Calcein Unilamellar Vesicles of DOPC/DOPS (1:10)**

Given the experimental conditions (peptide concentration, L/P, buffer composition), the results of ThT fluorescence and calcein leakage experiments can be easily compared. Fitting of the calcein leakage curves for all peptides at pH 7.4 was done with the Boltzmann equation, allowing the determination of the kinetic parameters of the experiments (table 24).

	ThT Fluorescence	Calcein Leakage
	(peptide concentration 10 $\mu$ M)	(peptide concentration 10 $\mu$ M)
	$t_{1/2}$ (hrs)	$t_{1/2}$ (hrs)
<b>hIAPP Wild-Type</b>	7.59 $\pm$ 0.02	16.49 $\pm$ 0.30
<b>IAPP H18K</b>	12.54 $\pm$ 0.04	-
<b>IAPP H18R</b>	14.79 $\pm$ 0.02	47.97 $\pm$ 0.30
<b>IAPP H18E</b>	35.44 $\pm$ 0.28	71.37 $\pm$ 1.08
<b>IAPP H18A</b>	45.15 $\pm$ 0.05	65.53 $\pm$ 0.46

**Table 24: Kinetic parameters ( $t_{1/2}$ ) of IAPP wild type and mutants determined by ThT fluorescence and calcein leakage experiments at pH 7.4.**

At pH 7.4, results showed that, to the exception of hIAPP H18K that did not induce any leakage from the vesicles the peptides started to aggregate before permeabilizing the membrane. This observation implies that the wild type peptide as well as mutants IAPP H18R, hIAPP H18E and hIAPP H18A formed membrane-disrupting oligomers over time. The capacity of mutant hIAPP H18R to induce calcein leakage was interesting as the substitution of the histidine by an arginine was motivated by the sequence of the non-toxic rat IAPP. The observed permeabilization therefore shows that, although the presence of an arginine instead of a histidine tended to slow down the kinetics of fibrillization, as shown with the results of the previously described experiments, it is not sufficient to disrupt the aggregation or to form non-toxic species. Rat IAPP differs from human IAPP by only six amino acids, and especially possesses three proline residues in position 25, 28 and 29, that are known to destabilize the structuration of the peptide into  $\beta$ -sheets.<sup>10</sup> These results therefore show the effect and significant role of both combined histidine 18 and residues 20-29 in promoting the aggregation of IAPP.

### 3. Conclusion

The present study focused on the effect of substitution of residue 18 of hIAPP sequence and of the pH on the oligomerization and fibrillization of the peptide, using a wide range of biophysical techniques.

The results at pH 7.4 showed that the substitution of the residue 18 had an inhibitory effect on the oligomerization of the peptides, as the different techniques showed that the kinetics of aggregation were slowed down for all mutants when compared to the kinetics of wild type hIAPP. Results have also shown that the global charge of the peptide as well as the nature of the side chain had an effect on the kinetics of oligomerization, as the introduction of a negatively charged peptide (hIAPP H18E) or of a short side chain (hIAPP H18A) had the most deleterious effect on the aggregation of the peptides. We also observed that mutants with a positively charged substitution (hIAPP H18K and hIAPP H18R) gave similar results and displayed kinetics of aggregation close to those of the wild-type peptide. This suggests that although the substitution had an inhibitory effect on the oligomerization, the introduction of a positive charge had only little effect on the kinetics of aggregation of hIAPP. However, ThT fluorescence results displayed low values of fluorescence intensity for both peptides, and NMR experiments have shown a significant residual monomer fraction for mutant hIAPP H18K and especially mutant hIAPP H18R. These results suggest that although these mutations were not the most deleterious and did not prevent oligomerization, their aggregation may lead to fewer fibrils or display a specific morphology.

Overall, the results at pH 7.4, showed that residue His18 displayed specific peptide-peptide interactions, inherent to the side chain of the residue, that contributed to the oligomerization and fibrillization of the peptide. The observation of the structure of the hIAPP fibrils, issued from a x-ray crystallography model structure<sup>11</sup>, shows that the residue His18 is indeed buried in the inside of the  $\beta$ -sheet, interacting with the side-chain of Ile26 and the backbone of Asn21 (figure 94). This localization of His18 and interaction with the envoning residues of the fibril implies that the mutation of His18 or the introduction of a positive or negative charge is likely to destabilize the fibril and therefore impair oligomerization. The study of the substitution of the histidine by other amino acids such as glutamine or asparagine, in order to maintain the hydrogen bonding between the residues, or also by tyrosin, in order to maintain aromatic properties.

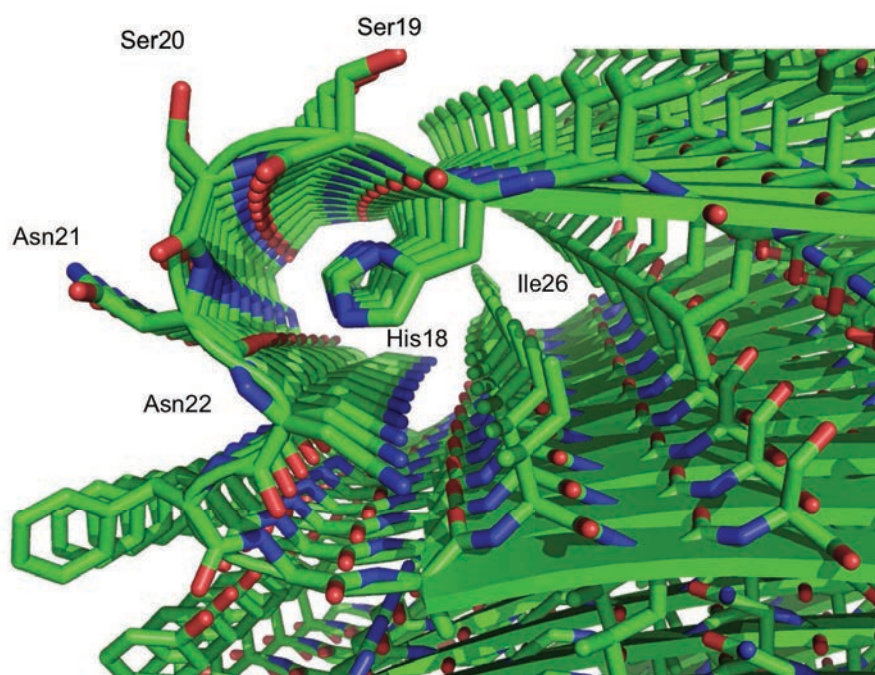


Figure 94: Environment of His18 in the hIAPP  $\beta$ -sheet structure of the fibril. Model issued from X-ray Cristallography (Wilztius and al., 2008<sup>11</sup>).

Results at pH 5.5 showed that at low pH, the interactions between monomers of the peptide or between the peptide and the anionic membrane were modulated in a complex way. The results for wild type peptide and mutants hIAPP H18K and hIAPP H18R were quite homogeneous, the mutants displaying slower kinetics of aggregations than at pH 7.4 for fluorescence and NMR experiments. On the contrary, although ThT fluorescence showed low kinetics of fibrillization (over 60 hours), NMR and CD experiments showed that mutants hIAPP H18E and hIAPP H18A seemed to aggregate faster at pH 5.5. Combined results of monolayer and calcein leakage experiments showed that the mutants had similar insertion efficiency into a lipid monolayer at both pH, but that low pH prevented the membrane permeabilization.

#### 4. Material and Methods

##### Sample preparation

Solid phase synthesis of IAPP was performed at Institut de Biologie Intégrative (IFR83) at the University Pierre et Marie Curie using Fmoc chemistry. The peptides were then purified by HPLC and characterized by MALDI-TOF mass spectrometry.

Peptides stock solution was obtained by dissolving the peptide at a concentration of 1 mM in hexafluoroisopropanol (HFIP) for one hour. Then, HFIP was evaporated and the sample was

dried by vacuum desiccation for at least 30 min. The resulting peptide film was dissolved at a concentration of 1 mM in DMSO (fluorescence experiments), 2 mM in DMSO (monolayer experiment) or in a 50 mM sodium phosphate, 100 mM NaF buffer, pH 7.4 or pH 5.5 (circular dichroism, NMR experiments).

### **Fluorescence assays**

The kinetics of fibril formation was measured using the fluorescence intensity increase upon binding of the fluorescent probes Thioflavin T (ThT) to fibrils. A plate reader (Fluostar Optima, BMG LabTech, Offenburg, Germany) and a standard 96 well black microtiter plate were used. Prior to the first measurement, the plate was shaken at 600 rpm for 10s. The fluorescence was measured at room temperature from the top of the plate every 10 minutes with excitation filter at 440 nm and emission filter at 480 nm for ThT. hIAPP and IAPP mutants were dissolved at a concentration of 1 mM in DMSO then diluted at a concentration of 200  $\mu$ M in a 50 mM Tris/HCl, 100 mM NaCl or 50 mM sodium phosphate, 100 mM NaCl buffers at adjusted pH of 5.5 or 7.4. Samples were then prepared in the wells. Final concentrations were of 10  $\mu$ M peptide, 100  $\mu$ M lipids (SUV of DOPC/DOPS, 7:3) and 10  $\mu$ M ThT.

Experiments were carried out three times at pH 7.4 and twice at pH 5.5. Each sample was prepared in triplicates in the plate reader.

Fluorescence values were, plotted as a function of time then fitted using a Boltzmann function with a home written program based on Mathematica 9 in order to determine the kinetic parameters associated to amyloid fibril formation.

### **Circular dichroism**

The changes in secondary structure for hIAPP and IAPP mutants were measured using a Jasco J-815 CD spectropolarimeter with a Peltier temperature-controlled cell holder over the wavelength range 190-260 nm.

Measurements were carried out in cells of 0.1 cm path length at 25°C in aqueous solution (50 mM sodium phosphate, 100 mM NaCl buffer, pH 7.4 or pH 5.5). For each sample, measurements were taken every 0.2 nm at a scan rate of 10 nm/min. Spectra were acquired every 30 minutes over a period of 7 to 24 hours. Peptide concentration was 10  $\mu$ M, lipid concentration (200 nm SUV of DOPC/DOPS, 7:3) was 100  $\mu$ M.



Ellipticity values at 205 nm were plotted as a function of time then fitted using a Boltzmann or function with a home written program based on Mathematica 9 in order to determine the kinetic parameters associated to the loss of dichroic signal.

### **NMR experiments**

NMR experiments were recorded on a Bruker Avance III 500 MHz spectrometer equipped with a  $^1\text{H}/^{13}\text{C}/^{15}\text{N}$  TCI cryoprobe with Z-axis gradient. NMR spectra were processed and analysed with TopSpin software (Bruker).

One-dimensional spectra were acquired over 8000 points using a spectral width of 6000 Hz. Solvent resonance was suppressed using a Watergate pulse sequence. The experiments were done at a temperature of 25°C.

Signals between 6.9 and 7.3 ppm were integrated, plotted as a function of time then fitted using a Boltzmann or a Richards function with a home-written program based on Mathematica 9.

### **Calcein Leakage experiments**

Calcein leakage experiments are done in a clear 96-well plate using a Fluostar Optima, BMG Labtech plate reader with an excitation filter at 480 nm and an emission filter at 530 nm. Peptides were added to the lipids (Ratio 1:10) just before the measurement, at a concentration of 10  $\mu\text{M}$  in a 50 mM Tris/HCl, 100 mM NaCl buffer at pH 7.4 or 5.5. Optimal gain is measured by the addition of 1  $\mu\text{L}$  of Triton-X-100 10% to three wells containing 200  $\mu\text{L}$  LUV/buffer mixture with the required concentration of lipids. The addition of the detergent to the medium induces 100% leakage and maximum fluorescence intensity. The plate was inserted in the plate reader and measurement is done immediately after a 10 second shaking of the plate. Measurements are done at a regular interval (5-10 minutes). After the experiment, plate is removed and 1  $\mu\text{L}$  of Triton-X-100 10% is added in every well. After shaking, an additional measurement is done (end point measurement).

Fluorescence values were plotted as a function of time then fitted using a Boltzmann function with a home-written program based on Mathematica 9 in order to determine the kinetic parameters associated to the leakage.

### **Monolayer experiments**

Experiments were done in the laboratory of the group of Membrane Biochemistry and Biophysics in Utrecht, in the Netherlands. The apparatus is a Langmuir-Blodgett trough containing 18 mL of buffer. The measure of the surface pressure is done over time with a



surface pressure sensor (the needle) after calibration of the surface tension of the air/water interphase. The DOPC/DOPS (7:3) monolayer is then deposited upon the buffer with a Hamilton® syringe until the desired surface pressure is reached. If needed, the surface pressure can be adjusted with a barrier, which compresses the monolayer on the surface of the buffer. Once the monolayer is stabilized, the peptide is injected into the buffer with a Hamilton® syringe.

The experiment is repeated five times, with different initial surface pressures ranging from 15 to 35 mN/m depending on the studied peptide.

- 
- <sup>1</sup> Westermark, P., Zhan-Chun Li, G. T. Westermark, A Leckström, and D. F. Steiner. “Effects of Beta Cell Granule Components on Human Islet Amyloid Polypeptide Fibril Formation.” *FEBS Letters* 379, no. 203–6 (1996).
  - <sup>2</sup> Li, Yang, Weixin Xu, Yuguang Mu, and John Z. H. Zhang. “Acidic pH Retards the Fibrillization of Human Islet Amyloid Polypeptide due to Electrostatic Repulsion of Histidines.” *The Journal of Chemical Physics* 139, no. 5 (August 7, 2013): 055102. doi:10.1063/1.4817000.
  - <sup>3</sup> Engel, Maarten F.M., HaciAli Yigittop, Ronald C. Elgersma, Dirk T.S. Rijkers, Rob M.J. Liskamp, Ben de Kruijff, Jo W.M. Höppener, and J. Antoinette Killian. “Islet Amyloid Polypeptide Inserts into Phospholipid Monolayers as Monomer.” *Journal of Molecular Biology* 356, no. 3 (February 2006): 783–89. doi:10.1016/j.jmb.2005.12.020.
  - <sup>4</sup> Grimsley, Gerald R., J. Martin Scholtz, and C. Nick Pace. “A Summary of the Measured P K Values of the Ionizable Groups in Folded Proteins.” *Protein Science*, 2008, NA – NA. doi:10.1002/pro.19.
  - <sup>5</sup> Khemtémourian, Lucie, Elena Doménech, Jacques P. F. Doux, Martijn C. Koorengel, and J. Antoinette Killian. “Low pH Acts as Inhibitor of Membrane Damage Induced by Human Islet Amyloid Polypeptide.” *Journal of the American Chemical Society* 133, no. 39 (October 5, 2011): 15598–604. doi:10.1021/ja205007j.
  - <sup>6</sup> Da Costa, Grégory, Liza Mouret, Soizic Chevance, Elisabeth Le Rumeur, and Arnaud Bondon. “NMR of Molecules Interacting with Lipids in Small Unilamellar Vesicles.” *European Biophysics Journal* 36, no. 8 (October 30, 2007): 933–42. doi:10.1007/s00249-007-0186-7.
  - <sup>7</sup> Wong, Pamela T., Joseph A. Schauerte, Kathleen C. Wissner, Hao Ding, and Edgar L. Lee. “Amyloid- $\beta$  Membrane Binding and Permeabilization Are Distinct Processes Influenced Separately by Membrane Charge and Fluidity.” *Journal of Molecular Biology* 386, no. 1 (February 13, 2009): 81–96. doi:10.1016/j.jmb.2008.11.060.
  - <sup>8</sup> Galvagnion, Céline, Alexander K. Buell, Georg Meisl, Thomas C. T. Michaels, Michele Vendruscolo, Tuomas P. J. Knowles, and Christopher M. Dobson. “Lipid Vesicles Trigger  $\alpha$ -Synuclein Aggregation by Stimulating Primary Nucleation.” *Nature Chemical Biology* 11, no. 3 (March 2015): 229–34. doi:10.1038/nchembio.1750.
  - <sup>9</sup> Bokvist, Marcus, Fredrick Lindström, Anthony Watts, and Gerhard Gröbner. “Two Types of Alzheimer’s  $\beta$ -Amyloid (1–40) Peptide Membrane Interactions: Aggregation Preventing Transmembrane Anchoring Versus Accelerated Surface Fibril Formation.” *Journal of Molecular Biology* 335, no. 4 (January 2004): 1039–49. doi:10.1016/j.jmb.2003.11.046.

- 
- <sup>10</sup> Abedini, Andisheh, and Daniel P. Raleigh. “Destabilization of Human IAPP Amyloid Fibrils by Proline Mutations Outside of the Putative Amyloidogenic Domain: Is There a Critical Amyloidogenic Domain in Human IAPP?” *Journal of Molecular Biology* 355, no. 2 (January 2006): 274–81. doi:10.1016/j.jmb.2005.10.052.
- <sup>11</sup> Wiltzius, Jed J.W., Stuart A. Sievers, Michael R. Sawaya, Duilio Cascio, Dmitriy Popov, Christian Riek, and David Eisenberg. “Atomic Structure of the Cross- $\beta$  Spine of Islet Amyloid Polypeptide (amylin).” *Protein Science* 17, no. 9 (September 2008): 1467–74. doi:10.1110/ps.036509.108.



# **Chapter 5:**

## **Interactions of amyloid peptides with inhibitors**



## 1. Introduction

Alzheimer's disease or Type 2 diabetes mellitus are two amyloid diseases that represent a major health concern given the ever increasing number of patients that suffer from these disorders. Currently, no available treatments exist in order to cure the disease but various therapeutic approaches have been developed in order to slow down the progress of the disease.

Although the mechanisms of oligomerization and fibrillization of the peptides are not yet known, significant evidence have linked amyloid intermediates species to cell-death. In this light, the toxic oligomers have become the main target for the development of therapeutic agents against amyloid disorders. Different classes of inhibitors have therefore been developed in order to inhibit the formation of toxic oligomers or to redirect the aggregation cascade toward non-toxic species.

One class of inhibitors consists of peptidomimetics that mimic the nucleation sites of the amyloid peptides. Theses peptidomimetics, designed to interact strongly with the amyloid peptides incorporate specific moieties or amino acids that act as  $\beta$ -sheet breakers by disturbing the regular hydrogen bonds between the amyloid  $\beta$ -strands.

Developments of peptidomimetics for the inhibition the fibril formation of A $\beta$  peptide, for example, were base on the KLVFF motif (residues 16-20), which was shown to be involved in the oligomerization and fibrillization.

Among those analogs, it was shown that a peptidomimetics containing a single proline (pentapeptide LPFFD) were able to disrupt fibrillization of A $\beta$ 42 by inducing unfavorable steric interactions.<sup>115</sup> Several investigations have also reported  $\alpha$ -aminoisobutyric acid (Aib) as a unique  $\beta$ -sheet breaker. Indeed in was shown that molecules incorporating an Aib motif strongly favoring a helical conformation. Therefore, the interaction between a potential inhibitor with an Aib motif with the nucleation sites of amyloid peptides is likely to prevent of the oligomerization and fibrillization by disrupting the interactions between the  $\beta$ -strands of the oligomers.<sup>116,117</sup> Other interesting molecules and peptidomimetics incorporating fluorine atoms, which modulates the hydrophobic properties and conformation of the analogs, were developed and have been shown to inhibit A $\beta$  aggregation.<sup>118,119</sup>

Another inhibitory approach of amyloid fibril formation was based on the investigation and development of small aromatic molecules, that were shown to interact with amyloid fibrils, in a similar way as Congo red or Thioflavin T, which are characteristic dyes for the detection of amyloid deposits.

Among this class of aromatic-rich molecules, investigation have been carried out on natural-based compounds, polyphenols, that were shown *in vitro* inhibitors of amyloid fibril formation.

Polyphenols are a class of natural or synthetic small molecules that are composed of one or more aromatic phenolic rings. Natural polyphenols are found in high concentrations in tea, berries, and a wide variety of other plants.

Investigation of the effect of polyphenols on amyloid peptides and proteins have shown that many of those compounds, including resveratrol, catechin, curcumin or (-)-epigallocatechin-3-gallate (EGCG), which will be the subject of paragraph 3 of this chapter, had an inhibitory effect on the fibril formation.<sup>120</sup>

During my thesis, I had the opportunity to collaborate on different projects involving potential inhibiting compounds, by carrying out NMR experiments in order to determine the mechanism of action of the studied compounds, their interactions with amyloid peptides and their effect on the kinetics of oligomerization and fibrillization.

The first project, in collaboration with the Laboratoire de Chimie Biologique (Group of Thierry Brigaud, Université de Cergy-Pontoise), involved the study of two tripeptides, incorporating  $\alpha,\alpha$ -disubstituted amino acids that were shown to inhibit fibril formation or to produce off-pathways species.

The second project, in collaboration with the group of Molécules Fluorées et Chimie Médicinale, (Sandrine Onger, Université d'Orsay), focused on the potential inhibitory effect of small and hydrosoluble sugar-based peptidomimetic analogs acting as  $\beta$ -sheet blockers of the fibrillization of A $\beta$ 42.

The third project was done in collaboration with the group Membrane Biophysics and Biochemistry (Antoinette Killian, Utrecht University), and focused on the study of (-)-epigallocatechin-3-gallate (EGCG), a natural compound extracted from green tea, which has shown promising results for the inhibition of fibrillization of amyloid peptides.

## 2. Effect of a (R)- $\alpha$ -trifluoromethylalanine containing short peptide in the inhibition of amyloid- $\beta$ fibrillation

Many inhibitors of A $\beta$  aggregation are peptides, which are designed to interact with one of two hydrophobic cores of A $\beta$ , the residues 17-21 (LVFFA) or 30-42 (AIIGLMVGGVVIA). Small peptides mimicking one of these hydrophobic sequences were demonstrated to modulate the kinetics of A $\beta$  aggregation. In particular, the KLVFF motif (residues 16-20) has been shown to be involved in the fibril formation. Among those compounds, peptides containing  $\alpha,\alpha$ -disubstituted amino acids were shown to impair fibril formation by interacting with the KLVFF motif of A $\beta$ 42<sup>121</sup>. Previous results reported that hydrophobic di- and hexapeptides incorporating the  $\alpha$ -aminoisobutyric acid (Aib) exhibited interesting inhibition properties of the oligomerization of amyloid- $\beta$  peptide, by disrupting the  $\beta$ -sheet assembly. The present study focused on the effect of a tripeptide incorporating an  $\alpha$ -trifluoromethylalanine in its sequence (Compound **2**: H-Ala-(R)-Tfm-Ala-Leu-OH, figure 95B) on the kinetics of fibrillization of A $\beta$ 42. The incorporation of fluorine atoms has been shown to modulate the proteolytic stability and hydrophobicity and to control the conformations of the peptide.<sup>122</sup> Therefore, the use of an  $\alpha$ -trifluoromethylalanine should combine both the characteristics of  $\alpha,\alpha$ -disubstituted amino acids and the specific properties of a fluorinated amino acid. Results were compared to the unfluorinated tripeptide containing the Aib analog of the peptide (Compound **1**: H-Ala-Aib-Leu-OH, figure 95A).

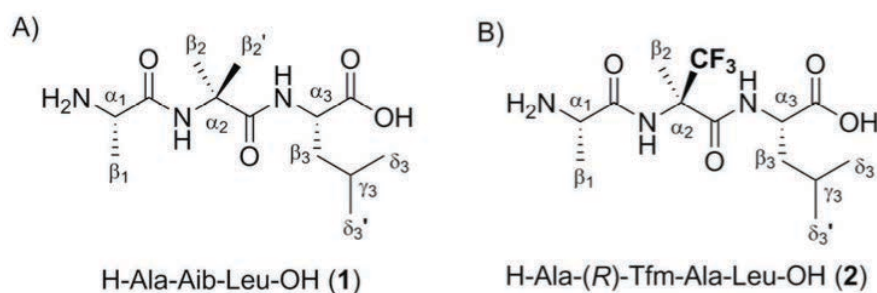


Figure 95: A) Structure of the peptide (1) H-Ala-Aib-Leu-OH  
B) Structure of the peptide (2) H-Ala-(R)-Tfm-Ala-Leu-OH

For this study, liquid state <sup>1</sup>H NMR studies were performed to measure the kinetics of depletion of monomeric soluble A $\beta$ 42 in the absence and in the presence of molecules **1** or **2**. Spectra of A $\beta$ 42 revealed a significant loss of signal intensity ( $\sim 50\%$ ) over a period of  $t_{1/2} = 4.2 \pm 1.0$  hrs indicating that the peptide undergoes oligomerization. After  $15 \pm 1.0$  hrs,



the peptide  $^1\text{H}$  signals decay to zero, corresponding to a complete disappearance of the monomeric peptide in solution (figure 96A). The presence of **1** does not affect this kinetics, as the loss of 50% signal intensity and the time needed to observe a complete disappearance of NMR signals were  $4.3 \pm 1.0$  hours and  $14 \pm 1.0$  hrs, respectively (figure 96B). In contrast, the NMR spectra of A $\beta$ 42 in presence of **2** showed that the kinetics of fibrillation were slowed down, with a 50% loss of signal intensity observed after  $8.0 \pm 1.0$  hrs. Result also showed that the signal corresponding to the monomeric A $\beta$ 42 was still present after over 20 hours of incubation, indicating that the monomer was not completely consumed (figure 96C). Intensity of the signals in the  $^1\text{H}$  aromatic region of the peptide were integrated, and values were plotted over time, and then fitted by a Boltzmann or exponential equation depending on the shape of the curve. The curves of A $\beta$ 42 alone and A $\beta$ 42 in the presence of **1** were fitted by a Boltzmann function. At time zero, only monomeric A $\beta$ 42 is present. The sharp drop in NMR intensities suggests that the monomer evolves into small oligomeric species, then into larger oligomers and finally protofibrils. At the end of the experiment, most monomers are consumed. The curve of A $\beta$ 42 in the presence of **2** could not be fitted by a Boltzmann function but was fitted by an exponential function suggesting that the fluorinated peptide **2** induces some changes in the kinetics of monomer depletion. Moreover, the peptide signal was still observed after 20 hours of incubation. These results suggest that in the presence of **2**, A $\beta$ 42 may follow another pathway of fibril formation.

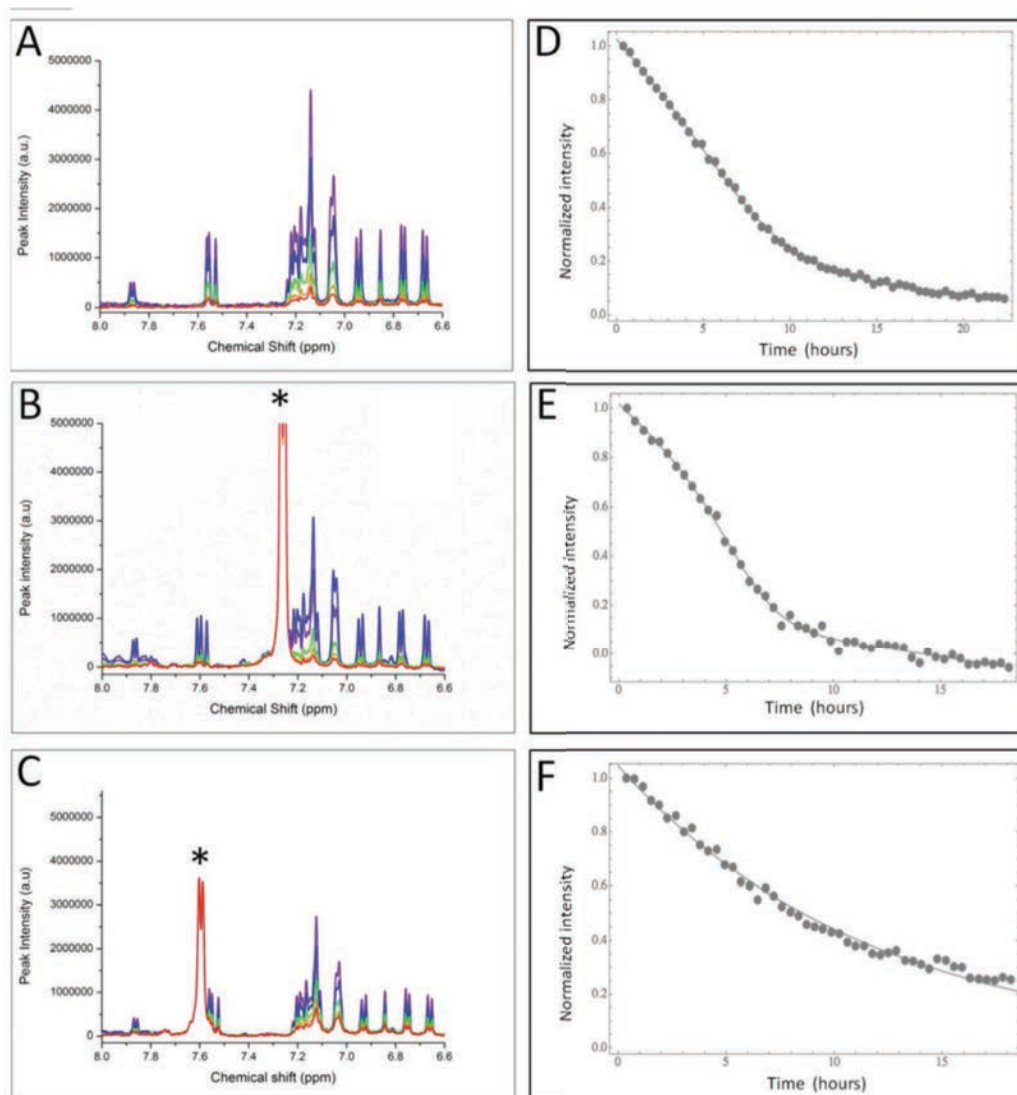


Figure 96: <sup>1</sup>H NMR spectra of Aβ42 (A), Aβ42:1 (1:10) (B) and Aβ42:2 (1:10) (C) over time. Purple: 0h, Blue: 2h, Green: 5h, Orange: 8h, Red: 10h. Peaks belonging to **1** and **2** are indicated by \* label on the relevant spectrum. Time course of normalized integrals of NMR signal between 6.6 and 7.1 ppm of Aβ42 (D), Aβ42:1 (1:10) (E) and Aβ42:2 (1:10) (F) over time.

Next, the interactions between the tripeptides with large oligomers of Aβ42 were probed by STD experiments. STD signals were observed for the resonances of **2** in the presence of Aβ42 proving that **2** interacts with Aβ42 species while no significant STD signal could be observed for compound **1**. The saturation transfer involves mostly protons of Leu side chain as well as the methyl groups of Ala and Tfm-Ala, enlightening the importance of van der Waals interactions through the aliphatic side chains of **2**. As the NMR saturation transfer is mediated by large molecular weight species, it is likely that the fluorinated peptide **2** interacts with aggregated Aβ42 species that are not visible on the <sup>1</sup>H NMR spectrum figure 97.

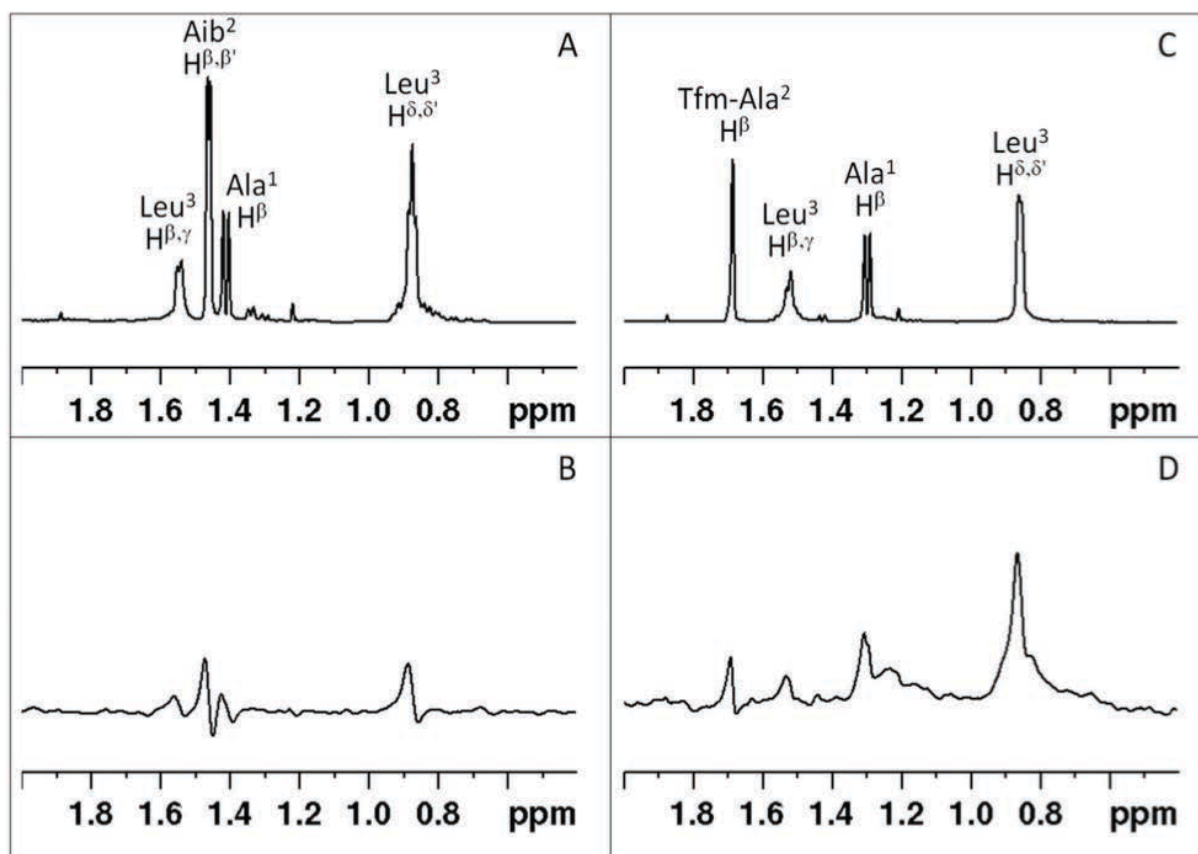


Figure 97: 1D  $^1\text{H}$  STD spectra of A $\beta$ 42:1 (1:10) (left) and A $\beta$ 42:2 (1:10) (right). A and C are reference spectra, mostly showing the signals of tripeptide 1 and 2 respectively (A : 0.8 ppm, 1.2-1.6 ppm; C : 0.8 ppm, 1.2 ppm, 1.4 ppm, 1.6 ppm). B and D are the resulting spectra of saturation transfer difference spectra for molecules 1 and 2 respectively. B shows almost no signal with weak dispersion peaks at 0.8 and 1.4 ppm while D shows the presence of STD signals with strong positive peaks at 0.8 and 1.2 ppm.

In conclusion, the two peptides that were studied during this project showed an inhibitory effect on the fibril formation at high concentration. This effect could be explained by the incorporation of Aib or the (R)- $\alpha$ -Tfm-Alanine  $\alpha,\alpha$ -disubstituted amino acids that acted as a  $\beta$ -sheet breaker, or by a good affinity of the peptides with the hydrophobic region of A $\beta$ , therefore contributing to the disruption of aggregation. Results have shown that the incorporation of a trifluoromethyl group in the compound gave significantly better inhibition results because of its increased hydrophobicity.

### 3. Study of the effect of small glycopeptidomimetics on the oligomerization and fibrillization of A $\beta$ 42

This study focused on a second class of compounds targeting the KVLFF region of A $\beta$ 42. These compounds are water-soluble peptidomimetics of the nucleation region of A $\beta$ 42 designed to interact with the peptide and modulate its kinetics of aggregation. Previous report has shown that the glycopeptide based on two hydrophobic dipeptides (Ala-Val and Val-Leu)

linked to a hydrophilic D-glucopyranosyl scaffold through aminoalkyl and carboxyethyl linkers in C1 and C6 positions (compound **1**, figure 98), had an inhibitory effect on the assembly of the peptide by interacting with the aggregated species of A $\beta$ 42.<sup>123</sup>

The present study described the effects of a new generation of derivatives incorporating the sugar-based moiety, with various peptidomimetics in the upper arm in the C6 position, designed to decrease the formation of  $\beta$ -sheets assemblies of A $\beta$ 42.

One of the peptidomimetics, compound **2**, kept the valine residue of compound **1** which was linked to a 5-amino-2-methoxybenzhydrazide unit (compound **2**, Figure 1), that mimics the  $\beta$ -strand unit and was reported to prevent protein-protein interactions involving intermolecular  $\beta$ -sheets of HIV-1 protease, and increasing the proteolytic stability of these molecules.<sup>124,125</sup>

The second peptidomimetic incorporated a lysine residue instead of the valine residue in order to provide the molecule to engage in electrostatic interactions with A $\beta$ 42, in order to increase their affinity for the peptide (compound **3**, Figure 1). The anomers  $\alpha$  and  $\beta$  of the C1 anomeric carbon of compound **3** were separated in order to further study the inhibitory effect of the  $\beta$  configuration (compound **3 $\beta$** ), which was previously reported to be the most effective on the kinetics of oligomerization of A $\beta$ 42.<sup>126</sup> The NMR experiments that are reported below were carried out on compound **3 $\beta$** .

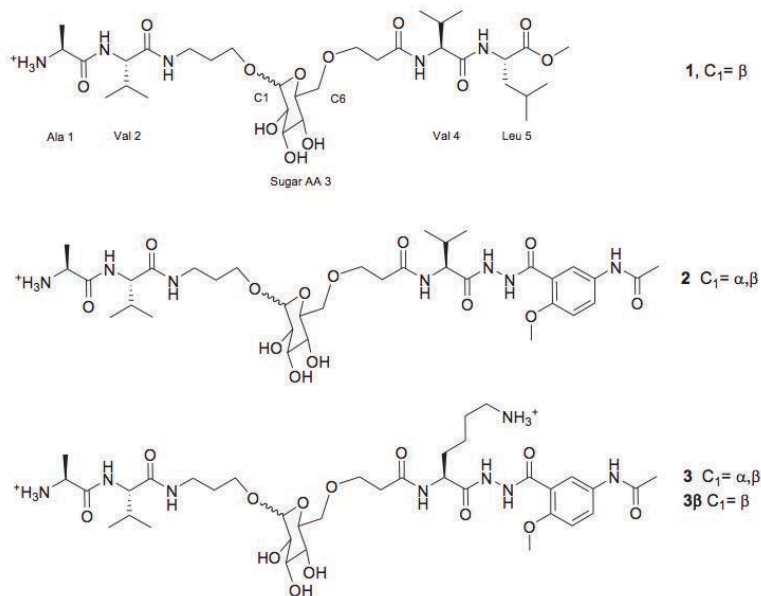


Figure 98: Structure of glycopeptidomimetic derivatives 1-3

To ensure that the A $\beta$ 42 peptide was mainly monomeric, experiments were carried out at a temperature of 5°C, with a low concentration of peptide (10-90  $\mu$ M).

The 2D  $^1\text{H}$ - $^{15}\text{N}$  and  $^1\text{H}$ - $^{13}\text{C}$  HSQC spectra of the  $^{15}\text{N}$ ,  $^{13}\text{C}$ -labeled A $\beta$ 42 in presence of a large excess of compound **3 $\beta$**  did not display any significant chemical shift perturbation of the observed  $^1\text{H}$ - $^{15}\text{N}$  and  $^1\text{H}$ - $^{13}\text{C}$  correlations of the monomeric A $\beta$ 42 (figure 99). These results show that the compound **3 $\beta$**  did not interact with the monomeric form of A $\beta$ 42.

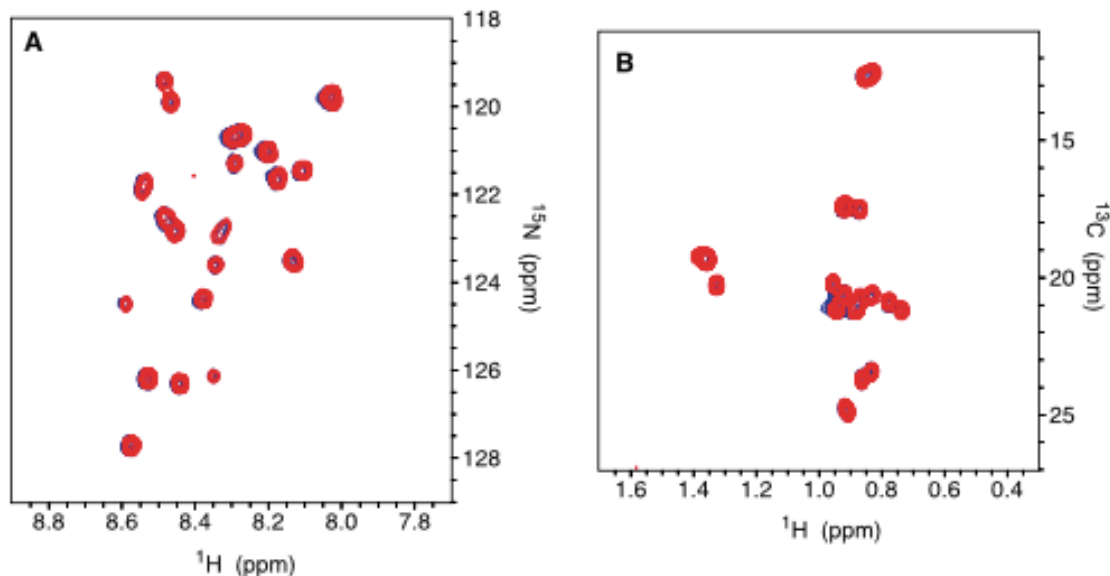


Figure 99: Supeposition of 2D  $^1\text{H}$ - $^{15}\text{N}$  HSQC (A) and 2D  $^1\text{H}$ - $^{13}\text{C}$  HSQC (B) spectra of 10  $\mu\text{M}$   $^{15}\text{N}$ ,  $^{13}\text{C}$ -labelled A $\beta$ 42 recorded at 5  $^\circ\text{C}$  in the absence (blue) and in the presence (red) of 400  $\mu\text{M}$  **3 $\beta$** . The region shown in A corresponds to backbone  $^1\text{H}$ - $^{15}\text{N}$  resonances and the region in B to methyl  $^1\text{H}$ - $^{13}\text{C}$  resonances.

STD experiments were recorded in the presence of compound **3 $\beta$** . Control experiments on **3 $\beta$**  showed that no STD signal could be detected on the compound alone, which was expected as the molecule does not aggregate in solution. Upon addition of A $\beta$ 42 in solution, a weak STD signal could be detected in the aromatic region of **3 $\beta$** . Interestingly, further experiments showed an increase of the STD signal over time (2.5 weeks), indicating an interaction between **3 $\beta$**  and larger species in solution (figure 100).

This apparition on of the STD signal on compound **3 $\beta$**  was concomitant with the decrease of the  $^1\text{H}$  NMR signal of A $\beta$ 42, which is linked to monomer depletion and formation of aggregated species that are too large to be observed by liquid state NMR (figure 101). Therefore, the gradual increase of the STD signal over time could be explained by the formation of oligomeric species of A $\beta$ 42 that bind to **3 $\beta$**  at a fast exchange rate on the NMR time scale.

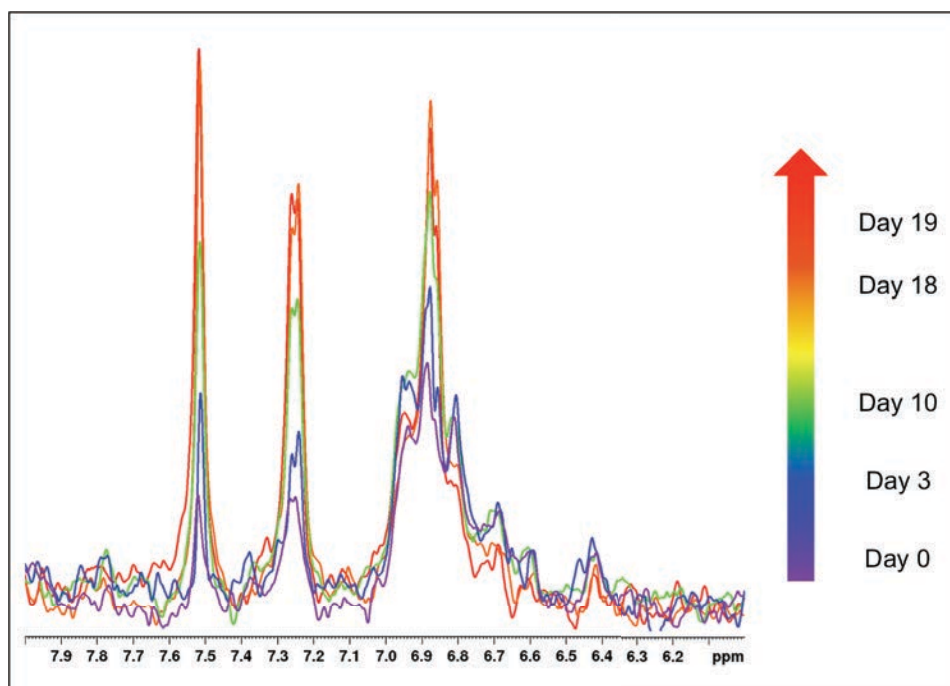


Figure 100: STD signal in the  $^1\text{H}$  aromatic region of  $3\beta$  (0,4 mM) in presence of  $\text{A}\beta_{42}$  (90  $\mu\text{M}$ ) at 5 °C over time. Spectra were recorded at  $t = 0$  (purple), after 3 days (blue), 10 days (green), 18 days (orange) and 19 days (red).

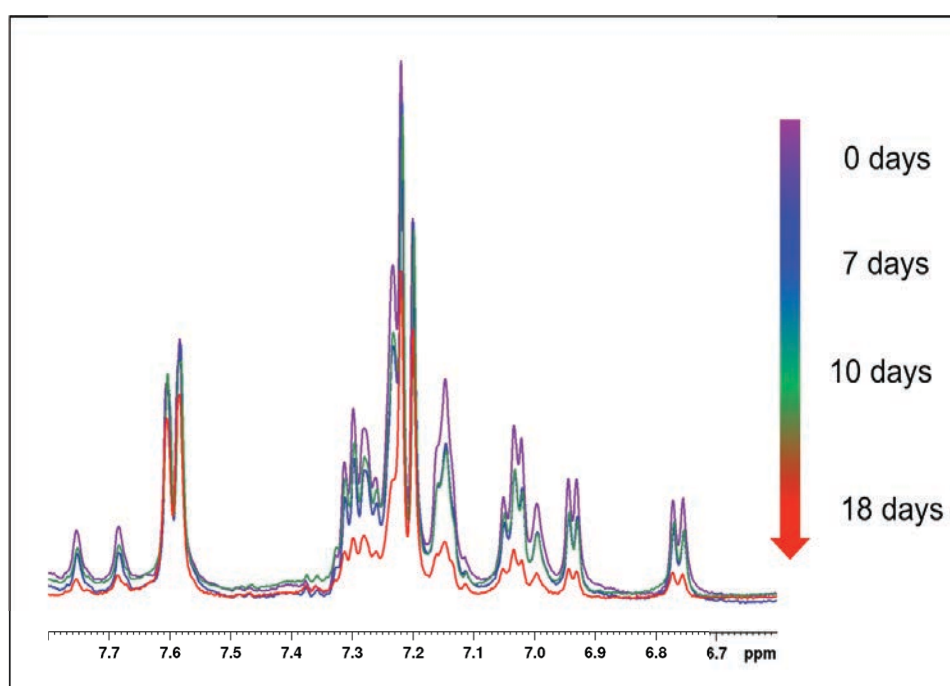
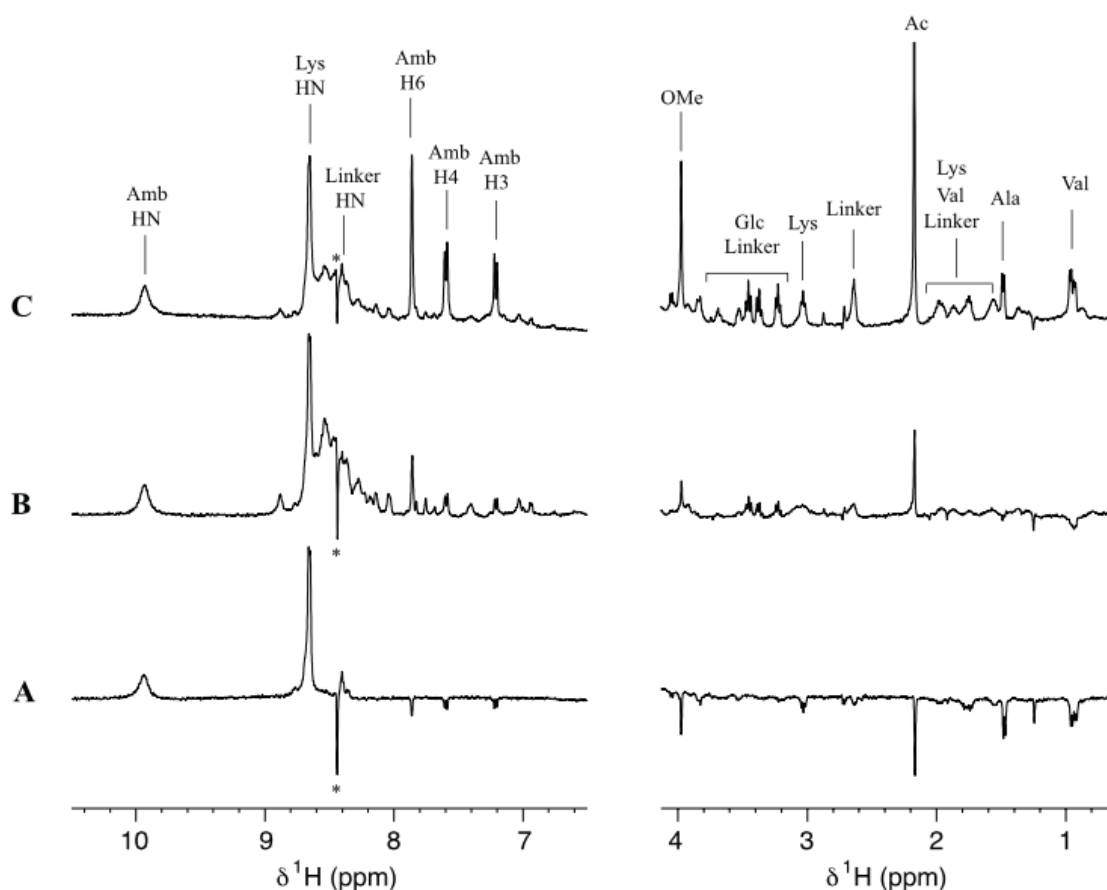


Figure 101: 1D  $^1\text{H}$  NMR spectra showing the aromatic signals of  $3\beta$  (0.4 mM) and  $\text{A}\beta_{42}$  (90  $\mu\text{M}$ ) at 5 °C over time. Spectra were recorded at  $t = 0$  (purple), after 7 days (blue), 10 days (green), and 18 days (red). The sample was kept at 5 °C during the whole period and heated to 30 °C for 12 hours just before recording spectra at 18 days to accelerate  $\text{A}\beta_{42}$  fibrillization.

The interactions between  $3\beta$  and  $\text{A}\beta_{42}$  were also observed by WaterLOGSY experiments, that detect a protein-ligand binding via the transfer of magnetization involving bulk water. In absence of  $\text{A}\beta_{42}$ , the protons of  $3\beta$  exhibited positive NOEs, which is expected

for a small molecule. Upon addition of A $\beta$ 42, we could observe a decrease of the positive NOEs and a following change of sign, from positive to negative. The NOEs became more negative over time, confirming that **3 $\beta$**  binds in a fast exchange rate on  $^1\text{H}$  NMR time scale to large oligomeric species that were formed following the aggregation of A $\beta$ 42 (figure 102).



**Figure 102:** 1D  $^1\text{H}$  WaterLOGSY spectra of **3 $\beta$**  (0.4 mM) in the absence (A) and in the presence (B, C) of A $\beta$ 42 (90  $\mu\text{M}$ ) after an incubation of 3 days (B) and 2.5 weeks. (C) Positive signals on the spectra correspond either to exchange peaks of amide protons with water or to negative NOEs with bulk water, while negative peaks correspond to positive NOEs with bulk water.

The positive NOEs observed in (A) are typical of a non-interacting low molecular weight molecule. The negative NOEs that appeared in B and C spectra are indicative of an interaction with A $\beta$ 42. Assignments of some **3 $\beta$**  resonances are indicated. The signal marked with an asterisk corresponds to formic acid impurity.

NMR experiments have therefore demonstrated the capacity of the compound **3 $\beta$**  to interact with A $\beta$ 42 aggregates and to delay both the early oligomerization and fibrillization of the peptide.

#### 4. Effect of (-)-epigallocatechin-3-gallate on the oligomerization of hIAPP

The following project focused on the interaction between a natural compound,

(-)-epigallocatechin-3-gallate (EGCG) and hIAPP.

EGCG (figure 103) is a polyphenol and an abundant biologically active compound of green tea, which was shown to have an inhibitory effect on amyloid formation *in vitro* of different amyloid peptides and proteins including hIAPP, A $\beta$  or  $\alpha$ -synuclein.

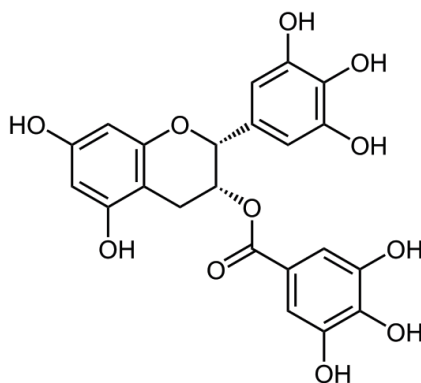


Figure 103: Chemical structure of (-)-epigallocatechin-3-gallate

Although the mechanisms of inhibition of amyloid formation by EGCG is not yet known, results have shown that the compound was able to interact with different intermediates of the fibril formation, either redirecting the pathway of oligomerization towards non-toxic aggregates or disaggregating large fibrils and protecting the cells of amyloid induced cytotoxicity.<sup>127,128</sup>

In order to have a better understanding of the mechanism of inhibition of amyloid formation by EGCG, we carried out 2D NMR experiments on hIAPP in the presence of compound. This experiments allowed to study the interaction between EGCG and hIAPP and to determine the presence of specific binding sites.

First, TOCSY and NOESY experiments were recorded on hIAPP in order to assign the observed resonances of the peptide in solution, which was compulsory for the further interaction studies between EGCG and hIAPP. These homonuclear experiments required higher concentration of peptide, compared to those that we commonly used for 1D <sup>1</sup>H, STD and PFG NMR (150  $\mu$ M instead of 50/75  $\mu$ M), which can significantly accelerate the aggregation. In order to prevent the aggregation or to slow down the kinetics of oligomerization, samples were prepared with cold buffers in a NMR Shigemi® 5 mm tube that was previously cooled down at 4°C and experiments were carried out at a temperature of 5°C (figure 104, table 25).



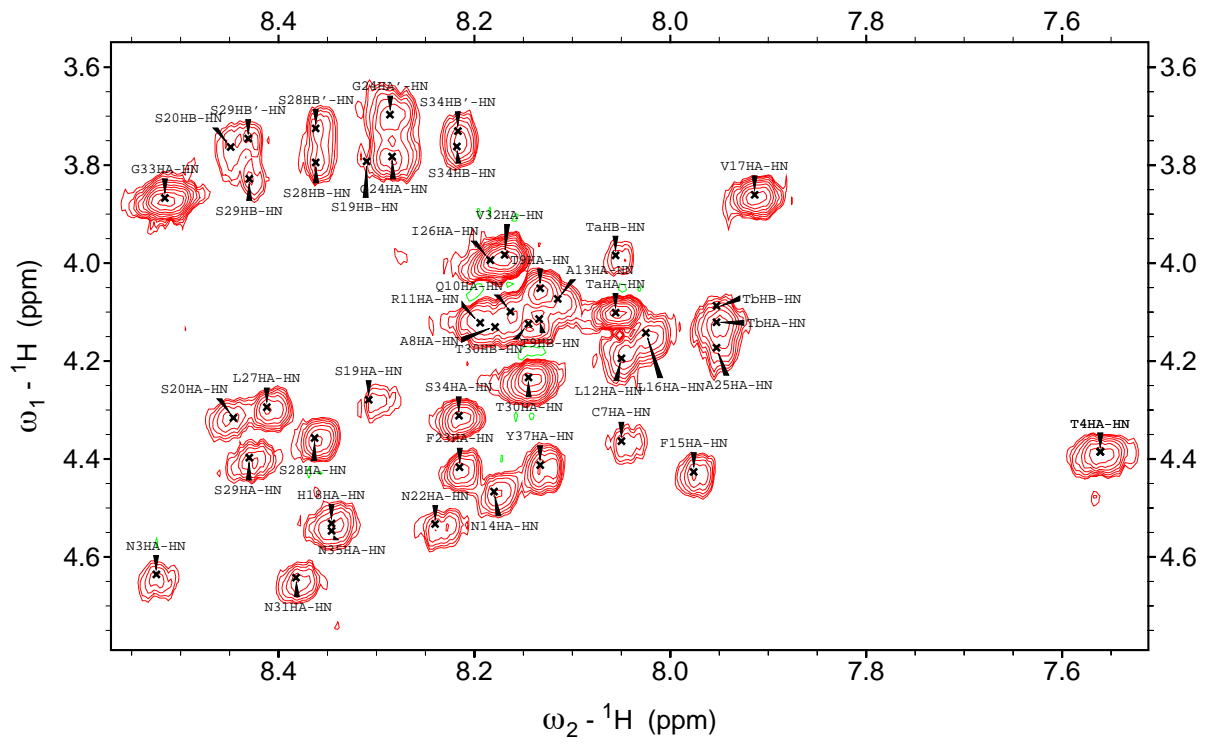


Figure 104: 2D  $^1\text{H}$ - $^1\text{H}$  TOCSY spectrum showing the HN-H $\alpha$  region of hIAPP (150  $\mu\text{M}$ ) at 5°C.

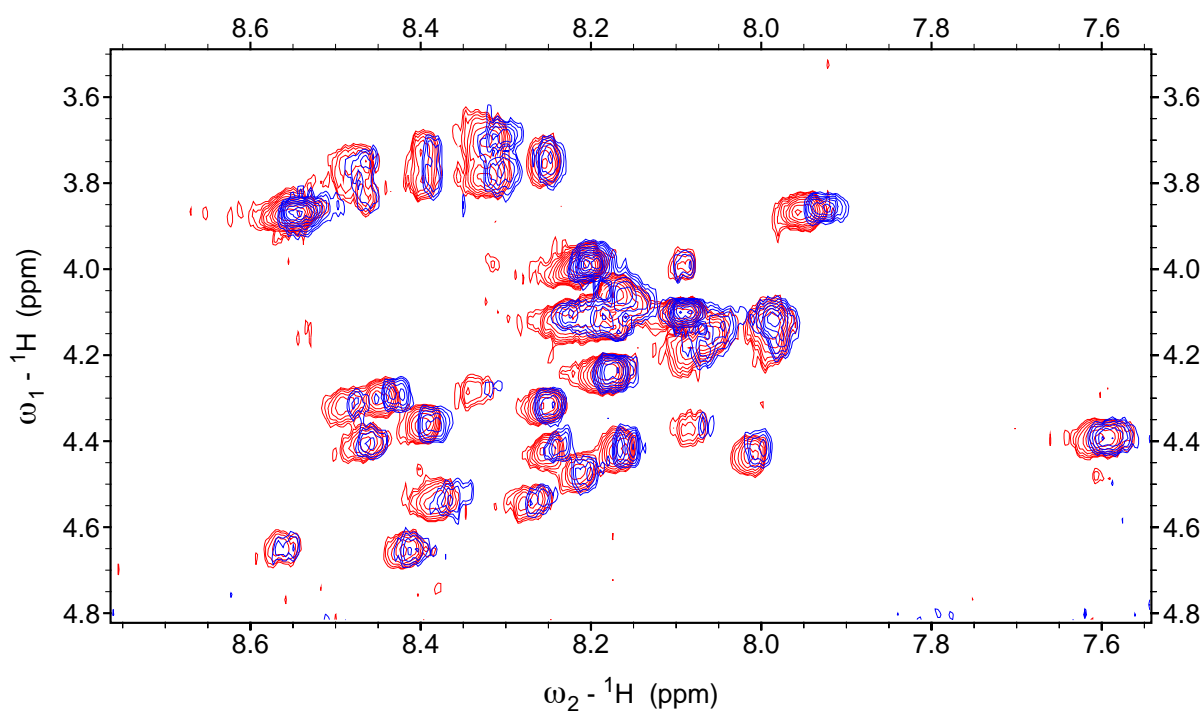
	HN	H $\alpha$	H $\beta$ /H $\beta'$	H $\gamma$	H $\gamma'$ /H $\gamma_2$	H $\delta$ /H $\delta'$	H $\delta'$ /H $\delta_2$	$\delta\epsilon$
K1	8.748	3.823	1.749	1.296		1.580		2.874
N3	8.526	4.636	2.652					
T4	7.561	4.385	4.473	1.180				
A5	8.748	4.095	1.372					
T6	7.953	4.121	4.087	1.081				
C7	8.050	4.364	3.195/2.942					
A8	8.179	4.131	1.344					
T9	8.134	4.051	4.114	1.122				
Q10	8.162	4.099	1.954	2.278				
R11	8.195	4.122	1.712	1.564	1.474	3.059		
L12	8.050	4.194	1.582	1.511		0.821	0.763	
A13	8.114	4.073	1.241					
N14	8.178	4.467	2.624					
F15	7.977	4.426	3.053/2.983					
L16	8.023	4.142	1.510	1.366		0.781	0.732	
V17	7.916	3.861	1.886	0.812	0.735			
H18	8.346	4.532	3.024/2.963			6.943		7.855
S19	8.309	4.279	3.792/3.653					
S20	8.447	4.316	3.763					
N22	8.239	4.533	2.630/2.520			7.498	6.835	
F23	8.216	4.417	3.073/2.929					
G24	8.285	3.782/3.697						
A25	7.952	4.173	1.240					
I26	8.184	3.994	1.715	0.766				
L27	8.411	4.294	1.525	1.466		0.730		
S28	8.362	4.357	3.794/3.725			0.792	0.727	
S29	8.430	4.397	3.828/3.746					
T30	8.145	4.233	4.124	1.075				
N31	8.382	4.642	2.714/2.626					
V32	8.169	3.983	1.998	0.811				
G33	8.516	3.867						
S34	8.217	4.312	3.762/3.730					
N35	8.347	4.547	2.586					
T36	8.056	4.101	3.984	0.952				
Y37	8.133	4.412	2.970/2.821			7.010		6.700

Table 25:  $^1\text{H}$  NMR assignment of IAPP residues (150  $\mu\text{M}$ ) at 5°C.

Second, TOCSY experiments were recorded on hIAPP in the presence of a fivefold excess of EGCG (750  $\mu\text{M}$ ), in order to observe: 1) a putative interaction between hIAPP and EGCG, 2) if this interaction was specific to hIAPP residues. As the preparation of hIAPP may induce some variability (concentration, HFIP treatment), EGCG was added, as a powder, in

the hIAPP solution that was used as a reference. Additionally,  $^1\text{H}$  1D experiments were carried out prior and after addition of EGCG, in between the TOCSY experiments in order to ensure that the peptide had not oligomerized over the time course of the experiments, which would lead to loss of signal and affect the quality of the 2D experiments.

The addition of EGCG in solution induced a downfield shift for the HN proton residues of many amino acids, indicating that the compound had bound to hIAPP or had an effect on the structure of the peptide (figure 106). The chemical shift differences were calculated in order to see if some for residues were more affected by the addition of EGCG in solution, suggesting a more specific binding site of the compound to the peptide. Results showed that residues Cys7, Val17, His18, Ser19, Gly24, Ile26 and Leu27 most of which correspond to the loop connecting the two  $\beta$ -strands of the structured monomer and the nucleation site of hIAPP (table 26).



**Figure 105: TOCSY  $^1\text{H}$ - $^1\text{H}$  spectrum of the HN-H $\alpha$  region of hIAPP (red) and hIAPP in presence of EGCG (blue) at 5°C. Peptide concentration was 150  $\mu\text{M}$ , EGCG concentration was 750  $\mu\text{M}$**

	<b>IAPP</b>	<b>IAPP + EGCG</b>	
<b>Residue</b>	$\delta_{\text{NH}}$ (ppm)	$\delta_{\text{NH}}$ (ppm)	<b>Chemical shift variation</b> (ppm)
N3	8,526	8,515	0,011
T4	7,561	7,549	0,012
A5	8,748	8,735	0,013
T6	7,953	7,943	0,01
C7	8,05	8,025	0,025
A8	8,179	8,164	0,015
T9	8,134	8,118	0,016
Q10	8,162	8,154	0,008
R11	8,195	8,178	0,017
L12	8,05	8,028	0,022
A13	8,114	8,096	0,018
N14	8,178	8,166	0,012
F15	7,977	7,963	0,014
L16	8,023	8,008	0,015
V17	7,916	7,885	0,031
H18	8,346	8,318	0,028
S19	8,309	8,278	0,031
S20	8,447	8,438	0,009
N22	8,239	8,221	0,018
F23	8,216	8,198	0,018
G24	8,285	8,26	0,025
A25	7,952	7,937	0,015
I26	8,184	8,158	0,026
L27	8,411	8,385	0,026
S28	8,362	8,345	0,017
S29	8,43	8,42	0,01
T30	8,145	8,132	0,013
N31	8,382	8,37	0,012
V32	8,169	8,157	0,012
G33	8,516	8,501	0,015
S34	8,217	8,208	0,009
N35	8,347	8,327	0,02
T36	8,056	8,047	0,009
Y37	8,133	8,116	0,017
Mean variation = $0,017 \pm 0,007$			

**Table 26: Chemical shift deviations for full length hIAPP.**  
Cells highlighted in red correspond to the values above the standard deviation range. Cells highlighted in blue correspond to the values below the standard deviation range

However, additional experiments showed that the sample evolved over time, with the monomer signal decreasing after 24 hours of incubation, indicating that at that concentration of hIAPP, a fivefold excess of EGCG did not completely inhibit the aggregation.

In light of these results, the same set of experiments was carried out on a hIAPP fragment composed of the first 19 residues of the peptide (figure 106).



Figure 106: Amino acid sequence of hIAPP<sub>1-19</sub>

The fragment hIAPP<sub>1-19</sub>, has been shown to be weakly amyloidogenic in solution.<sup>129</sup> Therefore, we ensure that any observed shift differences observed upon addition of EGCG are associated to the interaction between the peptide and the compound, and not because of a possible oligomerization of hIAPP.

In comparison with the full-length peptide, a set of TOCSY and NOESY experiments were recorded to assign the different resonances of the hIAPP<sub>1-19</sub>. The resulting spectra displayed similar chemical shifts than the full-length peptide, and were obtained with a better resolution, as the peptide did not aggregate, which allowed an easier assignment and to eliminate the uncertainties raised on the attribution of hIAPP (figure 107, table 27)

1D <sup>1</sup>H experiments showed that the signal of the peptide did not decrease significantly in the time course of the experiments, confirming that hIAPP<sub>1-19</sub> remained mainly monomeric, which is consistent with the fact that hIAPP<sub>1-19</sub> is stable and does not form oligomers. The addition of EGCG to the spectrum induces weak perturbation of the chemical shifts of the peptide, although the calculation of the chemical shift differences showed that residues Cys7, Ala8, Gln10 and His18 were slightly affected by the addition of the compound. The sites of interaction Cys7 and His18 between EGCG and hIAPP<sub>1-19</sub> were common to those observed for the full-length peptide, especially residue His18. These results show that EGCG interacts with some specific sites of hIAPP that are involved in the oligomerization and elongation of the fibrils.

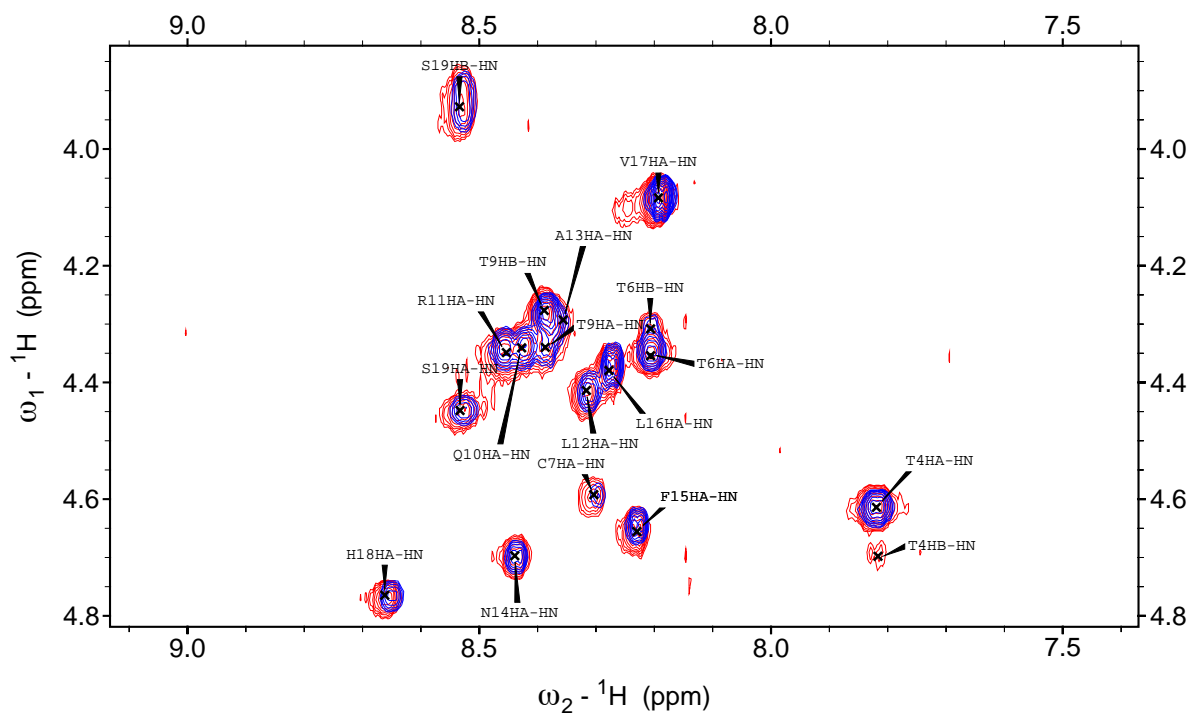


Figure 107: TOCSY  $^1\text{H}$ - $^1\text{H}$  spectrum of the HN-H $\alpha$  region of hIAPP $_{1-19}$  (red) and hIAPP $_{1-19}$  in presence of EGCG (blue) at 5°C. Peptide concentration was 150  $\mu\text{M}$ , EGCG concentration was 750  $\mu\text{M}$

Residue	hIAPP $_{1-19}$ $\delta\text{NH}$ (ppm)	hIAPP $_{1-19}$ + EGCG $\delta\text{NH}$ (ppm)	Chemical shift variation (ppm)
T4	7,819	7,819	0
A5	8,996	8,996	0
T6	8,206	8,206	0
C7	8,305	8,295	0,01
A8	8,438	8,428	0,01
T9	8,387	8,381	0,006
Q10	8,426	8,416	0,01
R11	8,459	8,457	0,002
L12	8,316	8,308	0,008
A13	8,366	8,366	0
N14	8,439	8,439	0
F15	8,232	8,229	0,003
L16	8,277	8,272	0,005
V17	8,196	8,189	0,007
H18	8,66	8,649	0,011
S19	8,534	8,526	0,008
Mean variation = 0,005 $\pm$ 0,004			

Table 27: Chemical shift deviations for hIAPP1-19.

Cells highlighted in red correspond to the values above the standard deviation range. Cells highlighted in blue correspond to the values below the standard deviation range

The results of our experiments showed that the addition of EGCG to monomeric hIAPP induced variations of the chemical shifts of the peptide, indicating an interaction between the polyphenol and amyloid peptide. A calculation of the chemical shifts perturbations allowed us to observe that the interactions were more specific with residues present in the loop and amyloidogenic region of IAPP. Experiments on hIAPP<sub>1-19</sub> allowed us to observe a no or little interaction with EGCG. Nevertheless, the calculation of chemical shifts deviations also indicated that the residue His18 was affected by the addition of EGCG, also suggesting that there existed a specific interaction between the compound and that residue.

The same experiments will have to be carried out on the fragment 20-37 of hIAPP, which includes the 20-29 amyloidogenic region of hIAPP as to observe the possible interactions between EGCG and the nucleation site of the peptide.

## 5. Conclusion`

The purpose of these projects was to probe the effects of different classes of inhibitors on the oligomerization and fibrillization of hIAPP and A $\beta$ 42 amyloid peptides by NMR experiments. The inhibitory effect of compounds on A $\beta$ 42 was carried out with peptides, developed through different strategies. The first project involved the incorporation of a trifluoromethyl group in tripeptides known to have a good affinity with the hydrophobic region of A $\beta$ 42. Results have shown that the presence of the trifluoromethyl amino acid lead to an inhibition of the oligomerization and fibrillization, due to its effect as a  $\beta$ -sheet breaker, an increased hydrophobicity that leads to an enhanced interaction with A $\beta$ 42. The second project focused on the effect of that sugar-based peptidomimetics of the amyloidogenic region of A $\beta$ 42. Results showed that the compound prevented the formation of toxic oligomers, by engaging hydrophobic interactions with A $\beta$ 42 as well as impairing the  $\beta$ -sheet elongation, by introduction of the sugar moiety and aromatic units acting as a  $\beta$ -breaker.

Results of both projects showed that the inhibitors either interacted with the monomeric peptide, or with A $\beta$ 42 oligomers in order to modulate the kinetics of oligomerization or fibrillization of the peptide.

Finally the natural compound EGCG was shown to interact with hIAPP peptide, especially with the nucleation (residue 20-29) and loop region (residue 16 to 20) that contribute to the oligomerization of the peptide. The perturbations observed on the 2D <sup>1</sup>H-<sup>1</sup>H TOCSY spectrum upon addition of EGCG in solution, showed that the compound interacted with the monomeric peptide prior the oligomerization. Additional experiments will be carried

out on samples of hIAPP full length, hIAPP<sub>1-19</sub> and hIAPP<sub>20-37</sub> and in presence of EGCG to further observe the interactions between the peptides and the compounds and determinate more accurately the specific binding sites to the peptide and mechanism of inhibition of the compound.

## Material and methods

### Part 1:

The two tripeptides **1** and **2** were synthesized by solid phase synthesis at Laboratoire de Chimie Biologique, Université de Cergy-Pontoise. A $\beta$ 42 was obtained from American Peptide Company, Inc. (Batch #1207090T). Peptide was dissolved at a concentration of 1 mM in a 1% ammoniac solution and diluted at a final concentration of 50  $\mu$ M in a 10 mM Tris/HCl, 100 mM NaF buffer, pH 6. The sample was then immediately transferred in a Shigemi® 5mm tube. One-dimensional spectra were acquired over 4000 points using a spectral width of 7000 Hz. A cosine bell apodisation function was applied to 1D  $^1\text{H}$  experiments. For each spectrum, 1024 scans were accumulated leading to an experimental time of about 23 minutes. Peptide  $^1\text{H}$  resonances (in the amide/aromatic region between 6.6 and 7.1 ppm) were then integrated and these values are plotted as a function of time (see Figure 3D-F), leading to a sigmoidal curve for A $\beta$ 42 alone and A $\beta$ 42 in the presence of **1** and to an exponential curve for A $\beta$ 42 in the presence of **2**. Since the analysis is done for the integrated intensity of peptide  $^1\text{H}$  resonances between 6.6 and 7.1 ppm, results are therefore average values. All raw NMR experimental data have been processed using the TopSpin program (Bruker) and further analyzed for the integration and the fit using the equations 2 and 3 with a home-written program based on Mathematica 8. The program is available upon request. 1D  $^1\text{H}$  STD experiments were acquired using a cascade of Gaussian shaped pulses (50 ms pulse,  $B_1$  field of 0.1 kHz, total duration of 3 s) applied on resonance ( $-0.7$  ppm) and off resonance ( $+30$  ppm), alternatively. An exponential window function with a line-broadening factor of 10 Hz was applied to  $^1\text{H}$  STD experiments prior to Fourier transform.

### Part 2:

NMR experiments were recorded on a Bruker Avance III 500 MHz spectrometer equipped with a  $^1\text{H}/^{13}\text{C}/^{15}\text{N}$  TCI cryoprobe with Z-axis gradient. NMR spectra were processed and analysed with TopSpin software (Bruker).

Samples of A $\beta$ 42 in the absence or in the presence of **3 $\beta$**  were prepared in Shigemi tubes



(280  $\mu$ L volume) in 50 mM sodium phosphate, pH 7.4 containing 10% D<sub>2</sub>O. Calibration of the <sup>1</sup>H and <sup>13</sup>C were calibrated using DSS (sodium 4,4 dimethyl-4-silapentane-1-sulfonate). Synthetic A $\beta$ 42 peptide was used in NMR experiments, with the exception of 2D HSQC experiments requiring <sup>15</sup>N, <sup>13</sup>C-labelled recombinant A $\beta$ 42. Solid phase peptide synthesis of A $\beta$ 42 was performed at the Institut de Biologie Intégrative (IFR83, Université Pierre et Marie Curie). Recombinant A $\beta$ 42 was obtained according to the protocol described in chapter 2 of the manuscript. NMR experiments were acquired at 5 °C. One-dimensional spectra were acquired over 8000 points using a spectral width of 6000 Hz. A cosine bell apodisation function was applied to 1D <sup>1</sup>H experiments. Solvent resonance was suppressed using a Watergate pulse sequence. For each spectrum, 512 scans were accumulated leading to an experimental time of about 11 minutes. 2D NOESY experiments were recorded with a mixing time of 0.2 s. 1D <sup>1</sup>H STD experiments were acquired using a cascade of Gaussian shaped pulses (50 ms pulse, B<sub>1</sub> field of 0.1 kHz, total duration of 3 s) applied on resonance (−0.7 ppm) and off resonance (+30 ppm), alternatively. The number of scans was set to 320, corresponding to an experiment duration of 50 min. 1D <sup>1</sup>H WaterLOGSY (water-ligand observed via gradient spectroscopy) experiments were recorded using a Gaussian pulse of 20 ms duration for selective inversion of water magnetization and a mixing period of 0.5 s. The recycling delay was set to 2 s and the total number of scans was 1200, corresponding to an experimental time of 1 hour.

### Part 3:

One-dimensional spectra were acquired over 8000 points using a spectral width of 6000 Hz. A cosine bell apodisation function was applied to 1D <sup>1</sup>H experiments. Solvent resonance was suppressed using a Watergate pulse sequence. For each spectrum, 64 scans were accumulated leading to an experimental time of about 2 minutes.

Proton assignment was obtained on the protonated samples, from the analysis of a 2D TOCSY experiment using a 60 ms MLEV 17 mixing time and 2D NOESY experiment (0.2 s mixing time). The experiments were collected as a 512 (t<sub>1</sub>) and 4096 (t<sub>2</sub>) time-domain matrix over a spectral width of 12 ppm with 32 and 64 scans per t<sub>1</sub> increments, respectively.

---

<sup>115</sup> Soto, Claudio, Einar M. Sigurdsson, Laura Morelli, R. Asok Kumar, Eduardo M. Castaño, and Blas Frangione. “ $\beta$ -Sheet Breaker Peptides Inhibit Fibrillogenesis in a Rat Brain Model of Amyloidosis: Implications for Alzheimer’s Therapy.” *Nature Medicine* 4, no. 7 (July 1998): 822–26. doi:10.1038/nm0798-822.

- 
- <sup>116</sup> Gilead, Sharon, and Ehud Gazit. "Inhibition of Amyloid Fibril Formation by Peptide Analogues Modified with  $\alpha$ -Aminoisobutyric Acid." *Angewandte Chemie International Edition* 43, no. 31 (August 6, 2004): 4041–44. doi:10.1002/anie.200353565.
- <sup>117</sup> Venkatraman, Janani, Sasalu C. Shankaramma, and Padmanabhan Balaram. "Design of Folded Peptides." *Chemical Reviews* 101, no. 10 (October 1, 2001): 3131–52. doi:10.1021/cr000053z.
- <sup>118</sup> Loureiro, Joana A., Rosa Crespo, Hans Börner, Pedro M. Martins, Fernando A. Rocha, Manuel Coelho, M. Carmo Pereira, and Sandra Rocha. "Fluorinated Beta-Sheet Breaker Peptides." *J. Mater. Chem. B* 2, no. 16 (March 14, 2014): 2259–64. doi:10.1039/C3TB21483D.
- <sup>119</sup> Török, Béla, Abha Sood, Seema Bag, Aditya Kulkarni, Dmitry Borkin, Elizabeth Lawler, Sujaya Dasgupta, et al. "Structure-Activity Relationships of Organofluorine Inhibitors of  $\beta$ -Amyloid Self-Assembly." *ChemMedChem* 7, no. 5 (May 2012): 910–19. doi:10.1002/cmdc.201100569.
- <sup>120</sup> Porat, Yair, Adel Abramowitz, and Ehud Gazit. "Inhibition of Amyloid Fibril Formation by Polyphenols: Structural Similarity and Aromatic Interactions as a Common Inhibition Mechanism." *Chemical Biology* <html\_ent Glyph="@amp;" Ascii="&"/> *Drug Design* 67, no. 1 (January 2006): 27–37. doi:10.1111/j.1747-0285.2005.00318.x.
- <sup>121</sup> Etienne, Marcus A., Jed P. Aucoin, Yanwen Fu, Robin L. McCarley, and Robert P. Hammer. "Stoichiometric Inhibition of Amyloid  $\beta$ -Protein Aggregation with Peptides Containing Alternating  $\alpha,\alpha$ -Disubstituted Amino Acids." *Journal of the American Chemical Society* 128, no. 11 (March 1, 2006): 3522–23. doi:10.1021/ja0600678.
- <sup>122</sup> Salwiczek, Mario, Elisabeth K. Nyakatura, Ulla I. M. Gerling, Shijie Ye, and Beate Koksche. "Fluorinated Amino Acids: Compatibility with Native Protein Structures and Effects on Protein–protein Interactions." *Chemical Society Reviews* 41, no. 6 (February 27, 2012): 2135–71. doi:10.1039/C1CS15241F.
- <sup>123</sup> Dorgeret, Bertrand, Lucie Khemtémourian, Isabelle Correia, Jean-Louis Soulier, Olivier Lequin, and Sandrine Ongeri. "Sugar-Based Peptidomimetics Inhibit Amyloid  $\beta$ -Peptide Aggregation." *European Journal of Medicinal Chemistry* 46, no. 12 (December 2011): 5959–69. doi:10.1016/j.ejmech.2011.10.008.
- <sup>124</sup> Khasanova, Tatyana V., Omid Khakshoor, and James S. Nowick. "Functionalized Analogues of an Unnatural Amino Acid That Mimics a Tripeptide  $\beta$ -Strand." *Organic Letters* 10, no. 22 (November 20, 2008): 5293–96. doi:10.1021/ol8021897.
- <sup>125</sup> Cheng, Pin-Nan, Cong Liu, Minglei Zhao, David Eisenberg, and James S. Nowick. "Amyloid  $\beta$ -Sheet Mimics That Antagonize Amyloid Aggregation and Reduce Amyloid Toxicity." *Nature Chemistry* 4, no. 11 (November 2012): 927–33. doi:10.1038/nchem.1433.
- <sup>126</sup> Kaffy, Julia, Dimitri Brinet, Jean-Louis Soulier, Lucie Khemtémourian, Olivier Lequin, Myriam Taverna, Benoît Crousse, and Sandrine Ongeri. "Structure–activity Relationships of Sugar-Based Peptidomimetics as Modulators of Amyloid  $\beta$ -Peptide Early Oligomerization and Fibrillization." *European Journal of Medicinal Chemistry* 86 (October 2014): 752–58. doi:10.1016/j.ejmech.2014.09.031.
- <sup>127</sup> Ehrnhoefer, Dagmar E., Jan Bieschke, Annett Boeddrich, Martin Herbst, Laura Masino, Rudi Lurz, Sabine Engemann, Annalisa Pastore, and Erich E. Wanker. "EGCG Redirects Amyloidogenic Polypeptides into

---

Unstructured, off-Pathway Oligomers.” *Nature Structural & Molecular Biology* 15, no. 6 (June 2008): 558–66. doi:10.1038/nsmb.1437.

- <sup>128</sup> Meng, Fanling, Andisheh Abedini, Annette Plesner, C. Bruce Verchere, and Daniel P. Raleigh. “The Flavanol (–)-Epigallocatechin 3-Gallate Inhibits Amyloid Formation by Islet Amyloid Polypeptide, Disaggregates Amyloid Fibrils and Protects Cultured Cells Against IAPP Induced Toxicity.” *Biochemistry* 49, no. 37 (September 21, 2010): 8127–33. doi:10.1021/bi100939a.
- <sup>129</sup> Khemtémourian, Lucie, Maarten F. M. Engel, Rob M. J. Liskamp, Jo W. M. Höppener, and J. Antoinette Killian. “The N-Terminal Fragment of Human Islet Amyloid Polypeptide Is Non-Fibrillogenic in the Presence of Membranes and Does Not Cause Leakage of Bilayers of Physiologically Relevant Lipid Composition.” *Biochimica et Biophysica Acta (BBA) - Biomembranes* 1798, no. 9 (September 2010): 1805–11. doi:10.1016/j.bbamem.2010.05.022.

# **Chapter 6:**

## **Conclusion**



The objectives of this thesis was to get an insight into the oligomerization and fibrillization properties of two amyloid peptides, A $\beta$ 42 and hIAPP and investigate how factors such as pH, substitution of a residue or addition of inhibitors could affect these processes.

The first part of my thesis followed the “toxic oligomer” hypothesis and focused on the early stages of oligomerization of A $\beta$ 42 and hIAPP. For this study, we carried out a panel of complementary biophysical experiments, each focusing on different stages of the fibril formation in order to better characterize the oligomerization and fibrillization of the peptides.

In order to compare the results obtained by different spectroscopic techniques, experimental conditions were designed to be as close as possible in term of physicochemical parameters and buffer composition. However, it appeared during the study that the experiments could be batch dependent and that the addition of fluorescent probes used for fluorescence experiments could induce a bias in our results, which was a drawback for the fine comparison of the kinetics of oligomerization and fibrillization between techniques.

The results of the experiments, have nevertheless allowed us to obtain mechanistic information on the oligomerization and fibrillization of the peptides. Overall, our results, obtained with NMR experiments, gel electrophoresis and CD experiments, showed that the fibrillization mechanism of hIAPP appeared to be a cooperative process, characterized by fast kinetics of aggregation leading to large insoluble fibrils. The different techniques that were used failed to detect small intermediate species, which was consistent with previous data that reported that hIAPP did not form stable low weight oligomers during the aggregation process.<sup>130,131</sup> In addition, investigation of the interaction between the different species showed no exchange between the monomer or small oligomers and larger species that aggregated in solution.

On the contrary, the oligomerization and fibrillization mechanism of A $\beta$ 42 showed a stepwise process, characterized by the co-existence of different species (monomeric peptide, intermediates and large oligomers) that were in fast-exchange with each other in solution, as was shown by NMR experiments.

The second part of my thesis focused on the effect of pH and substitution of residue 18 of hIAPP. The residue 18 was indeed shown to be a key residue in the oligomerization and the fibrillization given its variable of state of protonation within the

physiological pH range and its particular localization, in the loop of the ordered hIAPP monomer that forms fibrils.

This study on the effect of pH and substitution of residue 18 have been carried out at pH 5.5 and pH 7.4, which corresponds to the pH of the secretory granules of the cell and of the extracellular medium, respectively, and on five peptides including the wild type peptide and four mutants where residue 18 was substituted by a lysine, an arginine, a glutamic acid or an alanine. Given the interaction between hIAPP, especially the 19 residues of N-terminus region and the cell membrane, the experiments have been carried out in presence of membrane models composed of a mixture (7:3) of DOPC (zwitterionic head group) and DOPS (anionic head group).

Overall, our results at pH 7.4 showed that residue His18 was involved in specific peptide-peptide interactions that contributed to the elongation of the fibrils. The substitution of His18 by another amino acid was indeed shown to be deleterious and that the oligomerization and fibrillization was especially destabilized when His 18 was replaced by a negatively charged amino acid (glutamic acid) or with an amino acid with a short side chain (alanine). A possible outlook would be the study of the effect of the substitution of the histidine residue by other amino acids such as glutamine, asparagine or tyrosine that would maintain its hydrogen bonding or aromatic properties.

Our results at pH 5.5 showed that low pH was globally unfavorable to the oligomerization and the fibrillization of the peptides, modulating its aggregation in a complex way given the protonation state of either residue 18 and the N-terminus of the peptides.

To go further in this study, complementary experiments could be carried out on hIAPP wild type and mutants at pH 5.5 and pH 7.4. Among those experiments, microscopy would be especially interesting, as it would allow us to observe the morphology of the formed aggregates and/or fibrils of the different mutants over time.

Last but not least, the third part of my thesis focused on the study of potential inhibitors of amyloid oligomerization. As they are strongly linked to cell-death oligomeric species represent an interesting target for the development of therapeutic compounds that were developed through different strategies.

In particular, one of the main strategies, is to design peptides that incorporate moieties acting as  $\beta$ -breakers. Those peptides are described to have a good affinity with the nucleation regions of the amyloid peptides and disrupt the oligomerization by disturbing the interactions between the  $\beta$ -strands of the oligomers or fibrils.

Among this class of inhibitors, we studied the effect of a tripeptide incorporating a trifluoromethyl amino acid on the kinetics of oligomerization of A $\beta$ 42. Results have shown that the presence of the fluorinated amino acid led to an inhibition of the oligomerization and fibrillization, due to its effect as a  $\beta$ -sheet breaker, an increased hydrophobicity given by the presence of fluorine atoms that leads to an enhanced interaction with A $\beta$ 42. Second, we studied the interactions between a peptidomimetic incorporating a sugar moiety as well as aromatic units. Our results, obtained by NMR experiments, showed that the designed compound interacted with the oligomers of A $\beta$ 42, engaging hydrophobic interactions and therefore preventing the formation of toxic oligomers.

This work on inhibiting compounds has led to two scientific publications «*Use of a ( R )- $\alpha$ -Trifluoromethylalanine Containing Short Peptide in the Inhibition of Amyloid Peptide Fibrillation.*» (Botz, Alexandra, Vincent Gasparik, Emmanuelle Devillers, Anais R. F. Hoffmann, Lucie Caillon, Evelyne Chelain, Olivier Lequin, Thierry Brigaud, and Lucie Khemtémourian), which was accepted in *Biopolymers Peptide Science* and «*Small glycopeptidomimetics inhibit protein-protein interactions mediating amyloid  $\beta$ -peptide oligomerization and fibrillization.* » (Kaffy J., Brinet D., Soulier J.L., Correia I, Tonali N, Fera K.F., Iacone Y., Hoffmann A.R.F, Khemtémourian L., Crousse B., Taylor M., Allsop D., Taverna M., Lequin O., Ongeri S.), which was submitted in *Nature Chemistry*.

This last chapter also focused on the interactions between hIAPP and a natural polyphenol, EGCG that was shown to inhibit the fibril formation of several amyloid peptides. The results of 2D experiments that we carried out on full-length hIAPP and hIAPP<sub>1-19</sub> showed that EGCG interacted with hIAPP monomer, especially with the nucleation (residue 20-29) and loop region (His18) of the amyloid peptide. Additional experiments will be carried out on samples of hIAPP full length, hIAPP<sub>1-19</sub> and hIAPP<sub>20-37</sub> and in presence of EGCG to further observe the interactions between the peptides and the compounds and determinate more accurately the specific binding sites to the peptide and mechanism of inhibition of the compound.

---

<sup>130</sup> Soong, Ronald, Jeffrey R. Brender, Peter M. Macdonald, and Ayyalusamy Ramamoorthy. "Association of Highly Compact Type II Diabetes Related Islet Amyloid Polypeptide Intermediate Species at Physiological Temperature Revealed by Diffusion NMR Spectroscopy." *Journal of the American Chemical Society* 131, no. 20 (May 27, 2009): 7079–85. doi:10.1021/ja900285z.



- 
- <sup>131</sup> Vaiana, Sara M., Rodolfo Ghirlando, Wai-Ming Yau, William A. Eaton, and James Hofrichter. "Sedimentation Studies on Human Amylin Fail to Detect Low-Molecular-Weight Oligomers." *Biophysical Journal* 94, no. 7 (April 1, 2008): L45–47. doi:10.1529/biophysj.107.125146

## **Publications**



**Use of a (R)- $\alpha$ -trifluoromethylalanine containing short peptide in the inhibition of amyloid peptide  
fibrillation**

Alexandra Botz<sup>1,2,3</sup>, Vincent Gasparik<sup>4</sup>, Emmanuelle Devillers<sup>4</sup>, Anais R. F. Hoffmann<sup>1,2,3</sup>, Lucie  
Caillon<sup>1,2,3</sup>, Evelyne Chelain<sup>4</sup>, Olivier Lequin<sup>1,2,3</sup>, Thierry Brigaud<sup>\*4</sup>, Lucie Khemtémourian<sup>\*1,2,3</sup>

<sup>1</sup> Sorbonne Universités, UPMC Univ Paris 06, Laboratoire des Biomolécules, 4 place Jussieu, F-75005,  
Paris, France.

<sup>2</sup> Ecole Normale Supérieure-PSL Research University, Département de Chimie, 24 rue Lhomond, F-  
75005, Paris, France.

<sup>3</sup> CNRS, UMR 7203 Laboratoire des Biomolécules, F-75005, Paris, France.

<sup>4</sup> Laboratoire de Chimie Biologique, Université de Cergy-Pontoise, EA 4505, 5 Mail Gay-Lussac, 95000  
Cergy-Pontoise, France

Correspondence: thierry.brigaud@u-cergy.fr; lucie.khemtemourian@upmc.fr

**This article has been accepted for publication and undergone full peer review but has not been  
through the copyediting, typesetting, pagination and proofreading process which may lead to  
differences between this version and the Version of Record. Please cite this article as an  
'Accepted Article', doi: 10.1002/bip.22670  
© 2015 Wiley Periodicals, Inc.**

This article is protected by copyright. All rights reserved.

**Abstract (250 words)**

The extracellular deposition of insoluble amyloid fibrils resulting from the aggregation of the amyloid- $\beta$  ( $A\beta$ ) is a pathological feature of neuronal loss in Alzheimer's disease. Numerous small molecules have been reported to interfere with the process of  $A\beta$  aggregation. Compounds containing aromatic structures, hydrophobic amino acids and/or the  $\alpha$ -aminoisobutyric acid (Aib) as  $\beta$ -sheet breaker elements have been reported to be effective inhibitors of  $A\beta$  aggregation. We synthesized two peptides, one containing the Aib amino acid and the other including its trifluoromethylated analog (*R*)-Tfm-Alanine and we evaluated the impact of these peptides on  $A\beta$  amyloid formation. The compounds were tested by standard methods such as thioflavin-T fluorescence spectroscopy and transmission electron microscopy but also by circular dichroism, liquid state NMR and NMR saturation transfer difference experiments to further characterize the effect of the two molecules on  $A\beta$  structure and on the kinetics of depletion of monomeric, soluble  $A\beta$ . Our results demonstrate that the peptide containing Aib reduces the quantity of aggregates containing  $\beta$ -sheet structure but slightly inhibits  $A\beta$  fibril formation, while the molecule including the trifluoromethyl (Tfm) group slows down the kinetics of  $A\beta$  fibril formation, delays the random coil to  $\beta$ -sheet structure transition and induces a change in the oligomerization pathway. These results suggest that the hydrophobic Tfm group has a better affinity with  $A\beta$  than the methyl groups of the Aib and that this Tfm group is effective and important in preventing the  $A\beta$  aggregation.

### Introduction

The formation of protein amyloid deposits also named amyloid fibrils, composed of  $\beta$ -sheet aggregates, is associated with major human diseases including Alzheimer's disease (AD), Parkinson's disease, the spongiform encephalopathy and type 2 diabetes mellitus. AD is a neurodegenerative disorder associated with synaptic loss, abnormalities in functioning of neurons, neuronal cell death leading to memory loss and severe cognitive impairment. AD is characterized by the accumulation of extracellular amyloid- $\beta$  peptides ( $A\beta$ ) in senile plaques and intracellular neurofibrillary tangles composed of microtubule-associated protein tau.<sup>1</sup>

The amyloid- $\beta$  peptide, the main component of the senile plaques, was suggested to be the key factor in the development of AD pathology.<sup>2,3</sup> This peptide results from the cleavage of the transmembrane amyloid precursor protein (APP) by  $\beta$ - and  $\gamma$ -secretases. Depending on the site of APP cleavage by  $\gamma$ -secretase,  $A\beta$  peptides of various chain lengths from 39 to 43 amino acid residues are generated.<sup>4-7</sup> The two major alloforms of  $A\beta$  found in the cerebral tissue of AD patients are  $A\beta$ 40 and  $A\beta$ 42, which differ by the presence of two amino acids (Ile and Ala) at the C-terminal part. It has been shown that  $A\beta$ 42 forms fibril at a higher rate than  $A\beta$ 40 and that  $A\beta$ 42 is more toxic to cultured neurons than  $A\beta$ 40.<sup>8,9</sup>

In solution, the aggregation process of  $A\beta$  peptides involves a secondary structure transition from random coil to  $\beta$ -sheet conformation leading to cross  $\beta$ -sheet structure formation with  $\beta$ -strand repeats running perpendicular to the fibril axis.<sup>10-12</sup> As for all amyloid peptides,  $A\beta$  is produced as a soluble monomer and undergoes oligomerization and amyloid fibril formation via a nucleation-dependent polymerization process.<sup>13,14</sup> During the course of *in vitro* fibril formation, various non-fibrillar aggregation intermediates, collectively called soluble oligomers or protofibrils, have been shown to precede the emergence of fibrils. In the 90s, it was generally thought that  $A\beta$  fibrils were toxic to the neurons and therefore responsible for the initiation of AD.<sup>15</sup> Currently, the prevailing and well-documented view is that soluble  $A\beta$  oligomers are the most toxic species in AD pathogenesis.<sup>16</sup> However, the group of Lashuel hypothesized that  $A\beta$  toxicity is mediated by ongoing polymerization process rather than by a specific and stable  $A\beta$  molecular species.<sup>17</sup> In other words, they assume that the assembly of  $A\beta$  fibrils at the membrane causes membrane disruption, as it was also shown for the islet amyloid polypeptide involved in type 2 diabetes mellitus.<sup>18</sup> In view of these hypotheses, an attractive strategy for treating AD is to inhibit the early stages of  $A\beta$  aggregation or to redirect the aggregation cascade towards off-pathways and non toxic species.<sup>19</sup>

Many inhibitors of  $A\beta$  aggregation are peptides, which are designed to interact with one of two hydrophobic cores of  $A\beta$ , the residues 17-21 or 30-42. Small peptides mimicking one of these hydrophobic sequences were demonstrated to modulate the kinetics of  $A\beta$  aggregation.<sup>20</sup> Initial work

identified the KLVFF motif as capable of inhibiting fibril formation.<sup>21</sup> Then, variants of this motif containing a polycationic disrupting region added to the C terminus of KLVFF motif have been synthesized and showed differences in A $\beta$  fibril formation.<sup>22,23</sup> Another class of peptides which contained  $\alpha,\alpha$ -disubstituted amino acids was shown to abolish fibril formation or to produce off-pathways species.<sup>24</sup> According to the same rationale, di- and hexapeptides incorporating the  $\alpha$ -aminoisobutyric acid (Aib) as  $\alpha,\alpha$ -disubstituted amino acid were reported to present interesting inhibition properties of the oligomerization of  $\beta$ -amyloid polypeptide.<sup>25</sup> Other interesting molecules that inhibit A $\beta$  aggregation are  $\beta$ -breaker peptides containing N-methyl amino acids or proline.<sup>26,27</sup> As reported by several recent studies on ligand-A $\beta$  interactions, NMR constitutes an outstanding technique to provide insights into the role of intermolecular interactions.<sup>28</sup>

The incorporation of fluorine atoms into biologically relevant molecules is nowadays an expanding strategy for the improvement of their physical and biological properties<sup>29</sup>. The incorporation of fluorine atoms is known to increase the metabolic stability, the lipophilicity and to modulate the reactivity and the acido-basic properties of neighboring functional groups. As a class of biologically active compounds, fluorine atoms containing peptides are becoming very attracting target molecules. The incorporation of fluorinated amino acids into peptides has been reported to modulate their proteolytic stability and hydrophobicity<sup>30</sup> and to control the conformations of the peptides.<sup>31</sup> As an emerging feature, fluorinated amino acids are also used as powerful <sup>19</sup>F NMR probes for biological activity studies.<sup>32</sup> For example, <sup>19</sup>F was introduced into the islet amyloid polypeptide and into A $\beta$ 40 so as to follow the kinetics of oligomers formation using real-time <sup>19</sup>F NMR.<sup>33</sup> For several years we have developed efficient methods for the synthesis of enantiopure  $\alpha$ -alkyl- $\alpha$ -trifluoromethyl amino acids ( $\alpha$ -Tfm-AAs)<sup>34</sup> and the methodologies for their incorporation into short peptides for biological activity evaluation.<sup>35</sup> As these  $\alpha$ -trifluoromethyl amino acids constitute highly hindered  $\alpha,\alpha$ -disubstituted amino acids, their incorporation into peptides should constitute a promising tool to induce a  $\beta$  sheet breaker effect and an inhibition of A $\beta$  aggregation. In correlation with the recent literature results obtained with an  $\alpha$ -aminoisobutyric acid (Aib) containing dipeptide,<sup>25</sup> we wish to report herein the use of an hydrophobic (*R*)- $\alpha$ -trifluoromethylalanine containing tripeptide for the inhibition of A $\beta$  aggregation. The results will be compared with the unfluorinated analogue incorporating the Aib amino acid.

## Results

### Effect of (*R*)-trifluoromethylalanine containing short peptide on A $\beta$ 42 fibrillation

The aggregation of A $\beta$ 42 incubated at 25°C with the peptides H-Ala-Aib-Leu-OH (**1**) or H-Ala-(*R*)-Tfm-Ala-Leu-OH (**2**) (Figure 1) at a molar ratio of 1:10 was evaluated by the ThT binding assay, the

standard method used to monitor the time course of fibril formation.<sup>36</sup> The aggregation of A $\beta$ 42 can be described by a sigmoidal transition with a well-defined lag phase in which monomers and oligomers dominate the population, followed by a growth phase during which fibrils elongate and, finally, a plateau. The kinetics data were fitted according to a Boltzmann sigmoidal equation. Three parameters were derived from the ThT curves of A $\beta$ 42 alone and A $\beta$ 42 in the presence of the evaluated compound. The time at half fibril conversion ( $t_{1/2}$ ), the elongation or aggregation rate ( $\tau$ ), and the fluorescence intensity at the plateau (F) which is dependent in a first approximation on the amount of fibrillar material formed, were extrapolated from the fit. The fluorescence assay of A $\beta$ 42 at a concentration of 5  $\mu$ M shows a typical fibrillation process with a lag phase of approximately 10 h followed by a growth phase and a final plateau reached at 20 h (Figure 2A, black). Our results show that **1** exhibits inhibitory capabilities, however these properties were limited to a reduction in the equilibrium plateau of approximately 25%, while the initial lag phase and the aggregation rate were not significantly altered (Figure 2A, blue). In contrast, our results with the fluorinated molecule **2** shows i) an increase in the lag phase of A $\beta$ 42 from 10 to 15 h (Figure 2A, orange), ii) a reduced final fluorescence intensity by a factor of **2** and iii) an decrease of the aggregation rate from 0.8 to 0.2 h<sup>-1</sup>, indicating that this molecule slows down the kinetics of A $\beta$ 42 fibril formation. Control experiments, performed in the absence of A $\beta$ 42, indicated that under the experimental conditions used, the ThT fluorescence of the molecules **1** and **2** remained low (Figure 2A, dot). The results are summarized in Figure 2B with respect to their effect upon lag extension, elongation rate and equilibrium plateau reduction. The A $\beta$ 42 inhibitor molar ratio of 1:1 did not significantly change the aggregation parameters of A $\beta$ 42, which indicates that there is a threshold concentration for the A $\beta$ 42-molecule interactions.

Subsequently, we decided to study the characteristics and morphology of the A $\beta$ 42 fibril formation in the presence or absence of the molecule using transmission electron microscopy. The fibrils formed by A $\beta$ 42 exhibited the typical morphology of long and twisted amyloid fibrils with widths between 10 and 15 nm (Figure 2C). Similar observations were made in the presence of the peptide **1** indicating that this molecule does not significantly decrease the amounts of A $\beta$ 42 fibrils (Figure 2D). Nevertheless, the fibrils formed by A $\beta$ 42 sample containing 10-fold excess of the fluorinated peptide **2** showed a clear inhibition correlating to the ThT experiments (Figure 2E). Indeed, the fibrils were thinner and smaller and had a lower frequency compared to the fibrils formed by A $\beta$ 42 alone. Altogether, our TEM results are correlated with the ThT assay results, indicating that the molecule containing the trifluoromethyl group has a potential to serve as an inhibitor for the process of A $\beta$ 42 fibril formation.



### Stabilization of A $\beta$ 42 secondary structure in the presence of the peptide incorporating the (*R*)-trifluoromethylaniline

To evaluate the initial A $\beta$ 42 structure and to analyze the conformational changes of A $\beta$ 42 after a few hours of incubation in the absence or in the presence of an equimolar concentration of the two molecules **1** or **2**, inhibition studies were carried out by CD. The CD spectrum of A $\beta$ 42 freshly dissolved in 10 mM Tris.HCl, 100 mM NaF buffer at 50  $\mu$ M displays a peak with negative ellipticity at 200 nm that is characteristic of a random coil conformation, in agreement with previous reports (Figure 3A).<sup>37</sup> The same result is observed in the presence of peptides **1** and **2** (Figures 3B-C). However, after a few hours of incubation, A $\beta$ 42 alone and A $\beta$ 42 in the presence of **1** adopt a  $\beta$ -sheet structure, while A $\beta$ 42 in the presence of **2** retains its random coil conformation. The CD signal of A $\beta$ 42 in the presence of the fluorinated peptide **2** remains stable for at least 96 h and shows no evidence of  $\beta$ -sheet structure, indicative of amyloid fibril formation. The formation of  $\beta$ -sheet structure is indicated by the appearance of a negative band at 220 nm and the loss of the negative band at 200 nm. By plotting the CD ellipticity at 220 nm against time, a sigmoid curve is obtained for A $\beta$ 42 alone and A $\beta$ 42 in the presence of **1** in agreement with previous reports.<sup>38</sup> The lag phase, the  $t_{1/2}$  time required to reach half-value of the maximum of the CD signal at 220 nm and the time to reach the plateau are reported in Figure 3D. A $\beta$ 42 presented a random coil to  $\beta$ -sheet transition of 9 h. In the presence of **1**, the transition occurs at 50 h, while in the presence of **2** no transition is observed. Our results show that **1** has a slowing effect; this molecule interferes with  $\beta$ -sheet formation and monomer assembly. Interestingly, **2** has a stabilizing effect; this molecule is able to stabilize the unordered-soluble monomers/small oligomers and delay the conformational transition.

### Trifluoromethylaniline containing short peptide slows down the kinetics of monomeric A $\beta$ 42 depletion

Next, liquid state  $^1\text{H}$  NMR studies were performed to measure the kinetics of depletion of monomeric soluble A $\beta$ 42 in the absence and in the presence of molecules **1** or **2**, using the same experimental conditions as for CD (in terms of temperature, buffer composition, pH). The basis for using NMR peak intensities in kinetics studies of peptide self-assembly is simple in that as self-assembly occurs, the intensities of peaks due to monomer decrease as a result of the conversion of the NMR-visible monomer to NMR-invisible assemblies.<sup>39</sup> Figure 4A-C shows the amide/aromatic region of the 1D  $^1\text{H}$  NMR spectra recorded in the absence and in the presence of the molecules. Spectra of A $\beta$ 42 revealed a significant loss of signal intensity ( $\sim 50\%$ ) over a period of  $4.2 \pm 1.0$  hours suggesting that the peptide undergoes oligomerization. After  $15 \pm 1.0$  hours, the peptide  $^1\text{H}$  signals decay to zero indicating that the monomeric peptide form in solution disappears completely. The presence of **1** does not affect this kinetics, with the loss of signal intensity and the time needed to

observe a complete disappearance of NMR signals of  $4.3 \pm 1.0$  hours and  $14 \pm 1.0$  hours, respectively. In sharp contrast, in the presence of **2** the  $t_{1/2}$  corresponding to a 50% loss of signal intensity increases to  $8.0 \pm 1.0$  hours and the peak intensity does not decrease until 0 indicating that **2** slows down the kinetics of depletion of monomeric A $\beta$ 42 and that after 20 hours, there is still monomeric A $\beta$ 42 in solution. We then determined the integral of the  $^1\text{H}$  NMR in the amide/aromatic region and plotted it against incubation time (Figure 4D-F). The curves of A $\beta$ 42 alone and A $\beta$ 42 in the presence of **1** were fitted by a Boltzmann function. At time zero, only monomeric A $\beta$ 42 is present. The sharp drop in NMR intensities suggests that the monomer evolves into small oligomeric species, then into larger oligomers and finally protofibrils. At the end of the experiment, most monomers are consumed. The curve of A $\beta$ 42 in the presence of **2** could not be fitted by a Boltzmann function but was fitted by an exponential function suggesting that the fluorinated peptide **2** induces some changes in the kinetics of monomer depletion and that in the presence of **2**, A $\beta$ 42 may follow another pathway of fibril formation. It is important to note that the normalized peak intensity does not decrease till zero suggesting that monomeric A $\beta$ 42 is still present after 20 hours of incubation. Our results clearly indicate that molecule **2** is able to interact with A $\beta$ 42. We next studied the A $\beta$ 42:**2** interactions using saturation transfer difference (STD) experiments which enable to probe the interactions of small ligands that bind to macromolecular species (Figure 5A-D).<sup>40,20c</sup> STD signals were observed for the resonances of **2** in the presence of A $\beta$ 42 proving that **2** interacts with A $\beta$ 42 species while no significant STD signal could be observed for compound **1**. The saturation transfer involves mostly protons of Leu side chain as well as the methyl groups of Ala and Tfm-Ala, enlightening the importance of van der Waals interactions through the aliphatic side chains of **2**. As the NMR saturation transfer is mediated by large molecular weight species, it is likely that the fluorinated peptide **2** interacts with aggregated A $\beta$ 42 species that are not visible on the  $^1\text{H}$  NMR spectrum.

### Discussion

Protein misfolding and aggregation have been related to severe human disorders, which are all characterized by amyloid fibrils. Inhibition of the assembly of the mature monomeric peptide or protein into aggregated structures has emerged as a therapeutic strategy for those diseases. Numerous small molecule inhibitors of A $\beta$  aggregation, including fluorinated molecules, have been studied.<sup>20a,41</sup> Moreover, compounds containing among others hydrophobic amino acids and the non proteinogenic amino acid Aib, which has a much stronger  $\beta$ -breaking potential than proline are reported to inhibit A $\beta$  aggregation.<sup>25</sup> It is known that fluorinated amino acids can have drastic effects on peptides or protein stability and on peptide-peptide interactions due to the unique stereoelectronic properties of fluorine.<sup>42</sup> Although the effect of the incorporation of side chain fluorinated  $\alpha$ -amino acids into amyloid forming peptides have been recently investigated,<sup>43</sup> the use of

fluorinated amino acids containing peptides in amyloid aggregation inhibition have rarely been studied.<sup>44</sup> So far, to our knowledge, the  $\beta$ -sheet breaker ability of  $\alpha$ -trifluoromethylalanine containing peptides has never been evaluated yet. The  $\alpha$ -trifluoromethylalanine should combine both the characteristics of an  $\alpha,\alpha$ -disubstituted amino acids and the specific properties of a fluorinated amino acid. The Ala-Aib-Leu (**1**) and Ala-Tfm-Ala-Leu (**2**) sequences were chosen because of their great hydrophobicity in order to provide a good affinity with A $\beta$ .

The ThT fluorescence, EM, CD and NMR studies of A $\beta$  in the presence of peptides **1** or **2** reveal several interesting features. ThT fluorescence suggests that both molecules exhibited inhibitory potencies, ranging from a modest reduction of the equilibrium plateau for the peptide **1** to an important inhibition for the fluorinated peptide **2**. These results demonstrate that the  $\beta$ -sheet breaker effect due to incorporation of the  $\alpha,\alpha$ -disubstituted amino acids is confirmed in both cases. Moreover the inhibition of A $\beta$  aggregation is increased by the introduction of the hydrophobic trifluoromethyl group. This result constitutes a nice illustration of the hydrophobicity modulation of peptides by fluorinated groups. These ThT fluorescence data are consistent with our EM results that show a small number of thin and small fibrils of A $\beta$  in the presence of the peptide **2**, while in the presence of the molecule **1**, more abundant thick fibrils were found. In the presence of **2**, CD spectra data show predominantly random coil conformation even after several days of incubation, and no transition to  $\beta$ -sheet structure, characteristic of amyloid fibrils, occurs. Finally our NMR studies indicate that the peptide **2** slows down the depletion of monomeric A $\beta$  and likely interacts with oligomeric A $\beta$  species that lead to an inhibition of amyloid fibrils. Hence, all these experiments suggest that the presence of the trifluoromethyl group inhibit fibril formation of A $\beta$ . It is important to note that the inhibition effect of peptide **2** is stronger in the CD and NMR experiments, which were performed at a higher A $\beta$  concentration (50  $\mu$ M) than the ThT-fluorescence assay (5  $\mu$ M). These results suggest that the affinity of A $\beta$  to the molecule **2** is probably weak.

As the fluorination increases the hydrophobicity of the molecule, we believe that the peptide **2** will interact with the hydrophobic region of A $\beta$ . This interaction might contribute to the prevention of A $\beta$  peptides to interact with each other, thus inhibiting their interaction. Loureiro et al<sup>44</sup> showed using ThT-fluorescence and EM that fluorination of the hydrophobic residue valine or phenylalanine is effective in preventing the A $\beta$  aggregation at a molar ratio of 1:20. They hypothesized that this inhibition is due to the interaction between the fluorinated amino acid and the hydrophobic residues of A $\beta$ . We believe that the inhibition of A $\beta$  aggregation by the fluorinated tripeptide **2** can be explained by the same reasons.

#### Conclusions

The two tripeptides designed in this study showed an inhibition of the kinetics of fibril formation at high concentration. This inhibition could be explained by i) a  $\beta$ -sheet breaker effect promoted by the Aib or the (*R*)- $\alpha$ -Tfm-Alanine  $\alpha,\alpha$ -disubstituted amino acids and ii) a good affinity of the peptides with the hydrophobic region of A $\beta$ . The trifluoromethyl group containing peptide gave significantly better inhibition results because of its increased hydrophobicity. It is anticipated that a longer and more hydrophobic peptide sequence incorporating an  $\alpha$ -Tfm-Alanine will induce helicity and will provide a better affinity between the inhibitor and the A $\beta$  peptide and therefore a stronger inhibition. Moreover the fluorine atoms would constitute useful probes for the investigation of the inhibitors-A $\beta$  interactions by  $^{19}\text{F}$ NMR.

### Materials and Methods

#### Synthesis of H-Ala-Aib-Leu-OH (1)

A sample of *N*-Fmoc-Leu-Wang resin (loading : 0.8 mmol/g, 375 mg, 0.30 mmol, 1.0 equiv.) was placed in a dried 15 mL glass reaction vessel, stirred in a mixture of dry DCM (2 mL) and DMF (2 mL) for 40 min, and drained. The Fmoc group was removed with 10 ml of 20% piperidine in DMF (3 x 10 min) and the resin was washed with DMF (3 x 1 min) and DCM (3 x 1 min). To the resin were added a solution of Fmoc-Aib-OH (488 mg, 1.50 mmoles, 5.0 equiv), DIPEA (261 ml, 1.50 mmol, 5.0 equiv) and HATU (570 mg, 1.50 mmol, 5.0 equiv) in DMF (4 mL). The coupling reaction was stirred for 2 hours at room temperature, after which the resin was washed with 5 mL of DMF (3 x 2 min) and 5 mL of DCM (3 x 2 min). The same procedure was repeated for the coupling of *N*-Fmoc-Ala-OH (494 mg, 1.50 mmol, 5.0 equiv). The coupling reaction was stirred for 2 hours. The Fmoc group was then removed with 10 ml of 20% piperidine in DMF (3 x 10 min) and the resin was cleaved with a solution of TFA (95%) in dichloromethane for 3 hours. Purification by semi-preparative HPLC (Acetonitrile (TFA 0.1%)/water (TFA 0.1%), 10 : 9 to 30 : 70) afforded the tripeptide **1** (21 mg, 75  $\mu\text{mol}$ , 25%, > 95% purity) as a white solid.  $^1\text{H}$  NMR ( $\text{CD}_3\text{OD}$ ):  $\delta$  0.94–0.90 (m, 6 H,  $\text{H}_{\beta_3} + \text{H}_{\beta_3'}$ ), 1.47–1.52 (m, 9 H,  $\text{H}_{\beta_1} + \text{H}_{\beta_2} + \text{H}_{\beta_2'}$ ), 1.53–1.59 (m, 2 H,  $\text{H}_{\beta_3}$ ), 1.63 (m, 1 H,  $\text{H}_{\gamma_3}$ ), 3.93 (m, 1 H,  $\text{H}_{\alpha_1}$  or  $\text{H}_{\alpha_3}$ ), 4.43 (m, 1 H,  $\text{H}_{\alpha_1}$  or  $\text{H}_{\alpha_3}$ ) ppm.  $^{13}\text{C}$  NMR ( $\text{CD}_3\text{OD}$ ):  $\delta$  17.6, 22.0, 23.4, 25.2, 25.4, 25.9, 41.7, 50.3, 52.3, 58.1, 118.0 (q,  $^1J_{\text{C-F}} = 291$  Hz; TFA), 163.0 (q,  $^2J_{\text{C-F}} = 34$  Hz, TFA), 170.4, 176.1, 176.2 ppm.  $^{19}\text{F}$  NMR ( $\text{CD}_3\text{OD}$ ):  $\delta$  -80 ppm (s, TFA salt). MS (EI):  $m/z$  (%) = 288.2 ( $[\text{M}+\text{H}]^+$ ). HRMS (ESI)  $m/z$   $[\text{M}+\text{H}]^+$  Calcd for  $\text{C}_{14}\text{H}_{25}\text{N}_3\text{O}_4$  288.1923, found 288.1912.

#### Synthesis of H-Ala-(*R*)- $\alpha$ -Tfm-Ala-Leu-OH (2)

Pd/C (260 mg, 0.075 mmol, 0.5 equiv.) was added to a solution of *N*-Fmoc-Ala-(*R*)- $\alpha$ -Tfm-Ala-Leu-OBn<sup>34b</sup> (100 mg, 0.15 mmol, 1.0 equiv.) in MeOH (5 mL) under a nitrogen atmosphere. The reaction mixture was stirred under a hydrogen atmosphere (2 bars) for 2 hours. The catalyst was separated by

filtration and HCl gas was bubbled through the solution for 10 min. The resulting solution was evaporated under vacuum to afford H-Ala-(R)- $\alpha$ -Tfm-Ala-Leu-OH (**2**) (40 mg, 77%, > 95% purity) as a white solid.  $^1\text{H}$  NMR ( $\text{CD}_3\text{OD}$ ):  $\delta$  0.91 (m, 6H,  $\text{H}_{\beta 3} + \text{H}_{\beta 3'}$ ), 1.50 (d, 3H,  $J = 6$  Hz,  $\text{H}_{\beta 1}$ ), 1.60–1.62 (m, 3H,  $\text{H}_{\beta 3} + \text{H}_{\beta 3'}$ ), 1.76 (s, 3H,  $\text{H}_{\beta 2}$ ), 3.99 (m, 1H,  $\text{H}_{\alpha 1}$  or  $\text{H}_{\alpha 3}$ ), 4.47 (m, 1H,  $\text{H}_{\alpha 1}$  or  $\text{H}_{\alpha 3}$ ) ppm.  $^{13}\text{C}$  NMR ( $\text{CD}_3\text{OD}$ ):  $\delta$  17.5, 18.0, 21.9, 23.3, 25.8, 41.6, 50.3, 52.5, 63.9 (q,  $^2J_{\text{C-F}} = 26$  Hz), 117.5 (q,  $^1J_{\text{C-F}} = 296$  Hz; TFA), 125.8 (q,  $^1J_{\text{C-F}} = 285$  Hz), 162.5 (q,  $^2J_{\text{C-F}} = 28$  Hz, TFA), 167.4, 170.7, 175.4 ppm.  $^{19}\text{F}$  NMR ( $\text{CD}_3\text{OD}$ ):  $\delta$  -79.7 (s, 3 F,  $\text{CF}_3$ ), -80.1 (s, TFA salt) ppm. MS (EI):  $m/z$  (%) = 232 ( $[\text{M} + \text{H}]^+$ ).

#### Preparation of Peptide Samples

A $\beta$ 42 was obtained from American Peptide Company, Inc. (Batch #1207090T). Peptide was dissolved at a concentration of 1 mM in a 1% ammoniac solution and then diluted in 10 mM Tris.HCl, 100 mM NaCl (pH 7.4) for ThT and TEM experiments and in 10 mM Tris.HCl, 100 mM NaF (pH 6) for CD and NMR spectroscopy.

#### Aggregation Kinetics Measured by Thioflavin T Fluorescence

The kinetics of fibril formation was measured using the fluorescence intensity increase upon binding of the fluorescent dye ThT to fibrils. A plate reader (Fluostar Optima, BMG labtech) and standard 96-wells flat-bottom black microtiter plates in combination with a 440 nm excitation filter and a 485 nm emission filter were used. For the A $\beta$ 42:inhibitor experiments, the ThT assay was started by adding 5  $\mu\text{L}$  of a 0.2 mM A $\beta$ 42 stock solution and 10  $\mu\text{L}$  of a 1 mM peptide stock solution to a mixture of 10  $\mu\text{M}$  ThT and 10 mM Tris.HCl, 100 mM NaCl at pH 7.4. The concentration of A $\beta$ 42 was held constant at 5  $\mu\text{M}$  and the molecules **1** and **2** were added in equimolar amounts to yield 1:10 molar ratio mixtures. The microtiter plate was shaken for 10 seconds directly after the addition of all components, but not during the measurement. The ThT assays were performed three times, each in triplicate and on different days.

The assessment of inhibition of amyloid peptide aggregation by peptides was determined as followed. Amyloid peptide aggregation assays were performed in the absence and in the presence of molecules and fibril formation was monitored via ThT fluorescence to evaluate each compound's ability to alter both the lag time to aggregate formation ( $t_{1/2}$ ) and the equilibrium plateau indicative of the quantity of aggregate formed ( $F$ ). The extension of the lag time was evidenced as an increase in the experimental lag time in the presence of the molecule relative to the lag time observed without the molecule, and is evaluated as a ratio,  $t_{1/2}(\text{A}\beta + \text{molecule})/t_{1/2}(\text{A}\beta)$ . The reduction of the equilibrium plateau was evidenced as a decrease in the experimental fluorescence plateau with the molecule, relative to the fluorescence plateau observed without the molecule, and is evaluated as the percentage decrease from the experimental fluorescence plateau with the molecule,  $(F_{\text{A}\beta} - F_{\text{A}\beta + \text{molecule}})/F_{\text{A}\beta} \times 100\%$ .

#### Transmission electron microscopy

TEM was performed at the Institut de biologie Intégrative (IFR83) at the University Pierre et Marie Curie. Peptides were dissolved under the same conditions as in the ThT-assay. Aliquots (20  $\mu$ L) of A $\beta$ 42 alone and A $\beta$ 42 in the presence of **1** or **2** were absorbed onto glow-discharged carbon-coated 300-mesh copper grids for 2 min. Grids were then blotted and dried. Next, grids were negatively stained for 45 s on 2.5 % uranyl acetate, and again blotted, and dried. Grids were examined using a ZEISS 912 Omega transmission electron microscope operating at 80 kV.

#### CD Spectroscopy

CD spectra were measured on a Jasco J-815 spectropolarimeter over the wavelength range 190–260 nm, by using 0.1 cm path length quartz cell (internal volume 200  $\mu$ L) from Hellma GmbH. CD spectra were recorded at 25°C every 0.2 nm at a scan rate of 10 nm/min. Spectra were recorded every half or one hour. Measurements were carried out in 10 mM Tris.HCl, 100 mM NaF (pH 6). The concentration of A $\beta$ 42 was held constant at 50  $\mu$ M and the molecules **1** and **2** were added in equimolar amounts to yield 1:10 molar ratio mixtures. Data obtained were then collected and processed using the software Spectra Manager<sup>®</sup>. Following background correction, the CD data were normalized to molar ellipticity per residue. To follow A $\beta$ 42 conformational changes, spectra were recorded at regular intervals and the ellipticity at 220 nm was plotted vs. the time of incubation.

Experimental values were fitted to a Boltzmann sigmoidal equation:

$$\theta_{220} = \frac{\theta_i - \theta_f}{1 + e^{-(t-t_{0.5})/\tau}} + \theta_f \quad \text{with elongation rate } (h^{-1}) = 1/\tau \quad \text{Equation 1}$$

In this equation,  $\theta_i$  and  $\theta_f$  are the initial and final ellipticity values at 220 nm,  $t_{0.5}$  is the time corresponding to 50% of transition conformational and  $\tau$  a time constant. In order to estimate the peptide secondary structure content, an analysis of relevant CD spectra was carried out using the CDFriend software<sup>45</sup>.

#### NMR Experiments

Peptide was dissolved at a concentration of 1 mM in a 1% ammoniac solution, and then diluted at a final concentration of 50  $\mu$ M in a 10 mM TrisHCl, 100 mM NaF (pH 6) buffer, in the presence of 10 % of D<sub>2</sub>O and immediately transferred in a Shigemitsu Tube of 5 mm diameter. Experiments were recorded at 298 K on a Bruker AVANCE III NMR spectrometer operating at a <sup>1</sup>H frequency of 500 MHz, equipped with a TCI cryoprobe. One-dimensional spectra were acquired over 4000 points using a spectral width of 7000 Hz. A cosine bell apodisation function was applied to 1D <sup>1</sup>H experiments. Solvent resonance was suppressed using a Watergate pulse sequence.

For each spectrum, 1024 scans were accumulated leading to an experimental time of about 23 minutes. Peptide <sup>1</sup>H resonances (in the amide/aromatic region between 6.6 and 7.1 ppm) were then integrated and these values are plotted as a function of time (see Figure 3D-F), leading to a

sigmoidal curve for A $\beta$ 42 alone and A $\beta$ 42 in the presence of **1** (Equation 2) and to an exponential curve for A $\beta$ 42 in the presence of **2** (Equation 3).

$$I = I_i + \frac{I_i - I_f}{1 + e^{(t - t_{0.5})/\tau}} \quad \text{Equation 2}$$

$$I = I_i e^{-\frac{x}{b}} \quad \text{with} \quad t_{0.5} = b \ln 2 \quad \text{Equation 3}$$

where  $I$  is peptide signal intensity obtained from 1D  $^1\text{H}$  NMR experiments,  $I_i$  and  $I_f$  are the initial and final  $^1\text{H}$  NMR intensities,  $t_{0.5}$  is the time when the  $^1\text{H}$  NMR intensity reaches 50% of the maximum  $^1\text{H}$  NMR signal.

Since the analysis is done for the integrated intensity of peptide  $^1\text{H}$  resonances between 6.6 and 7.1 ppm, results are therefore average values. All raw NMR experimental data have been processed using the TopSpin program (Bruker) and further analyzed for the integration and the fit using the equations 2 and 3 with a home-written program based on Mathematica 8. The program is available upon request.

For STD experiments, saturation was realized using a cascade of Gaussian shaped selective pulses (50 ms duration,  $B_1$  field of 0.1 kHz) for a total duration of 2 s, applied at -1 and +30 ppm, alternatively. An exponential window function with a line broadening factor of 10 Hz was applied to  $^1\text{H}$  STD experiments prior to Fourier transform.

#### Acknowledgments

We thank Luminita Duma for helping in the NMR fit and for valuable discussion; Julien Pytkowicz for helping in the molecules synthesis; and Géraldine Toutirais (IBPS FRE 3631 - Institut de Biologie Paris-Seine, service de microscopie électronique - Université Pierre et Marie Curie, France) for the electron microscopy.

#### References

1. Selkoe, D.J. *Nature* 2003, 426, 900–904.
2. Kaye, R.; Head, E.; Thompson, J. L.; McIntire, T. M.; Milton, S. C.; Cotman, C. W.; Glabe, C. G. *Science* 2003, 301, 486–489.
3. Vigo-Pelfrey, C.; Lee, D.; Keim, P.; Lieberburg, I.; Schenk, D. B. *J. Neurochem* 1993, 61, 1965–1968.
4. Seubert, P.; Oltsdorf, T.; Lee, M. G.; Barbour, R.; Blomquist, C.; Davis, D. L.; Bryant, K.; Fritz, L. C.; Galasko, D.; Thal, L. J.; Lieberburg, I.; Schenk, D. B. *Nature* 1993, 361, 260–263.
5. Bibl, M.; Mollenhauer, B.; Esselmann, H.; Lewczuk, P.; Trenkwalder, C.; Brechlin, P.; Rütger, E.; Kornhuber, J.; Otto, M.; Wiltfang, J. *J. Neural Transm* 2006, 113, 1771–1778.

6. Jensen, M.; Schröder, J.; Blomberg, M.; Engvall, B.; Pantel, J.; Ida, N.; Basun, H.; Wahlund, L.-O.; Werle, E.; Jauss, M.; Beyreuther, K.; Lannfelt, L.; Hartmann, T. *Ann Neurol* 1999, 45, 504–511.
7. Lue, L.-F.; Kuo, Y.-M.; Roher, A. E.; Brachova, L.; Shen, Y.; Sue, L.; Beach, T.; Kurth, J. H.; Rydel, R. E.; Rogers, J. *Am J Pathol* 1999, 155, 853–862.
8. Dahlgren, K. N.; Manelli, A. M.; Stine, Jr, W. B.; Baker, L. K.; Krafft, G. A.; LaDu, M. J. *J Biol Chem* 2002, 277, 32046–32053.
9. Jan, A.; Adolfsson, O.; Allaman, I.; Buccarello, A. L.; Magistretti, P. J.; Pfeifer, A.; Muhs, A.; Lashuel, H. A. *J Biol Chem* 2011, 286, 8585–8596.
10. Vivekanandan, S.; Brender, J. R.; Lee, S. Y. *Ramamoorthy, A. Biochem Biophys Res Commun* 2011, 312–316.
11. Petkova, A. T.; Yau, W.-M.; Tycko, R. *Biochemistry* 2006, 45, 498–512.
12. Yu, L.; Edalji, R.; Harlan, J. E.; Holzman, T. F.; Lopez, A. P.; Labkovsky, B.; Hillen, H.; Barghorn, S.; Ebert, U.; Richardson, P. L.; Miesbauer, L.; Solomon, L.; Bartley, D.; Walter, K.; Johnson, R. W.; Hajduk, P. J.; Olejniczak, E. T. *Biochemistry* 2009, 48, 1870–1877.
13. Harper, J. D.; Wong, S. S.; Lieber, C. M.; Lansbury, Jr., P. T. *Chem Biol* 1997, 4, 119–125.
14. Jarrett, J. T.; Lansbury, Jr., P. T. *Cell* 1993, 73, 1055–1059.
15. Hardy, J. A.; Higgins, G. A. *Science* 1992, 184–185.
16. Hardy, J.; Selkoe, D. J. *Science* 2002, 353–356.
17. (a) Jan, A.; Adolfsson, O.; Allaman, I.; Buccarello, A.-L.; Magistretti, P. J.; Pfeifer, A.; Muhs, A.; Lashuel, H. A. *J Biol Chem* 2011, 286, 8585–8596. (b) Lau, T.-L.; Ambroggio, E.E.; Tew, D.J.; Cappai, R.; Masters, C.L.; Fidelio, G.D.; Barnham, K.J.; Separovic, F. *J Mol Biol* 2006, 356, 759–770.
18. Engel, M. F. M.; Khemtémourian, L.; Kleijer, C. C.; Meeldijk, H. J.; Jacobs, J.; Verkleij, A. J.; de Kruijff, B.; Killian, J. A.; Höppener, J. W. M. *Proc Natl Acad Sci USA* 2008, 105, 6033–6038.
19. Ladiwala, A. R. A.; Dordick, J. S.; Tessier, P. M. *J Biol Chem* 2011, 286, 3209–3218.
20. (a) Stains, C.I.; Mondal, K.; Ghosh, I. *ChemMedChem* 2007, 2, 1674–1692. (b) Kaffy, J.; Brinet, D Soulier, J.-L.; Khemtémourian, L.; Lequin, O.; Taverna, M.; Crousse, B.; Onger, S. *Eur. J. Med. Chem.* 2014, 86, 752–758. (c) Dorgeret, B.; Khemtémourian, L.; Correia, I.; Soulier, J.-L.; Lequin, O.; Onger, S. *Eur J Med Chem* 2011, 46, 5959–5969.
21. Tjernberg, L. O.; Lilliehöök, C.; Callaway, D. J. E.; Näslund, J.; Hahne, S.; Thyberg, J.; Terenius, L.; Nordstedt, C. *J Biol Chem* 1997, 272, 12601–12605.
22. Lowe, T. L.; Strzelec, A.; Kiessling, L. L.; Murphy, R. M. *Biochemistry* 2001, 40, 7882–7889.
23. Cairo, C. W.; Strzelec, A.; Murphy, R. M.; Kiessling, L. L. *Biochemistry* 2002, 41, 8620–8629.
24. Etienne, M. A.; Aucoin, J. P.; Fu, Y.; McCarley, R. L.; Hammer, R. P. *J Am Chem Soc* 2006, 128, 3522–3523.



25. (a) Frydman-Marom, A.; Rechter, M.; Shefler, I.; Bram, Y.; Shalev, D. E.; Gazit, E. *Angew Chem Int Ed* 2009, 48, 1981–1986. (b) Gilead, S.; Gazit, E. *Angew Chem Int Ed* 2004, 43, 4041–4044.
26. Gordon, D. J.; Sciarretta, K. L.; Meredith, S. C. *Biochemistry* 2001, 40, 8237–8245.
27. Soto, C.; Sigurdsson, E. M.; Morelli, L.; Kumar, R. A.; Castano, E. M.; Frangione, B. *Nat Med* 1998, 4, 822–826.
- 28 (a) Yesuvadian, R.; Krishnamoorthy, J., Ramamoorthy, A.; Bhunia, A. *Biochem Biophys Res Commun* 2014, 447, 590–595. (b) Savelieff, M. G.; Liu, Y.; Senthamarai, R. R. P.; Korshavn, K. J.; Lee, H. J.; Ramamoorthy, A.; Lim, M. H. *Chem Commun* 2014, 50, 5301–5303. (c) Yoo, S.I.; Yang, M.; Brender, J. R.; Subramanian, V.; Sun, K.; Joo, N. E.; Jeong, S.-H.; Ramamoorthy, A.; Kotov, N. A. *Angew Chem Int Ed* 2011, 50, 5110–5115. (d) Choi, J.-S.; Braymer, J. J.; Nanga, R. P.R.; Ramamoorthy, A.; Lim, M. H. *Proc Natl Acad Sci U. S. A.* 2010, 107, 21990–21995.
- 29 (a) Ojima, I., Ed. *Fluorine In Medicinal Chemistry And Chemical Biology*; Wiley-Blackwell: Hoboken, NJ, 2009. (b) Gouverneur, V.; Muller, K., Eds. *Fluorine in Pharmaceutical and Medicinal Chemistry: From Biophysical Aspects to Clinical Applications*; Imperial College Press: London, 2012. (c) Wang, J.; Sanchez-Rosello, M.; Acena, J.-L.; del Pozo, C.; Sorochinsky, A. E.; Fustero, S.; Soloshonok, V. A.; Liu, H. *Chem Rev* 2014, 114, 2432–2506.
30. (a) Salwiczek, M.; Nyakatura, E. K.; Gerling, U. I. M.; Ye, S.; Koksche, B. *Chem Soc Rev* 2012, 41, 2135–2171. (b) Koksche, B.; Sewald, N.; Hofmann, H.-J.; Burger, K.; Jakubke, H.-D. *J Pept Sci* 1997, 3, 157–167. (c) Asante, V.; Mortier, J.; Wolber, G.; Koksche, B. *Amino Acids* 2014, 46, 2733–2744. (d) Meng, H.; Kumar, K. *J Am Chem Soc* 2007, 129, 15615–15622.
31. (a) Molteni, M.; Pesenti, C.; Sani, M.; Volonterio, A.; Zanda, M. *J Fluorine Chem* 2004, 125, 1335–1743. (b) Zanda, M. *New J Chem* 2004, 28, 1401–1411. (c) Feytens, D.; Chaume, G.; Chassaing, G.; Lavielle, S.; Brigaud, T.; Byun, B. J.; Kang, Y. K.; Miclet, E. *J Phys Chem B* 2012, 116, 4069–4079.
32. (a) Kubyskin, V. S.; Komarov, I. V.; Afonin, S.; Mykhailiuk, P. K.; Grage, S. L.; Ulrich, A. S. in *Fluorine in Pharmaceutical and Medicinal Chemistry: From Biophysical Aspects to Clinical Applications*. V. Gouverneur; K. Muller Eds.; Imperial College Press, London, 2012, p. 91–139. (b) Vulpetti, A., Dalvit C. *Drug Discovery Today* 2012, 17, 890–897. (c) Dalvit, C.; Ardini, E.; Fogliatto, G. P.; Mongelli, N.; Veronesi, M. *Drug Discovery Today* 2004, 9, 595–602.
- 33.(a) Suzuki, Y.; Brender, J. R.; Hartman, K.; Ramamoorthy, A.; Marsh, E. N. G. *Biochemistry* 2012, 51, 8154–8162. (b) Suzuki, Y.; Brender, J. R.; Soper, M. T.; Krishnamoorthy, J.; Zhou, Y.; Ruotolo, B. T.; Kotov, N. A.; Ramamoorthy, A.; Marsh, E. N. G. *Biochemistry* 2013, 52, 1903–1912.
34. (a) Huguenot, F.; Brigaud, T. *J Org Chem* 2006, 71, 7075–7078. (b) Chaume, G.; Lensen, N.; Caupène, N.; Brigaud, T. *Eur J Org Chem* 2009, 5717–5724. (c) Chaume, G.; Van Severen, M. C.; Marinkovic, S.; Brigaud, T. *Org Lett* 2006, 8, 6123–6126. (d) Caupène, C.; Chaume, G.; Ricard, L.; Brigaud, T. *Org Lett* 2009, 11, 209–212.

35. Jlalia, I.; Lensen, N.; Chaume, G.; Dzhambazova, E.; Astasidi, L.; Hadjiolova, R.; Bocheva, A.; Brigaud, T. *Eur J Med Chem* 2013, 62, 122–129.
36. Le Vine 3<sup>rd</sup>, H. *Methods Enzymol* 1999, 309, 274-284.
37. Bartolini, M.; Bertucci, C.; Bolognesi, M.L.; Cavalli, A.; Melchiorre, C.; Andrisano, V. 2007. *ChemBioChem* 2007, 8, 2152–2161.
38. Caillon, L.; Lequin, O.; Khemtemourian, L. *Biochem Biophys Acta* 2013, 1828, 2091–2098.
39. Caillon, L.; Duma, L., Lequin, O.; Khemtemourian, L. *Mol Membr Biol* 2015, 7-8, 239–249.
40. Meyer, B.; Peters, T. *Angew Chem Int Ed* 2003, 42, 864–890.
41. (a) Torok, B.; Dasgupta, S.; Torok, M. *Current Bioact. Comp.* 2008, 4, 159-174. (b) Torok, B.; Sood, A.; Bag, S.; Kulkarni, A.; Borkin, D.; Lawler, E.; Dasgupta, S.; Landge, S.; Abid, M.; Zhou, W.; Foster, M.; LeVine III, H.; Torok, M. *ChemMedChem* 2012, 7, 910–919.
42. For a review see : Salwiczek, M., Nyakatura, E. K.; Gerling, U. I. M.; Ye, S. Kocsch, B. *Chem Soc Rev* 2012, 41, 2135–2171.
43. Gerling, U. I. M.; Salwiczek, M.; Cadicamo, C. D.; Erdbrink, H.; Czekelius, C.; Grage, S. L.; Wadhwani, P.; Ulrich, A. S.; Behrends, M.; Haufe, G.; Kocsch, B. *Chem Sci* 2014, 5, 819–830.
44. Loureiro, J. A.; Crespo, R.; Börner, H.; Martins, P. M.; Rocha, F. A.; Coelho, M.; Pereira, M. C.; Rocha, S. J. *Mater Chem B* 2014, 2, 2259–2264.
45. Khemtemourian, L.; Buchoux, S.; Aussenac, F.; Dufourc, E. J. *Eur Biophys* 2007, 36, 107-112.

**Figures caption**

**FIGURE 1.** (A) Structure of the peptide **1** H-Ala-Aib-Leu-OH; (B) structure of the peptide **2** H-Ala-(R)-Tfm-Ala-Leu-OH; (C) Amino acid sequence of A $\beta$ 42.

**FIGURE 2.** (A) Inhibition of A $\beta$ 42 fibril formation by the compounds. The kinetics of A $\beta$ 42 (10  $\mu$ M) fibril formation in the absence (black) or in the presence of **1** (blue) or **2** (orange) as assessed by ThT fluorescence in 10 mM Tris.HCl 100 mM NaCl (pH 7.4) over the course of 50 h. ThT traces are shown for molecules **1** and **2** (dash grey). (B) Ratio of half-life times of A $\beta$ 42 fibril formation in the presence of **1** or **2** or alone and percentage of the plateau intensity decrease (See supporting information for the calculation). TEM images obtained by negative staining of A $\beta$ 42 at 5  $\mu$ M after 22 h of incubation, alone (C), in the presence of **1** (D) and in the presence of **2** (E).

**FIGURE 3.** CD spectra of (A) A $\beta$ 42 alone, (B) A $\beta$ 42 in the presence of **1** and (C) A $\beta$ 42 in the presence of **2** obtained immediately after the addition of the molecule and after few hours of incubation. (D) Kinetic parameters (lag time,  $t_{1/2}$  and equilibration time) of A $\beta$ 42  $\beta$ -sheet formation in the absence and in the presence of the molecules determined using the time course of absolute CD ellipticity at 220 nm. (E) Calculated secondary structure contents of A $\beta$ 42 in the absence and in the presence of molecules **1** or **2**. Deconvolution of CD spectra was accomplished using CDFriend software (see Materials and Methods).

**FIGURE 4.**  $^1\text{H}$  NMR spectra of A $\beta$ 42 (A), A $\beta$ 42:**1** (1:10) (B) and A $\beta$ 42:**2** (1:10) (C) over time. Purple: 0h, Blue: 2h40, Green: 5h20, Orange: 8h, Red: 10h20. Peaks belonging to **1** and **2** are indicated by \* label on the relevant spectrum. Time course of normalized integrals of NMR signal between 6.6 and 7.1 ppm of A $\beta$ 42 (D), A $\beta$ 42:**1** (1:10) (E) and A $\beta$ 42:**2** (1:10) (F) over time.

**FIGURE 5.** 1D  $^1\text{H}$  STD spectra of A $\beta$ 42:**1** (1:10) (left) and A $\beta$ 42:**2** (1:10) (right). A and C are reference spectra, mostly showing the signals of tripeptide **1** and **2** respectively (A : 0.8 ppm, 1.2-1.6 ppm; C : 0.8 ppm, 1.2 ppm, 1.4 ppm, 1.6 ppm). B and D are the resulting spectra of saturation transfer difference spectra for molecules **1** and **2** respectively. B shows almost no signal with weak dispersion peaks at 0.8 and 1.4 ppm and D shows the presence of STD signals with strong positive peaks at 0.8 and 1.2 ppm.

FIGURE 1.

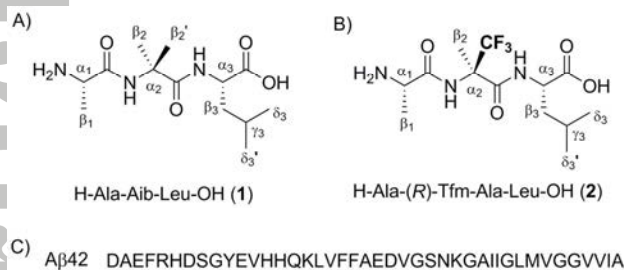


FIGURE 2.

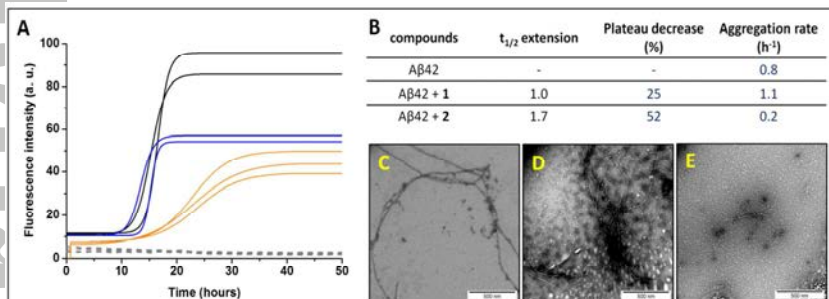


FIGURE 3.

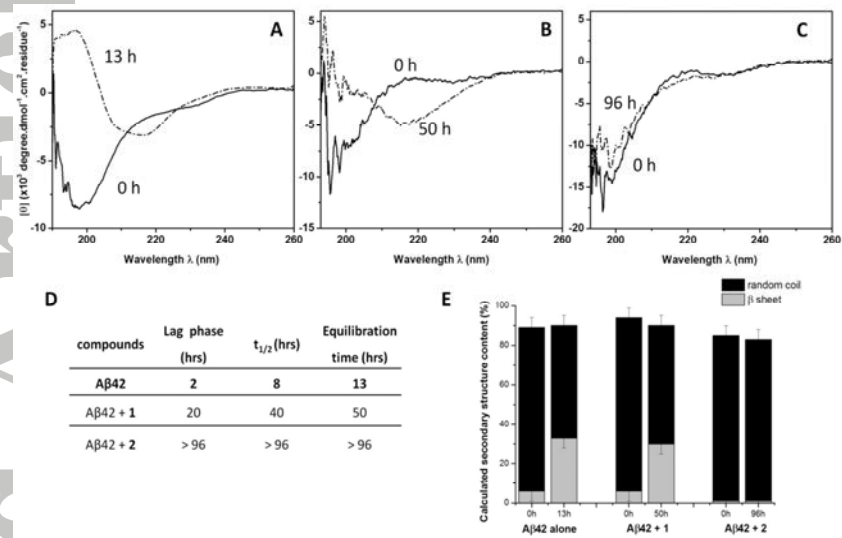


FIGURE 4

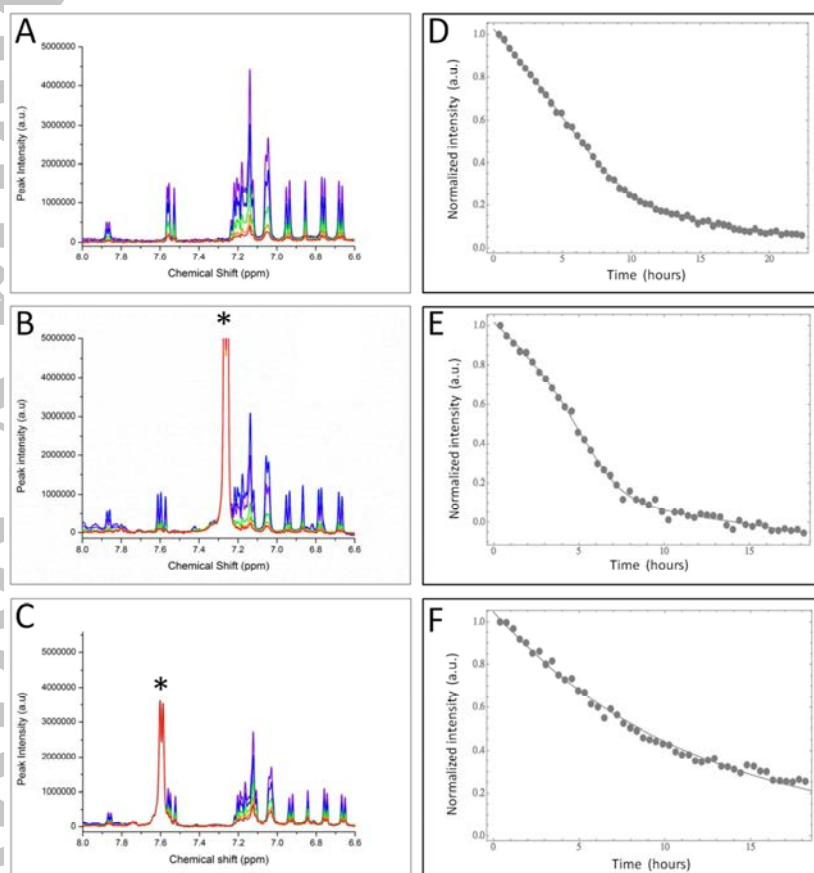
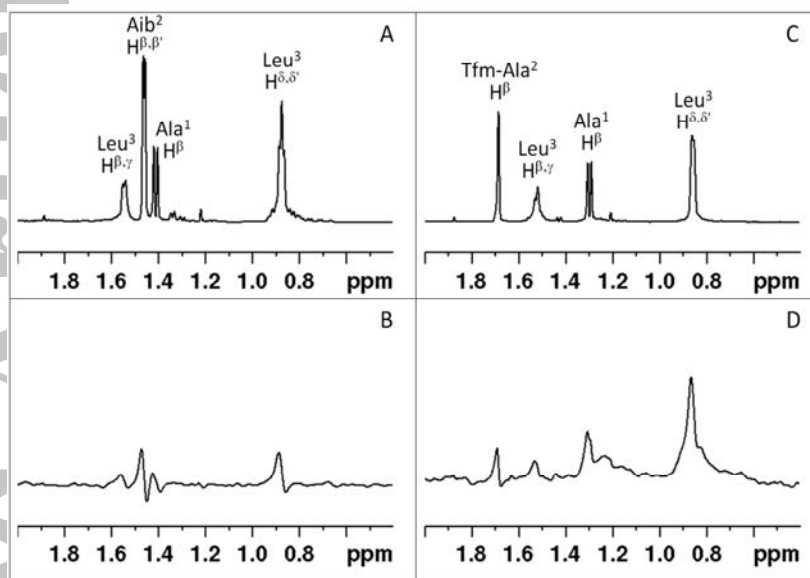


FIGURE 5





## Small glycopeptidomimetics inhibit protein-protein interactions mediating amyloid $\beta$ -peptide oligomerization and fibrillization

Julia Kaffy<sup>1</sup>, Dimitri Brinet<sup>1,2</sup>, Jean-Louis Soulier<sup>1</sup>, Isabelle Correia<sup>3</sup>, Nicolo Tonali<sup>1</sup>, Katia Fabiana Fera<sup>1</sup>, Yasmine Iacone<sup>1,2</sup>, Anaïs R. F. Hofmann<sup>3</sup>, Lucie Khemtémourian<sup>3</sup>, Benoit Crousse<sup>1</sup>, Mark Taylor<sup>4</sup>, David Allsop<sup>4</sup>, Myriam Taverna,<sup>2</sup> Olivier Lequin<sup>3</sup>, Sandrine Onger<sup>1\*</sup>

<sup>1</sup>Molécules Fluorées et Chimie Médicinale, BioCIS UMR-CNRS 8076, LabEx LERMIT, Université Paris-Sud, Faculté de Pharmacie, 5 rue Jean-Baptiste Clément, 92296 Châtenay-Malabry Cedex, France

<sup>2</sup>Protéines et Nanotechnologies en Sciences Séparatives, Institut Galien de Paris Sud, UMR-CNRS 8612, Université Paris-Sud, Faculté de Pharmacie, 5 rue Jean-Baptiste Clément, 92296 Châtenay-Malabry Cedex, France

<sup>3</sup>Sorbonne Universités - UPMC Univ Paris 06, Ecole Normale Supérieure - PSL Research University, CNRS UMR 7203 LBM, 4 place Jussieu, 75252 Paris Cedex 05, France

<sup>4</sup>Lancaster University, Division of Biomedical and Life Sciences, Faculty of Health and Medicine, Lancaster LA1 4YQ, UK

Email: Sandrine.onger@u-psud.fr

**ABSTRACT:** Drugs have failed to slow the progression of Alzheimer's disease, which affects more than 35 million people worldwide. How drug candidates that reduce fibril formation interact with the most neurotoxic forms of amyloid peptide  $A\beta_{1-42}$  is unknown. We report herein the capacity of small and hydrosoluble sugar-based peptidomimetic analogs to inhibit both  $A\beta_{1-42}$  early oligomerization and fibrillization. A wide range of bio- and physico-chemical techniques, such as innovative capillary electrophoresis, nuclear magnetic resonance, and surface plasmon resonance, was used in order to identify the  $A\beta_{1-42}$  species targeted by the synthesized peptidomimetic compounds. We clearly demonstrate that these molecules rationally designed and having physicochemical properties for drug-likeness can delay the aggregation of  $A\beta_{1-42}$  by interacting with soluble oligomers in order to prevent the further fibrillization and to maintain the presence of non-toxic monomers. Furthermore, these compounds suppress totally the toxicity of  $A\beta_{1-42}$  towards SH-SY5Y human neuroblastoma cells, even at sub-stoichiometric concentrations.

**KEYWORDS:** amyloid  $\beta$ -peptide, Alzheimer's disease, peptidomimetics, glycopeptides, aggregation, oligomers, capillary electrophoresis, nuclear magnetic resonance, surface plasmon resonance.

### Introduction

Protein-protein interactions mediating protein aggregation concern at least 30 different proteins and are associated with more than 20 serious human diseases, including Alzheimer's (AD), Parkinson's disease and type 2 diabetes mellitus. The accumulation of extra- or intracellular protein deposits, often referred to as amyloid, characterize these protein misfolding diseases. AD, which is the most common form of late-life dementia,<sup>1</sup> is associated with accumulation of intraneuronal neurofibrillary tangles and extracellular 'senile' plaques containing insoluble fibrils composed of 40 or 42-residue amyloid- $\beta$  peptides ( $A\beta_{1-40}$  or  $A\beta_{1-42}$ ).<sup>2</sup> Monomeric  $A\beta$  peptides convert into fibrils through a complex nucleation process involving the formation of various aggregated species such as soluble oligomers and protofibrils of increasing size.<sup>3-5</sup> Structural studies have reported that oligomeric and fibrillar species share a  $\beta$ -sheet rich conformation,<sup>6-10</sup> however the structure of the different oligomeric species is far from being understood. Although  $A\beta_{1-42}$  is not the most abundant amyloid peptide produced *in vivo*, it is the major constituent of amyloid plaques and is far more aggregative and neurotoxic than  $A\beta_{1-40}$ .<sup>11,12</sup> Experimental evidence supports the hypothesis that low molecular weight oligomers are primarily responsible for the neurodegeneration observed in AD.<sup>2,11,13-16</sup> However, the role of fibrils should not be neglected, because they have been demonstrated not to be inert species, but are able to generate damaging redox activity and promote the nucleation of toxic oligomers.<sup>17,18</sup>

Hence it remains crucial to develop inhibitors that can reduce the prevalence of small transient oligomers and also prevent the formation of fibrils. Numerous compounds have been reported as inhibitors or modulators of  $A\beta_{1-42}$  aggregation. The main drawbacks of the described molecules that jeopardize their development as drug candidates are: a lack of binding selectivity leading to a high risk for various side-effects for dyes or polyphenol natural products<sup>19</sup>; poor bioavailability and high propensity to self-aggregate for peptide derivatives<sup>20,21</sup>; and a general lack of information regarding their mechanism of action, and in particular on their effects on toxic oligomer formation.<sup>19-21</sup> To our knowledge, rationally designed small and 'druggable' pseudo- or non-peptidic aggregation inhibitors have been very scarcely reported.<sup>22,23</sup> Some of us have described retro-inverso peptide inhibitors of both early oligomerization and fibrillization.<sup>22</sup>

We previously reported a novel class of glycopeptide derivatives, based on two hydrophobic dipeptides (Ala-Val and Val-Leu) linked to a hydrophilic D-glucopyranosyl scaffold through aminoalkyl and carboxyethyl linkers in C1 and C6 positions, respectively (compound **1**, Figure 1).<sup>24</sup> These pentapeptide analogs were shown to modulate  $A\beta_{1-40}$  and  $A\beta_{1-42}$  aggregation, as demonstrated by fluorescence Thioflavin-T (ThT) assays and transmission electron microscopy (TEM).<sup>24</sup> The flexible and hydrophilic sugar moiety is believed to act as a  $\beta$ -sheet breaker, playing a major role in preventing the interactions between  $A\beta$  species and thus inhibiting the aggregation. The introduction of a

carbohydrate in peptides can also have a multifaceted impact on the properties of these molecules, such as modulating the hydrophilicity/hydrophobicity balance and conferring resistance to proteolytic cleavage.<sup>25</sup>

In order to further decrease the number of potential sites for proteolytic attack, we have now introduced peptidomimetics in the upper arm in the C6 position. A wide range of bio- and physico-chemical techniques was then used in order to evaluate the activity of the synthesized small hydrosoluble peptidomimetic compounds on the early oligomerization, fibrillization and toxicity of A $\beta$ <sub>1-42</sub> and also to identify the A $\beta$ <sub>1-42</sub> species targeted by these molecules.

## Results

### Design

As we have already demonstrated the superiority of the  $\beta$  configuration of the C1 anomeric carbon in our previously reported glycopeptides,<sup>24b</sup> we decided in a first attempt to evaluate the mixture of  $\alpha$  and  $\beta$  anomers, to avoid a difficult separation of the two anomers. Furthermore, as we have also clearly demonstrated the superiority of the amino propoxy link relative to the amino ethoxy link, in the C1 position of the sugar moiety,<sup>24b</sup> we decided to prepare glycopeptidomimetics bearing the amino propoxy link. For the design of the peptidomimetic strands, we chose to replace the C-terminal leucine (Leu5 in compound **1**, Figure 1) by the 5-amino-2-methoxybenzhydrazide unit (compounds **2** and **3**, Figure 1), which is a part of the  $\beta$ -strand mimic ("Hao" unit) reported by Nowick and co-workers.<sup>21,26</sup> The introduction of a 5-amino-2-methoxybenzhydrazide unit into  $\beta$ -strand mimics was shown, by some of us, to be extremely effective in the prevention of protein-protein interactions involving intermolecular  $\beta$ -sheets of HIV-1 protease in order to inhibit its dimerization, while increasing the proteolytic stability of the molecules.<sup>27</sup> In a first generation, the valine residue (Val4 in compound **1**, Figure 1) was kept and linked to the 5-amino-2-methoxybenzhydrazide unit (compound **2**, Figure 1). Next, the valine residue was replaced by a lysine residue, to further provide these molecules with the possibility of engaging in electrostatic interactions with A $\beta$ <sub>1-42</sub>, in order to increase their affinity for A $\beta$ <sub>1-42</sub> (compound **3**, Figure 1).

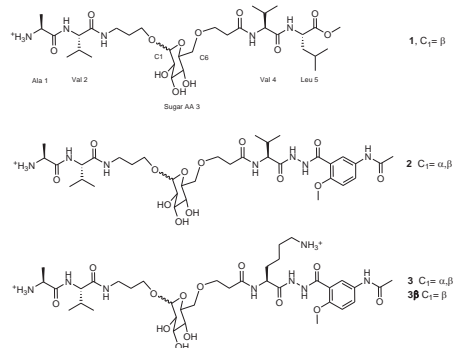


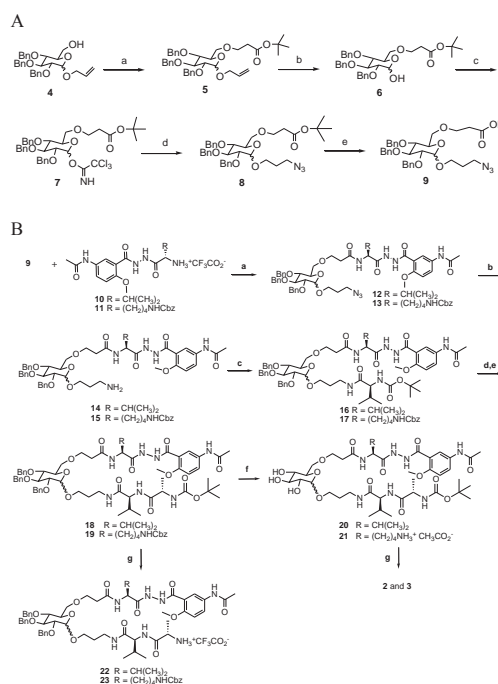
**Figure 1.** Structure of glycopeptidomimetic derivatives **1-3**

### Synthesis of the glycopeptidomimetics.

A short and robust synthesis of the intermediate **9** was developed (Figure 2A). We started from the C1 allylic protected D-glucose

which was transformed into **4** following the procedure described in the literature.<sup>28</sup> The Michael addition of **4** on *tert*-butylacrylate was performed to give **5**. The allyl group of **5** was then removed from the C<sub>1</sub> hydroxyl group with PdCl<sub>2</sub> to give compound **6** in good yield. The anomeric hydroxyl of **6** was converted into the trichloroacetimidate intermediate **7**, in the presence of trichloroacetonitrile and using NaH as a base. The nucleophilic substitution reaction by 3-azidopropan-1-ol was then carried out in the presence of AuCl (10%) affording **8** in good yield. The  $\alpha$  and  $\beta$  epimers **8** were obtained in equal proportion and could not be separated at this stage. The *tert*-butyl group was finally cleaved in acidic conditions to give the carboxylic acid **9**.

The scaffold **9** was then coupled with the peptidomimetic arms **10** and **11** prepared according to our published procedure<sup>27</sup>, using DMTMM<sup>29</sup> as coupling agent (Figure 2B). Compounds **12** and **13** were obtained in good yield. The azido group of **12** and **13** was then reduced via a Staudinger reaction<sup>30</sup> to give the corresponding amines, **14** and **15** in satisfactory yields. In order to build the peptic arm in C1, the two amino acids *N*-Boc-L-Val-OH and *N*-Boc-L-Ala-OH were successively coupled by a standard coupling/deprotection protocol to afford **18** and **19** from **14** and **15** respectively, in good yields. Hydrogenolysis of **18** and **19** afforded **20** and **21**, which underwent an acidic cleavage of the *tert*-butyl carbamate to give **2** and **3**. The acidic cleavage of the *tert*-butyl carbamate was also performed on benzylated compounds **18** and **19** to afford **22** and **23**. All the desired compounds were obtained as a mixture of  $\alpha$  and  $\beta$  anomers. The  $\beta$  anomer **3 $\beta$**  was isolated after separation by HPLC.



2

**Figure 2. Synthesis of glycopeptidomimetics.** A- Synthesis of the scaffold **9**. Reagents and conditions: a) *tert*-butyl acrylate, TBAB, 20% NaOH aq., rt, 24h, 79%; b) PdCl<sub>2</sub>, CH<sub>3</sub>OH/EtOH, N<sub>2</sub> atm. rt, overnight 75%; c) CCl<sub>4</sub>/CN, NaH, CH<sub>2</sub>Cl<sub>2</sub>, rt, overnight, 75%; d) 3-azidopropan-1-ol, AuCl (10% w/w), CH<sub>2</sub>Cl<sub>2</sub>, N<sub>2</sub> atm., rt, 2 days, 82%; e) TFA, CH<sub>2</sub>Cl<sub>2</sub>, rt, overnight, 72%. B- Synthesis of glycopeptidomimetics **2** and **3**. Reagents and conditions: a) NMM, DMTMM, DMF, rt, overnight, 86% (**12**), 68% (**13**); b) Ph<sub>3</sub>P, THF/H<sub>2</sub>O (9:1), 40 °C, 24h, 63% (**14**), 50% (**15**); c) *N*-Boc-L-Val-OH, NMM, DMTMM, DMF, rt, overnight, 79% (**16**), 68% (**17**); d) TFA, CH<sub>2</sub>Cl<sub>2</sub>, rt, 3h, quantitative; e) *N*-Boc-L-Ala-OH, NMM, DMTMM, rt, overnight, 68% (**18**), 73% (**19**); f) H<sub>2</sub> Pd/C, rt, MeOH, 48h, 88% (**20**); 75% (**21**); g) TFA, CH<sub>2</sub>Cl<sub>2</sub>, rt, 3h, quantitative.

#### Inhibition of A $\beta$ <sub>1-42</sub> fibrillization by glycopeptidomimetics ThT-fluorescence assays

The ability of compounds **1-3** and of intermediates **19-23** to inhibit the fibrillization of A $\beta$ <sub>1-42</sub> was studied by ThT fluorescence spectroscopy.<sup>31</sup> The fluorescence curve for A $\beta$ <sub>1-42</sub> at a concentration of 10  $\mu$ M followed the typical sigmoidal pattern with a lag phase of 8–9 h followed by an elongation phase and a final plateau reached after 17–18 h (purple curve, figure 3A). Two parameters were derived from the ThT curves of A $\beta$ <sub>1-42</sub> alone and A $\beta$ <sub>1-42</sub> in the presence of the evaluated compound: (1)  $t_{1/2}$ , which is defined as the time at which the half maximal ThT fluorescence is observed and gives insight on the rate of the aggregation process; (2) F, the fluorescence intensity at the plateau which is assumed to be dependent on the amount of fibrillar material formed (Table 1, Figures 3A-C).

**Table 1. Effects of compounds 1, 2, 3, 3 $\beta$ , 20 and 21 on A $\beta$ <sub>1-42</sub> fibrillization assessed by ThT-fluorescence spectroscopy at a compound/ A $\beta$ <sub>1-42</sub> ratio of 10/1 and 1/1 (the concentration of A $\beta$ <sub>1-42</sub> in this assay is 10  $\mu$ M). The effect of **3** and **3 $\beta$**  at a compound/A $\beta$  ratio of 0.1/1 is also reported.**

Compounds (Compound/A $\beta$ ratio)	$t_{1/2}$ increase (%) <sup>[a]</sup>	Plateau decrease <sup>[b]</sup>
<b>1</b> 10/1	280 $\pm$ 70	-56 $\pm$ 9 %
<b>1</b> 1/1	ne	ne
<b>2</b> 10/1	325 $\pm$ 12	-31 $\pm$ 7%
<b>2</b> 1/1	155 $\pm$ 10	ne
<b>3</b> 10/1	NA	-87 $\pm$ 1%
<b>3</b> 1/1	148 $\pm$ 12	-29 $\pm$ 9%
<b>3</b> 0.1/1	ne	-23 $\pm$ 6%
<b>3<math>\beta</math></b> 10/1	NA	-90 $\pm$ 2%
<b>3<math>\beta</math></b> 1/1	165 $\pm$ 11	-34 $\pm$ 7%
<b>3<math>\beta</math></b> 0.1/1	129 $\pm$ 12	-16 $\pm$ 6%
<b>20</b> 10/1	379 $\pm$ 15	-41 $\pm$ 22%
<b>20</b> 1/1	138 $\pm$ 10	ne
<b>21</b> 10/1	NA	-84 $\pm$ 3%
<b>21</b> 1/1	154 $\pm$ 8	-26 $\pm$ 6%

ne = no effect, NA = no aggregation, parameters are expressed as mean  $\pm$  SE, n=3-6. [a] See supporting information for the calculation of the  $t_{1/2}$  extension/reduction. A compound displaying a  $t_{1/2}$  extension/reduction > 100 is a delayer of aggregation. [b] See supporting information for the calculation of the plateau decrease.

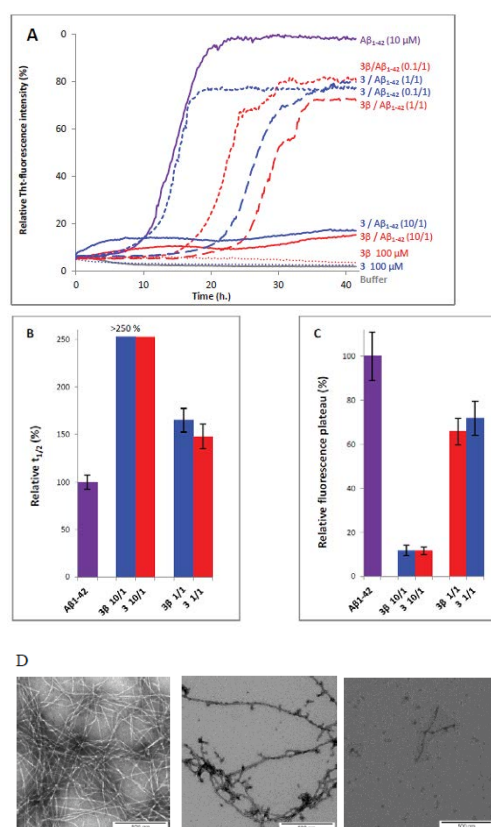


**Figure 3. Effects of derivatives 3 and 3 $\beta$  on the fibrillization kinetics of A $\beta$ <sub>1-42</sub> monitored by Thioflavin-T fluorescence and TEM.** A) Representative curves of ThT fluorescence assays over time showing A $\beta$ <sub>1-42</sub> (10  $\mu$ M) aggregation in the absence (purple curve) and in the presence of compounds **3** (blue curves) and **3 $\beta$**  (red curves) at compound/A $\beta$ <sub>1-42</sub> ratios of 10/1, 1/1 and 0.1/1. B)  $t_{1/2}$  extension relative to A $\beta$ <sub>1-42</sub> alone, in the presence of compounds **3** (blue curves) and **3 $\beta$**  (red curves) at compound/A $\beta$ <sub>1-42</sub> ratios of 10/1 and 1/1. C) Fluorescence plateau decrease relative to A $\beta$ <sub>1-42</sub> alone, in the presence of compounds **3** (blue curves) and **3 $\beta$**  (red curves). D) Effects of derivative **3** on the fibril formation of A $\beta$ <sub>1-42</sub> visualized by TEM. Negatively stained images were recorded after 42 h of incubation of A $\beta$ <sub>1-42</sub> (10  $\mu$ M in 10 mM Tris.HCl, 100 mM NaCl at pH = 7.4) alone (left) or in the presence of 10  $\mu$ M of **3** (middle) and of 100  $\mu$ M of **3** (right). Scale bars, 500 nm

The glycopeptidomimetic molecules **2** and **3** were dramatically more efficient inhibitors of A $\beta$ <sub>1-42</sub> aggregation than the glycopeptide compound **1** in particular at lower compound/ A $\beta$ <sub>1-42</sub> ratios of 1/1 and even 0.1/1. It is noteworthy that a lysine residue attached to the 5-amino-2-methoxybenzhydrazide unit was highly beneficial for the activity compared to a valine residue (compare **3** vs **2** and **21** vs **20**). The free amine of the lysine residue side chain is thus beneficial for the activity. However, no dramatic effect of the

3

N-terminal free amine of the dipeptide Val-Ala chain was observed in both lysine and valine series. Indeed, a similar activity was obtained for the free amine **3** and the Boc protected **21** from one hand and for the free amine **2** and the Boc protected **20** on the other hand. It was also remarkable that the  $\beta$  anomer **3 $\beta$**  showed a superior activity to the mixture of  $\alpha$  and  $\beta$  anomers in **3** at low compound/ $A\beta_{1-42}$  ratios (1/1 and 0.1/1, Table 1 and Figure 3A-C). As also observed in our previous glycopeptides series<sup>24b</sup>, benzylated derivatives **19**, and **22-23** tended to self-aggregate and to slightly accelerate the aggregation process (Table 3S and Figure 1S in supporting information), confirming that polar hydroxyl groups of the sugar moiety were essential to prevent the aggregation.

#### TEM experiments

Transmission electron microscopy (TEM) analyses were performed on compound **3** that showed the most significant effect on  $A\beta_{1-42}$  aggregation in the ThT-fluorescence assays. Images were recorded after 42 h of preincubation, corresponding to maximum aggregation in the ThT assays, with and without **3** (Figure 3D). Differences were observed regarding the amount of aggregates formed in the presence of **3** at both ratios. A very dense network of fibers displaying a typical morphology was observed for  $A\beta_{1-42}$  alone. Only few scattered, very short and scarce fibers were visible on the grid containing the  $A\beta$  sample incubated with **3** at 10/1 ratio. This result validated the ThT-fluorescence data, indicating that compound **3** dramatically slowed down the aggregation of  $A\beta_{1-42}$  (at a **3**/ $A\beta_{1-42}$  ratio of 10/1) and efficiently reduced the amount of typical amyloid fibrils formed. It is noteworthy that even if at a **3**/ $A\beta_{1-42}$  ratio of 1/1 the fluorescence was not dramatically decreased in the ThT assays, but the morphology of the network observed by TEM was very different and less dense and the sample contained some globular aggregates.

#### Inhibition of $A\beta_{1-42}$ oligomerization by glycopeptidomimetics Capillary electrophoresis

In order to determine their effect on small soluble oligomer formation, **3** and **3 $\beta$**  were studied by Capillary Electrophoresis (CE). We recently proposed an improved CE method to monitor easily over time the very early steps of the  $A\beta_{1-42}$  oligomerization process.<sup>32,24b</sup> This technique has the advantage of being able to follow three kinds of soluble species, (i) the monomer (peak ES), (ii) different small metastable oligomers grouped under peak ES' and (iii) transient species formed later and which correspond to species larger than dodecamers (peak LS). Aggregation kinetics of  $A\beta_{1-42}$  alone showed that over time, the monomer ES peak decreased in favor of the oligomer peaks ES' and LS, and of insoluble species, forming spikes in the profile (Figure 2S in supporting information for the detailed kinetics). At time 0, the monomer peak ES was almost the only visible species, while after 12 h, only a small monomer peak remained and many insoluble aggregates, giving spikes, were present (Figure 4A).

In the presence of **3 $\beta$**  (**3 $\beta$** / $A\beta_{1-42}$  ratio of 1/1), the electrophoretic profile clearly indicated that the kinetics of oligomerization was significantly slowed down. Indeed, **3 $\beta$**  maintained dramatically the presence of the monomer (peak ES). In addition, the large oligomer species grouped under the peak LS were still present at 12 h while they completely disappeared in the control electrophoretic profile (figure 4B, and Figure 3S in supporting information for the detailed kinetics). The preservation of the monomer was statistically significant, after 12 h, only 19% remained in the

control experiment while 52% remained in the presence of **3 $\beta$**  (Figure 4C). Similar results were observed with the mixture of  $\alpha$  and  $\beta$  anomers in **3**, however a slightly superior effect was observed for **3 $\beta$**  (41% of monomer species remained after 12 h in the presence of the mixture **3**) (Figures 4S and 5S in supporting information).

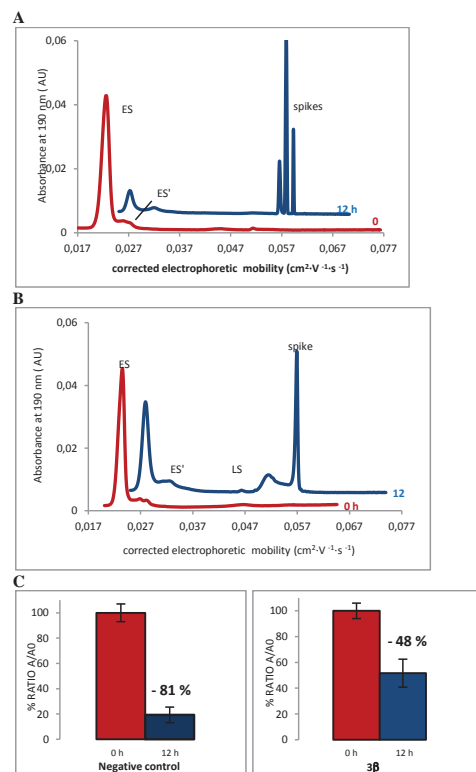


**Figure 4.** Effect of **3 $\beta$**  on the early oligomerization steps by CE. Electrophoretic profile of  $A\beta_{1-42}$  peptide (100  $\mu$ M) obtained immediately (0 h), and 12 h after sample reconstitution (t0) alone (A) and in the presence of compound **3 $\beta$**  at compound/ $A\beta_{1-42}$  ratio of 1/1 (B). Results in panel C show the effect of **3 $\beta$**  on the monomer ES (C). Results are a mean of 3 experiments.

#### Interaction of **3 $\beta$** with oligomeric species of $A\beta_{1-42}$

##### NMR experiments

The goal of the NMR experiments was to study if compound **3 $\beta$**  was able to adopt any preferred conformation in solution and if it interacted in solution either with the monomeric species or with soluble aggregated forms of  $A\beta_{1-42}$ .

We first examined mixtures of  $A\beta_{1-42}$  and **3 $\beta$**  at a temperature of 5°C and using low concentrations of  $A\beta_{1-42}$  (10–90  $\mu$ M) to ensure that  $A\beta_{1-42}$  was mainly monomeric in freshly prepared samples.<sup>34</sup> The 2D  $^1\text{H}$ - $^{15}\text{N}$  and 2D  $^1\text{H}$ - $^{13}\text{C}$  HSQC spectra of 10  $\mu$ M  $^{15}\text{N}$ ,  $^{13}\text{C}$ -

labelled  $A\beta_{1-42}$ <sup>35</sup> recorded in the absence and in the presence of a large excess of **3** $\beta$  (0.4 mM) displayed no significant chemical shift perturbations of  $A\beta_{1-42}$   $^1H$ - $^{15}N$  and  $^1H$ - $^{13}C$  correlations (Figure 6S in supporting information). Similarly, no chemical shift differences could be detected for the  $^1H$  signals of **3** $\beta$  in 1D  $^1H$  and 2D  $^1H$ - $^1H$  experiments (data not shown), even when higher concentrations of  $A\beta_{1-42}$  were used (up to 90  $\mu M$ ). Thus our NMR experiments demonstrated that **3** $\beta$  did not interact with monomeric  $A\beta_{1-42}$  peptide.

We then turned to magnetization transfer experiments that are commonly used to detect the binding of small ligands to large molecular weight species. Saturation Transfer Difference (STD) experiments were recorded to characterize binding properties and map binding epitopes of **3** $\beta$ .<sup>24a,35</sup> No STD signals could be detected in a control experiment with **3** $\beta$  alone, as expected for a low molecular weight molecule that did not aggregate in solution. The addition of  $A\beta_{1-42}$  peptide led to the apparition of weak STD signals (Figure 5). Interestingly, an increase in the STD signal was observed over time, reaching a maximum after 2.5 weeks. Concomitantly, a slow decay of the 1D  $^1H$  NMR signals of  $A\beta_{1-42}$  was observed (Figure 7S in supporting information), corresponding to the formation of high molecular weight  $A\beta_{1-42}$  aggregates that were too large to be observed by solution NMR spectroscopy.<sup>33</sup> Thus the gradual increase of the STD signal over several weeks could be explained by the slow conversion of monomeric  $A\beta_{1-42}$  to aggregated species that bind **3** $\beta$ . The STD signals were the strongest for the aromatic and methyl resonances of **3** $\beta$ , suggesting that the hydrophobic groups of the dipeptide and peptidomimetic strands were directly involved in the interaction with  $A\beta_{1-42}$  species.

WaterLOGSY experiments also enabled us to detect the binding of **3** $\beta$  to  $A\beta_{1-42}$  species, through intermolecular magnetization transfers involving bulk water. The protons of **3** $\beta$  exhibited positive NOEs in the absence of  $A\beta_{1-42}$  (Figure 8S in supporting information), as expected for a small molecule. The addition of  $A\beta_{1-42}$  caused a decrease of positive NOEs and a change of sign of the NOEs that became more negative over time, confirming that **3** $\beta$  binds to high molecular weight species in fast exchange on the NMR time scale.

Finally, NMR spectroscopy was used to analyze the structure of **3** $\beta$  in the free and bound forms. The 1D  $^1H$  NMR spectra of **3** $\beta$  alone were characterized by sharp line widths and concentration-independent chemical shifts (0.04–2 mM range), demonstrating that **3** $\beta$  was highly soluble and not prone to aggregation in the (sub) millimolar range. Chemical shifts, vicinal coupling constants and ROEs analysis showed that the peptidic/pseudopeptidic arms and the aminoalkyl and carboxyethyl linkers were highly flexible, as supported by small diastereotopic splitting of methylenic protons, averaged vicinal coupling constants (Table S1), intraresidual and sequential ROE intensities, and the absence of long-range ROEs. Furthermore the amide protons exhibited strong temperature dependence of their chemical shifts (Table S1), which is an indicator of high solvent accessibility. Altogether, these NMR data indicated that **3** $\beta$  did not adopt *per se* hydrogen-bonded  $\beta$ -sheet conformations and had no self-association properties in solution. Interestingly, 2D NOESY experiments recorded on **3** $\beta$  in the presence of  $A\beta_{1-42}$  were characterized by modifications in the intensity of intraresidual and sequential NOEs which became more negative (Figure 9S in supporting information). These changes correspond to transferred NOEs due to transient binding of **3** $\beta$  to  $A\beta_{1-42}$  aggregated species. However

no additional long-range NOE correlations were detected, suggesting that **3** $\beta$  conformation remained largely extended and did not adopt a compact shape upon  $A\beta_{1-42}$  binding.

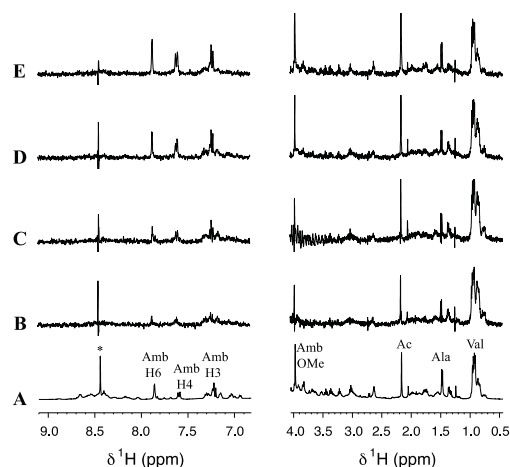


**Figure 5. Interaction of **3** $\beta$  with  $A\beta_{1-42}$  monitored by NMR.** Aromatic/amide (left) and aliphatic (right) regions of 1D  $^1H$  NMR spectra of **3** $\beta$  (0.4 mM) and  $A\beta_{1-42}$  (90  $\mu M$ ) at 5 °C. (A) Reference 1D  $^1H$  spectrum recorded at  $t = 0$ . (B–E) 1D  $^1H$  STD spectra recorded at  $t = 0$  (B), after 2 days (C), 1 week (D) and 2.5 weeks (E). The assignment of the aromatic and methyl resonances of **3** $\beta$  is indicated. Amb means 5-amino-2-methoxybenzoyl. The signal marked with an asterisk corresponds to formic acid impurity.

#### SPR experiments

SPR was then used to evaluate the affinity between compound **3** and its  $\beta$ -anomer **3** $\beta$  and  $A\beta_{1-42}$  monomer bound to the gold surface.

To our knowledge, the few SPR experiments described in the literature to detect the affinity of ligands for  $A\beta_{1-42}$  have used either the depsi-peptide molecule described by Taniguchi *et al.*<sup>36,37,22</sup> or biotinylated  $A\beta_{1-42}$  immobilized onto streptavidin-coated chips.<sup>38</sup> An SPR-based immunoassay has been also developed to recognize  $A\beta_{1-42}$  oligomers.<sup>39</sup> The main drawbacks we found in these methods are the necessity to synthesize the non-commercial depsi-peptide, the modest SPR provided with these other approaches, and the use of modified peptides which may alter their affinity behavior. We thus developed a new method to immobilize the commercial  $A\beta_{1-42}$  peptide monomer by a classical peptide coupling through its amino groups. We paid particular attention to maintaining  $A\beta_{1-42}$  in its monomeric form upon immobilization. Recently a similar method has been reported, however no clear evidence on the nature of the immobilized species was provided.<sup>40</sup>

We optimized the immobilization of  $A\beta_{1-42}$  peptide by varying different parameters (pH and concentration of the sample preparation, and injection parameters such as the flow, the time and the number of injections). To ensure that only monomeric species were mainly immobilized, a rinsing step using an aqueous solution of  $NH_4OH.H_2O$  0.1 % was employed (see the procedure in



the supporting information), as we demonstrated previously by CE that these conditions were able to disaggregate oligomers and regenerate monomeric species.<sup>32</sup> The characterization of the Gold chip was performed using specific antibodies directed against the N- or C-term of A $\beta$ <sub>1-42</sub> (6E10 and MD 19-0016, respectively, see supporting information). Curcumin, which is a well-known disaggregant compound<sup>41</sup> did not lead to a decrease of the signal and was even found to bind to A $\beta$ <sub>1-42</sub> fixed on the SPR chips (Figure 18S in supporting information).

Finally, the affinity of ThT toward the peptide immobilized on the chip surface was evaluated before and after our optimized rinsing step, which used an aqueous solution of NH<sub>4</sub>OH.H<sub>2</sub>O 0.1 %. Both SPR signal and fluorescence (visualized by fluorescence microscopy images of the channel) were higher before the rinsing step. The rinsing step is therefore crucial to disaggregate large species present initially on the chip surface in order to lead to a surface mainly composed by A $\beta$  in its monomeric form (Figure 14S in supporting information).

We conducted SPR measurements with compounds **3**, **3 $\beta$**  and **1** to check their affinity for A $\beta$ <sub>1-42</sub> peptide. A concentration-dependent signal was observed, however, the response was very low in the range of the tested concentrations (up to 200  $\mu$ M) indicating that these compounds have a very low affinity for the immobilized A $\beta$ <sub>1-42</sub> (Figures 15S, 16S and 17S in the supporting information). This result is in accordance with the NMR data.

#### Protection against A $\beta$ <sub>1-42</sub> cell toxicity

The inhibitors were investigated to determine their ability to reduce the toxicity of aggregated A $\beta$ <sub>1-42</sub> to SH-SY5Y neuroblastoma cells. The addition of either **1** or **3** showed a protective effect on cell survival (MTS assay, Figure 6) and membrane damage (LDH membrane integrity assay, Figure 20S in supporting information) in the presence of cytotoxic 5  $\mu$ M A $\beta$ <sub>1-42</sub>. Remarkably, this protective effect was seen at equimolar amounts of inhibitor to A $\beta$ <sub>1-42</sub> and was still present at a ratio of 0.05/1 (inhibitor/A $\beta$ <sub>1-42</sub>) in the MTS assay.

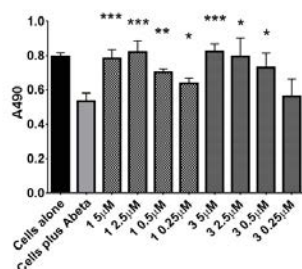


**Figure 6. Effect of **1** and **3** on A $\beta$ <sub>1-42</sub> toxicity towards SH SY5Y cells.** Cell viability in the presence of 5  $\mu$ M aggregated A $\beta$ <sub>1-42</sub> and decreasing concentrations of **1** or **3**. The black bar on the left shows cell viability in the absence of A $\beta$ <sub>1-42</sub>. Statistical significance is indicated by \*, where \* is  $p < 0.05$ , \*\* is  $p < 0.01$  and \*\*\* is  $p < 0.001$  comparing cells incubated with A $\beta$ <sub>1-42</sub> plus inhibitor to those with A $\beta$ <sub>1-42</sub> alone. Statistical significance is described.

#### Plasma stability

The ability to withstand enzymatic cleavage in the circulatory system is an important requirement for any potential drug. Incu-

bating the two inhibitors **1** and **3** in plasma gives an idea of how stable they will be once injected into the body. **3** withstood 24 hours at 37°C with no obvious degradation in 10% plasma (Figure 11S in supporting information). **1** appeared to show some degradation over the same period, although the total area of the peaks did not change (Figure 21S in supporting information). Unmodified polypeptides are usually degraded within minutes under these incubation conditions.

#### Discussion

The introduction of a peptidomimetic strand based on a 5-amino-2-methoxybenzhydrazide unit linked through the carboxyethyl in the C6 position of the D-glucopyranosyl scaffold not only increased the stability towards proteolytic degradation but also dramatically increased the capacity of these pentapeptide analogs to inhibit the fibrillization of A $\beta$ <sub>1-42</sub>, as demonstrated by the ThT fluorescence and TEM experiments. The polar hydroxyl groups of the sugar moiety were essential to prevent the aggregation, as demonstrated by the lack of inhibitory activity of the benzyl analogues **19**, **22-23**. A slightly superior effect was observed for the  $\beta$  anomer **3 $\beta$**  compared to the mixture of  $\alpha$  and  $\beta$  anomers in **3** (confirmed in the CE experiments). The presence of the amine of the side chain of the lysine residue in compound **3** proved to be beneficial for the inhibitory activity in comparison with the valine residue in compound **2**. This result suggests that an ionic interaction is likely to be established between this amine and acidic residues of A $\beta$ <sub>1-42</sub>, strengthening the hydrophobic interactions involving aliphatic and aromatic moieties. Indeed, several computational and experimental studies on A $\beta$ <sub>1-42</sub> have shown that, in addition to the hydrophobic interactions involving in particular the 16-21 sequence (KLVFFA), the formation of a salt-bridge between amino acids Asp23 and Lys28 might stabilize a turn motif involving residues 24-28.<sup>9,42</sup> An interaction with Glu22 might also be beneficial for the activity of the molecules.<sup>42b</sup> We can thus suggest, and this is supported by the NMR binding experiments (STD), that this novel class of glycopeptidomimetics is likely to interact through the hydrophobic sequences of the peptidomimetic and dipeptide sequences, presumably with a hydrophobic sequence of A $\beta$ <sub>1-42</sub> (such as the central K<sub>16</sub>-A<sub>21</sub> or the C-terminal part I<sub>31</sub>-V<sub>40</sub>) and through an electrostatic interaction. The flexible and hydrophilic sugar moiety acts as a  $\beta$ -sheet breaker to prevent the aggregation. The effect of the glycopeptidomimetic on the early steps of oligomerization has been also been demonstrated clearly by CE. Compound **3 $\beta$**  dramatically preserved the non-toxic monomer of A $\beta$ <sub>1-42</sub> (ES). Oligomers larger than dodecamers (LS) were also stabilized. Both types of cell viability assay proved that pre-incubation of cytotoxic A $\beta$ <sub>1-42</sub> with glycopeptidomimetic **3** completely rescued the SH-SY5Y neuroblastoma cells. The protective effect was observed even at sub-stoichiometric concentrations (**3** reduced cell death by 100% with 0.5 eq and by 75% with 0.1 eq. in the MTS assay). It is also notable that glycopeptide **1** showed also a dramatic effect on cell survival, but was more sensitive to proteolytic attack.

The NMR and SPR experiments clearly indicated that this novel glycopeptidomimetic series does not bind to monomers with substantial affinity. NMR indicated that the A $\beta$ <sub>1-42</sub> species recognized by **3 $\beta$**  are oligomeric forms whose concentration slowly increased with time. Thus, even if **3 $\beta$**  is a small molecule that does not *per se* adopt a preferential conformation, it is able to recognize and bind to the early  $\beta$ -structured A $\beta$ <sub>1-42</sub> oligomers. The observation of magnetization transfers in STD, WaterLOGSY and

trNOESY experiments implied that the interconversion between the free and the  $A\beta_{1-42}$ -bound forms of **3** $\beta$  occurred in fast exchange on the NMR time scale. We can thus hypothesize that such transient binding of **3** $\beta$  to oligomers may impede the subsequent addition of monomers or the association of oligomers into larger species and/or disrupt these early oligomers so that they revert back to monomers (Figure 7A).

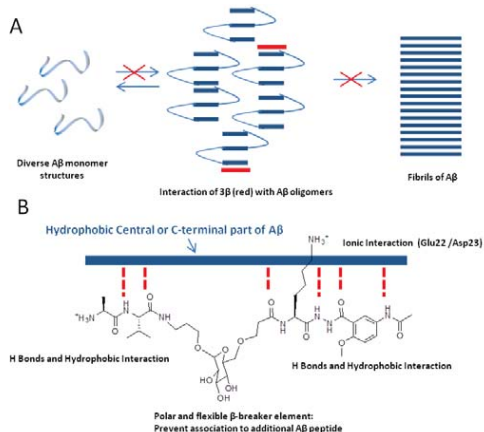


**Figure 7.** Hypothesis of mechanism of  $A\beta_{1-42}$  aggregation inhibition by **3** $\beta$ . A- Proposed model of inhibition of fibrillization of  $A\beta_{1-42}$  and of preservation of  $A\beta_{1-42}$  monomer by **3** $\beta$ . B- Proposed model of interaction of **3** $\beta$  with  $A\beta_{1-42}$ .

### Conclusion

In conclusion, the present work validates the singular effect of sugar-based peptidomimetic analogs of pentapeptides on  $A\beta_{1-42}$  oligomerization and fibrillization. This new series has been designed in order to achieve three objectives: first, to engage in both hydrophobic and ionic interactions with  $A\beta_{1-42}$ , thanks to small peptide and peptidomimetic arms; secondly, to prevent cross  $\beta$ -sheet elongation of  $A\beta_{1-42}$  due to the hydrophilic sugar, considered as a  $\beta$ -sheet breaker element (Figure 7B). Finally, it has been designed also to be druggable, particularly to be a small molecule (MW around 800) with a good hydrophobicity/ hydrophilicity balance and resistance to proteolytic degradation. A wide range of bio- and physico-chemical techniques was used to demonstrate the capacity of the compounds (in particular **3** $\beta$ ) to delay both the early oligomerization and fibrillization of  $A\beta_{1-42}$ . To the best of our knowledge, this is the first example of a small molecule that is able to preserve the non-toxic monomeric species of  $A\beta_{1-42}$ . The strong protective effect on cells, even at sub-stoichiometric concentrations, also highlights the considerable therapeutic potential of this novel series of peptidomimetics.

### Additional informations

Supplementary data associated with this article, ie synthetic procedures and characterization of glycopeptidomimetic compounds; experimental procedure for fluorescence-detected ThT binding assay; representative curves of ThT fluorescence assays; experimental procedure for TEM studies, CE, NMR and SPR, can be found in the online version, at doi:

### Acknowledgements

Chiara Bernardi (CB) (BioCIS, UMR 8076) is thanked for her help with the synthesis. Claire Troufflard and Karine Leblanc (BioCIS, UMR 8076) are thanked for their help with the NMR experiments and the HPLC analysis respectively. Magali Noiray (CIBLOT-Bia, Université Paris-Sud) and G erardine Toutirais (Institut de Biologie Paris Seine (IBPS)/ FR3631, Service de Microscopie Electronique, Universit e Pierre et Marie Curie, France) are acknowledged for their advices in SPR and TEM experiments respectively. The Minist ere de l'Enseignement Sup erieur et de la Recherche (MESR) is thanked for financial support for DB. The European Union is thanked for funding the research training of NT, KF, CB and YI in the frame of the European student exchange Erasmus programme.

### Author contributions

JK and SO designed and supervised the research and wrote the paper. JLS and BC designed and supervised the synthesis of the glycopeptidomimetics performed by NT and KF. JK performed the ThT fluorescence and TEM experiments. DB and YI performed the EC and SPR experiments under the supervision of MTav. IC and AH performed the NMR experiments under the supervision of LK and OL. MT and DA performed the cell viability assays. All authors commented on the initial draft.

### Abbreviations

$A\beta$ , Amyloid-beta peptide; AD, Alzheimer's disease; CE, Capillary Electrophoresis; STD, Saturation Transfer Difference; ThT, Thioflavin T; TEM, Transmission Electron Microscopy; SPR, Surface Plasmon resonance; SAR, Structure-activity relationships; DMTMM, [4-(4,6-Dimethoxy-1,3,5-triazin-2-yl)-4-methyl-morpholinium tetrafluoroborate]; DMAP, 4-dimethylaminopyridine.

### Competing financial interests

The authors declare no competing financial interests.

### REFERENCES

1. a) <http://www.alz.co.uk/research/world-report>. b) Mucke, L. Alzheimer's disease. *Nature*, **461**, 895-897 (2009).
2. a) Goedert, M. & Spillantini, M. G. A Century of Alzheimer's Disease. *Science*, **314**, 777-780 (2006). b) Haas, C. & Selkoe, D. J. Soluble protein oligomers in neurodegeneration: Lessons from the Alzheimer amyloid  $\beta$ -peptide. *Nat. Rev. Mol. Cell Biol.*, **8**, 101-112 (2007).
3. Cohen, S. I. A., Linse, S., Luheshi, M., Hellstrand, E., White, D. A., Rajah, L., Otzen, D. L., Vendruscolo, M., Dobson, C. M. & Knowles, T. P. J. Proliferation of amyloid- $\beta$ 42 aggregates occurs through a secondary nucleation mechanism. *Proc. Natl. Acad. Sci. USA*, **110**, 9758-9763 (2013).
4. Matsumura, S., Shinoda, K., Yamada, M., Yokojima, S., Inoue, M *et al.* Two Distinct Amyloid  $\beta$ -Protein ( $A\beta$ ) Assembly Pathways Leading to Oligomers and Fibrils Identified by Combined Fluorescence Correlation Spectroscopy, Morphology, and Toxicity Analyses. *J. Biol. Chem.* **286**, 11555-11562 (2011).
5. Jeong, J. S., Ansaloni, A., Mezzenga, R., Lashuel, H. A. & Dietler, G. Novel Mechanistic Insight into the Molecular Basis of Amyloid Polymorphism and Secondary Nucleation during Amyloid Formation. *J. Mol. Biol.* **425**, 1765-1781 (2013).
6. L uhres, T., Ritter, C., Adrian, M., Riek-Loher, D., Bohrmann, B., D obeli, H., Schubert, D & Riek, R. 3D structure of Alzheimer's amyloid- $\beta$ (1-42) fibrils. *Proc. Natl. Acad. Sci. USA* **102**, 17342-17347 (2005).
7. Laganowsky, A., Liu, C.; Sawaya, R. M., Whitelegge, J. P., Park, J & Zhao, M. Atomic View of a Toxic Amyloid Small Oligomer. *Science* **335**, 1228-1231 (2012).
8. Yu, L., Edalji, R.; Harlan, J. E., Holzman, T. F., Pereda Lopez, A.; Labkovsky, B., Hillen, H., Barghorn, S. *et al.* Structural Characterization of a soluble Amyloid  $\beta$ -peptide Oligomer. *Biochemistry* **48**, 1870-1877 (2009).
9. Ahmed, M., Davis, J., Aucoin, D., Sato, D., Ahuja, S., Aimoto, S., Elliott, J. J., Van Nostrand W. E. & O Smith, S. Structural conversion of neurotoxic amyloid- $\beta_{1-42}$  oligomers to fibrils. *Nat. Struct. Mol. Biol.* **17**, 561-567 (2010).
10. W alti M. A., Orts J., Veggeli B., Campioni S. & Riek R. Solution NMR Studies of Recombinant  $A\beta$ (1-42): From the Presence of a Micellar Entity to

- Residual  $\beta$ -Sheet Structure in the Soluble Species, *ChemBioChem* **16**, 659–669 (2015).
11. Dahlgren, K. N., Manelli, A. M., Blaine Stine, W., Baker, L. K., Krafft, G. A. & LaDu, M. J. Oligomeric and Fibrillar Species of Amyloid- $\beta$  Peptides Differentially Affect Neuronal Viability. *J. Biol. Chem.* **277**, 32046-32053 (2002).
  12. Jan, A., Gokce, O., Luthi-Carter R. & Lashuel, H. A. The ratio of Monomeric to Aggregated Forms of A $\beta$ 40 and A $\beta$ 42 Is an Important Determinant of Amyloid- $\beta$  Aggregation, Fibrillogenesis, and Toxicity. *J. Biol. Chem.* **283**, 28176-28189 (2008).
  13. Ono, K., Condrón, M. M. & Teplow, D. B. Structure-neurotoxicity relationships of amyloid  $\beta$ -protein oligomers. *Proc. Natl. Acad. Sci. USA* **106**, 14745-14750 (2009).
  14. Shankar, G. M., Li, S., Mehta, T. H., Garcia-Munoz A., Shepardson, N. E., Smith I. *et al.* Amyloid  $\beta$ -Protein Dimers Isolated Directly from Alzheimer Brains Impair Synaptic Plasticity and Memory. *Nat. Med.* **14**, 837-842 (2008).
  15. Pranglio, P., Yusko, E. C., Sept, D., Yang, J. & Mayer, M. Multivariate Analyses of Amyloid-Beta Oligomer Populations Indicate a Connection between Pore Formation and Cytotoxicity. *PLoS ONE*, **7**, e47261 (2012).
  16. Cizas, P., Budvytyte, R., Morkuniene, R., Moldovan, R., Broccio, M., Lösche, M., Niaura, G., Valincius, G. & Borutaite, V. Size-dependent neurotoxicity of  $\beta$ -amyloid oligomers. *Arch. Biochem. Biophys.* **496**, 84–92 (2010).
  17. Mayes, J., Tinker-Mill, C., Kolosov, O., Zhang, H., Tabner, B. J. & Allsop, D.  $\beta$ -Amyloid fibrils in Alzheimer's disease are not inert when bound to copper ions but can degrade hydrogen peroxide and generate reactive oxygen species. *J. Biol. Chem.* **289**, 12052-62 (2014).
  18. Cohen, S. I. A., Linse, S., Luheshi, L. M., Hellstrand, E., White, D. A., Rajah, L., Otzen, D. E., Vendruscolo, M., Dobson, C. M. & Knowles, T. P. J. Proliferation of amyloid- $\beta$ 42 aggregates occurs through a secondary nucleation mechanism. *Proc Natl Acad Sci U S A.* **110**, 9758-9763 (2013).
  19. a) Belluti, F., Rampa, A., Gobbi, S. & Bisi, A. Small-molecule inhibitors/modulators of amyloid- $\beta$  peptide aggregation and toxicity for the treatment of Alzheimer's disease: a patent review (2010 - 2012). *Expert Opin. Ther. Patents* **23**, 581-596 (2013); b) Hård, T. & Lendel, C. Inhibition of Amyloid Formation. *J. Mol. Biol.* **421**, 441–465 (2012); c) Doig, A. J. & Derreumaux P. Inhibition of protein aggregation and amyloid formation by small molecules. *Current Opinion in Structural Biology* **30**, 50–56 (2015).
  20. For a review, see a) Stains, C.I., Mondal, K., & Ghosh, I. Molecules that Target beta-Amyloid. *ChemMedChem* **2**, 1674-1692 (2007). b) Takahashi, T. & Mihara, H. Peptide and Protein Mimetics Inhibiting Amyloid Peptide Aggregation. *Acc. Chem. Res.* **41**, 1309-1318 (2008). c) Neddenriep, B., Calciano, A., Conti, D.; Saue, E., Paterson, M., Bruno, E. & Moffet, D. A. Short Peptides as Inhibitors of Amyloid Aggregation *The Open Biotechnology Journal* **5**, 39-46 (2011). d) Luo, J. & Abrahams, J. P. Cyclic Peptides as Inhibitors of Amyloid Fibrillation. *Chem. Eur. J.* **20**, 2410–2419 (2014).
  21. Cheng, P.-N., Liu, C., Zhao, M., Eisenberg, D., Nowick, J. S. Amyloid  $\beta$ -sheet mimics that antagonize protein aggregation and reduce amyloid toxicity. *Nat. Chem.* **4**, 927-933 (2012).
  22. Taylor, M., Moore, S., Mayes, J., Parkin, E., Beeg, M., Canovi, M., Gobbi, M., Mann, D. M. A. & Allsop, D. Development of a Proteolytically Stable Retro-Inverso Peptide Inhibitor of  $\beta$ -Amyloid Oligomerization as a Potential Novel Treatment for Alzheimer's Disease. *Biochemistry* **49**, 3261–3272 (2010).
  23. Arai, T., Araya, T., Sasaki, D., Taniguchi, A., Sato, T., Sohma, Y. & Kanai, M. Rational Design and Identification of a Non-Peptide Aggregation Inhibitor of Amyloid- $\beta$  Based on a Pharmacophore Motif Obtained from cyclo[-Lys-Leu-Val-Phe-Phe-]. *Angew. Chem. Int. Ed.* **53**, 8236–8239 (2014).
  24. a) Dorgeret, B., Khemtémourian, L., Correia, I., Soulier, J.-L., Lequin, O. & Ongeri, S. Sugar-based peptidomimetics inhibit amyloid  $\beta$ -peptide aggregation. *Eur. J. Med. Chem.*, **46**, 5959-5969 (2011). b) Kaffy, J., Brinet, D., Soulier, J.-L., Khemtémourian, L., Lequin, O., Taverna, M., Crousse, B. & Ongeri, S. Structure-activity Relationships of Sugar-based peptidomimetics as modulators of amyloid  $\beta$ -peptide early oligomerization and fibrillization *Eur. J. Med. Chem.* **86**, 752-758 (2014).
  25. a) Gruner, S. A. W., Truffault, V., Voll, G., Locardi, E., Stöckle, M. & Kessler, H. Design, Synthesis, and NMR Structure of Linear and Cyclic Oligomers Containing Novel Furanoid Sugar Amino Acids *Chem. Eur. J.* **8**, 4366-4376 (2002). b) Schweizer, F. Glycosamino Acids: Building Blocks for Combinatorial Synthesis—Implications for Drug Discovery. *Angew. Chem. Int. Ed.* **41**, 230-253 (2002). c) Risseuuew, M. DM P., Overhand, M., Fleet, G. W. J. & Simone, M. I. A compendium of sugar amino acids (SAA): scaffolds, peptide- and glyco-mimetics. *Tetrahedron: Asymmetry* **18**, 2001-2010 (2007).
  26. Nowick, J. S., Chung, D. M., Maitra, K., Maitra, S., Stigers, K. D. & Sun, Y. An Unnatural Amino Acid that Mimics a Tripeptide  $\beta$ -Strand and Forms  $\beta$ -Sheetlike Hydrogen-Bonded Dimers *J. Am. Chem. Soc.* **122**, 7654-7661 (2000).
  27. a) Bannwarth, L., Kessler, A., Pêthe, S., Collinet, B., Merabet, N., Boggetto, N., Sicsic, S., Reboud-Ravaux, M. & Ongeri, S. Molecular tongs containing amino acid mimetic fragments : new inhibitors of wild-type and mutated HIV-1 protease dimerization. *J. Med. Chem.*, **49**, 4657 (2006). b) Vidu, A., Dufau, L., Bannwarth, L., Soulier, J.-L., Sicsic, S., Piarulli, U., Reboud-Ravaux, M. & Ongeri, S. Towards the first non peptidic molecular tong inhibitor of wild-type and mutated HIV-1 protease dimerization. *ChemMedChem*, **5**, 1899 (2010).
  28. a) Yamanai, T., Inoue, R., Matsuda, S., Iwao, K., Oda, Y., Yoshida, A., Hamasaki, K. Formation of *O*-glycosidic linkages from 1-hydroxy sugars by bismuth(III) triflate-catalyzed dehydrative glycosidation. *Heterocycles* **77**, 445–460 (2009). b) Yamazaki, T. *et al.* US. Patent Appl. Publ. US 20020052327 A1 20020502 (2002).
  29. a) Kaminski, Z.J., Kolesinska B. *et al.* N-Triazinylammonium Tetrafluoroborates. A New Generation of Efficient Coupling Reagents Useful for Peptide Synthesis *J. Am. Chem. Soc.* **127**, 16912-16920 (2005). b) Jastrzabek K.G. *et al.* 4-(4,6-Di[2,2,2-trifluoroethoxy]-1,3,5-triazin-2-yl)-4-methylomor-pholinium Tetrafluoroborate. Triazine-Based Coupling Reagents Designed for Coupling Sterically Hindered Substrates *J. Org. Chem.*, **76**, 4506-4513 (2011).
  30. Komarova, B. S., Maryasina, S. S., Tsvetkov, Y. E. & Nifantiev, N. E. Water-Dependent Reduction of Carbohydrate Azides by Dithiothreitol *Synthesis*, **45**, 471-478 (2013).
  31. LeVine 3rd, H. Quantification of  $\beta$ -Sheet Amyloid Fibril Structures with Thioflavin T. *Methods Enzymol.* **309**, 274-284 (1999).
  32. Brinet, D., Kaffy, J., Oukacine, F., Glumm, S., Ongeri, S. & Taverna, M. An improved CE method for the *In vitro* monitoring of the challenging early steps of the A $\beta$ <sub>1-42</sub> peptide oligomerization: application to anti-Alzheimer's drug discovery. *Electrophoresis* **35**, 3302-3309 (2014).
  33. Fawzi, N.L., Ying, J., Ghirlando, R., Torchia, D.A. & Clore, G.M.. Atomic-resolution dynamics on the surface of amyloid- $\beta$  protofibrils probed by solution NMR. *Nature* **480**, 268-272 (2011).
  34. Walsh, D.M., Thulin, E., Minogue, A.M., Gustavsson, N., Pang, E., Teplow, D.B. & Linse, S. A facile method for expression and purification of the Alzheimer's disease-associated amyloid  $\beta$ -peptide. *FEBS J.* **276**, 1266-1281 (2009).
  35. Airoldi, C., Cardona, F., Sironi, E., Colombo, L., Salmona, M., Silva, A., Nicotra, F. & La Ferla, B. cis-Glyco-fused benzopyran compounds as new amyloid- $\beta$  peptide ligands. *Chem. Commun.* **47**, 10266-10268 (2011).
  36. Taniguchi, A., Sohma, Y., Hirayama, Y., Mukai, H., Kimura, T., Hayashi, Y., Matsuzaki, K., and Kiso, Y. "Click peptide": pH-triggered in situ production and aggregation of monomer A $\beta$ <sub>1-42</sub>. *ChemBioChem* **10**, 710–715 (2009).
  37. Canovi, M., Lucchetti, J., Stravalaci, M., Re, F., Moscatelli, D., Bigini, P., Salmona, M., and Gobbi, M. Applications of Surface Plasmon Resonance (SPR) for the Characterization of Nanoparticles Developed for Biomedical Purposes. *Sensors* **12**, 16420–16432 (2012).
  38. a) Amjhee, H., Bate, C., Williams, A., Virdee, J., Jeggo, R., Spanswick, D., Scopes, D.I.C., Treherne, J.M., Mazzitelli, S., Chawner, R., *et al.* The N-Methylated Peptide SEN304 Powerfully Inhibits A $\beta$ <sub>1-42</sub> Toxicity by Perturbing Oligomer Formation. *Biochemistry* **51**, 8338–8352 (2012). b) Maezawa, I. *et al.* Congo red and thioflavin-T analogs detect A $\beta$  oligomers. *J. Neurochem.* **104**, 457-468 (2008).
  39. Stravalaci, M. *et al.* Specific Recognition of Biologically Active Amyloid- $\beta$  Oligomers by a New Surface Plasmon Resonance-based Immunoassay and an *in Vivo* Assay in *Caenorhabditis elegans*. *J. Biol. Chem.* **287**, 27796-27805 (2012).
  40. Kai, T. *et al.* Tabersonine Inhibits Amyloid Fibril Formation and Cytotoxicity of A $\beta$ <sub>1-42</sub>. *ACS Chem. Neuroscience*, **6**, 879-888 (2015).
  41. Yang, F. *et al.* Curcumin Inhibits Formation of Amyloid  $\beta$  Oligomers and Fibrils, Binds Plaques, and Reduces Amyloid *in Vivo*. *J. Biol. Chem.* **280**, 5901 (2005).
  42. (a) Smith, M.D. & Cruz, L. Changes to the Structure and Dynamics in Mutations of A $\beta$ <sub>21-30</sub> Caused by Ions in Solution. *J. Phys. Chem. B* **117**, 14907–14915 (2013). (b) Hochdörfer, K., März-Berberich, J., Nagel-Steger, L., Epple, M., Meyer-Zaika, W., Horn, A.H.C., Sticht, H., Sinha, S., Bitan, G. & T. Schrader Rational Design of  $\beta$ -Sheet Ligands Against A $\beta$ <sub>1-42</sub>-Induced Toxicity. *J. Am. Chem. Soc.* **133**, 4348-4358 (2011).



## Review Article

# Molecular Structure, Membrane Interactions, and Toxicity of the Islet Amyloid Polypeptide in Type 2 Diabetes Mellitus

Lucie Caillon,<sup>1,2,3</sup> Anais R. F. Hoffmann,<sup>1,2,3</sup>  
Alexandra Botz,<sup>1,2,3</sup> and Lucie Khemtémourian<sup>1,2,3</sup>

<sup>1</sup>Sorbonne Universités, UPMC Univ Paris 06, Laboratoire des Biomolécules, 4 Place Jussieu, 75005 Paris, France

<sup>2</sup>Département de Chimie, Ecole Normale Supérieure, PSL Research University, 24 Rue Lhomond, 75005 Paris, France

<sup>3</sup>CNRS, UMR 7203 Laboratoire des Biomolécules, 75005 Paris, France

Correspondence should be addressed to Lucie Khemtémourian; lucie.khemtemourian@upmc.fr

Received 27 November 2014; Accepted 3 March 2015

Academic Editor: Hiroshi Okamoto

Copyright © 2015 Lucie Caillon et al. This is an open access article distributed under the Creative Commons Attribution License, which permits unrestricted use, distribution, and reproduction in any medium, provided the original work is properly cited.

Human islet amyloid polypeptide (hIAPP) is the major component of the amyloid deposits found in the pancreatic islets of patients with type 2 diabetes mellitus (T2DM). Mature hIAPP, a 37-aa peptide, is natively unfolded in its monomeric state but forms islet amyloid in T2DM. In common with other misfolded and aggregated proteins, amyloid formation involves aggregation of monomers of hIAPP into oligomers, fibrils, and ultimately mature amyloid deposits. hIAPP is coproduced and stored with insulin by the pancreatic islet  $\beta$ -cells and is released in response to the stimuli that lead to insulin secretion. Accumulating evidence suggests that hIAPP amyloid deposits that accompany T2DM are not just an insignificant phenomenon derived from the disease progression but that hIAPP aggregation induces processes that impair the functionality and the viability of  $\beta$ -cells. In this review, we particularly focus on hIAPP structure, hIAPP aggregation, and hIAPP-membrane interactions. We will also discuss recent findings on the mechanism of hIAPP-membrane damage and on hIAPP-induced cell death. Finally, the development of successful anti-amyloidogenic agents that prevent hIAPP fibril formation will be examined.

## 1. Introduction

Type 2 diabetes mellitus (T2DM) is classified as a protein-misfolding disease and shares the debilitating consequences of misfolded and aggregated peptides and proteins with more than 20 other diseases, such as Alzheimer's disease, Parkinson's disease, and spongiform encephalopathy [1–3]. T2DM is characterized metabolically by defects in both insulin secretion and insulin action, resulting in hyperglycemia, and is histopathologically characterized by the presence of fibrillar amyloid deposits in the pancreatic islets of Langerhans (islet amyloid) [4]. Amyloid is a generic term for a protein aggregation state in which the proteins bind to each other in a  $\beta$ -sheet conformation [5, 6]. In T2DM, amyloid deposits were initially assumed to be composed of insulin; however, in 1987 two different groups discovered that the major component of islet amyloid is a 37-residue polypeptide pancreatic hormone [7, 8], initially named insulinoma amyloid peptide [9], then

diabetes-associated peptide [7], and finally islet amyloid polypeptide (IAPP) [8] or amylin [10]. The presence of these amyloid deposits in T2DM has been linked to the death of the insulin producing islet  $\beta$ -cells, thereby contributing to the development of this disease [4].

IAPP, found in all mammals, is coproduced and cosecreted with insulin in a molar IAPP:insulin ratio of 1:100 in healthy individuals, a ratio that can increase to 1:20 in T2DM. The function of hIAPP is still not entirely clear. As a paracrine hormone, hIAPP may be involved in the regulation of glucose metabolism, the control gastric emptying, the suppression of glucagon, the control of satiety, and other cellular processes [11–16]. Along with these functions hIAPP disrupts cell coupling and is also reported to induce apoptosis in isolated human islets [17]. Although hIAPP is a hormone, no specific receptors have yet been found. However, specific binding sites have been identified in the brain and in the renal cortex [18–20].

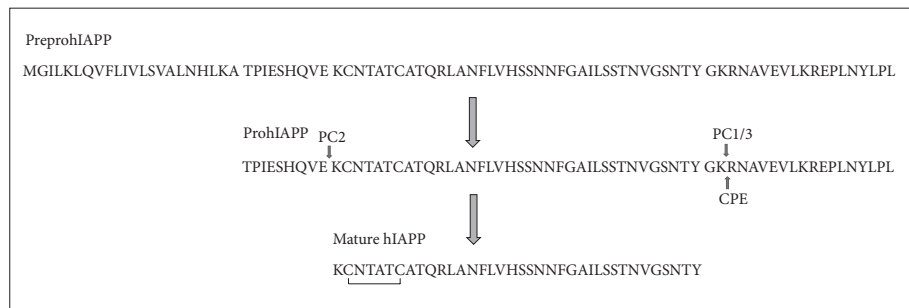


FIGURE 1: Processing of human PreproIAPP that lead to the formation of mature hIAPP. The cleavage site for PC2 and PC1/3 is indicated by arrows. The residues KR, indicated by arrow, which remain after the cleavage is induced by PC1/3 are removed by the carboxypeptidase E. This results in the amidation of the C-terminus of mature hIAPP. The disulfide bridge is shown on the mature hIAPP.

hIAPP is stored with insulin by the pancreatic islet  $\beta$ -cells and is released in response to the stimuli that lead to insulin secretion [21–23]. hIAPP is initially expressed by  $\beta$ -cells as an 89-aa residue prohormone containing a 22-aa signal sequence which is cleaved off upon translocation across the endoplasmic reticulum, resulting in the prohormone precursor prohIAPP (Figure 1). Further processing of the prohormone proIAPP (67-aa in humans) involves cleavage at the C-terminal end either in the trans-Golgi network or in secretory granules, resulting in an intermediate 48-aa residue peptide. The second cleavage, at the N-terminal end, generates the mature 37-aa peptide, hIAPP, in the secretory granules. The two flanking peptides from prohIAPP remain in the secretory granules. Cleavage is initiated at two conserved dibasic sites and involves the two endoproteases prohormone convertase 2 (PC2) and prohormone convertase 1/3 (PC1/3) and the carboxypeptidase E (CPE), which are the same enzymes that process proinsulin to mature insulin [24–27]. A glycine residue at the start of the C-terminal propeptide acts as an amidation donor. The mature peptide undergoes posttranslational modification via formation of a disulfide bond between cysteine residues 2 and 7 (Figure 1).

There is a large and growing body of work on the biophysics of hIAPP amyloid formation and on the biological consequences of islet amyloid deposition. In this review, the current knowledge of hIAPP structure, hIAPP-membrane interactions, hIAPP toxicity, and the development of inhibitors of hIAPP toxicity will be presented and analysed.

## 2. Conformation and Structure of IAPP in Solution

hIAPP can appear in various states (monomer, oligomer, or fibril) all with very different structures. In solution, it has been shown, using circular dichroism, that monomeric hIAPP is a natively unfolded peptide which is predominantly random coil, aside from a rigid ring structure formed by the disulfide bridge between Cys2 and Cys7 residues. As for all amyloid forming peptides, hIAPP undergoes a conformational

transition from its nonfolded state to a  $\beta$ -sheet structure, which increases over time [28–30]. This initial peptide conformational change is the key step leading to the formation of oligomers to highly ordered and insoluble amyloid fibrils.

Little information on the structure of hIAPP oligomers (and other oligomers associated with amyloid diseases) is available, mainly due to the instability of the species and to the relatively fast aggregation process of hIAPP. Both  $\beta$ -sheet-rich hIAPP oligomers and  $\alpha$ -helix-rich hIAPP oligomers have been observed [31, 32]. High resolution microscopy (electron and atomic-force) and spectroscopy techniques (NMR) are most often used to detect oligomeric species, although NMR generally lacks the time resolution necessary to obtain a snapshot of oligomers. A handful of microscopy studies have confirmed that hIAPP oligomers consist of 10–20 hIAPP monomers with large variations in size and shape [33–35]. However, data on the size of hIAPP oligomers is somewhat scarce, where one study showed a range of 25–500 monomers and another showed a range of 20–40 monomers [36, 37].

The structure of hIAPP fibrils is more comprehensively described, probably due to the stable nature of the fibrils. Observation by electron microscopy (EM) of hIAPP fibrils reveals a polymorphism among the fibrils. In some cases, they organise themselves as helical fibrils of variable width, presenting some periodical twists. In other cases, the oligomers, also called “protofibrils” at this point, associate themselves laterally in long and striated ribbon-like strands. These strands, whose structure will be made more explicit later on, can be several nanometers long and have a width ranging from 5 to 15 nm [6, 38]. Further observation into the atomic organisation of these ribbon-like fibrils finds that the mature amyloid fibrils are characterized by a cross  $\beta$  structure, where all  $\beta$  strands, linked by interstrand hydrogen bonds, are oriented perpendicularly to the fibril axis. The insoluble and noncrystalline nature of hIAPP fibrils has complicated the determination of their molecular structure; however, further investigations using different techniques such as solid-state NMR spectroscopy or X-ray crystallography have provided two similar atomic level models for hIAPP fibrils. The first

model was obtained using solid-state NMR spectroscopy in association with molecular modelling. The resulting model suggests that a single protofibril is made of two symmetric hIAPP monomers. The backbone of those hIAPP monomers possesses two  $\beta$ -strand segments formed by residues 8–17 and 29–37 separated by a bend or loop that is formed by residues 18–27. As the monomer structures itself into this hairpin, different orientations of the side chains of the residues between the two  $\beta$ -sheets have been obtained by Langevin dynamics. Either side chains of Gln10, Leu12, Asn14, and Leu16 are in contact with the  $\beta$ -sheet formed by residues 28–37, whereas side chains of Arg11, Ala13, and Phe15 are located on the outside of the fibril, or the organisation of the side chains is reversed, meaning that side chains of Gln10, Leu12, Asn14, and Leu16 are located outside the protofibril when side chains of Arg11, Ala13, and Phe15 are facing the core of the block. Each single monomer then interacts with another, as a pair, via the side chains of residues 26 to 32, thus forming the single protofilament. Protofilaments then laterally associate, leading to the mature fibril [6]. The second model for hIAPP fibrils was obtained by using X-ray crystallography and is based on steric zippers and on crystal structures that were obtained on segments 20–27 (NNFGAIL) and 29–33 (SSTNVG) of the peptide. This model, similar to that obtained by solid-state NMR with the exception of atomic distances between  $\beta$ -sheet layers, suggests that a monomer of hIAPP has a hairpin structure consisting of two  $\beta$ -strands. Each monomer then associates with another, with the SSTNVG segment of the first molecule creating a steric zipper that interacts with the NNFGAIL segment of the second. These stacks of peptides then associate themselves one on top of another, perpendicular to the fibril axis, to form the mature amyloid fibril [39].

### 3. Structure of Membrane-Bound hIAPP

Aggregation of hIAPP on the membrane proceeds through a different pathway than in solution, as the structure of membrane-bound hIAPP is different to that of hIAPP in solution. The conformation of hIAPP has been examined using CD and NMR spectroscopy in different membrane models. In the presence of negatively charged membranes, hIAPP initially displays  $\alpha$ -helical structure [40]. After a few minutes of incubation, the conformation of hIAPP changes to  $\beta$ -sheet, characteristic of fibril formation. hIAPP freshly added to zwitterionic membrane models (including among others phosphatidylcholine, phosphatidylethanolamine, cholesterol, or sphingomyelin) displays typical random coil conformation, which undergoes a typical change to  $\beta$ -sheet secondary structure in a few hours (Figure 2) [41]. In both anionic and zwitterionic micelles, the  $\alpha$ -helical structure is predominant for several days, suggesting that in these media the peptide is kept in a monomeric conformation [41]. The micelle models enabled two groups to characterize the conformation of monomeric hIAPP, in SDS or DPC micelles using NMR [42, 43]. Both groups have found that the core (residues 7 to 28) is an  $\alpha$ -helix structure with a kink region near residues 18–22. However, the presence of this kink is likely due to the high curvature of the micelles.

The C-terminal part of hIAPP is unfolded with a high degree of flexibility, while the N-terminal part (residues 1–7) forms a hairpin due to the presence of the disulfide bond. The structure of hIAPP in the presence of membranes was also studied using microscopy techniques [44]. This study showed that hIAPP forms ion-channel-like structures in reconstituted membranes suggesting that these oligomeric hIAPP pores could insert in membranes and therefore change their barrier properties.

### 4. Mechanism of hIAPP Fibril Formation

As for all amyloid peptides, hIAPP is produced as a soluble monomer and undergoes oligomerization and amyloid fibril formation via a nucleation-dependent polymerization process [45]. This process is divided into three main steps, in the first step, also named the lag phase, the peptide is in a monomeric form and/or in small soluble oligomers and no fibrils are present; the second step, called the elongation phase, is indicated by the propagation of the fibril growth with consumption of monomer and finally the plateau is reached when the amount of fibril remains constant. The kinetics of hIAPP fibril formation can be monitored in time by the commonly used method of specific binding of the fluorescent molecule Thioflavin T (ThT) to amyloid fibrils [46]. A kinetic trace of hIAPP fibril formation shows a lag phase and a sigmoidal transition which are both typical for fibril growth of amyloidogenic proteins and peptides (Figure 3). The lag phase is dependent on experimental conditions such as the peptide concentration, the ionic strength, the temperature, and the pH [47, 48].

In most species, IAPP is expressed as an immature 89-membered amino acid peptide which is ultimately processed into a mature peptide of 37 amino acid residues [49]. Most of the N- and C-terminal residues, the intramolecular disulfide bridge, and the amidated C-terminus are strongly conserved throughout the mammalian species (Figure 4). There is a correlation between the sequence of IAPP and its propensity to form amyloid fibrils. For example, rat or mouse IAPP (rIAPP or mIAPP) differ from human IAPP by only six residues out of 37 and do not form fibrils. Note that those five of six positions between hIAPP and the nonamyloidogenic mIAPP are located between residues 20 and 29, the region which is known to be important in hIAPP fibrillation [50] and that three of the six residues involve a proline (at positions 25, 28, and 29) which is well-known as a disrupter of secondary structure and acts as a  $\beta$ -sheet breaker. Unlike rodents, dogs, and cow that do not form fibrils, primates, cats, porcine, ferret, and guinea pigs can form amyloid fibrils and are prone to T2DM [51].

Several studies have shown that hIAPP sequence can be divided into three parts, (i) the 1–19 region which is responsible for hIAPP/membrane interaction and insertion [52, 53], (ii) the 20–29 region, which is essential for amyloid fibril formation [29, 50], and (iii) the amyloidogenic 30–37 region which favours fibrils formation [54–56]. The N-terminal region contains all charged residues: Lys1, Arg11, and His18 [56]. In particular, the protonation state of the His18 is affected by the change in pH between the  $\beta$ -cell granules of

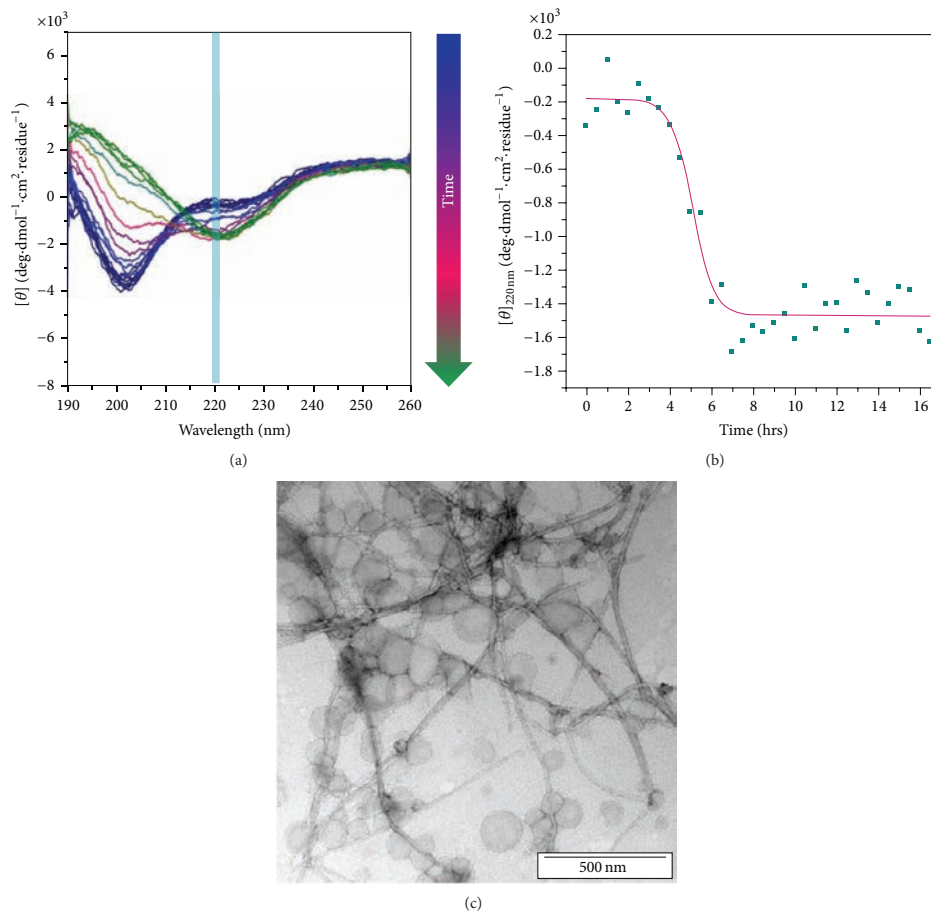


FIGURE 2: (a) CD kinetic study of hIAPP in vesicles. Plot color code: dark blue: CD spectrum recorded after 5 minutes and green: CD spectrum recorded after few hours. (b) Time course of CD ellipticity at 220 nm. (c) Negatively stained microscopy images of hIAPP after incubation with vesicles.

the pancreas where hIAPP is stored at a pH of approximately 5.5 and released into the extracellular compartment, which has a pH of 7.4. Studies in solution have shown that hIAPP aggregation is faster at a pH of 8.8 than at 4.0 and that the fibril morphology is affected by a pH of 2.4 [56, 57], indicating that in solution the pH really plays a role in hIAPP aggregation. hIAPP contains one aromatic residue in each of the three main parts (Phe15, Phe23, and Tyr37), that raise the question of the importance of aromatic-aromatic and aromatic-hydrophobic interactions in IAPP aggregation. Studies using single, double, and triple mutants in which the aromatic residues were replaced by Leu residues (F15L, F23L, and Y37L) indicated that aromatic residues are not required for fibril formation. However, the substitution decreases

the rate of fibril formation and alters the tendency of fibrils to aggregate [58–60]. The 20–29 region is the segment in which most mutations occur between the species (*vide supra*). Many substitutions that impact amyloid formation fall within the 20–29 domain confirming the importance of this region. A mutation (Ser → Gly) at position 20, which is found at low levels in certain Asian populations, was found to affect amyloid fibril formation and the development of T2DM *in vivo*. Indeed, this mutation seems to constitute a risk factor for diabetes, and it has been shown to increase the fibril formation rate *in vitro* [11, 61]. The effect of the proline residue has been further investigated on an 8–37 fragment of hIAPP, known to be amyloidogenic [62], but presenting substitutions by prolines in positions 17, 19, and 30. This study has shown

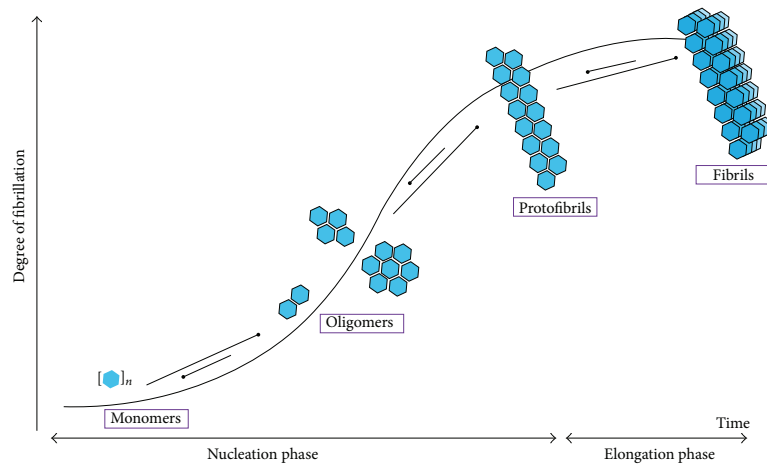


FIGURE 3: Schematic representation of fibrillation of hIAPP over time. During nucleation phase, hIAPP monomers associate themselves in order to form oligomers of various sizes. As the nucleation phase extends to the elongation phase, we can observe the formation of protofibrils, building blocks of the mature fibrils that characterize amyloidoses.

	1	10	20	30
Human	KCNTATCATQRLANFLVHSSNMF	GAIL	SSTNV	GSNTY
Rat/mouse	KCNTATCATQRLANFLVRSNNL	GPVLP	PPTNV	GSNTY
Monkey	KCNTATCATQRLANFLVRSNNM	FGTIL	SSTNV	GSNTY
Porcine	KCNMATCATQHLANFLDRSR	NNLGTIF	SPTKV	GSNTY
Cow	KCGTATCETQRLANFLAPSSN	KLGAIF	SPTKM	GSNTY
Cat	KCNTATCATQRLANFLIRSSNN	LGAILL	SPTNV	GSNTY
Dog	KCNTATCATQRLANFLVRSNNL	GAIL	SPTNV	GSNTY
Guinea pig	KCNTATCATQRLTNFLVRS	SHNLGA	LLPTD	VGSNTY
Hamster	KCNTATCATQRLANFLVHSSNN	LGPVLS	PPTNV	GSNTY
Ferret	KCNTATCVTQRLANFLIHSSNN	LGAILL	PPTD	VGSNTY
Rabbit	CNTVT	CATQRLANFLIHSSNN	F	FLPPS
Hare	T	QRLANFLIHSSNN	F	FLPPT

FIGURE 4: Primary sequence of IAPP from different species. Only partial sequences are available for rabbit and hare. Residues that differ from the human IAPP sequences are highlighted in red.

that proline substitution outside the core 20–29 region of hIAPP not only reduces the aggregation of hIAPP in solution but also induces instability in the  $\beta$ -sheet structure. It is therefore suggested that proline substitution has a dominant negative role in fibril formation by either disruption of the nucleation process of hIAPP or by favouring the nonstructured state of the peptide [63]. A «reverse study» has been performed by Green and coworkers on rIAPP [64]. In this case, the proline residues have been conserved while Arg18, Leu23 and Val26 have been substituted by His18, Phe23, and Ile26 as in hIAPP. Results have shown that although the modified rIAPP does not complete the fibril formation to its maturity as would the wild type hIAPP, the peptide is able

to form fibrils. This implies that the presence of the prolines in rIAPP does disrupt fibril formation but is not completely sufficient to avoid it. Moreover, these different studies also show the importance of key residues in hIAPP that influence its structure and induce mature fibril formation.

The mechanism of islet amyloid formation is not well understood. One potential cause has been proposed to be alterations in the processing of the hIAPP precursor molecule, proIAPP, by the islet  $\beta$ -cells [26, 65]. Recent investigations have demonstrated that the precursor does not form amyloid aggregates in solution and may be important in early intracellular amyloid formation [27, 66, 67]. For example, several studies demonstrated that proIAPP interacts with heparin sulphate proteoglycan of the basement membranes that may act as a seed for amyloid formation [68]. In addition, it was shown that incomplete processing has large consequences for the properties of hIAPP and that these consequences point toward a less cytotoxic activity of the precursor as compared to mature hIAPP [69].

Another characteristic of hIAPP is the intramolecular disulfide bridge between Cys2 and Cys7 at its N-terminal, which was shown to be essential for its biological activity [70]. *In vitro* studies highlight that the disulfide bond is not involved in the amyloid fibril core structure, prohibiting the N-terminal region of hIAPP from forming  $\beta$ -sheet structures. However, it does contribute to the assembly mechanism since the loss of the disulfide bond reduces fibril formation [62].

## 5. The Role of Lipid Membranes in hIAPP Aggregation

Membranes are implicated in hIAPP aggregation, both as the target of toxicity and as a catalyst [32, 71, 72]. hIAPP is

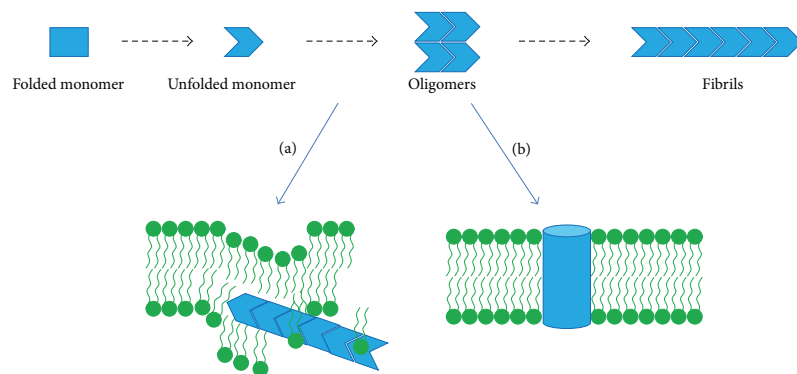


FIGURE 5: Schematic representation of permeabilization hypothesis. The natively fold peptide first starts to unfold. The first hypothesis (a) proposes that the monomeric peptide or small oligomers interact with the membranes and insert into the membranes. Fibril formation leads to membrane permeabilization by changes in membrane curvature and lipids recruitment. The second hypothesis (b) suggests that oligomeric species are toxic for the membrane interacting with it and forming pores.

known to interact with the membranes and to be inserted into the membranes, which affect hIAPP aggregation [52, 73]. The analysis of the first step of hIAPP/membrane interaction shows that hIAPP is inserted into phospholipid membranes most likely as a monomer and that the N-terminal part (1–19) is responsible for insertion [49]. This is in agreement with theoretical predictions from the amino acid sequence which suggest that only the 1–8 region has a membrane-interacting ability [74]. A study found that the disulfide bridge located in the N-terminal part (1–19) has a minor effect on membrane insertion properties and peptide conformational behaviour, suggesting that this disulfide bridge does not play a significant role in hIAPP/membrane interactions [75].

It is known that lipid membranes can promote hIAPP aggregation [71]. Lipid composition is a key factor that governs the extent to which membranes alter peptide aggregation. Several compositions were studied, highlighting the influence of various lipids on hIAPP aggregation and fibrillation. It has been shown that anionic lipids such as phosphatidylserine (PS) and phosphatidylglycerol (PG) strongly accelerate the kinetics of fibrils formation, thus reducing the lag time of the kinetics [40, 41, 71, 76]. In the presence of such membranes, hIAPP fibril formation occurs within a few minutes as opposed to a few hours in their absence. In contrast, the zwitterionic phosphatidylethanolamine (PE) is prone to slowing down these kinetics [41, 77]. Literature data thus indicate that the lipid composition of membranes has a large effect on hIAPP fibril formation kinetics but does not affect fibril morphology.

The modifications of fibril formation kinetics by lipid membrane composition could be attributed to peptide/lipid interactions. In particular, electrostatic interactions between anionic lipids and the positively charged hIAPP could explain the enhancement of hIAPP aggregation. Thus, as in solution, changes of pH, as well as ionic strength, could affect hIAPP aggregation and fibrillation in the presence of membranes

[47, 48]. It has been shown that in the presence of membranes, a low pH decreases the rate of fibril formation, suggesting that a low pH prevents aggregation of hIAPP as well as membrane damage in the secretory granules [48]. The ionization state of the histidine residue significantly affected the kinetics of hIAPP conformational changes and concomitant fibril formation and this is directly related to the kinetics of hIAPP-membrane damage. These results confirmed that the change of protonation of His18 is very important in the kinetics of hIAPP aggregation and fibril formation.

Despite considerable progress in the field of hIAPP-membrane interaction, the mechanism of peptide-lipid interactions and membrane permeabilization still remains to be elucidated and it is not known how hIAPP-membrane interactions are related to cytotoxicity in T2DM.

## 6. hIAPP-Induced Membrane Damage

The most widely accepted hypothesis is that hIAPP-induced cytotoxicity occurs via a membrane disruption mechanism (Figure 5). The first experimental evidence that an amyloid protein could cause membrane damage came from the work of Pollard [78]. It was found that the peptide A $\beta$ , involved in Alzheimer's disease, could form cation-selective channels in planar lipid bilayers. A few years later, similar experiments were done on hIAPP and showed that hIAPP could also form cation-selective channels and ultimately disrupt the membranes [79]. On the other hand, neither the nonamyloidogenic mouse IAPP nor the amyloid hIAPP fibrils formed channels. These ion-channels have been also observed for other amyloidogenic proteins suggesting that the toxicity of amyloid proteins seems to be linked to their shared potential to form channels (or pores) in membrane [80, 81]. At this stage, it was clear that hIAPP could induce membrane damage; however, the exact mechanism of hIAPP-induced membrane disruption is far from clear and numerous models



have been described during the last 15 years [33, 34, 36, 37, 52, 71, 79, 82–84]. A report concluded that soluble oligomers from several types of amyloids, including hIAPP, specifically increase lipid bilayer conductance, while fibrils and soluble low molecular weight species have no effect, suggesting that this may represent the common primary mechanism of pathogenesis in amyloid-related diseases [82]. It was also suggested that antimicrobial and amyloid peptides may share membrane-permeabilization mechanisms since these peptides share many characteristics. Indeed, for both peptides, a threshold peptide concentration is required to induce the oligomerization on the membrane surface which leads to the membrane damage. Recent studies on hIAPP and A $\beta$  suggested that the amyloid fibril formation on the membrane surface induces membrane damage [84–86]. It was postulated that it is the growth of hIAPP fibrils at the membrane surface rather than the formation of oligomeric species that causes hIAPP-induced membrane damage. Thus, as soon as the fibril develops on the membrane surface, the structural integrity of the membrane is compromised, possibly by forcing the curvature of the bilayer to an unfavourable angle or by uptake of lipids by hIAPP fibrils during fibril elongation at the membrane (Figure 4). Uptake of membrane phospholipids in amyloid that forms at the membrane, as observed from *in vitro* studies [72, 76], as well as *in vivo* studies [87], could indeed be an additional factor that contributes to membrane leakage. Coarse-grained molecular dynamics simulation results agree with this hypothesis and showed that amyloidogenic peptides, including hIAPP, fibrillate on the surface of the membrane, damaging the vesicles and promoting leakage [88]. In all of these hypotheses, the membranes have an important role as mediator or accelerator of the conversion of one hIAPP species to the other. However, membrane disruption by hIAPP is not the only mechanistic hypothesis that has been proposed regarding  $\beta$ -cell death linked to the presence of the peptide; other mechanisms will be discussed next.

## 7. hIAPP-Induced Cell Toxicity

A primary question resides in the main location of hIAPP in the islet of Langerhans. As it has been described that amyloid deposits that are involved in T2DM appear to be extracellular, some evidence has suggested that the amyloid formation actually starts intercellularly. Indeed, several studies, performed either on transgenic mice capable of secretion of hIAPP or on baboons, have reported that hIAPP fibrils or in prefibrillar states could be observed either freely in the intracellular medium, locating the development site of the peptide's oligomers in the endoplasmic reticulum (ER), Golgi, or secretory granules of the  $\beta$ -cells [27]. Localisation of fibrillar species intracellularly may be particularly important as it could be the root of extracellular deposition of amyloid fibrils on pancreatic  $\beta$ -cells and imply different mechanisms of cellular death. Since the presence and oligomerization of hIAPP is related to dysfunction followed by apoptosis of pancreatic  $\beta$ -cells, different cell factors have been investigated in order to determine the origin and mechanism of the decrease of  $\beta$ -cell mass in the pancreas. As the source of

amyloid formation is the misfolding of a specific peptide, studies have focused on the likely correlation between hIAPP synthesis and ER stress.

The ER serves many different functions in the cell, including assuring the correct native folding and posttranslational modification of peptides and proteins synthesized within the cell but also transportation of those molecules to the Golgi and secretory granules and release into the extracellular matrix. Those properties of the ER are well-balanced and regulated to avoid any misfolding and aggregation of proteins or peptides. However, this equilibrium can be disrupted by any ill-factors such as disturbances in redox regulation or calcium regulation and viral infection, applied on the ER. In particular, and as previously stated, insulin resistance results in a higher biosynthesis of insulin and thus of hIAPP. The consequent overproduction of protein and peptide in the  $\beta$ -cells then results in ER stress and triggers some malfunction in the folding process of the molecules, as it reaches overcapacity. The accumulation of misfolded protein in the cells along with ER stress cascades into the unfolded protein response (UPR). This regulation process involves simultaneously the production of chaperones to both assist the folding of proteins and limit their aggregation; reducing ER workload by inhibiting the protein synthesis triggering the UPR; enhancing the transportation of misfolded protein to the ubiquitin-proteasome system for degradation; and, as a last resort, triggering of the apoptosis process.

In spite of the various regulation responses to counteract the misfolding of proteins or peptides following ER stress, it is observed that hIAPP still autoassociates and forms toxic oligomers. This behaviour suggests that the prevention mechanism against hIAPP misfolding and therefore aggregation can be saturated and rendered noneffective. Different hypotheses regarding this fact can be evoked among which is the decrease in  $\beta$ -cell mass, also linked to apoptosis, enhancing once more the joint synthesis of insulin and hIAPP or the inability of the cell to eliminate cytotoxic oligomers once they are formed in the system.

To a larger extent, whether the cells are exposed to high concentration of hIAPP and/or if the responses to the peptide's aggregation are revealed to be inefficient,  $\beta$ -cell apoptosis is observed. Although mechanisms of the apoptotic behaviour of  $\beta$ -cells have yet to be fully elucidated, there have been some hypotheses that have been proposed concerning the different pathways and triggers that induce cell death. The first pathway, called the extrinsic pathway, involves extracellular factors such as membrane disruption, as described previously, or the binding to cell receptors. In particular, it has been described that exogenous or endogenous hIAPP could interact and thus activate the FAS receptor, present on the surface of cells. The activation of this "death receptor" results in apoptosis by in turn activating specific proteins such as caspase-3 [89]. The second pathway that has been described is the exogenous pathway and is linked to intracellular factors. Besides ER stress and UPR, mentioned before and mainly involved in pancreatic  $\beta$ -cells death, other factors disturbing the main function of ER are likely to enhance hIAPP oligomerization and cell death. Among those,

mitochondrial dysfunction, generation of oxygen free radical, defects in autophagy can also be mentioned [90].

Lastly, it has also been suggested that  $\beta$ -cell toxicity can be induced by an inflammatory response linked to hIAPP. Indeed, it has been found that the insulin resistance and production of hIAPP initiate an increase in the concentration of proinflammatory cytokines such as interleukin  $1\beta$  (IL- $1\beta$ ), which has been previously described to be cytotoxic to pancreatic islets of Langerhans [11, 27, 90–97].

## 8. Inhibition of hIAPP Fibril Formation

The amyloid pathway leading to fibrils is supposed to be responsible for  $\beta$ -cell death and T2DM. The development of inhibitors of amyloid formation is therefore of considerable interest in treating patients suffering from T2DM. However, although hIAPP is extremely amyloidogenic, most research has focused on other amyloidogenic proteins like A $\beta$  peptide or  $\alpha$ -synuclein, involved in Alzheimer's and Parkinson's disease, respectively. Different classes of inhibitors of hIAPP amyloid formation have been identified and have been tested for their ability to reduce amyloid cytotoxicity, using either cells or *in vitro* model systems [98–104].

First of all, insulin is one of the most effective inhibitors of hIAPP amyloid formation [71, 105–111]. However, little is known about the mechanism of this inhibition process. Some studies have demonstrated that insulin interacts with the growing hIAPP fibril [106, 108]. Another study showed that the mechanism of inhibition of hIAPP fibril formation by insulin is related to strong binding of the insulin  $\beta$ -chain to hIAPP [112]. A recent molecular modelling study has shown that it involves a helix-helix interaction between the helical insulin and the N-terminal helix of hIAPP. The interaction between insulin and hIAPP may stabilize hIAPP in a nonamyloidogenic monomeric state [111].

Another valuable class of inhibitors are the polyphenols, which are thought to interact with amyloidogenic proteins via aromatic  $\pi$ - $\pi$  interactions, although the precise mechanism is an issue still under debate [102, 113–116]. The molecule (–)-Epigallocatechin 3-Gallate (EGCG), a natural component of green tea, is of particular interest [117, 118]. Indeed, EGCG could have the ability to bind the unaggregated hIAPP, leading to the formation of noncytotoxic oligomers through another pathway. Nevertheless, the mechanism remains under some debate [114, 115]. In addition to its inhibitory activity, EGCG is one of the few molecules able to disaggregate preformed hIAPP amyloid fibrils in bulk solution [117, 118]. Effects are observed for a 2:1 hIAPP to EGCG ratio and even for a 5:1 IAPP to EGCG ratio [118]. On the contrary, a 1:1 hIAPP to EGCG ratio is necessary to increase the cell viability in the presence of EGCG. This molecule is then less effective in the presence of cell membranes than in solution [118]. Morin hydrate (2',3,4',5,7-pentahydroxyflavone) is a polyphenol as well, and more precisely a flavonoid. This molecule inhibits the amyloid formation of hIAPP, since the inhibition is effective from a 1:1 hIAPP to Morin hydrate ratio. The molecule acts in a ratio-dependent manner, because the effects on fibrils formation are even more pronounced than when the molecule is

introduced in excess [119]. As with EGCG, Morin hydrate is able to disaggregate preexisting fibrils at a one to one ratio. Unfortunately, all not hydroxyflavones are inhibitors of hIAPP amyloid formation. For example, Myricetin is an inhibitor of A $\beta$  amyloid formation but is totally ineffective against hIAPP at a one to one ratio. The number and position of hydroxyl groups may also play a role in the mechanism of inhibition. However, it has been demonstrated that Myricetin slows down hIAPP amyloid formation in a 10-fold excess, that is, at very high concentrations. Nevertheless, this molecule is effective *in vivo* and merits further consideration. Equally of interest is phenol red, a small aromatic polyphenol molecule, which elicits an effect on hIAPP fibril formation at a 4-fold excess of molecule *in vitro*. Its high efficiency in protecting pancreatic  $\beta$ -cells from the cytotoxic effect of hIAPP makes it a particularly attractive target molecule. In addition, phenol red is a nontoxic and noncarcinogenic compound, in contrast to many polycyclic aromatics [120]. Unfortunately, the mode of action of this class of molecules on the hIAPP amyloid formation is not known and no clear mechanism has yet been suggested. Their interest lies in their ability to not only inhibit the formation of amyloid fibrils but also disaggregate existing fibrils, protecting cells against hIAPP amyloid cytotoxicity.

A third class of molecules which are active against hIAPP fibrillation are molecular mimics. This particular strategy is based on molecular recognition thanks to similar molecular structure. For example, rat IAPP (rIAPP) whose sequence differs from hIAPP at only six positions is nonamyloidogenic *in vitro* or *in vivo*. rIAPP inhibits hIAPP amyloid formation in a dose-dependent manner. Even if the slowdown of the aggregation kinetics exists at 1:1 or 1:2 hIAPP to rIAPP ratios, the effect on fibril morphology and final quantity is only observed in a 5-fold or 10-fold excess of rIAPP [121]. As in the case of insulin, a mechanism involving interactions between helical N-terminal regions of the two peptides has been suggested. In addition, efficient inhibition of hIAPP amyloid formation has been demonstrated by the modified aromatic peptide fragment NFGAILSS in which phenylalanine was substituted with tyrosine (NYGAILSS) [33, 120]. Replacement of this aromatic amino acid leads to the formation of a nonamyloidogenic peptide, aromatic residues playing a role in accelerating the process of fibrillation. Unfortunately, this peptide proved to be cytotoxic toward  $\beta$ -cells and thus cannot be used as an inhibitor [120]. A study showed that Aib modified peptide induced a high inhibition effect on the full-length hIAPP [122]. More recently, another analogue of hIAPP was designed by N-methylation of the amide bonds at G24 and I26, called IAPP-GI [123]. This molecular mimic is a nonamyloidogenic hIAPP analog that is able to associate with hIAPP and thus inhibits the process of fibrillation and cytotoxicity. hIAPP-GI was found to be a remarkable inhibitor of hIAPP amyloid formation. In fact, a 1:1 hIAPP to hIAPP-GI ratio is sufficient to completely inhibit amyloid formation. Moreover, hIAPP-GI dissociates existing oligomers and fibrils and reverses their cytotoxicity [123].

Finally, an original compound, selenium phycocyanin (Se-PC), has been discovered as an inhibitor, acting in a dose-dependent manner [124]. The combination of Se and phycocyanin proved to be particularly effective at stopping



the fibrillation process of hIAPP. In fact, Se-PC is effective at even a 4-fold less concentration relative to hIAPP. A mode of action has been proposed according to which Se-PC interferes with hIAPP to interrupt the fibrillation process thanks to the formation of nanoscale oligomers. This compound is a good inhibitor of the  $\beta$ -cell death induced by hIAPP. Se-PC is thus a promising candidate for antidiabetes drug development due to its activity on the cell media.

Unfortunately and despite considerable effort, the mechanism of hIAPP amyloid formation is not understood nor the mode of action of most of the hIAPP amyloid inhibitors. It is even more difficult to understand these mechanisms as most of the experiments described refer to studies in bulk solution [125]. *In vitro* studies in diluted bulk solution do not adequately reflect the complexity of the cellular surrounding. Thus, the effect of inhibitors can be widely changed according to the medium. This is especially the case for the inhibitor EGCG whose inhibitory activity is lower than that in bulk solution [117]. AFM images confirm the presence of abundant fibrils at the phospholipid interface, even in a large excess of EGCG, whereas this molecule is very effective in bulk solution.

It is important to note that some publications referencing hIAPP inhibitors only draw conclusions from ThT assays. The monitoring of amyloid fibril formation via ThT experiments is a very convenient and common technique, but with a large disadvantage concerning the study of inhibitors. Indeed, many potential inhibitors can interfere with the ThT dye, thereby inhibiting the fluorescence of the probe and leading to false positive inhibitors. This is particularly the case for rifampicin or hydroxyflavones that interfere with ThT and might suggest that they inhibit hIAPP amyloid formation, which is contradicted by TEM images [119, 126]. It is thus necessary to check the results obtained by ThT fluorescence and to confirm the inhibitory activity with other techniques such as circular dichroism (CD), nuclear magnetic resonance (NMR), transmission electron microscopy (TEM), or atomic force microscopy (AFM).

## 9. Conclusions

Today, there are 382 million people living with diabetes. Diabetes is on the rise all over the world and medical practitioners are struggling to keep pace. Worldwide, one person dies as a consequence of diabetes (such as cardiovascular disease, kidney failure, and lower limb amputation) every 6 seconds. In this regard, there is currently great interest in the field of islet amyloid. However there are important outstanding issues. Important questions that remain to be answered include the following. What is the mechanism of hIAPP fibril formation *in vivo*? What are the morphology and structure of hIAPP oligomers and hIAPP fibrils *in vivo*? Why do oligomers and amyloidogenic protein form? What is the exact nature of the toxic species? Much of the research work on hIAPP-membrane structure and hIAPP-membrane interactions is performed on membrane models. Progresses have been made and the results from the biophysical studies have generated some hypotheses. However, an important

challenge will be now to connect these biophysical results with the *in vivo* experiments.

## Conflict of Interests

The authors declare that there is no conflict of interests regarding the publication of this paper.

## Acknowledgments

The authors thank Professor Olivier Lequin and Dr. Cillian Byrne for reading this paper.

## References

- [1] F. Chiti and C. M. Dobson, "Protein misfolding, functional amyloid, and human disease," *Annual Review of Biochemistry*, vol. 75, pp. 333–366, 2006.
- [2] J. D. Sipe, "Amyloidosis," *Critical Reviews in Clinical Laboratory Sciences*, vol. 31, no. 4, pp. 325–354, 1994.
- [3] D. J. Selkoe, "Folding proteins in fatal ways," *Nature*, vol. 426, no. 6968, pp. 900–904, 2003.
- [4] J. W. M. Höppener, B. Ahrén, and C. J. M. Lips, "Islet amyloid and type 2 diabetes mellitus," *The New England Journal of Medicine*, vol. 343, no. 6, pp. 411–419, 2000.
- [5] G. G. Glenner, E. D. Eanes, H. A. Bladen, R. P. Linke, and J. D. Termine, " $\beta$ -pleated sheet fibrils. A comparison of native amyloid with synthetic protein fibrils," *Journal of Histochemistry & Cytochemistry*, vol. 22, no. 12, pp. 1141–1158, 1974.
- [6] S. Luca, W.-M. Yau, R. Leapman, and R. Tycko, "Peptide conformation and supramolecular organization in amylin fibrils: constraints from solid-state NMR," *Biochemistry*, vol. 46, no. 47, pp. 13505–13522, 2007.
- [7] G. J. S. Cooper, A. C. Willis, A. Clark, R. C. Turner, R. B. Sim, and K. B. M. Reid, "Purification and characterization of a peptide from amyloid-rich pancreases of type 2 diabetic patients," *Proceedings of the National Academy of Sciences of the United States of America*, vol. 84, no. 23, pp. 8628–8632, 1987.
- [8] P. Westermark, C. Wernstedt, E. Wilander, D. W. Hayden, T. D. O'Brien, and K. H. Johnson, "Amyloid fibrils in human insulinoma and islets of Langerhans of the diabetic cat are derived from a neuropeptide-like protein also present in normal islet cells," *Proceedings of the National Academy of Sciences of the United States of America*, vol. 84, no. 11, pp. 3881–3885, 1987.
- [9] P. Westermark, C. Wernstedt, E. Wilander, and K. Sletten, "A novel peptide in the calcitonin gene related peptide family as an amyloid fibril protein in the endocrine pancreas," *Biochemical and Biophysical Research Communications*, vol. 140, no. 3, pp. 827–831, 1986.
- [10] G. J. S. Cooper, B. Leighton, G. D. Dimitriadis et al., "Amylin found in amyloid deposits in human type 2 diabetes mellitus may be a hormone that regulates glycogen metabolism in skeletal muscle," *Proceedings of the National Academy of Sciences of the United States of America*, vol. 85, no. 20, pp. 7763–7766, 1988.
- [11] P. Westermark, A. Andersson, and G. T. Westermark, "Islet amyloid polypeptide, islet amyloid, and diabetes mellitus," *Physiological Reviews*, vol. 91, no. 3, pp. 795–826, 2011.
- [12] M. Samsom, L. A. Szarka, M. Camilleri, A. Vella, A. R. Zinsmeister, and R. A. Rizza, "Pramlintide, an amylin analog,

- selectively delays gastric emptying: potential role of vagal inhibition," *American Journal of Physiology: Gastrointestinal and Liver Physiology*, vol. 278, no. 6, pp. G946–G951, 2000.
- [13] I. Chapman, B. Parker, S. Doran et al., "Effect of pramlintide on satiety and food intake in obese subjects and subjects with type 2 diabetes," *Diabetologia*, vol. 48, no. 5, pp. 838–848, 2005.
- [14] I. Chapman, B. Parker, S. Doran et al., "Low-dose pramlintide reduced food intake and meal duration in healthy, normal-weight subjects," *Obesity*, vol. 15, no. 5, pp. 1179–1186, 2007.
- [15] B. Åkesson, G. Panagiotidis, P. Westermark, and I. Lundquist, "Islet amyloid polypeptide inhibits glucagon release and exerts a dual action on insulin release from isolated islets," *Regulatory Peptides*, vol. 111, no. 1–3, pp. 55–60, 2003.
- [16] P. A. Rushing, M. M. Hagan, R. J. Seeley et al., "Inhibition of central amylin signaling increases food intake and body adiposity in rats," *Endocrinology*, vol. 142, no. 11, pp. 5035–5038, 2001.
- [17] R. A. Ritzel, J. J. Meier, C.-Y. Lin, J. D. Veldhuis, and P. C. Butler, "Human islet amyloid polypeptide oligomers disrupt cell coupling, induce apoptosis, and impair insulin secretion in isolated human islets," *Diabetes*, vol. 56, no. 1, pp. 65–71, 2007.
- [18] P. J. Wookey, C. Tikellis, D. U. He-Cheng, H.-F. Qin, P. M. Sexton, and M. E. Cooper, "Amylin binding in rat renal cortex, stimulation of adenyllyl cyclase, and activation of plasma renin," *The American Journal of Physiology*, vol. 270, no. 2, pp. F289–F294, 1996.
- [19] P. M. Sexton, G. Paxinos, X.-F. Huang, and F. A. O. Mendelsohn, "In vitro autoradiographic localization of calcitonin binding sites in human medulla oblongata," *Journal of Comparative Neurology*, vol. 341, no. 4, pp. 449–463, 1994.
- [20] G. Paxinos, S. Y. Chai, G. Christopoulos et al., "In vitro autoradiographic localization of calcitonin and amylin binding sites in monkey brain," *Journal of Chemical Neuroanatomy*, vol. 27, no. 4, pp. 217–236, 2004.
- [21] M. Stridsberg, S. Sandler, and E. Wilander, "Cosecretion of islet amyloid polypeptide (IAPP) and insulin from isolated rat pancreatic islets following stimulation or inhibition of  $\beta$ -cell function," *Regulatory Peptides*, vol. 45, no. 3, pp. 363–370, 1993.
- [22] A. Lukinius, E. Wilander, G. T. Westermark, U. Engstrom, and P. Westermark, "Co-localization of islet amyloid polypeptide and insulin in the B cell secretory granules of the human pancreatic islets," *Diabetologia*, vol. 32, no. 4, pp. 240–244, 1989.
- [23] S. E. Kahn, D. A. D'Alessio, M. W. Schwartz et al., "Evidence of cosecretion of islet amyloid polypeptide and insulin by  $\beta$ -cells," *Diabetes*, vol. 39, no. 5, pp. 634–638, 1990.
- [24] M. Furuta, H. Yano, A. Zhou et al., "Defective prohormone processing and altered pancreatic islet morphology in mice lacking active SPC2," *Proceedings of the National Academy of Sciences of the United States of America*, vol. 94, no. 13, pp. 6646–6651, 1997.
- [25] M. Marcinkiewicz, D. Ramla, N. G. Seidah, and M. Chrétien, "Developmental expression of the prohormone convertases PC1 and PC2 in mouse pancreatic islets," *Endocrinology*, vol. 135, no. 4, pp. 1651–1660, 1994.
- [26] L. Marzban, C. J. Rhodes, D. F. Steiner, L. Haataja, P. A. Halban, and C. B. Verchere, "Impaired NH<sub>2</sub>-terminal processing of human proislet amyloid polypeptide by the prohormone convertase PC2 leads to amyloid formation and cell death," *Diabetes*, vol. 55, no. 8, pp. 2192–2201, 2006.
- [27] J. F. Paulsson, A. Andersson, P. Westermark, and G. T. Westermark, "Intracellular amyloid-like deposits contain unprocessed pro-islet amyloid polypeptide (proIAPP) in beta cells of transgenic mice overexpressing the gene for human IAPP and transplanted human islets," *Diabetologia*, vol. 49, no. 6, pp. 1237–1246, 2006.
- [28] C. E. Higham, E. T. A. S. Jaikaran, P. E. Fraser, M. Gross, and A. Clark, "Preparation of synthetic human islet amyloid polypeptide (IAPP) in a stable conformation to enable study of conversion to amyloid-like fibrils," *FEBS Letters*, vol. 470, no. 1, pp. 55–60, 2000.
- [29] C. Goldsbury, K. Goldie, J. Pellaud et al., "Amyloid fibril formation from full-length and fragments of amylin," *Journal of Structural Biology*, vol. 130, no. 2–3, pp. 352–362, 2000.
- [30] R. Kaye, J. Bernhagen, N. Greenfield et al., "Conformational transitions of islet amyloid polypeptide (IAPP) in amyloid formation *in vitro*," *Journal of Molecular Biology*, vol. 287, no. 4, pp. 781–796, 1999.
- [31] R. Kaye, A. Pensalfini, L. Margol et al., "Annular protofibrils area structurally and functionally distinct type of amyloid oligomer," *The Journal of Biological Chemistry*, vol. 284, no. 7, pp. 4230–4237, 2009.
- [32] J. D. Knight, J. A. Hebda, and A. D. Miranker, "Conserved and cooperative assembly of membrane-bound  $\alpha$ -helical states of islet amyloid polypeptide," *Biochemistry*, vol. 45, no. 31, pp. 9496–9508, 2006.
- [33] Y. Porat, A. Stepsensky, F.-X. Ding, F. Naider, and E. Gazit, "Completely different amyloidogenic potential of nearly identical peptide fragments," *Biopolymers*, vol. 69, no. 2, pp. 161–164, 2003.
- [34] J. D. Green, L. Kreplak, C. Goldsbury et al., "Atomic force microscopy reveals defects within mica supported lipid bilayers induced by the amyloidogenic human amylin peptide," *Journal of Molecular Biology*, vol. 342, no. 3, pp. 877–887, 2004.
- [35] J. D. Green, C. Goldsbury, J. Kistler, G. J. S. Cooper, and U. Aebi, "Human amylin oligomer growth and fibril elongation define two distinct phases in amyloid formation," *The Journal of Biological Chemistry*, vol. 279, no. 13, pp. 12206–12212, 2004.
- [36] M. Anguiano, R. J. Nowak, and P. T. Lansbury Jr., "Protofibrillar islet amyloid polypeptide permeabilizes synthetic vesicles by a pore-like mechanism that may be relevant to type II diabetes," *Biochemistry*, vol. 41, no. 38, pp. 11338–11343, 2002.
- [37] J. Janson, R. H. Ashley, D. Harrison, S. McIntyre, and P. C. Butler, "The mechanism of islet amyloid polypeptide toxicity is membrane disruption by intermediate-sized toxic amyloid particles," *Diabetes*, vol. 48, no. 3, pp. 491–498, 1999.
- [38] C. S. Goldsbury, G. J. S. Cooper, K. N. Goldie et al., "Polymorphic fibrillar assembly of human amylin," *Journal of Structural Biology*, vol. 119, no. 1, pp. 17–27, 1997.
- [39] J. J. W. Wiltzius, S. A. Sievers, M. R. Sawaya et al., "Atomic structure of the cross- $\beta$  spine of islet amyloid polypeptide (amylin)," *Protein Science*, vol. 17, no. 9, pp. 1467–1474, 2008.
- [40] S. A. Jayasinghe and R. Langen, "Lipid membranes modulate the structure of islet amyloid polypeptide," *Biochemistry*, vol. 44, no. 36, pp. 12113–12119, 2005.
- [41] L. Caillon, O. Lequin, and L. Khemtémourian, "Evaluation of membrane models and their composition for islet amyloid polypeptide-membrane aggregation," *Biochimica et Biophysica Acta—Biomembranes*, vol. 1828, no. 9, pp. 2091–2098, 2013.
- [42] S. M. Patil, S. Xu, S. R. Sheftic, and A. T. Alexandrescu, "Dynamic alpha-helix structure of micelle-bound human amylin," *The Journal of Biological Chemistry*, vol. 284, no. 18, pp. 11982–11991, 2009.

- [43] R. P. R. Nanga, J. R. Brender, S. Vivekanandan, and A. Ramamoorthy, "Structure and membrane orientation of IAPP in its natively amidated form at physiological pH in a membrane environment," *Biochimica et Biophysica Acta*, vol. 1808, no. 10, pp. 2337–2342, 2011.
- [44] A. Quist, I. Doudevski, H. Lin et al., "Amyloid ion channels: a common structural link for protein-misfolding disease," *Proceedings of the National Academy of Sciences of the United States of America*, vol. 102, no. 30, pp. 10427–10432, 2005.
- [45] S. B. Padrick and A. D. Miranker, "Islet amyloid: phase partitioning and secondary nucleation are central to the mechanism of fibrillogenesis," *Biochemistry*, vol. 41, no. 14, pp. 4694–4703, 2002.
- [46] H. Naiki, K. Higuchi, M. Hosokawa, and T. Takeda, "Fluorometric determination of amyloid fibrils in vitro using the fluorescent dye, thioflavine T," *Analytical Biochemistry*, vol. 177, no. 2, pp. 244–249, 1989.
- [47] P. J. Marek, V. Patsalo, D. F. Green, and D. P. Raleigh, "Ionic strength effects on amyloid formation by amylin are a complicated interplay among debye screening, ion selectivity, and Hofmeister effects," *Biochemistry*, vol. 51, no. 43, pp. 8478–8490, 2012.
- [48] L. Khemtémourian, E. Doménech, J. P. F. Doux, M. C. Koorengevel, and J. A. Killian, "Low pH Acts as inhibitor of membrane damage induced by human islet amyloid polypeptide," *Journal of the American Chemical Society*, vol. 133, no. 39, pp. 15598–15604, 2011.
- [49] T. Sanke, G. I. Bell, C. Sample, A. H. Rubenstein, and D. F. Steiner, "An islet amyloid peptide is derived from an 89-amino acid precursor by proteolytic processing," *Journal of Biological Chemistry*, vol. 263, no. 33, pp. 17243–17246, 1988.
- [50] P. Westermark, U. Engstrom, K. H. Johnson, G. T. Westermark, and C. Betsholtz, "Islet amyloid polypeptide: pinpointing amino acid residues linked to amyloid fibril formation," *Proceedings of the National Academy of Sciences of the United States of America*, vol. 87, no. 13, pp. 5036–5040, 1990.
- [51] C. Betsholtz, L. Christmansson, U. Engstrom et al., "Sequence divergence in a specific region of islet amyloid polypeptide (IAPP) explains differences in islet amyloid formation between species," *FEBS Letters*, vol. 251, no. 1-2, pp. 261–264, 1989.
- [52] M. F. M. Engel, H. Yigittop, R. C. Elgersma et al., "Islet amyloid polypeptide inserts into phospholipid monolayers as monomer," *Journal of Molecular Biology*, vol. 356, no. 3, pp. 783–789, 2006.
- [53] L. Khemtémourian, M. F. M. Engel, R. M. J. Liskamp, J. W. M. Höppener, and J. A. Killian, "The N-terminal fragment of human islet amyloid polypeptide is non-fibrillogenic in the presence of membranes and does not cause leakage of bilayers of physiologically relevant lipid composition," *Biochimica et Biophysica Acta: Biomembranes*, vol. 1798, no. 9, pp. 1805–1811, 2010.
- [54] M. R. Nilsson and D. P. Raleigh, "Analysis of amylin cleavage products provides new insights into the amyloidogenic region of human amylin," *Journal of Molecular Biology*, vol. 294, no. 5, pp. 1375–1385, 1999.
- [55] R. P. R. Nanga, J. R. Brender, J. Xu, G. Veglia, and A. Ramamoorthy, "Structures of rat and human islet amyloid polypeptide IAPP1-19 in micelles by NMR spectroscopy," *Biochemistry*, vol. 47, no. 48, pp. 12689–12697, 2008.
- [56] E. T. A. S. Jaikaran, C. E. Higham, L. C. Serpell et al., "Identification of a novel human islet amyloid polypeptide  $\beta$ -sheet domain and factors influencing fibrillogenesis," *Journal of Molecular Biology*, vol. 308, no. 3, pp. 515–525, 2001.
- [57] A. Abedini and D. P. Raleigh, "The role of His-18 in amyloid formation by human islet amyloid polypeptide," *Biochemistry*, vol. 44, no. 49, pp. 16284–16291, 2005.
- [58] S. M. Tracz, A. Abedini, M. Driscoll, and D. P. Raleigh, "Role of aromatic interactions in amyloid formation by peptides derived from human amylin," *Biochemistry*, vol. 43, no. 50, pp. 15901–15908, 2004.
- [59] P. Marek, A. Abedini, B. Song et al., "Aromatic interactions are not required for amyloid fibril formation by islet amyloid polypeptide but do influence the rate of fibril formation and fibril morphology," *Biochemistry*, vol. 46, no. 11, pp. 3255–3261, 2007.
- [60] L.-H. Tu and D. P. Raleigh, "Role of aromatic interactions in amyloid formation by islet amyloid polypeptide," *Biochemistry*, vol. 52, no. 2, pp. 333–342, 2013.
- [61] S. Sakagashira, H. J. Hiddinga, K. Tateishi et al., "S20G mutant amylin exhibits increased in vitro amyloidogenicity and increased intracellular cytotoxicity compared to wild-type amylin," *The American Journal of Pathology*, vol. 157, no. 6, pp. 2101–2109, 2000.
- [62] B. W. Koo and A. D. Miranker, "Contribution of the intrinsic disulfide to the assembly mechanism of islet amyloid," *Protein Science*, vol. 14, no. 1, pp. 231–239, 2005.
- [63] A. Abedini and D. P. Raleigh, "Destabilization of human IAPP amyloid fibrils by proline mutations outside of the putative amyloidogenic domain: is there a critical amyloidogenic domain in human IAPP?" *Journal of Molecular Biology*, vol. 355, no. 2, pp. 274–281, 2006.
- [64] J. Green, C. Goldsbury, T. Mini et al., "Full-length rat amylin forms fibrils following substitution of single residues from human amylin," *Journal of Molecular Biology*, vol. 326, no. 4, pp. 1147–1156, 2003.
- [65] J. F. Paulsson and G. T. Westermark, "Aberrant processing of human proislet amyloid polypeptide results in increased amyloid formation," *Diabetes*, vol. 54, no. 7, pp. 2117–2125, 2005.
- [66] I. T. Yonemoto, G. J. A. Kroon, H. J. Dyson, W. E. Balch, and J. W. Kelly, "Amylin proprotein processing generates progressively more amyloidogenic peptides that initially sample the helical state," *Biochemistry*, vol. 47, no. 37, pp. 9900–9910, 2008.
- [67] M. Krampert, J. Bernhagen, J. Schmucker et al., "Amyloidogenicity of recombinant human pro-islet amyloid polypeptide (ProIAPP)," *Chemistry & Biology*, vol. 7, no. 11, pp. 855–871, 2000.
- [68] F. Meng, A. Abedini, B. Song, and D. P. Raleigh, "Amyloid formation by pro-islet amyloid polypeptide processing intermediates: Examination of the role of protein heparan sulfate interactions and implications for islet amyloid formation in type 2 diabetes," *Biochemistry*, vol. 46, no. 43, pp. 12091–12099, 2007.
- [69] L. Khemtémourian, G. L. Casarramona, D. P. L. Suylen et al., "Impaired processing of human pro-islet amyloid polypeptide is not a causative factor for fibril formation or membrane damage in vitro," *Biochemistry*, vol. 48, no. 46, pp. 10918–10925, 2009.
- [70] A. N. Roberts, B. Leighton, J. A. Todd et al., "Molecular and functional characterization of amylin, a peptide associated with type 2 diabetes mellitus," *Proceedings of the National Academy of Sciences of the United States of America*, vol. 86, no. 24, pp. 9662–9666, 1989.

- [71] J. D. Knight and A. D. Miranker, "Phospholipid catalysis of diabetic amyloid assembly," *Journal of Molecular Biology*, vol. 341, no. 5, pp. 1175–1187, 2004.
- [72] E. Sparr, M. F. M. Engel, D. V. Sakharov et al., "Islet amyloid polypeptide-induced membrane leakage involves uptake of lipids by forming amyloid fibers," *FEBS Letters*, vol. 577, no. 1–2, pp. 117–120, 2004.
- [73] K. Sasahara, K. Morigaki, T. Okazaki, and D. Hamada, "Binding of islet amyloid polypeptide to supported lipid bilayers and amyloid aggregation at the membranes," *Biochemistry*, vol. 51, no. 35, pp. 6908–6919, 2012.
- [74] E. Ahmad, A. Ahmad, S. Singh, M. Arshad, A. H. Khan, and R. H. Khan, "A mechanistic approach for islet amyloid polypeptide aggregation to develop anti-amyloidogenic agents for type-2 diabetes," *Biochimie*, vol. 93, no. 5, pp. 793–805, 2011.
- [75] L. Khemtémourian, M. F. M. Engel, J. A. W. Kruijtzter, J. W. M. Höppener, R. M. J. Liskamp, and J. A. Killian, "The role of the disulfide bond in the interaction of islet amyloid polypeptide with membranes," *European Biophysics Journal*, vol. 39, no. 9, pp. 1359–1364, 2010.
- [76] H. Zhao, E. K. J. Tuominen, and P. K. J. Kinnunen, "Formation of amyloid fibers triggered by phosphatidylserine-containing membranes," *Biochemistry*, vol. 43, no. 32, pp. 10302–10307, 2004.
- [77] M. F. M. Sciacca, J. R. Brender, D.-K. Lee, and A. Ramamoorthy, "Phosphatidylethanolamine enhances amyloid fiber-dependent membrane fragmentation," *Biochemistry*, vol. 51, no. 39, pp. 7676–7684, 2012.
- [78] N. Arispe, E. Rojas, and H. B. Pollard, "Alzheimer disease amyloid  $\beta$  protein forms calcium channels in bilayer-membranes: blockade by tromethamine and aluminum," *Proceedings of the National Academy of Sciences of the United States of America*, vol. 90, no. 2, pp. 567–571, 1993.
- [79] T. A. Mirzabekov, M.-C. Lin, and B. L. Kagan, "Pore formation by the cytotoxic islet amyloid peptide amylin," *The Journal of Biological Chemistry*, vol. 271, no. 4, pp. 1988–1992, 1996.
- [80] M. Kawahara, Y. Kuroda, N. Arispe, and E. Rojas, "Alzheimer's  $\beta$ -amyloid, human islet amylin, and priori protein fragment evoke intracellular free calcium elevations by a common mechanism in a hypothalamic GnRH neuronal cell line," *The Journal of Biological Chemistry*, vol. 275, no. 19, pp. 14077–14083, 2000.
- [81] N. Arispe, H. B. Pollard, and E. Rojas, "Giant multilevel cation channels formed by Alzheimer-disease amyloid beta-protein [a-beta-P-(1-40)] in bilayer-membranes," *Proceedings of the National Academy of Sciences of the United States of America*, vol. 90, no. 22, pp. 10573–10577, 1993.
- [82] R. Kayed, Y. Sokolov, B. Edmonds et al., "Permeabilization of lipid bilayers is a common conformation-dependent activity of soluble amyloid oligomers in protein misfolding diseases," *The Journal of Biological Chemistry*, vol. 279, no. 45, pp. 46363–46366, 2004.
- [83] R. Kayed, E. Head, J. L. Thompson et al., "Common structure of soluble amyloid oligomers implies common mechanism of pathogenesis," *Science*, vol. 300, no. 5618, pp. 486–489, 2003.
- [84] M. F. M. Engel, L. Khemtémourian, C. C. Kleijer et al., "Membrane damage by human islet amyloid polypeptide through fibril growth at the membrane," *Proceedings of the National Academy of Sciences of the United States of America*, vol. 105, no. 16, pp. 6033–6038, 2008.
- [85] A. Jan, O. Adolfsson, I. Allaman et al., "A $\beta$ 42 neurotoxicity is mediated by ongoing nucleated polymerization process rather than by discrete A $\beta$ 42 species," *The Journal of Biological Chemistry*, vol. 286, no. 10, pp. 8585–8596, 2011.
- [86] L. Khemtémourian, J. A. Killian, J. W. Höppener, and M. F. M. Engel, "Recent insights in islet amyloid polypeptide-induced membrane disruption and its role in  $\beta$ -cell death in type 2 diabetes mellitus," *Experimental Diabetes Research*, vol. 2008, Article ID 421287, 9 pages, 2008.
- [87] G. P. Gellermann, T. R. Appel, A. Tannert et al., "Raft lipids as common components of human extracellular amyloid fibrils," *Proceedings of the National Academy of Sciences of the United States of America*, vol. 102, no. 18, pp. 6297–6302, 2005.
- [88] R. Friedman, R. Pellarin, and A. Caflich, "Amyloid aggregation on lipid bilayers and its impact on membrane permeability," *Journal of Molecular Biology*, vol. 387, no. 2, pp. 407–415, 2009.
- [89] E. Law, S. Lu, T. J. Kieffer et al., "Differences between amyloid toxicity in alpha and beta cells in human and mouse islets and the role of caspase-3," *Diabetologia*, vol. 53, no. 7, pp. 1415–1427, 2010.
- [90] J. F. Rivera, T. Gurlo, M. Daval et al., "Human-IAPP disrupts the autophagy/lysosomal pathway in pancreatic B-cells: Protective role of p62-positive cytoplasmic inclusions," *Cell Death and Differentiation*, vol. 18, no. 3, pp. 415–426, 2011.
- [91] S. Zhang, J. Liu, M. Dragunow, and G. J. S. Cooper, "Fibrillogenic amylin evokes islet  $\beta$ -cell apoptosis through linked activation of a caspase cascade and JNK1," *The Journal of Biological Chemistry*, vol. 278, no. 52, pp. 52810–52819, 2003.
- [92] S. L. Subramanian, S. Zraika, K. Aston-Mourney, J. Udayasankar, and S. E. Kahn, "CJUN N-terminal kinase (JNK) activation mediates islet amyloid-induced beta cell apoptosis in cultured human islet amyloid polypeptide transgenic mouse islets," *Diabetologia*, vol. 55, no. 1, pp. 166–174, 2012.
- [93] Y. J. Park, S. Lee, T. J. Kieffer et al., "Deletion of *Fas* protects islet beta cells from cytotoxic effects of human islet amyloid polypeptide," *Diabetologia*, vol. 55, no. 4, pp. 1035–1047, 2012.
- [94] C. J. Huang, T. Gurlo, L. Haataja et al., "Calcium-activated calpain-2 is a mediator of beta cell dysfunction and apoptosis in type 2 diabetes," *The Journal of Biological Chemistry*, vol. 285, no. 1, pp. 339–348, 2010.
- [95] S. Zraika, R. L. Hull, J. Udayasankar et al., "Oxidative stress is induced by islet amyloid formation and time-dependently mediates amyloid-induced beta cell apoptosis," *Diabetologia*, vol. 52, no. 4, pp. 626–635, 2009.
- [96] C. Westwell-Roper, D. L. Dai, G. Soukhatcheva et al., "IL-1 blockade attenuates islet amyloid polypeptide-induced proinflammatory cytokine release and pancreatic islet graft dysfunction," *Journal of Immunology*, vol. 187, no. 5, pp. 2755–2765, 2011.
- [97] S. L. Masters, A. Dunne, S. L. Subramanian et al., "Activation of the NLRP3 inflammasome by islet amyloid polypeptide provides a mechanism for enhanced IL-1 $\beta$  2 in type 2 diabetes," *Nature Immunology*, vol. 11, no. 10, pp. 897–904, 2010.
- [98] M. M. Alhamadsheh, S. Connelly, A. Cho et al., "Potent kinetic stabilizers that prevent transthyretin-mediated cardiomyocyte proteotoxicity," *Science Translational Medicine*, vol. 3, no. 97, 2011.
- [99] J. Bieschke, J. Russ, R. P. Friedrich et al., "EGCG remodels mature  $\alpha$ -synuclein and amyloid- $\beta$  fibrils and reduces cellular toxicity," *Proceedings of the National Academy of Sciences of the United States of America*, vol. 107, no. 17, pp. 7710–7715, 2010.
- [100] A. K. Buell, E. K. Esbjörner, P. J. Riss et al., "Probing small molecule binding to amyloid fibrils," *Physical Chemistry Chemical Physics*, vol. 13, no. 45, pp. 20044–20052, 2011.



- [101] M. Daval, S. Bedrood, T. Gurlo et al., "The effect of curcumin on human islet amyloid polypeptide misfolding and toxicity," *Amyloid*, vol. 17, no. 3-4, pp. 118-128, 2010.
- [102] E. Gazit, "A possible role for  $\pi$ -stacking in the self-assembly of amyloid fibrils," *The FASEB Journal*, vol. 16, no. 1, pp. 77-83, 2002.
- [103] M. Necula, R. Kaye, S. Milton, and C. G. Glabe, "Small molecule inhibitors of aggregation indicate that amyloid  $\beta$  oligomerization and fibrillization pathways are independent and distinct," *Journal of Biological Chemistry*, vol. 282, no. 14, pp. 10311-10324, 2007.
- [104] D. Sellin, L.-M. Yan, A. Kapurniotu, and R. Winter, "Suppression of IAPP fibrillation at anionic lipid membranes via IAPP-derived amyloid inhibitors and insulin," *Biophysical Chemistry*, vol. 150, no. 1-3, pp. 73-79, 2010.
- [105] P. Westermark, Z.-C. Li, G. T. Westermark, A. Leckström, and D. F. Steiner, "Effects of beta cell granule components on human islet amyloid polypeptide fibril formation," *FEBS Letters*, vol. 379, no. 3, pp. 203-206, 1996.
- [106] E. T. A. S. Jaikaran, M. R. Nilsson, and A. Clark, "Pancreatic  $\beta$ -cell granule peptides form heteromolecular complexes which inhibit islet amyloid polypeptide fibril formation," *Biochemical Journal*, vol. 377, no. 3, pp. 709-716, 2004.
- [107] Y. C. Kudva, C. Mueske, P. C. Butler, and N. L. Eberhardt, "A novel assay in vitro of human islet amyloid polypeptide amyloidogenesis and effects of insulin secretory vesicle peptides on amyloid formation," *Biochemical Journal*, vol. 331, no. 3, pp. 809-813, 1998.
- [108] J. D. Knight, J. A. Williamson, and A. D. Miranker, "Interaction of membrane-bound islet amyloid polypeptide with soluble and crystalline insulin," *Protein Science*, vol. 17, no. 10, pp. 1850-1856, 2008.
- [109] W. Cui, J.-W. Ma, P. Lei et al., "Insulin is a kinetic but not a thermodynamic inhibitor of amylin aggregation," *FEBS Journal*, vol. 276, no. 12, pp. 3365-3371, 2009.
- [110] S. Janciauskiene, S. Eriksson, E. Carlemalm, and B. Ahrén, "B cell granule peptides affect human islet amyloid polypeptide (IAPP) fibril formation in vitro," *Biochemical and Biophysical Research Communications*, vol. 236, no. 3, pp. 580-585, 1997.
- [111] A. C. Susa, C. Wu, S. L. Bernstein et al., "Defining the molecular basis of amyloid inhibitors: human islet amyloid polypeptide-insulin interactions," *Journal of the American Chemical Society*, vol. 136, no. 37, pp. 12912-12919, 2014.
- [112] S. Gilead, H. Wolfenson, and E. Gazit, "Molecular mapping of the recognition interface between the islet amyloid polypeptide and insulin," *Angewandte Chemie—International Edition*, vol. 45, no. 39, pp. 6476-6480, 2006.
- [113] A. H. Armstrong, J. Chen, A. F. McKoy, and M. H. Hecht, "Mutations that replace aromatic side chains promote aggregation of the Alzheimers A $\beta$  peptide," *Biochemistry*, vol. 50, no. 19, pp. 4058-4067, 2011.
- [114] D. E. Ehrnhoefer, J. Bieschke, A. Boeddrich et al., "EGCG redirects amyloidogenic polypeptides into unstructured, off-pathway oligomers," *Nature Structural & Molecular Biology*, vol. 15, no. 6, pp. 558-566, 2008.
- [115] S. A. Hudson, H. Ecroyd, F. C. Dehle, I. F. Musgrave, and J. A. Carver, "(-)-Epigallocatechin-3-gallate (EGCG) maintains  $\kappa$ -casein in its pre-fibrillar state without redirecting its aggregation pathway," *Journal of Molecular Biology*, vol. 392, no. 3, pp. 689-700, 2009.
- [116] J. M. Lopez del Amo, U. Fink, M. Dasari et al., "Structural properties of EGCG-induced, nontoxic Alzheimer's disease A $\beta$  oligomers," *Journal of Molecular Biology*, vol. 421, no. 4-5, pp. 517-524, 2012.
- [117] M. F. M. Engel, C. C. Vandenakker, M. Schleegeer, K. P. Velikov, G. H. Koenderink, and M. Bonn, "The polyphenol EGCG inhibits amyloid formation less efficiently at phospholipid interfaces than in bulk solution," *Journal of the American Chemical Society*, vol. 134, no. 36, pp. 14781-14788, 2012.
- [118] F. Meng, A. Abedini, A. Plesner, C. B. Verchere, and D. P. Raleigh, "The Flavanol (-)-epigallocatechin 3-gallate inhibits amyloid formation by islet amyloid polypeptide, disaggregates amyloid fibrils, and protects cultured cells against IAPP-induced toxicity," *Biochemistry*, vol. 49, no. 37, pp. 8127-8133, 2010.
- [119] H. Noor, P. Cao, and D. P. Raleigh, "Morin hydrate inhibits amyloid formation by islet amyloid polypeptide and disaggregates amyloid fibers," *Protein Science*, vol. 21, no. 3, pp. 373-382, 2012.
- [120] Y. Porat, Y. Mazor, S. Efrat, and E. Gazit, "Inhibition of islet amyloid polypeptide fibril formation: a potential role for heteroaromatic interactions," *Biochemistry*, vol. 43, no. 45, pp. 14454-14462, 2004.
- [121] P. Cao, F. Meng, A. Abedini, and D. P. Raleigh, "The ability of rodent islet amyloid polypeptide to inhibit amyloid formation by human islet amyloid polypeptide has important implications for the mechanism of amyloid formation and the design of inhibitors," *Biochemistry*, vol. 49, no. 5, pp. 872-881, 2010.
- [122] S. Gilead and E. Gazit, "Inhibition of amyloid fibril formation by peptide analogues modified with alpha-aminoisobutyric acid," *Angewandte Chemie International Edition*, vol. 43, no. 31, pp. 4041-4044, 2004.
- [123] L.-M. Yan, M. Taterek-Nossol, A. Velkova, A. Kazantzis, and A. Kapurniotu, "Design of a mimic of nonamyloidogenic and bioactive human islet amyloid polypeptide (IAPP) as nanomolar affinity inhibitor of IAPP cytotoxic fibrillogenesis," *Proceedings of the National Academy of Sciences of the United States of America*, vol. 103, no. 7, pp. 2046-2051, 2006.
- [124] X. Li, L. Ma, W. Zheng, and T. Chen, "Inhibition of islet amyloid polypeptide fibril formation by selenium-containing phyco-cyanin and prevention of beta cell apoptosis," *Biomaterials*, vol. 35, no. 30, pp. 8596-8604, 2014.
- [125] J. Seeliger, A. Werkmüller, and R. Winter, "Macromolecular crowding as a suppressor of human IAPP fibril formation and cytotoxicity," *PLoS ONE*, vol. 8, no. 7, Article ID e69652, 2013.
- [126] F. Meng, P. Marek, K. J. Potter, C. B. Verchere, and D. P. Raleigh, "Rifampicin does not prevent amyloid fibril formation by human islet amyloid polypeptide but does inhibit fibril thioflavin-T interactions: implications for mechanistic studies of  $\beta$ -cell death," *Biochemistry*, vol. 47, no. 22, pp. 6016-6024, 2008.

# Summary (French)

## *I. Introduction*

Le terme « amyloïde » fut introduit par le médecin et biologiste Rudolph Virchow à la fin du 19<sup>ème</sup> siècle, lorsqu'il s'est aperçu qu'un tissu cérébral d'apparence anormale réagissait positivement à la coloration à l'iode comme l'amidon (d'où le terme « amyloïde »)<sup>1</sup>. Cette découverte initiale fut ensuite suivie par une phase descriptive de dépôts amyloïdes par microscopie électronique. Les images obtenues ont montré des amas de fibres droites et rigides, d'épaisseur comprise entre 6 et 13 nm et de 100 nm à 1,6 µm de long<sup>2,3</sup>. Cette morphologie ainsi que la capacité de lier le rouge Congo et l'apparition d'une biréfringence verte sous lumière polarisée sont devenues les caractéristiques des amyloïdes. A l'heure actuelle, plus de 20 peptides et protéines amyloïdes ont été identifiées, intervenant dans des maladies systémiques ou locales, neurodégénératives ou non neuropathiques. Les maladies d'Alzheimer, de Parkinson, de Huntington et le diabète de type 2 sont les plus connues.

Les maladies amyloïdes sont des affections sévères caractérisées par la présence de dépôts extracellulaires susceptibles de toucher un ou plusieurs tissus du corps humain dont le système nerveux central. Ces agrégats fibreux non solubles, appelés amyloïdes, dont l'origine est liée à divers facteurs tels que par exemple des surconcentrations peptidiques locales, un mauvais repliement de peptides, sont la cause de nombreux dommages tissulaires et cellulaires au sein de l'organe affecté, provoquant une altération de ses fonctions au cours du temps.

Bien que le mécanisme de formation des fibres reste mal connu, il a été décrit comme un processus mettant en jeu deux grandes étapes : la nucléation, cinétiquement déterminante conduisant à la formation d'oligomères et la phase d'élongation conduisant à la formation des fibres (figure 1). La formation des fibres amyloïdes est associée à changement conformationnel des peptides qui passent d'un état non structuré ou d'une structure native qui leur est propre à une structure  $\beta$  croisée. A l'état fibrillaire, les peptides adoptent une structure secondaire en feuillets  $\beta$  dont les axes des brins sont perpendiculaires à l'axe de la fibre et les liaisons hydrogène inter-brins parallèles à celui-ci.

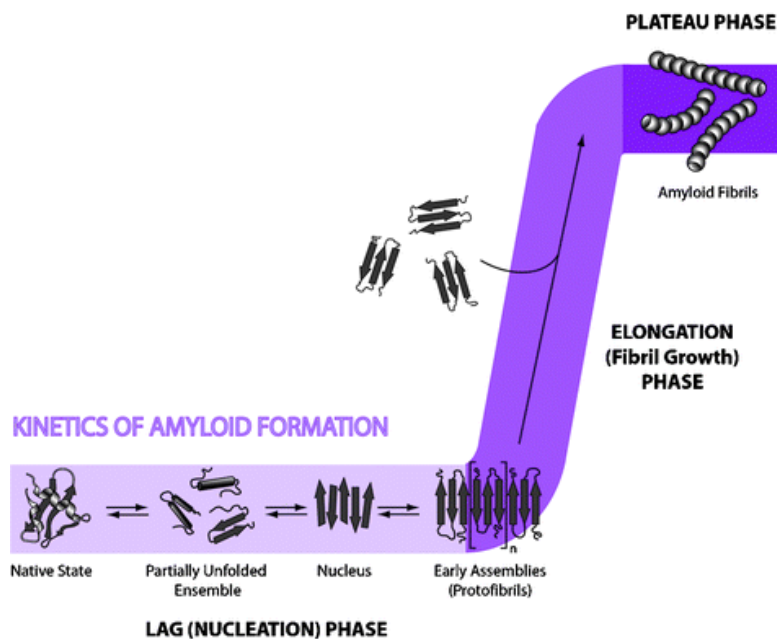


Figure 108 :Représentation schématique de la formation de fibres amyloïdes (adapté de Wilson et al., 2007<sup>4</sup>)

#### a) Hypothèses de cytotoxicité

Plusieurs hypothèses ont été émises concernant l'origine de la cytotoxicité des peptides amyloïdes. De par la présence d'agrégats fibreux au niveau des tissus affectés, une première hypothèse a lié le caractère cytotoxique des peptides amyloïdes aux fibres matures. Cependant, des études plus récentes réalisées *in vitro* ont montré que plus que les fibres, des espèces oligomériques ou les premières étapes du processus d'oligomérisation étaient responsables du caractère cytotoxique des peptides amyloïdes<sup>5,6</sup>.

#### b) Le diabète de type 2 et la sécrétion de l'IsletAmyloidPolyPeptide (hIAPP)

Le diabète de type 2 est lié à un trouble du métabolisme du glucose conduisant à une hyperglycémie. D'un point de vue histopathologique, des dépôts insolubles de fibres amyloïdes, principalement constitués par le peptide hIAPP, sont observés au niveau des îlots de Langerhans.

hIAPP est un peptide composé de 37 résidus et co-sécrété avec l'insuline par les cellules  $\beta$  du pancréas. Il est initialement synthétisé comme un pré-pro-peptide de 89 résidus, qui est par la suite clivé dans le réticulum endoplasmique pour former le précurseur proIAPP de 67 résidus. Le peptide proIAPP est converti en peptide mature de 37 résidus dans l'appareil de Golgi et les granules de sécrétion<sup>7,8</sup>. Une fois le peptide hIAPP formé et fonctionnel, celui-ci est libéré dans le milieu extracellulaire. A ce jour, son rôle physiologique reste mal connu, néanmoins,

il semble être impliqué, entre autres, dans la vidange gastrique et dans la régulation de la glycémie et de la satiété.

### *c) La maladie d'Alzheimer et la synthèse du peptide $\beta$ -amyloïde ( $A\beta$ )*

La maladie d'Alzheimer se caractérise entre autres par des dépôts amyloïdes, appelées « plaques séniles », au sein du cortex cérébral, constitués en majorité d'un peptide de 4 kDa appelé peptide  $\beta$ -amyloïde ( $A\beta$ ) qui forme le motif de répétition de ces fibres et sur lequel nous allons focaliser notre étude. Le peptide  $A\beta$  est un fragment issu du clivage d'une protéine transmembranaire appelée « AmyloidPrecursorProtein » (APP) par les enzymes  $\beta$  et  $\gamma$ -sécrétases. Selon le site de clivage de la  $\gamma$ -sécrétase dans la région transmembranaire de l'APP, le peptide  $A\beta$  peut être constitué de 38, 40 ou 42 résidus. Ce site de clivage influence la propension du peptide à l'auto-association ainsi que son caractère pathogène<sup>9</sup>.

### *d) Interactions avec les membranes*

La membrane cellulaire étant trop complexe pour être étudiée, nous avons fait appel à plusieurs modèles membranaires afin de pouvoir mener nos expériences. Selon les expériences nous avons utilisé soit des vésicules unilamellaires, constituées d'une seule bicouche lipidique, dont la taille allait de 50 (SUV) à 200 nm (LUV), soit une monocouche lipidique (figure 2). Les monocouches lipidiques se forment spontanément en déposant des lipides à une interface air/eau. Les lipides s'orientent de telle sorte que les têtes polaires sont en contact avec la solution aqueuse tandis que les queues hydrophobes sont dirigées vers l'air, formant ainsi une monocouche pour laquelle il est possible de mesurer une tension de surface.

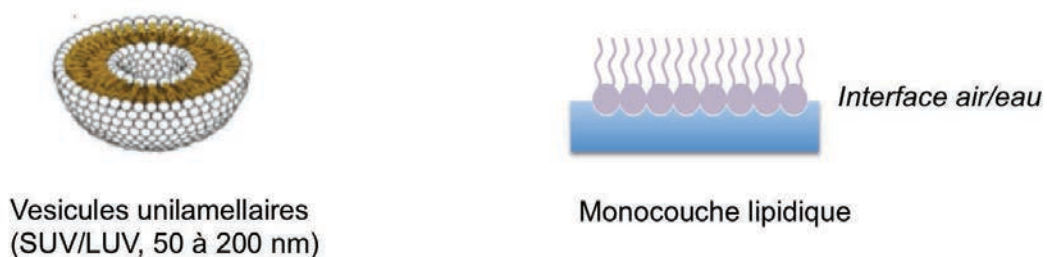


Figure 109 : Représentation schématique d'une vésicule unilamellaire et d'une monocouche lipidique



### *e) Développement d'inhibiteurs potentiels*

En raison de leur affinité avec la membrane cellulaire et de leur caractère cytotoxique, les espèces intermédiaires sont devenues des cibles majeures pour le développement de composés thérapeutiques visant à limiter le développement des maladies amyloïdes. Plusieurs stratégies ont été utilisées à cet effet : la stabilisation du monomère, l'accélération du processus afin de former des fibres inertes ou la redirection du mécanisme d'association vers la formation d'espèces non toxiques.

Des molécules peptidomimétiques incluant un sucre ou des tripeptides incorporant un acide aminé trifluorométhyl dans leurs chaînes peptidiques. Ces molécules ont pour but de déstabiliser les interactions peptide-peptide menant à la formation d'espèces toxiques.

En parallèle à la conception et au développement de composés synthétiques, d'autres études ont été menées sur des composés naturels, particulièrement les polyphénols, susceptibles d'inhiber la formation de fibres amyloïdes.

### *f) Objectifs de la thèse*

Mon travail s'est articulé selon 3 axes de recherches.

Dans un premier temps, nous nous sommes intéressés aux premières étapes d'oligomérisation des peptides hIAPP et A $\beta$ 42 dans l'optique d'obtenir des informations sur les propriétés mécanistiques propres aux deux peptides.

Ensuite, une analyse mutationnelle réalisée à deux pH (5,5 et 7,4) a permis de déterminer l'influence du résidu His18 de la séquence d'hIAPP ainsi que l'effet de la charge globale du peptide sur ses propriétés d'oligomérisation.

Enfin, la troisième partie de ma thèse traite de l'influence de plusieurs inhibiteurs potentiels sur l'auto-association des peptides hIAPP et A $\beta$ 42.

## *II. Méthodes d'analyse*

Mes projets ont fait appel à différentes techniques biophysiques permettant d'observer différents états d'agrégation des peptides amyloïdes ainsi que les différentes interactions entre les espèces présentes en solution.

La fluorescence de la thioflavine T (ThT) est une technique utilisée de manière fréquente pour

le suivi de formation des fibres. La ThT a pour caractéristique de ne pas émettre de signal de fluorescence en présence d'espèces monomériques en solution. Son signal de fluorescence augmente au fur et à mesure de la formation des fibres avant d'atteindre un plateau en présence de fibres matures, conduisant à une courbe sigmoïdale.

La fluorescence du tryptophanol (TROL) possède quant à elle des propriétés différentes de celles de la ThT, sa liaison aux espèces pré-fibrillaires entraînant une extinction de la fluorescence et la décroissance du signal.

Les expériences de dichroïsme circulaire ont permis d'analyser les changements de structure secondaire des peptides amyloïdes inhérents à leur oligomérisation au cours du temps.

Les expériences de résonance magnétique nucléaire (RMN) ont permis à la fois de caractériser la cinétique de disparition du monomère au cours du temps (expériences 1D  $^1\text{H}$ ) ainsi que de mettre en évidence des interactions avec des espèces de plus haut poids moléculaire en solution (expériences de transfert de saturation).

La morphologie des agrégats de haut poids moléculaire et des fibres amyloïdes a été étudiée par microscopie électronique à transmission.

D'autres expériences ont permis l'observation des interactions entre les peptides amyloïdes et les membranes. Les expériences de fuite de la calcéïne, fluorophore encapsulé dans des vésicules lipidiques, ont permis de déterminer la perméabilisation membranaire induite par un peptide. Les premières étapes de l'insertion d'un peptide dans une membrane ont été étudiées sur un système simplifié de monocouches lipidiques.

Afin d'effectuer des comparaisons entre les résultats obtenus pour les différents peptides étudiés, plusieurs de nos résultats (intensité de la fluorescence ThT, intensité du signal RMN et ellipticité au cours du temps) ont pu être tracés et ajustés par des fonctions de Boltzmann et de Richards. Cet ajustement nous a notamment permis d'obtenir des paramètres cinétiques inhérents à la cinétique de fibrillation de hIAPP et A $\beta$ 42 tels que le temps de demi-vie ( $t_{1/2}$ ), temps auquel 50% de la variation de signal observée est atteinte (figure 3).

$$F_t = \frac{F_i - F_f}{1 + e^{\left(\frac{t-t_1}{2}\right)/\tau}} + F_f$$

$$I_t = \frac{I_i - I_f}{1 + e^{\left(\frac{t-t_1}{2}\right)/\tau}} + I_f$$

$$\theta_t = \frac{\theta_i - \theta_f}{1 + e^{\left(\frac{t-t_1}{2}\right)/\tau}} + \theta_f$$

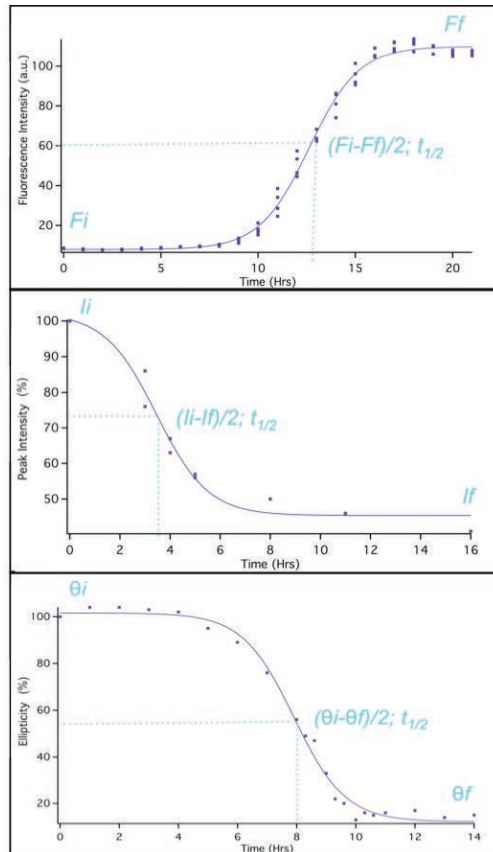


Figure 110 : Ajustement des données de fluorescence de la ThT, de RMN et de dichroïsme circulaire par une fonction sigmoïdale de Boltzmann (équations à gauche)

### III. Etude des mécanismes d'oligomérisation et de fibrillation des peptides amyloïdes

Les cinétiques rapides d'auto-association et la présence de plusieurs espèces intermédiaires ont rendu difficile la caractérisation des mécanismes d'oligomérisation et fibrillation des peptides. Les premières étapes du processus d'oligomérisation des peptides seraient associées avec le caractère cytotoxique de ces derniers, de ce fait, dans cette partie nous nous sommes intéressés à la première phase d'auto-association de deux peptides amyloïdes : hIAPP et Aβ42.

Ces deux peptides amyloïdes présentent des séquences proches (24% d'identité, 40% de similitude, figure 4) et sont de taille proche (37 et 42 acides aminés respectivement). Ces similitudes observées entre les deux peptides pourraient suggérer un mécanisme de fibrillation commun. Cependant, s'il a été possible de mettre en évidence et de caractériser des oligomères de faible poids moléculaire lors d'études sur Aβ, des études sur hIAPP dans des conditions expérimentales similaires n'ont pas permis de détecter la présence de petits oligomères.



Figure 111 : Séquences des peptides Aβ42 et hIAPP

Les expériences menées ont eu pour but de caractériser les interactions entre les différentes espèces présentes en solution afin de mieux comprendre les mécanismes d'oligomérisation et de fibrillation des deux peptides étudiés.

Afin de pouvoir comparer au mieux nos résultats, les expériences ont été menées dans les mêmes conditions expérimentales (concentration peptidique, solution tampon, pH, température).

Les expériences de fluorescence de la ThT (figure 5) ont montré qu'hIAPP avait une cinétique de formation de fibres très rapide, caractérisée par un temps de latence court, et une pente élevée suggérant un processus coopératif. Dans le cas du peptide Aβ42, la cinétique de formation des fibres est plus lente, avec une sigmoïde moins pentue, suggérant un mécanisme de fibrillation plus graduel. Nous avons également pu observer que le maximum de fluorescence différait selon le peptide étudié, celui pour Aβ42 étant inférieur à celui d'hIAPP après normalisation des valeurs. Ce résultat peut indiquer des différences d'affinité ou de mode de liaison entre la ThT et Aβ42 mais également que la quantité et/ou la morphologie des fibres formées pour les deux peptides diffère.

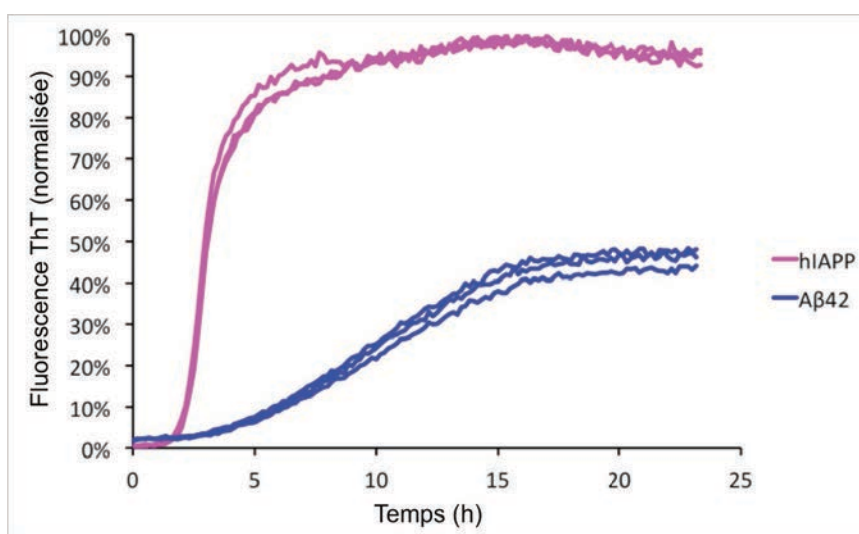


Figure 112 : Courbes de fluorescence de la ThT au cours du temps (hIAPP en rose, Aβ42 en bleu)

Bien que le TROL ait permis de montrer la formation de petits oligomères, la sonde s'est avérée être peu sélective, ne permettant pas d'identifier les espèces présentes en solution pour les 2 peptides (figure 5).

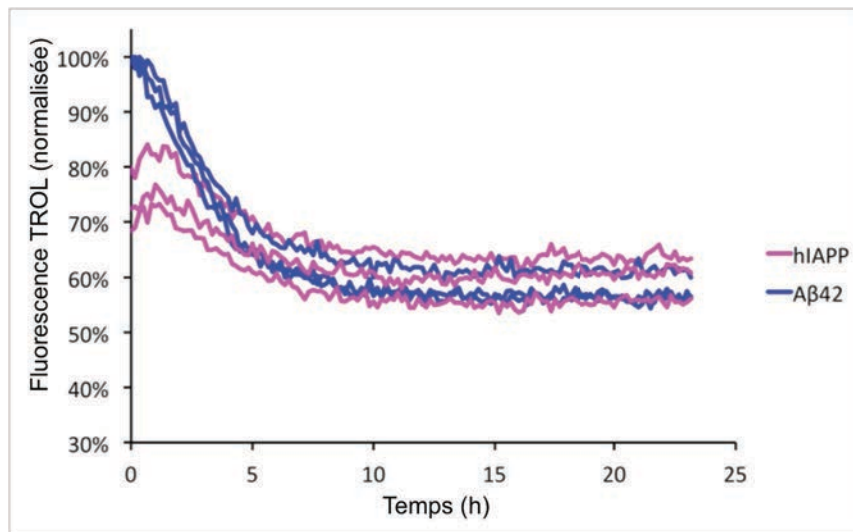


Figure 113 : Courbe de fluorescence du TROL au cours du temps (hIAPP en rose, Aβ42 en bleu)

En raison de l'utilisation de sondes fluorescentes à une concentration élevée de 75  $\mu\text{M}$ , une étude a été réalisée dans le but d'examiner les interactions entre les peptides amyloïdes et la ThT ou le TROL ainsi que la possible influence de ces fluorophores sur la cinétique d'oligomérisation et de fibrillation des peptides.

Les résultats des expériences RMN et de dichroïsme circulaire sur les deux peptides en présence des sondes fluorescentes ont montré que si celles-ci avaient peu d'influence sur la cinétique de fibrillation du peptide A $\beta$ , elles ralentissaient fortement la cinétique du peptide hIAPP. Cette interaction entre les sondes fluorescentes et les peptides amyloïdes montrent qu'il n'était pas possible de comparer les résultats obtenus par fluorescence, qui nécessitent l'utilisation des fluorophores, à ceux obtenus par dichroïsme circulaire ou par RMN.

Il reste cependant possible d'effectuer des comparaisons entre les expériences de RMN et de dichroïsme circulaire qui ne nécessitent pas l'utilisation de sondes fluorescentes. Les résultats obtenus pour ces expériences, en particulier ceux de la RMN, ont permis de mettre en évidence les interactions entre les espèces de différent poids moléculaire en solution et d'obtenir des informations mécanistiques d'oligomérisation pour les peptides hIAPP et A $\beta$ .

La cinétique de formation de fibres d'hIAPP est très rapide et caractérisée par l'auto association rapide des monomères. Espèces intermédiaires n'ont pas été détectées par l'ensemble des techniques biophysiques utilisées.

Au contraire, le mécanisme de formation de fibres d'A $\beta$  est plus graduel et est caractérisé par la présence d'échanges rapides entre des espèces de faible poids moléculaires (monomères, petits oligomères) qui ne sont pas totalement consommées et des espèces plus larges qui ne sont pas détectables par RMN (figure 7).

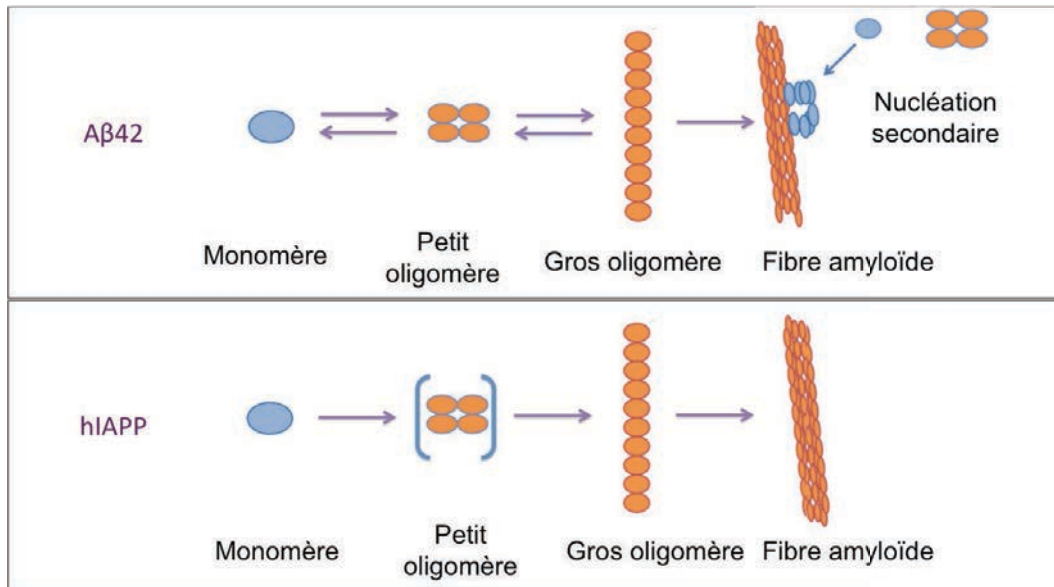


Figure 114 : Représentation schématique des mécanismes de fibrillation de hIAPP et A $\beta$ 42

#### IV. Effet de la substitution du résidu 18 et du pH sur les propriétés d'auto association de IAPP

Dans cette partie, nous nous sommes intéressés à l'effet du pH et de la substitution du résidu 18, sur les propriétés d'oligomérisation et de fibrillation du peptide IAPP. En effet, le résidu 18, une histidine, a la particularité de voir son degré de protonation changer en fonction du pH d'un point de vue physiologique (l'acide aminé est protoné à pH 5,5, correspondant au pH dans les granules de sécrétion, tandis qu'il est déprotoné à pH 7,4, dans le milieu extracellulaire). Situé dans la boucle inter-brins entre les deux brins  $\beta$  du peptide, le résidu 18 a également été identifié comme un résidu impliqué dans le processus d'élongation des fibres amyloïdes ainsi que dans l'interaction du peptide avec la membrane cellulaire<sup>10</sup>.

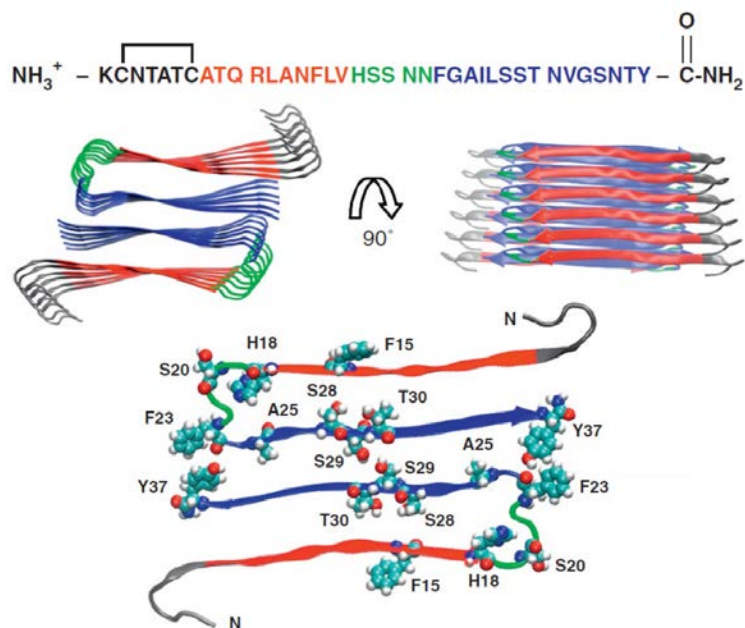


Figure 115 : Modèle structural des fibres d'hIAPP (Cao et al. 2013)<sup>11</sup>

Afin de mener cette étude, l'histidine a été substituée par une lysine, une arginine, qui sont des acides aminés chargés positivement, un glutamate, acide aminé chargé négativement à pH 7, ou une alanine, qui est neutre et dont la chaîne latérale est courte (figure 9). Ces différentes substitutions permettent ainsi de faire varier la charge globale des peptides et d'étudier les interactions entre la chaîne latérale du résidu 18 avec son environnement fibrillaire.

hIAPPsauvage :	KCNTATCAT	QRLANFLVHS	SNNFGAILSS	TNVGSNTY-NH <sub>2</sub>
IAPP H18K :	KCNTATCAT	QRLANFLVKS	SNNFGAILSS	TNVGSNTY-NH <sub>2</sub>
IAPP H18R :	KCNTATCAT	QRLANFLVRS	SNNFGAILSS	TNVGSNTY-NH <sub>2</sub>
IAPP H18E :	KCNTATCAT	QRLANFLVES	SNNFGAILSS	TNVGSNTY-NH <sub>2</sub>
IAPP H18A :	KCNTATCAT	QRLANFLVAS	SNNFGAILSS	TNVGSNTY-NH <sub>2</sub>

Figure 116 : séquence peptidique de hIAPP sauvage et des quatre mutants d'hIAPP

De par l'interaction entre hIAPP et la membrane des cellules  $\beta$  du pancréas, l'ensemble des expériences a été mené en présence de modèles membranaires (vésicules unilamellaires ou monocouche lipidique) composés d'un mélange 7:3 de 1,2-dioléoyl-*sn*-glycéro-3-phosphocholine (DOPC, à tête zwitterionique) et de 1,2-dioléoyl-*sn*-glycéro-3-phospho-L-sérine (DOPS, négativement chargé, figure 10).

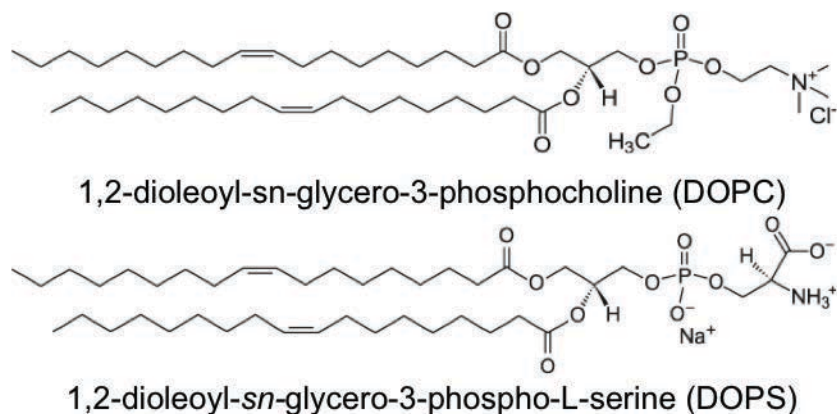


Figure 117 : Structure moléculaire de la 1,2-dioléoyl-*sn*-glycéro-3-phosphocholine (DOPC) et de la 1,2-dioléoyl-*sn*-glycéro-3-phospho-L-sérine (DOPS)

Les résultats de l'étude à pH 7,4 ont montré que la substitution de l'histidine par un des quatre acides aminés cités précédemment ralentissait la cinétique de fibrillation des peptides (tableau 1).

	Fluorescence ThT Concentration peptidique : 10 $\mu\text{M}$	NMR Concentration peptidique : 50 $\mu\text{M}$	CD Concentration peptidique : 25 $\mu\text{M}$
	$t_{1/2}(\text{h})$	$t_{1/2}(\text{h})$	$t_{1/2}(\text{h})$
<b>hIAPP sauvage</b>	7.59 $\pm$ 0.02	0.40 $\pm$ 0.23	2.30 $\pm$ 0.04
<b>IAPP H18K</b>	12.54 $\pm$ 0.04	3.28 $\pm$ 0.06	11.70 $\pm$ 0.08
<b>IAPP H18R</b>	14.79 $\pm$ 0.02	2.39 $\pm$ 0.09	9.94 $\pm$ 0.22
<b>IAPP H18E</b>	35.44 $\pm$ 0.28	> 24	Pas de transition (jours)
<b>IAPP H18A</b>	45.15 $\pm$ 0.05	9.53 $\pm$ 0.05	17.46 $\pm$ 0.089

Tableau 1 : Paramètres cinétiques (temps de demi-vie  $t_{1/2}$ ) obtenus pour hIAPP sauvage et les quatre peptides mutants par les expériences de fluorescence de la ThT, de RMN et CD à pH 7,4

L'analyse d'un modèle de fibre d'hIAPP obtenu à partir de données de cristallographie des rayons X montre que l'histidine 18 est orientée vers l'intérieur de la fibre, interagissant ainsi avec le squelette de l'asparagine 22 et la chaîne latérale de l'isoleucine 26. Ces interactions de l'histidine avec les résidus environnants impliquent par conséquent que la mutation du résidu 18 induit une déstabilisation de la structure de la fibre (figure 11).



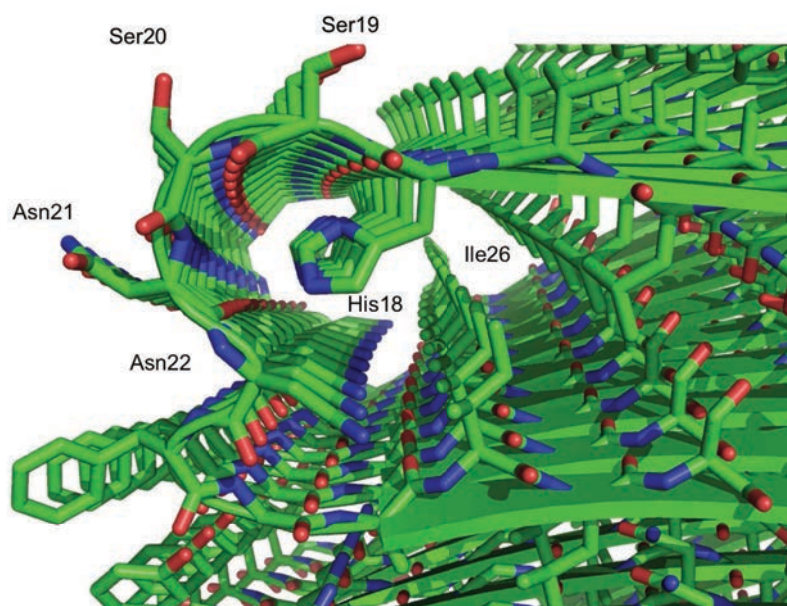


Figure 118 : Représentation de l'environnement de l'histidine 18 dans une fibre amyloïde d'hIAPP. Modèle obtenu à partir de données de cristallographie aux rayons X (Wiltzius et al., 2008<sup>12</sup>)

Les résultats de fluorescence de la ThT ont montré que de manière globale, la cinétique de fibrillation des peptides était ralentie à pH 5,5 par rapport à la cinétique à pH 7,4. De manière comparable aux résultats obtenus à pH 7,4, nous avons pu observer que la substitution de His18 par des acides aminés Lys/Arg/Glu/Ala était défavorable pour la cinétique d'oligomérisation du peptide, les substitutions par un acide aminé acide (Glu) ou à chaîne courte (Ala) étant les plus délétères. Cependant, les résultats des expériences de RMN et de CD ont montré que la cinétique de disparition du monomère et du signal dichroïque à 205 nm était plus rapide à pH 5,5 qu'à pH 7,4 pour les mutants IAPP H18E et IAPP H18A, indiquant que le pH acide modulait la fibrillation des peptides de manière complexe (tableau 2).

	Fluorescence ThT	RMN	CD
	Concentration peptidique : 10 $\mu$ M	Concentration peptidique : 50 $\mu$ M	Concentration peptidique : 25 $\mu$ M
	$t_{1/2}$ (h)	$t_{1/2}$ (h)	$t_{1/2}$ (h)
<b>hIAPPsauvage</b>	10.55 $\pm$ 0.05	1.38 $\pm$ 0.08	2.74 $\pm$ 0.35
<b>IAPP H18K</b>	21.98 $\pm$ 0.09	5.45 $\pm$ 0.27	6.36 $\pm$ 0.09
<b>IAPP H18R</b>	28.50 $\pm$ 0.10	4.12 $\pm$ 0.10	6.55 $\pm$ 0.45
<b>IAPP H18E</b>	67.97 $\pm$ 0.08	6.77 $\pm$ 0.08	3.52 $\pm$ 0.11
<b>IAPP H18A</b>	63.09 $\pm$ 0.06	4.09 $\pm$ 0.20	15.28 $\pm$ 0.06

Tableau 2 : Paramètres cinétiques (temps de demi-vie  $t_{1/2}$ ) obtenus pour hIAPP sauvage et les quatre peptides mutants par les expériences de fluorescence de la ThT, de RMN et CD à pH 5,5

Les expériences de fuite de calcéïne et de monocouches, réalisés dans le groupe de Membrane Biophysics and Biochemistry (Utrecht University) ont permis de montrer que les différents peptides s'inséraient de manière analogue dans la monocouche mais que le pH acide ralentissait ou empêchait la perméabilisation membranaire.

## V. Interactions avec molécules inhibitrices des maladies amyloïdes

La maladie d'Alzheimer et le diabète de type 2 représentent de nos jours deux problèmes de santé majeure. Malgré le développement de différentes approches visant à ralentir la progression de ces maladies, il n'existe à l'heure actuelle aucun traitement qui permette de soigner ces deux pathologies. En raison du caractère cytotoxique des espèces de faible poids moléculaire, celles-ci sont devenues une cible thérapeutique majeure pour le développement de différentes classes d'inhibiteurs de la formation de fibres amyloïdes.

Une classe d'inhibiteurs développés consiste en des peptidomimétiques qui miment le site de nucléation des peptides amyloïdes. Ces peptidomimétiques sont conçus afin d'interagir avec les peptides amyloïdes et incorporent des motifs visant à déstabiliser les interactions entre les feuillets  $\beta$ des peptides. En particulier, il a été montré que des molécules incorporant une proline ou un acide  $\alpha$ -aminoisobutyrique pouvaient inhiber la formation de fibres en induisant une gêne stérique ou en favorisant une conformation des peptides en hélice  $\alpha$ <sup>13,14</sup>. D'autres inhibiteurs potentiels possédant des atomes de fluor, qui permettent de moduler l'hydrophobicité des peptides ont également été développés.

En parallèle au développement d'inhibiteurs potentiels synthétiques, des études ont été réalisées sur les molécules naturelles, en particulier des polyphénols, dont l'effet inhibiteur sur la fibrillation des peptides amyloïdes a été montré *in vitro*.<sup>15</sup>

Lors de ma thèse, j'ai eu l'occasion de participer à plusieurs projets, en collaboration avec d'autres laboratoires, s'intéressant à l'effets d'inhibiteurs synthétiques et naturels sur la formation de fibres amyloïdes d'hIAPP et A $\beta$ 42.

Un premier projet a été réalisé en collaboration avec le laboratoire de chimie Biologique (groupe du Pr Thierry Brigaud, Université de Cergy-Pontoise) et a porté sur l'étude de deux tripeptides incorporant des acides  $\alpha,\alpha$ -disubstitués (acide  $\alpha$ -aminoisobutyrique et acide aminé trifluorométhylé).

Des résultats précédents ont en effet permis de montrer que l'incorporation d'un acide  $\alpha$ -aminoisobutyrique dans des peptides hydrophobes avait un effet inhibiteur sur la cinétique d'agrégation de peptides amyloïdes en perturbant l'auto-association des monomères.

La présence du fluor permet d'augmenter le caractère donneur de liaison hydrogène de l'amide, donc la stabilisation conformationnelle du tripeptide en feuillet  $\beta$  et l'augmentation de l'hydrophobie, ce qui pourrait conférer une plus grande affinité avec le site de nucléation de A $\beta$  (séquence KLVFF). Dans cette étude, nous nous sommes intéressés à l'influence d'un tripeptide incorporant un acide aminé trifluorométhylé (composé **2**, figure 12) sur la cinétique de fibrillation de A $\beta$  ainsi que son interaction avec le peptide, que nous avons comparées à celles de son homologue incorporant un acide  $\alpha$ -aminoisobutyrique (composé **1**).

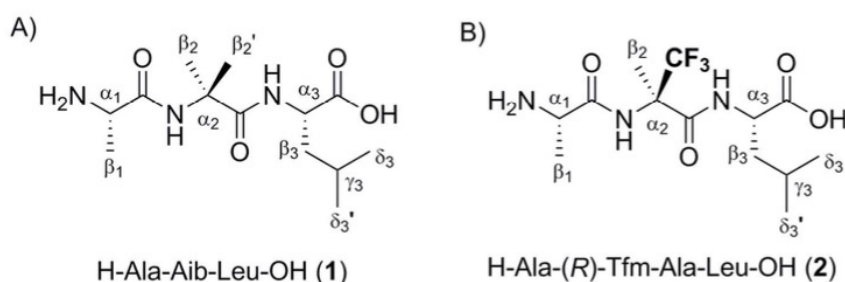


Figure 119 : Structure chimique des composés **1** et **2**

Nos résultats ont montré que si la cinétique de fibrillation du peptide A $\beta$ 42 était peu affectée par l'ajout du composé **1** en solution, elle était ralentie par la présence du composé **2** avec une perte de 50% de signal observée au bout de  $8.0 \pm 1.0$  heures (au lieu de  $4.2 \pm 1.0$  heures et  $4.3 \pm 1.0$  heures lorsque le peptide est seul en solution et en présence du composé **1**, respectivement). Par la suite, des expériences de STD ont permis d'observer la présence d'un échange rapide, à l'échelle de temps de la RMN entre le composé **2** et le peptide A $\beta$ 42, avec une apparition d'un signal au cours du temps. Ce signal n'est pas observé sur les échantillons d'A $\beta$ 42 avec le composé **1**.

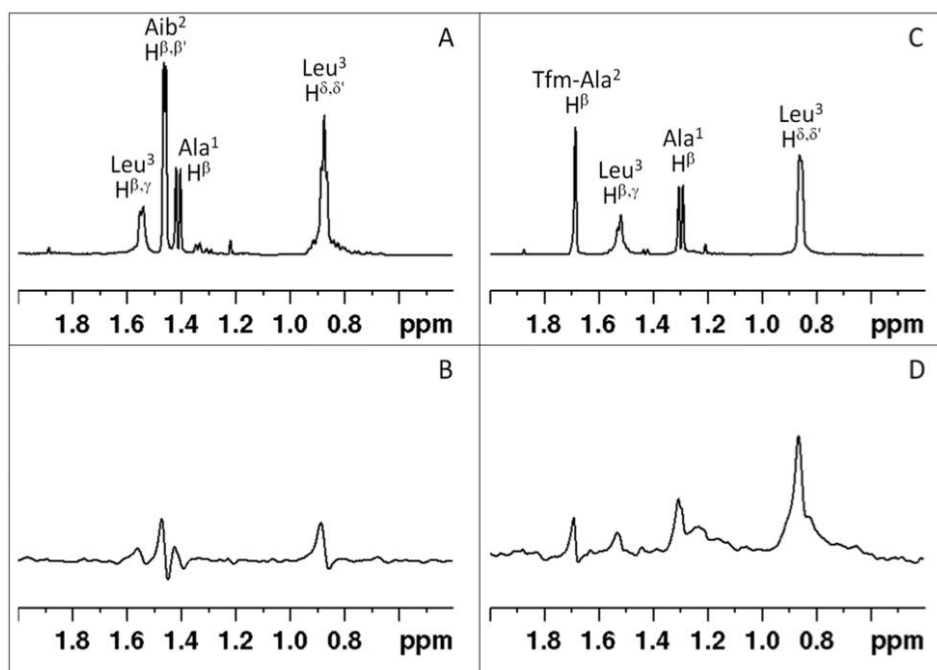


Figure 120 : (A,C) Spectres 1D  $^1\text{H}$  de la région aliphatique des composés 1 et 2 respectivement. (B,D) Signaux STD observés dans la région aliphatique  $^1\text{H}$  du composé 1 et 2 en présence du peptide A $\beta$ 42 au cours du temps.

Les résultats de ces expériences ont montré que des composés incorporant un motif Aib ou un acide aminé (R)- $\alpha$ -Tfm-Ala interfèrent avec le processus d'oligomérisation de A $\beta$  en perturbant la formation des feuilletts  $\beta$  du peptide et en interagissant avec la région hydrophobe du peptide. De plus, nous avons pu observer que l'incorporation du groupe trifluorométhylé dans le tripeptide, de par son hydrophobicité, permettait d'augmenter l'inhibition de l'oligomérisation d'A $\beta$ 42.

Un second projet a été mené en collaboration avec le groupe Molécules Fluorées et Chimie Médicinale, (Pr Sandrine Onger, Université d'Orsay). Cette étude a porté sur l'effet inhibiteur de peptidomimétiques incorporant un sucre (composé **3 $\beta$** , figure 14), qui a pour effet de défavoriser les interactions entre les monomères et oligomères présents en solution<sup>16</sup>, sur l'oligomérisation d'A $\beta$ 42.

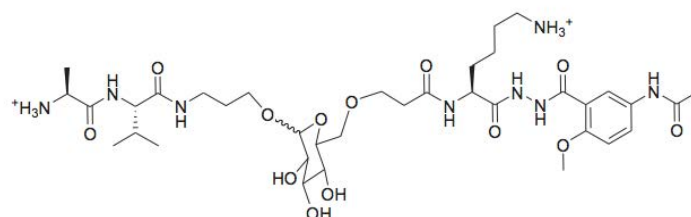


Figure 121 : Structure du composé **3 $\beta$**

L'absence de variation de déplacement chimique sur les spectres HSQC  $^{15}\text{N}$ - $^1\text{H}$  et  $^{13}\text{C}$ - $^1\text{H}$  a permis de montrer que le composé n'interagissait pas avec A $\beta$ 42 dans son état monomérique.

Cependant, l'apparition d'un signal STD au cours du temps, concomitante à la décroissance du signal RMN correspondant au monomère, ainsi que des expériences WaterLOGSY ont permis de mettre en évidence une interaction entre le composé et les espèces oligomériques présentes en solution (figure 15).

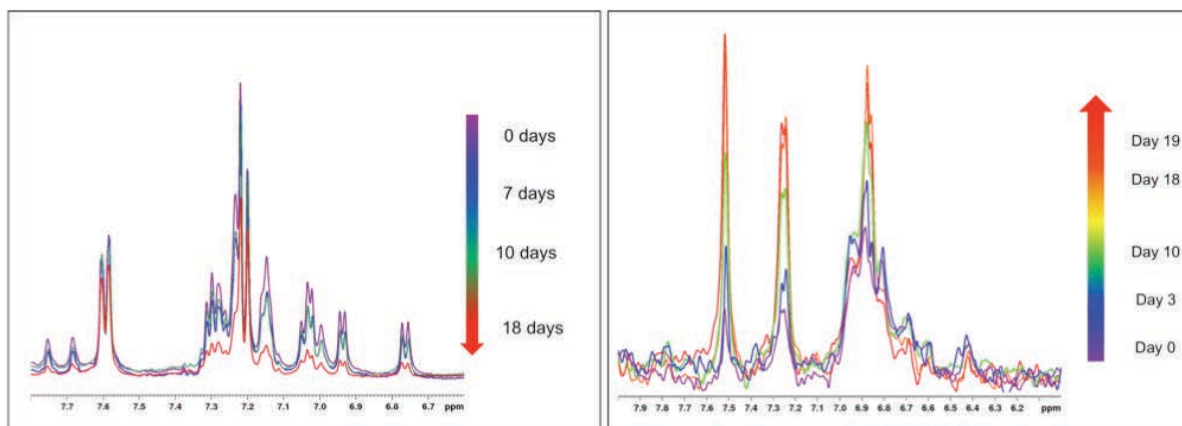


Figure 122 : (gauche) spectre RMN 1D  $^1\text{H}$  des signaux aromatiques du composé  $3\beta$  (0.4 mM) et  $A\beta_{42}$  (90  $\mu\text{M}$ ) à 5°C au cours du temps. (Droite) : signaux STD observés dans la région aromatique  $^1\text{H}$  du composé  $3\beta$  (0,4 mM) en présence du peptide  $A\beta_{42}$ (90  $\mu\text{M}$ ) à 5 °C au cours du temps

Enfin, une troisième collaboration, réalisée avec le groupe Membrane Biophysics and Biochemistry (Pr Antoinette Killian, Utrecht University) a consisté en l'étude de l'interaction d'un composé naturel, l'épigallocatechine gallate (EGCG), un polyphénol extrait du thé, avec hIAPP<sup>17</sup>. L'analyse par RMN a permis de montrer que EGCG interagissait avec hIAPP monomérique, induisant des variations de déplacement chimique, notamment dans la boucle inter-feuillets  $\beta$  (résidu 18) et dans la région amyloïdogénique (résidus 20-29) du peptide. Des expériences similaires ont été menées sur le fragment 1-19 du peptide hIAPP. Les résultats ont montré que l'ajout d'EGCG dans l'échantillon n'induisait pas ou de faibles variations de déplacement chimiques sur les spectres RMN, ce qui implique que le fragment hIAPP<sub>1-19</sub> interagit peu avec l'inhibiteur.

## VI. Conclusion

Les objectifs de cette thèse étaient d'étudier les propriétés d'oligomérisation et de fibrillation de deux peptides amyloïdes  $A\beta_{42}$  et hIAPP et d'étudier comment différents facteurs tels que le pH, la substitution d'un résidu ou l'ajout d'inhibiteurs pouvaient moduler le mécanisme d'auto association.

La première partie de ma thèse a porté sur l'étude des premières étapes d'oligomérisation des

peptides. Cette étude, qui a fait appel à différentes techniques biophysiques complémentaires a permis de mettre en évidence des différences de mécanismes d'oligomérisation des deux peptides. En particulier, nous avons montré que le mécanisme d'oligomérisation et fibrillation d'IAPP était coopératif et caractérisé par l'absence d'espèces de faible poids moléculaire en solution.

Dans la seconde partie de ma thèse, je me suis intéressée au rôle de l'histidine 18 de IAPP, ainsi qu'à l'effet de la charge globale du peptide sur ses propriétés d'oligomérisation. Pour cela, une étude mutationnelle a été réalisée et l'analyse biophysique des mutants en présence de modèles lipidiques a été effectuée à pH 5,5 et à pH 7,4. Les résultats de cette étude ont montré que la substitution de l'histidine 18 ralentissait la formation des fibres en interférant avec le processus d'auto-association des monomères et que le pH acide était globalement défavorable à l'oligomérisation. Dans la suite de ce projet, il serait intéressant d'effectuer des expériences de microscopie, afin d'observer la morphologie des différents agrégats formés lors de l'oligomérisation des peptides aux différents pH. De même nous pourrions nous intéresser à des mutants IAPP H18Q et H18N, qui permettraient de conserver le caractère accepteur/donneur de liaisons hydrogène, mais également un mutant IAPP H18Y, qui permettrait de conserver le caractère aromatique du résidu.

Enfin, j'ai étudié les interactions entre les peptides amyloïdes et des inhibiteurs potentiels, d'origine synthétique (peptides incorporant un sucre ou un acide aminé trifluorométhylé) ou naturelle (épigallocatechinegallate). Différents modes d'action des molécules inhibitrices ont ainsi pu être caractérisés, selon leur interaction avec les monomères ou les oligomères des peptides étudiés.

---

<sup>1</sup> Rather, L. J., and Rudolf Ludwig Karl Virchow. A Commentary on the Medical Writings of Rudolf Virchow: Based on Schwalbe's Virchow-Bibliographie, 1843-1901. Norman Publishing, 1990.

<sup>2</sup> Sipe, Jean D., and Alan S. Cohen. "Review: History of the Amyloid Fibril." *Journal of Structural Biology* 130, no. 2-3 (June 2000): 88-98. doi:10.1006/jsbi.2000.4221.

- 
- <sup>3</sup> Buxbaum, Joel N., and Reinhold P. Linke. "A Molecular History of the Amyloidoses." *Journal of Molecular Biology* 421, no. 2–3 (August 2012): 142–59. doi:10.1016/j.jmb.2012.01.024.
- <sup>4</sup> Wilson, Mark R., Justin J. Yerbury, and Stephen Poon. "Potential Roles of Abundant Extracellular Chaperones in the Control of Amyloid Formation and Toxicity." *Molecular BioSystems* 4, no. 1 (December 13, 2007): 42–52. doi:10.1039/B712728F.
- <sup>5</sup> Fändrich, Marcus. "Oligomeric Intermediates in Amyloid Formation: Structure Determination and Mechanisms of Toxicity." *Journal of Molecular Biology* 421, no. 4–5 (August 2012): 427–40. doi:10.1016/j.jmb.2012.01.006.
- <sup>6</sup> Haataja, Leena, Tatyana Gurlo, Chang J. Huang, and Peter C. Butler. "Islet Amyloid in Type 2 Diabetes, and the Toxic Oligomer Hypothesis." *Endocrine Reviews* 29, no. 3 (May 2008): 303–16. doi:10.1210/er.2007-0037.
- <sup>7</sup> Lukinius, A., E. Wilander, G. T. Westermark, U. Engström, and P. Westermark. "Co-Localization of Islet Amyloid Polypeptide and Insulin in the B Cell Secretory Granules of the Human Pancreatic Islets." *Diabetologia* 32, no. 4 (1989): 240–44.
- <sup>8</sup> Sanke, T., G. I. Bell, C. Sample, A. H. Rubenstein, and D. F. Steiner. "An Islet Amyloid Peptide Is Derived from an 89-Amino Acid Precursor by Proteolytic Processing." *Journal of Biological Chemistry* 263, no. 33 (November 25, 1988): 17243–46.
- <sup>9</sup> Selkoe, Dennis J. "The Molecular Pathology of Alzheimer's Disease." *Neuron* 6, no. 4 (January 4, 1991): 487–98. doi:10.1016/0896-6273(91)90052-2.
- <sup>10</sup> Engel, Maarten F.M., Haci Ali Yigit, Ronald C. Elgersma, Dirk T.S. Rijkers, Rob M.J. Liskamp, Ben de Kruijff, Jo W.M. Höppener, and J. Antoinette Killian. "Islet Amyloid Polypeptide Inserts into Phospholipid Monolayers as Monomer." *Journal of Molecular Biology* 356, no. 3 (February 2006): 783–89. doi:10.1016/j.jmb.2005.12.020.
- <sup>11</sup> Cao, Ping, Andisheh Abedini, and Daniel P. Raleigh. "Aggregation of Islet Amyloid Polypeptide: From Physical Chemistry to Cell Biology." *Current Opinion in Structural Biology* 23, no. 1 (February 2013): 82–89. doi:10.1016/j.sbi.2012.11.003.
- <sup>12</sup> Wiltzius, Jed J.W., Stuart A. Sievers, Michael R. Sawaya, Duilio Cascio, Dmitriy Popov, Christian Riek, and David Eisenberg. "Atomic Structure of the Cross- $\beta$  Spine of Islet Amyloid Polypeptide (amylin)." *Protein Science* 17, no. 9 (September 2008): 1467–74. doi:10.1110/ps.036509.108.
- <sup>13</sup> Soto, Claudio, Einar M. Sigurdsson, Laura Morelli, R. Asok Kumar, Eduardo M. Castaño, and Blas Frangione. " $\beta$ -Sheet Breaker Peptides Inhibit Fibrillogenesis in a Rat Brain Model of Amyloidosis: Implications for Alzheimer's Therapy." *Nature Medicine* 4, no. 7 (July 1998): 822–26. doi:10.1038/nm0798-822.
- <sup>14</sup> Gilead, Sharon, and Ehud Gazit. "Inhibition of Amyloid Fibril Formation by Peptide Analogues Modified with  $\alpha$ -Aminoisobutyric Acid." *Angewandte Chemie International Edition* 43, no. 31 (August 6, 2004): 4041–44. doi:10.1002/anie.200353565.
- <sup>15</sup> Loureiro, Joana A., Rosa Crespo, Hans Börner, Pedro M. Martins, Fernando A. Rocha, Manuel Coelho, M. Carmo Pereira, and Sandra Rocha. "Fluorinated Beta-Sheet Breaker Peptides." *J. Mater. Chem. B* 2, no. 16 (March 14, 2014): 2259–64. doi:10.1039/C3TB21483D.

- 
- <sup>16</sup> Dorgeret, Bertrand, Lucie Khemtémourian, Isabelle Correia, Jean-Louis Soulier, Olivier Lequin, and Sandrine Onger. “Sugar-Based Peptidomimetics Inhibit Amyloid  $\beta$ -Peptide Aggregation.” *European Journal of Medicinal Chemistry* 46, no. 12 (December 2011): 5959–69. doi:10.1016/j.ejmech.2011.10.008.
- <sup>17</sup> Meng, Fanling, Andisheh Abedini, Annette Plesner, C. Bruce Verchere, and Daniel P. Raleigh. “The Flavanol (–)-Epigallocatechin 3-Gallate Inhibits Amyloid Formation by Islet Amyloid Polypeptide, Disaggregates Amyloid Fibrils and Protects Cultured Cells Against IAPP Induced Toxicity.” *Biochemistry* 49, no. 37 (September 21, 2010): 8127–33. doi:10.1021/bi100939a.





# Résumé

Les maladies amyloïdes sont des affections sévères caractérisées par la présence de dépôts extracellulaires fibreux susceptibles de toucher un ou plusieurs tissus du corps humain. Au cours de ma thèse, je me suis intéressée au peptide  $\beta$ -amyloïde ( $A\beta$ ), impliqué dans la maladie d'Alzheimer, ainsi que l'amyline ou Islet Amyloid PolyPeptide (IAPP), impliqué dans le diabète de type 2.

Le mécanisme de formation des fibres a été décrit comme un processus en deux étapes : la nucléation, conduisant à la formation d'oligomères et la phase d'élongation conduisant à la formation des fibres. La première partie de ma thèse est consacrée à l'étude des premières étapes d'oligomérisation d'IAPP. Ce projet, qui a fait appel à différentes techniques biophysiques, a permis de montrer que le mécanisme d'oligomérisation d'IAPP était coopératif et caractérisé par l'absence d'espèces de faible poids moléculaire en solution.

Ensuite, je me suis intéressée au rôle de l'histidine 18 d'IAPP et l'effet de la charge globale du peptide sur ses propriétés d'oligomérisation. Pour cela, une étude mutationnelle a été réalisée et l'analyse biophysique des mutants en présence de modèles lipidiques a été effectuée à pH 5,5 et à pH 7,4. Les résultats de cette étude ont montré que la substitution du résidu 18 ralentissait la formation des fibres et que le pH acide était globalement défavorable à l'oligomérisation.

Enfin, j'ai étudié les interactions entre les peptides amyloïdes et des inhibiteurs potentiels d'origine synthétique ou naturelle. Différents modes d'action de ces inhibiteurs ont ainsi pu être caractérisés, selon leur interaction avec les monomères ou les oligomères des peptides étudiés.